THE UNIVERSITY OF QUEENSLAND

AUSTRALIA

Investigation of Semi-Inverted Hydrocyclone with Novel Design

Muhammad Abdur Rasyid

B.Sc. (Metallurgical Engineering)

A thesis submitted for the degree of Master of Philosophy at

The University of Queensland in 2017

Sustainable Mineral Institute

Julius Kruttschnitt Mineral Research Centre

Abstract

Classification is a vital stage in mineral processing process which separates mineral particles on size by size basis. One classifier that is very common in industry is the hydrocyclone, equipment which has no moving parts and which utilizes centrifugal force to separate mineral particles suspended in a liquid into overflow (fines) and underflow (coarse) products.

The amount of water in the feed recovered to the underflow stream has a significant impact on classification efficiency. Bypass flow, a natural phenomenon where a fraction of fine particles entrained by water reports to the coarse product without being subjected to the classification mechanism, has been believed to be the cause of inefficiency of hydrocyclone. As a result, the hydrocyclone inefficiency causes the overgrinding of valuable minerals. Developing a hydrocyclone classifier which can minimize the amount of water recovery to underflow is an important opportunity.

Non-vertical hydrocyclones (inclination less than horizontal) started to get attention in the late 1980's, where higher throughput and elimination of spigot blockage on non-vertical operation were initially reported (Hochsheid, 1987, Orwe and Noreen, 1988, Johnstone and Rais, 1988, 1997). Specific investigations of hydrocyclone classification performance under influence of different inclinations were investigated in the next two decades (Asomah, 1996, Rong and Napier-Munn, 2003, Banisi and Deghan-Nayeri, 2005, Vakamalla et al., 2014). Review of the literature on these previous works provides that inclining the hydrocyclone beyond horizontal (semi-inverted position) has the potential to be a much more efficient classifier by reducing water recovery to underflow. A specific parametric investigation of hydrocyclone operating at semi-inverted has not been reported. The influences of pressure and different density on semi-inverted hydrocyclone have not been reported.

This thesis is aimed to study the fundamental behaviour of the semi-inverted hydrocyclone and its potential to address inefficiency problem.

Preliminary work comprising 15 tests was done using a standard 250 mm hydrocyclone treating low feed slurry concentration of 25% solids of silica at four different angles with the highest inclination 120 degrees from vertical operation (30 degrees above horizontal). Pressure was varied in order to tests the influence of pressure on semi-inverted operation. Additionally, a limited test on a standard hydrocyclone with higher concentration solids of 40% has been conducted at 135 degrees position. The results of the preliminary work indicated that semi-inverted hydrocyclone can effectively

reduce water recovery to underflow and increase cut size. Sharpness of separation was also found to be increased with inclination. Higher pressure reduced both cut size and water recovery and increased sharpness at semi-inverted positions. It was found that the standard hydrocyclone could not perform at 135 degrees. The cone angle of the hydrocyclone was modified to enable operation at 135 degrees (45 degrees above horizontal).

A total of 45 tests of primary work using the modified JKMRC hydrocyclone have been performed. Three types of slurry feed with different solids concentration and solids density were used: 40% silica, 50% silica, and 40% silica-magnetite solids concentration. Four different pressure levels of pressure (80 kPa to 140 kPa) were tested on semi-inverted positions and compared with conventional operation.

The main finding from all tests was that higher inclination could reduce water recovery significantly. At 135 degrees, water recovery dropped to 5 percent with 40% feed solids and 10% with 50% feed solids. The reductions were followed by a significant increase in cut size of two to three times of vertical hydrocyclone cut size. Sharpness of separation remained unaffected. The pressure – cut size relationship on semi-inverted hydrocyclone followed the conventional trend while and pressure – water recovery relationship did not follow the general trends for conventional hydrocyclones.

A comparison of the experimental results and simulated result using existing hydrocyclone models was done to evaluate the ability of the existing model to predict semi-inverted hydrocyclone operations. Two empirical hydrocyclone models developed by Narasimha and Mainza (2014) and Asomah and Napier-Munn (1997) were used. Although both models did not work well at semi-inverted operations, the trends were in the same order as the experimental results. Performance constant parameters of both models also underwent a gradual yet consistent shift. These results open the possibility of further model development.

The air core of a hydrocyclone is believed to be affected by inclination (Vakamalla et al., 2014), and it is likely that slurry flow pattern was asymmetrical on semi-inverted operation due to influence of gravity. Limited tests were included in the attempt to observe this asymmetric pattern by installing a modified vortex finder with a 10 mm offset centre. It was found that the offset vortex finder produced a lower cut size than the original vortex finder at 135 degrees while sharpness was maintained. A similar result was also found for individual components using JKMRC Model Development Kit analysis tools. These findings have not fully proved asymmetrical flow pattern effect on semi-inverted hydrocyclone performance but have supported the theory.

Declaration by author

This thesis is composed of my original work, and contains no material previously published or written by another person except where due reference has been made in the text. I have clearly stated the contribution by others to jointly-authored works that I have included in my thesis.

I have clearly stated the contribution of others to my thesis as a whole, including statistical assistance, survey design, data analysis, significant technical procedures, professional editorial advice, and any other original research work used or reported in my thesis. The content of my thesis is the result of work I have carried out since the commencement of my research higher degree candidature and does not include a substantial part of work that has been submitted to qualify for the award of any other degree or diploma in any university or other tertiary institution. I have clearly stated which parts of my thesis, if any, have been submitted to qualify for another award.

I acknowledge that an electronic copy of my thesis must be lodged with the University Library and, subject to the policy and procedures of The University of Queensland, the thesis be made available for research and study in accordance with the Copyright Act 1968 unless a period of embargo has been approved by the Dean of the Graduate School.

I acknowledge that copyright of all material contained in my thesis resides with the copyright holder(s) of that material. Where appropriate I have obtained copyright permission from the copyright holder to reproduce material in this thesis.

Publications during candidature

No publications

Publications included in this thesis

No publications included

Contributions by others to the thesis

Dr. Robert Morrison was responsible for framing the ideas of the project in developing a new classifier into this thesis research.

Dr. Vladimir Jokovic organized several resources accessibility needed in this research such as experimental devices and materials. He also assisted in experimental work, model simulations, and provided MDK analysis results.

Dr. Vladimir Jokovic and Dr. Robert Morrison critically reviewed the structure and content of this thesis. Dr. Robert Morrison helped by reviewing the English.

Dr. Nirmal Weerasekara provided simulation results on CFD regarding the asymmetric particle flow pattern on semi-inverted hydrocyclone. Although the simulation results are not included as part of this thesis, his contribution supported this experiment.

Mr. Michael Kilmartin manufactured the modified hydrocyclone cone, vortex finder with offset, and hydrocyclone "catch box" which are critical to the experimental work of this thesis. Mr. Michael Kilmartin also assisted in adjustments and repairs of experimental devices.

Statement of parts of the thesis submitted to qualify for the award of another degree

None

Acknowledgements

First and foremost, all praise and thanks be to Allah the Almighty, Who has given me everything I need to complete this thesis. There are so many people that have given their contributions and support to me from prior to the commencement until the completion of my research, but I would like to specifically address certain institutions and people:

LPDP, for offering me full financial supports during my whole two years studying in Australia; and Metso Minerals, for their funding support to this research.

Julius Kruttschnitt Mineral Research Centre (JKMRC) and the University of Queensland (UQ), for giving me this special opportunity to learn from the best mineral research centre and one of the top universities in the world. It is an honour and big achievement to me.

Dr. Vladimir Jokovic, my principle supervisor, mainly for his remarkable support, encouragements and patience. He always gives me timely feedback to my writing. He has guided me through the whole research and has helped me more than an ordinary supervisor would do.

Dr. Robert Morrison, my associate supervisor, for his extraordinary support. His guidance has been very purposeful since day one and his valuable advice has been very helpful throughout the research. He was even willing to review the English of this thesis.

Dr. Nirmal Weerasekara, for providing CFD simulation results of semi-inverted hydrocyclone flow pattern, which is very important to this research.

Mr. Michael Kilmartin, for his brilliant work in manufacturing the hydrocyclone cone and vortex finder provided for this experiment. He also assisted on hydrocyclone rig adjustment and device maintenances.

All SMI-JKMRC staff, especially Mrs. Sherrin Brundle, Mrs. Tess Dobinson, Mrs. Jacqueline Ross-Hagebaum, and Dr. Elaine Wightman for their kind assistance on the administration; and Mrs. Karen Holtham for her library support and her unlimited cupcakes.

All JK Jackals past and present members, especially Pascal, Juan Jo, German, Yogesh, Farhad, and Maruf my only muslim brother at JKMRC, for the fun talk together and other good times.

Second to last, I would like to thank my parents and my family. Their endless supports always strengthen me. And lastly but most especially, I would like to send my deepest gratitude to my beloved wife, Icha, who just came to my life in the perfect moment. Please bear with me if I get the chance to take a PhD degree.

Keywords

hydrocyclone, semi-inverted, inclination, cut size, water recovery, efficiency, novel design

Australian and New Zealand Standard Research Classifications (ANZSRC)

ANZSRC code: 091404, Mineral Processing/Beneficiation, 100%

Fields of Research (FoR) Classification

FoR code: 0914, Resources Engineering and Extractive Metallurgy, 100%

Table of Contents

List of Figures

List of Tables

List of Abbreviations

Conc.	: Concentration
cm	: Centimeter
cm^3/s	: Cubic centimeter per second
cP	: Centipoise
F_{80}	: Feed 80% passing size
g/cm^3	: Gram per centimeter cubic
JKMRC	: Julius Kruttschnitt Mineral Research Centre
kg	: Kilogram
kPa	: Kilopascal
LDV	: Laser Doppler Velocimeter
LES	: Large Eddy Simulation
l/min	: litre per minute
MDK	: Model Development Kit
MIM	: Mount Isa Mines
mm	: Millimeter
mN.m	: Millinewton meter
m^3/h	: cubic meter per hour
O/F	: Overflow
Pa	: Pascal
PEPT	: Positron Emission Particle Tracking
P_{70}	: Product 70% passing size
P_{80}	: Product 80% passing size
RSM	: Reynold Stress equation Model
SG	: Specific gravity
TPH	: Tonnage per hour solids

t/m^3	: tonnes per meter cubic
U/F	: Underflow
US gal/min	: US gallon per minute volumetric flow rate

CHAPTER 1 : Introduction

The hydrocyclone is a type of centrifugal separator where water is used as the fluid medium. The term “cyclone” used is in relevant to the shape of the flow patterns within. These patterns resemble the air flows in a cyclonic motion on typhoon – on a smaller scale.

The cyclone separator was firstly used as dust removal system from air. It was Bretney (1891), an inventor from USA, who then patented the hydrocyclone, for use as a water purifier.

Since then, hydrocyclones have been widely used in industry for many decades. Mining industries have been using hydrocyclone in their processing plant since it was introduced commercially as particle classifier in the early 1970’s. Other industries such as chemical plant, coal washing plant, and oil refineries also utilise it.

This wide range application of hydrocyclone is caused by its versatile capability as a multi-phase separator. Hydrocyclone operation can be categorized into several areas of application based on its separation phases (Bradley, 1965), which are:

- solid-solid separator, generally referred to as a classifier in mineral processing plant,
- solid-liquid separator, as is used in cyclone thickener,
- liquid-liquid separator, mainly used in oil refinery,
- gas-solid separator.

It is important to take note that the way to operate hydrocyclone and the preferred performances within these applications can be very different. Thus, in this project, the focus is on the hydrocyclone as a classifying device for use in the comminution circuit of a mineral processing plant. However, there are many other possibilities.

It is mentioned in several textbooks (Bradley, 1965, Svarovsky, 1984, Napier-Munn et al., 1996) that the hydrocyclone provides some advantages as a classifier. The most notable one is that it has a simple design with no moving parts. This means decreased maintenance and low operating costs. The operating cost dominantly comes from power draw for pumping the feed slurry into the hydrocyclone. The maintenance cost mainly consumed by liner erosion inside the hydrocycyclone body or vortex finder and spigot. Also, the hydrocyclone only needs a relatively small area for installation.

Residence time of the slurry inside a cyclone is very short, helping to maintain a high flow of the processing plant throughput. The final overflow product solid percentage can also be customized relatively easily compared with other types of classifier such as spiral or rake classifier so that it will favour the downstream process such as flotation cells or leaching tanks.

Although the hydrocyclone was invented a long time ago, up until today engineers and researchers are still facing problem to get a comprehensive understanding of the complex nature of it, mainly owing to its enclosed body which make it difficult to see what really happen inside. It has become an intriguing challenge to develop and to explore the best setting and design of hydrocyclone in term of efficiency.

1.1 Hydrocyclone Parts and Classification Mechanism

Hydrocyclones in general have more than one design with a very wide range of sizes, but a typical hydrocyclone consists of a cylindrical body attached to a lower conical part, as shown in Figure 1-1. On the cylinder body there is an inlet line which provide a tangential flow for the feed and a vortex finder on the top of it to let the undersize product (overflow) out of the cyclone. Vortex finder is extended into the body of the cyclone into a certain length to prevent short-circuiting of the feed into the overflow. On the bottom, a spigot or an apex is mounted as a stream for the oversize product (underflow).

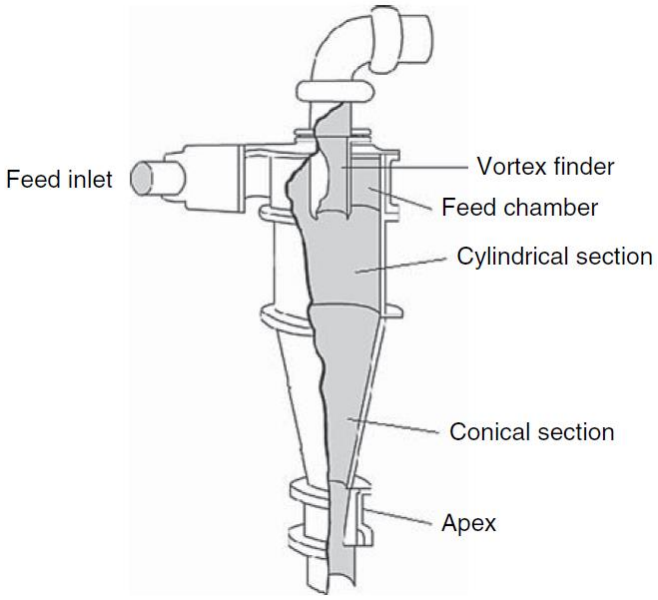

Figure 1-1 : Hydrocyclone parts (after Napier-Munn et al., 1996; Courtesy JKMRC, The University of Queensland)

Generally, industrial scale hydrocyclones are installed in a cluster that consists of several hydrocyclones. To ensure an equal feed distribution, the distribution chamber or feed-chamber is placed in the middle of a cluster. This chamber is surrounded by a number of hydrocyclones which are linked to the chamber through the inlet pipe of each cyclone. Two small sumps are usually set up to collect the products, one for each product stream. The underflow comes out from the each spigot (which is left opened to the atmosphere) and then collected to underflow sump, before commonly being passed back to mill feed stream in a typical milling circuit. On the other hand, each vortex finder is connected to a pipe that ends in the overflow sump to supply downstream process. This pipe is often vented to eliminate siphoning.

Many previous scientists have given a detail description the process mechanisms inside a hydrocyclone (Kelsall, 1953, Rietema, 1961a, Bradley, 1965, Svarovsky, 1984, Cullivan et al., 2004). The slurry is pumped through the tangential inlet pipe. Hydrocyclone is designed so that the structure can provide swirling flow to the pressurized feed entering the cylindrical body. This high speed rotating motion promotes centrifugal force and drag force which triggers relative particles movement in the fluid. The centrifugal force will throw particles outward radial direction closer to the cyclone wall, while drag force draw the solids inward closer to the centre. Figure 1-2 illustrates the flow of the slurry as described.

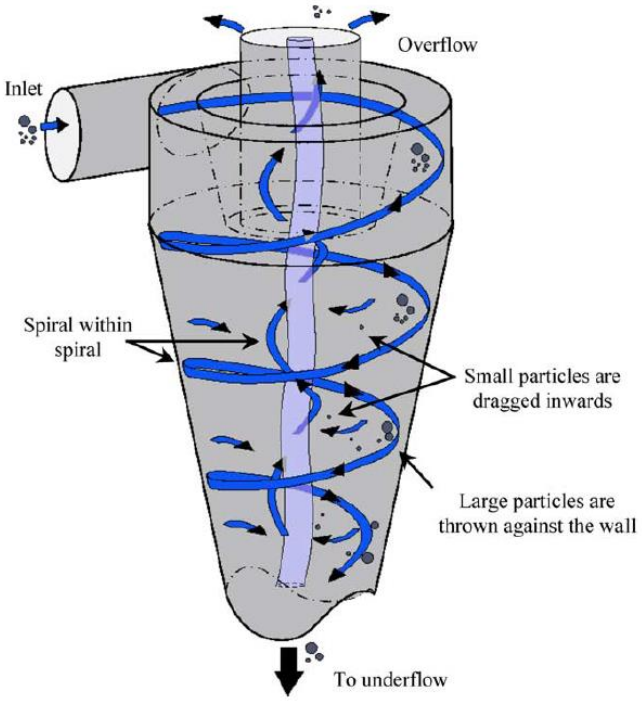

Figure 1-2 : Material flow in a hydrocyclone (Cullivan et al., 2004)

Solid-solid separation occurs because each particle experiences a different resultant of these two contradictory forces. There are several factors that affect the variation of resultant forces. It is mainly dependant on the physical characteristic of the particles such as size, density, and shape, though fluid density and viscosity also have effect on the separation.

As the separation mechanism takes place, the slurry moves to the lower conical part of cyclone body due to gravitational force. The outer portion of slurry flow, containing relatively large and dense particles, is discharged from the bottom through the spigot. The conical part is responsible for creating upward flow on the inner portion of slurry, comprising small and light material, goes out the hydrocylone through the vortex finder.

1.2 Background

One major concern in hydrocyclone operation is classification inefficiency. Hydrocyclone inefficiency is commonly caused by a substantial portion of by-pass fraction, which is a fine fraction of entrained particles that sweep along with water that report to underflow products. An efficient classification happens not only when most of particles separated by mechanism mentioned previously, but also when by-pass fraction is the lowest.

The search for a classifier with better efficiency has been a demanding task, as classification can consume as much as 10% of the comminution energy in a circuit (Musa and Morrison, 2009).

Non-vertical operation of hydrocyclone started to get attention in the late 1980s. Originally, the inclined hydrocyclone was intended to get rid of spigot blockages (Orwe and Noreen, 1988, Johnstone and Rais, 1988, Hochsheid, 1987). Another reported benefit was a substantial reduction of water recovery to underflow which resulted in a reduced circulating load for closed milling circuits. Hence feed tonnage could be increased with the cyclones set to 15 to 20 degrees below the horizontal position sloping downwards towards the coarse product discharge. These researchers also reported significant cost reduction with less pumping power required.

The idea of increasing plant throughput whilst reducing unnecessary high circulating load has made the application of non-vertical hydrocyclone more appealing. More investigations (Asomah, 1996, Rong and Napier-Munn, 2003, Banisi and Deghan-Nayeri, 2005, Vakamalla et al., 2014) were done to get a better understanding of the influence of hydrocyclone inclination on its operation and

performance. The most pronounced differences were an increase in cyclone separation cut size and a reduction of water recovery to underflow, as inclination was increased.

However, only a small quantity of attention was given by those researchers to operate at higher angles more than 90^{o} (Asomah, 1996, Rong and Napier-Munn, 1997). This mode of operation make the conical part to point upwards while in conventional or inclined operation the cone are pointing downwards. In order to better define this particular hydrocyclone operation, a term "semi-inverted" has been coined and is used for the rest of this thesis.

Even though the literature has indicated that semi-inverted operation is an effective way of reducing water recovery to underflow, increasing angles to higher than the horizontal raises several important practical issues.

Operating hydrocyclone at inclination above horizontal seems to have some operation limitations. In Asomah's report (1996), the maximum feed concentration he could achieve with half a meter diameter hydrocyclone at 135 degrees (45 degrees above horizontal) was only 33% solids using limestone. In industrial practice, the hydrocyclone usually operates with 40 – 70% feed solids concentration. Thus, extending the operation range of semi-inverted hydrocyclone is also important.

By turning the cyclone above horizontal position, it seems likely that gravity will pull the majority of unclassified feed slurry through (short-circuiting) through the vortex finder if hydrocyclone is not operating properly. This unwanted condition can be avoided if range of operating parameters such as flowrate and pressure drop at various inclinations can be established and understood.

The effect of gravity on semi-inverted hydrocyclone is also likely to have some influence on structure of flow pattern inside the hydrocyclone body. Vakamalla et al (2014) reported that there was a shift in air core diameter on inclined hydrocyclone below horizontal. It is possible that the impact is not only limited to the air core, but also to the particle orbits which will affect separation. Hence, it is worthwhile to investigate this idea.

1.3 Research Question and Hypotheses

The proportion of fine material which short circuits to the coarse product leads to the following question: “How can a more efficient hydrocyclone be achieved?”. This research is based on four hypotheses:

1. If the range of operation of semi-inverted hydrocyclone can be extended from Asomah’s work (1996), a hydrocyclone with superior performance can be achieved.
2. The effect of mineral specific gravity and shape is well defined in vertical hydrocyclone operation. Semi-inverted operation will not affect hydrocyclone responses to mineral specific gravity and shape.
3. Gravity force will give substantial influence to semi-inverted hydrocyclone performance by initiating asymmetrical flow patterns.
4. The range of operation in semi-inverted hydrocyclone to produce coarse product can be better defined.

1.4 Aims and Objectives

The aim of this work is to study the fundamental behaviour of semi-inverted hydrocyclone. This project can be divided into four specific objectives:

1. To observe the operation of semi-inverted hydrocyclone in terms of water recovery to underflow, size of separation, and separation sharpness.
2. To observe the effects of pressure, feed concentration and density on semi-inverted hydrocyclone.
3. To compare experimental results on semi-inverted with existing hydrocyclone models to investigate applicability of its model parameters.
4. To observe operating condition and limitations as well as to address practical difficulties in operating semi-inverted hydrocyclone.

CHAPTER 2 : Literature Review

2.1 Classification Efficiency

Classification efficiency has a different meaning to efficiency in comminution which is quantified by energy measurement. The term efficiency for a hydrocyclone is used for assessing how well the performance of a hydrocyclone in separating mixture of large and fine material particles. Although in reality density of particle can vary even if they are the same minerals, by convention separation efficiency of hydrocyclone is assessed on the basis of size.

One of the earliest means to quantify hydrocyclone efficiency was proposed by Kelsall (1952, cited in Bradley, 1965). He proposed an efficiency equation per size fraction for "centrifugal efficiency" as:

$$\boldsymbol{E^1 = \frac{G_1/G_0 - H_1/H_0}{1 - H_1/H_0}} \tag{2.1}$$

with G_0 and G_1 represent the solid flow in feed and underflow respectively, and H_0 and H_1 represent water flow in feed and underflow respectively. G_1/G_0 is defined as gross efficiency.

In reality, feed slurry does not enter hydrocyclone fraction by fraction. It always has a size distribution. As a result, the efficiency value will be in a function of size. Usually, the curve is asymptotic to fine and coarse size, generally accepted as a result of short circuit and bypass flows. Schubert and Neesse (1980, cited in Dueck et al., 2014) hypothesised that the superposition of turbulence and settling flow generate on S-shaped curve. Plitt and Kawatra (1979) additionally gave an illustration of misplacing behaviour, mentioning that there were coarse particles in finer product and, conversely, fines in underflow stream (Figure 2-1).

Kelsall (1953) then proposed a way to present classification performance by using graphical illustration, which is now widely known as the efficiency curve. This is analogous to the "partition"curve long used in gravity separators. The classification curve is produced by plotting the calculation data of feed fractions (F_i) that go to underflow fraction (U_i) for each size fraction (i). This can be put into a simple equation:

$$\boldsymbol{Y_i = \frac{U_i}{F_i} x\ 100\%} \tag{2.2}$$

where Y_i is the feed to underflow percentage.

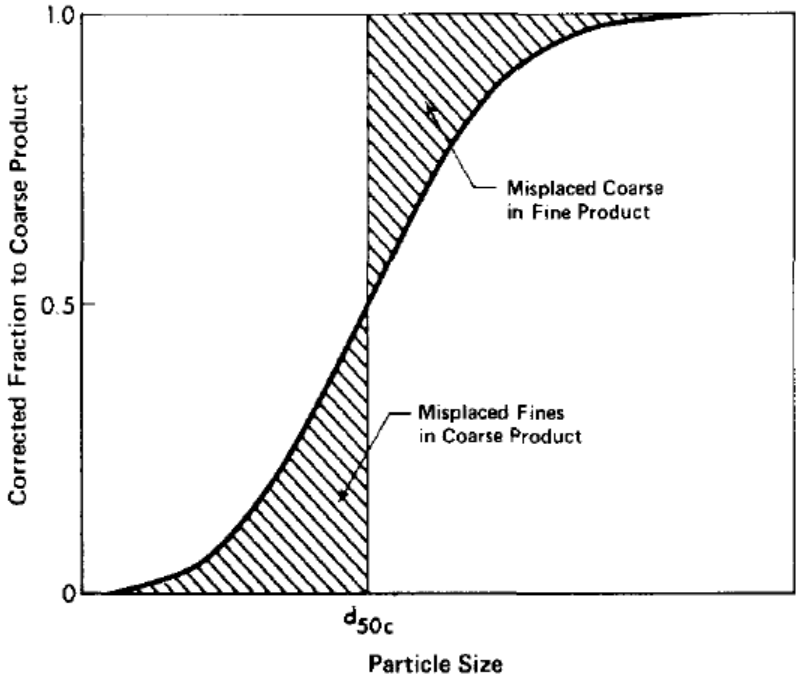

Figure 2-1: Misplaced particles shown in efficiency curve (after Plitt and Kawatra, 1979).

As mentioned in the previous section, a small portion of feed particles will inevitably become by-passing material that is entrapped in the underflow stream. These particles are exempted from the classification process. Accordingly, the efficiency curve is shifted from its true classification value. Furthermore, the efficiency value could not reach zero when there is no particles reporting to underflow. To diminish the effect of by-pass material, we can apply the following equation:

$$\boldsymbol{Y_i' = \frac{(Y_i - R_f)}{(1 - R_f)}} \tag{2.3}$$

where R_f symbolise the fraction of feed water recovered in the underflow stream in percentage units, widely known as the water recovery. The amount of by-passing material is believed to have the same ratio as the water. This theory was originally proposed by Kelsall in his report (1953). By this deduction, the unclassified particles flow fraction can be eliminated from the actual curves conceptually. Another way to normalise the curve is proposed by Nageswararao (1999). He argued the value of efficiency at zero size particles should not necessarily be zero, and the curve can be normalized in many possible forms.

To compare the performance between one curve and the other easily, the middle value of d_{50} is generally used. Dahlstrom (1949, cited in Kelsall, 1953) introduced d_{50} as the size of particles in micron that has equal chances to report to the overflow or the underflow. D_{50}, or widely known as cut size or cut point, and its corrected value, d_{50c} ,can be determined from the corrected efficiency curve (Figure 2-2) or from the mathematical model which will be presented on the next section.

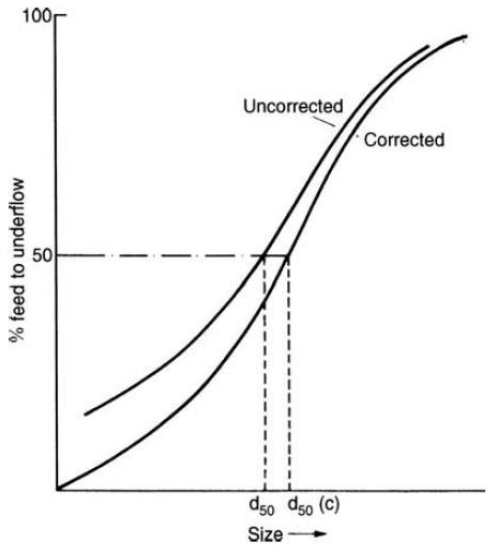

Figure 2-2: Actual and corrected curve and cut size (after Wills, 2006).

Besides separation cut size, another feature of the graph that can be used to assess classification performance is separation sharpness. A sharpness parameter, α (alpha), is Rosin-Ramler type parameter that is generated from Whiten's exponential sum equation (Napier-Munn et al., 1996). This parameter is expressed by equation 2.4:

$$\boldsymbol{E_{oa} = R_f \left(\frac{e^{\alpha} - 1}{e^{\alpha x} + e^{\alpha} - 2} \right)} \tag{2.4}$$

Where E_{oa} is the efficiency curve to overflow and x is the reduced size, d/d_{50c}. Higher values of α indicate a better separation, with $\alpha > 4$ is said to be a very sharp separation.

2.2 Flow Patterns inside a Hydrocyclone

It has been explained that the separation process in a hydrocyclone comes from the different resultant of forces that work on particles in a rotating water medium. However, this description simplifies the actual complicated mechanism. To get a better understanding of the operation of this apparatus, it is important to have a fundamental idea of flow pattern within a hydrocyclone.

As described previously, slurry is injected to the hydrocyclone conical top body from inlet pipe to give a tangential velocity. To provide this motion, conventional tangential inlet type and involute inlet type design have been widely adapted to the inlet of the hydrocyclone body. Studies in investigating other inlet methods such as axial inlet (Yalcin et al., 2003, Zhen-bo et al., 2011) have also been carried out but have not been commercialized on hydrocyclone in mineral industries.

The major feature of separation process inside a hydrocyclone is the directional change of inner part of the rotating slurry towards the top outlet (vortex finder). This flow pattern can be observed in three dimensions component: tangential velocity, vertical velocity, and radial velocity.

2.2.1 Tangential, Axial, and Radial Velocity

Bradley (1965) mentioned tangential velocity as the most significant velocity on a hydrocyclone flow. He started with the very basic concept of angular momentum conservation of a single phase system. A free-vortex condition was selected, with the following relation:

$$\boldsymbol{v\, r^n = constant} \tag{2.5}$$

where *n* value normally varies from 0.5 to 1. This relation remains true in solid body rotation case in which tangential velocity, *v*, value can approach infinity when radius of the particle from the centre, *r*, is zero. However in actual practice of hydrocyclone, the velocity will begin to drop in a certain radius before moving further towards the centre.

It was Kelsall (1952, cited in Bradley, 1965, Bergström and Vomhoff, 2007) who firstly did the experimental study on determining the behaviour of tangential velocity. In his work, he used the microscope tracking method to illustrate the detailed tangential velocity profiles within a cyclone (Figure 2-3). From the figure we can see tangential velocity increased as the particle move closer to the air core, but there was a turning point at radius of 0.2 inch where the tangential velocity starts to drop significantly. This point, located at ~$D_c/8$ from the centre, separated the region which behaves similarly as free-vortex in the outer part with the forced-vortex region which located in the inner part.

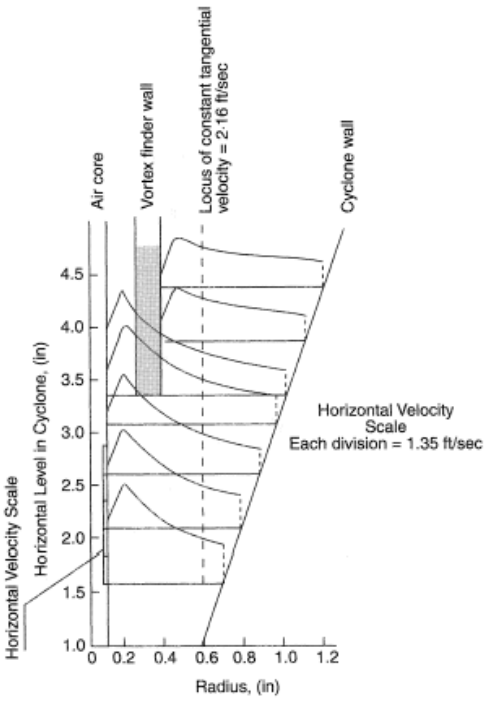

Figure 2-3: Profile of tangential velocity distribution (after Kelsall, 1952 cited in Bradley, 1965)

Knowles (1973) also did an observation on hydrocyclone tangential velocity field but with the absence of air core. The study was done by using anisole ($CH_3OC_6H_5$) with specific gravity 0.99327 as tracer particle with the help of cine photography. With the cyclone body diameter of 7.5cm, the same with Kelsall's size, and similar operating Reynolds number, he recorded 55 tracer positions in the cyclone. There were extracted into tangential velocity profiles. The patterns, in fact, show similar trends with Kelsall's flow field profile, even though it was operated without an air-core. However, the correcting factor, *n*, has a different range from 0.12 to 0.33. He deduced the huge gap came from the insufficiency of Reynolds number to form free-vortex flow.

While Kelsall and Bradley approaches are fully empirical. A theoretical approach by applying Navier-Stokes equation was used by Rietema (1961a). He used the theoretical derivation of hydrodynamic of fluid flow behaviour to predict the tangential velocity profile inside a hydrocyclone. The simplification of the derivation is as followed. The derivation was started with the following motion equation:

$$U\frac{\partial V}{\partial r}+W\frac{\partial V}{\partial z}+\frac{UV}{r}=(\nu+\epsilon)\left\{\frac{1}{r}\frac{\partial}{\partial r}\left(r\frac{\partial V}{\partial r}\right)+\frac{\partial^2 V}{\partial z^2}-\frac{V}{r^2}\right\} \tag{2.6}$$

With an assumption *z* was independent from *V*, which was proven previously by Kelsall's experiment, then the equation could be simplified as:

$$-\frac{\boldsymbol{U}}{\boldsymbol{r}}\frac{\boldsymbol{dVr}}{\boldsymbol{dr}}+(\boldsymbol{v}+\boldsymbol{\epsilon})\left\{\frac{\boldsymbol{d}}{\boldsymbol{dr}}\frac{\boldsymbol{1}}{\boldsymbol{r}}\frac{\boldsymbol{Vr}}{\boldsymbol{dr}}\right\}=\boldsymbol{0} \tag{2.7}$$

Also justified by Kelsall (Kelsall, 1952 cited in Bradley, 1965), it could be assumed that cyclone radial velocity was constant within the hydrocyclone, Rietema (1961a) modified the final relationship became:

$$\boldsymbol{\phi}=\boldsymbol{C_2}-\boldsymbol{C_1}\,\boldsymbol{exp}(-\boldsymbol{\lambda\sigma})\left(\frac{\boldsymbol{\sigma}}{\boldsymbol{\lambda}}+\frac{\boldsymbol{1}}{\boldsymbol{\lambda^2}}\right) \tag{2.8}$$

where C_1 and C_2 were functions of Rietema parameters λ and σ, with λ is dimensionless parameter for tangential velocity profile and σ is ratio of particle distance to radius of hydrocyclone. At $\sigma = 1$ for different values of λ, Rietema considered a value of at least 10 would be fit with Kelsall's tangential velocity distribution profile.

Bergström and Vomhoff (2004) tried to measure tangential velocity of particle loaded fluid. The result showed that pulp suspension would smooth the transition point between free-vortex region and forced vortex region.

Investigation on vertical velocity profile inside a hydrocyclone was done by Kelsall (1952, cited in Bradley, 1965) and Bradley (1965). They discovered an upward velocity profile around the air-core centre and downward velocity profile near the hydrocyclone wall. A short-circuit flow was also indicated from Kelsall's data. Despite high fluctuation on the data, Bradley concluded the locus line was appeared and divided into the cylindrical part (the mantle) and the conical form. In the radial direction, he also found that velocity is reduced as the particle radius from the centre decreases.

More recent works using Computational Fluid Dynamics (CFD) and Laser Doppler Velocimeter (LDV) have confirmed these flow patterns (Brennan, 2006, Rajamani, 1987). More recently still, Positron Emission Particle Tracking (PEPT) method has been used to follow activated particle in a hydrocyclone (Chang et al., 2011, Collins, 2016).

2.2.2 Short circuiting flow

The phenomena of short-circuit inside a hydrocyclone seems to be unavoidable. It is generally believed that this particular flow hugely impacts the classification performance of hydrocyclone. Short circuit flow passes unclassified input material directly to overflow product.

One of the earliest report on short-circuit came from Kelsall (1952, cited in Bradley, 1965). While studying the axial pattern of the flow within the hydrocyclone, he reported an unusual downward flow near the vortex finder wall, which he called as short circuit flow.

Bradley (1965) argued that this particular flow was caused by the "obstruction from vortex finder wall friction. The pressure difference assists a proportion of feed material to flow through the cyclone roof, move down along the vortex finder wall and join the main upward overflow." From his experimental work, he found that around 15% of feeds experience this short-circuit mechanism. Similar result was also reported Lynch (1974). Further, he reported that the most critical variable that could initiate short-circuiting is vortex finder diameter. A smaller diameter vortex finder might improve efficiency at coarse end, but only to a certain limit before it collapsed due to the appearance of short circuit flow.

Another unwelcome flow called "by-pass" flow was firstly discussed by Kelsall (1960, cited in Kelly, 1991). Kelsall argued that classification curve did not reach zero as the particle size got finer. He said then that there was a possibility of a proportion of small particles were not subjected to classification and carried away by water to the underflow instead. This particle entrainment phenomena was modelled by Finch (1983) as a function of particle size. However, Kelly (1991) stated that the previous thought on the likelihood of constant by-pass portion for all characteristic value of particle was very unlikely.

Another type for short-circuit, termed as "leakage", was introduced by Milin et al (1992). He investigated leakage phenomena from both experimental result and theoretical approach. From his experiment he identified a secondary flow. Secondary flow is a fraction of classified coarse stream that is forced to flow upward because the spigot is unable to accommodate the whole coarse stream. He concluded that this mechanism was dependent on spigot size, and hence spigot size is the limiting factor for solid amount in the fluid.

2.2.3 Air Core

A typical hydrocyclone operates with the appearance of an air core. The qualitative explanation of formation of air core has been proposed by several researchers (Dyakowski and Williams, 1993, Dyakowski and Williams, 1995, Concha et al., 1996, Gupta et al., 2008, Hararah et al., 2010). The highly pressurized slurry rotates inside the body and approaches the spigot. A low pressure area along the axis is created due to high angular momentum of the slurry near the centre. The spigot, which is opened to the atmosphere, inhales the air and develops the air core. Hence, the air-liquid surface has the same pressure with the atmosphere. Cullivan (2004) argued this common understanding by suggested the air core formation was transport driven instead of pressure driven. Computational prediction by Narasimha (2006) also supported this argument. Neesse and Dueck (2007) proposed another theory that air core could be formed not only from penetrated air from spigot, but also from dispersed or diluted air on feed inlet.

It was Barrientos et al. (1993, cited in Concha et al., 1996) who firstly developed air core model to predict the diameter of the core for water-only operating hydrocyclone. The proposed equation for the air core diameter is:

$$\boldsymbol{d_a = \frac{2\,\sigma_{gl}}{2\,\mu_l\,\alpha_i - \Delta p_a}} \tag{2.9}$$

where σ is surface tension of gas-liquid, μ is liquid viscocity, α is normal component of liquid radial velocity gradient at the interface, and Δp_a is pressure drop.

Concha et al. (1996) then developed the model into:

$$\boldsymbol{d_a = \frac{3.03\,\sigma\,D_o}{270.3\,\mu\left(1+\frac{1.18x10^{15}}{\Delta p^{2.61}}\right)\left(\frac{D_u}{D_o}\right)^{-0.20} - 1.38x10^{-3}}} \tag{2.10}$$

with Δp_a and α were assumed as empirical function of external pressure drop an geometrical ratio. Again, this equation was exclusive for water only operation.

Computational approaches in predicting air core diameter have been done by several researchers. Dyakowski and Williams (1995) produced air core profile by solving fluid motion equations for axisymmetric flow. Narasimha et al., (2006) applied Large Eddy Simulation (LES) turbulence model to get a better prediction on air core diameter compare to Reynold Stress Equation Model (RSM).

Air core can affect classification performance from its strong correlation with underflow discharge. Roping discharge is an unwanted physical phenomenon occurred on the underflow discharge due to hydrocyclone overcapacity, marked by thick stream lacking of rotational motion coming out from spigot. Spray discharge, on the other hand, is the preferable operating condition.

Concha et al. (1996) established his ideal criteria for spigot/vortex finder ratio (D_u/D_o) regarding roping or spray condition by acknowledging works from Plitt et al. (1987, cited in Concha et al., 1996) and Bustamante (1991, cited in Concha et al., 1996). He argued that the ratio that allows to give spray discharge has value of $D_u/D_o > 0.56$, while $0.56 > D_u/D_o > 0.45$ will produce either spraying to roping depending on operating variable, and D_u/D_o less than 0.45 will always result in roping discharge.

2.3 Qualitative Effect of Variables

To meet its potential of being an optimal classifier unit, an operation of hydrocyclones comprises a wide range of variables. Lilge (1962) mentioned there have been seventeen variables investigated which could affect classification performance of this piece of equipment. Each variable has its own influence and some of them have correlation with each other to add the complexity of hydrocyclones operation.

2.3.1 Vortex Finder and Spigot

Changing the overflow orifices (vortex finder) diameter seems to be more relevant in terms of operation optimisation, but it needs some consideration in design. Bradley (1965) pointed out that there was an optimum range for overflow diameter based on work by Kelsall (1953). He argued that the limit of vortex finder should not be smaller than 1/8 of hydrocyclone diameter, the point where the maximum tangential velocity is located at. This is to prevent coarse particles being an overflow stream due to short circuit flow. On one point, we would want the radius of vortex finder be as small as possible to give the opportunity for particles that are carried away by short circuit flow to re-enter the separation zone. On the opposite end, the diameter should not be larger than the radius of locus of zero vertical velocity, which is estimated at $D_c/2.3$. Therefore, theoretically $D_c/8$ to $D_c/2.3$ could be the optimum range for vortex finder diameter, and $D_c/7$ had been favoured by Bradley as the most effective overflow diameter.

Vortex finder length could also affect classification efficiency. Kelsall (1953) demonstrated that decreasing vortex finder length to a certain point would result in maximum efficiency of fine particles classification at the expense coarse particles separation impairment.

Compared with the vortex finder, customising the spigot is less problematic. Hydrocyclone manufacturers nowadays have adopted some ways for plant technicians to easily change the spigot. It is very common for a processing plant which is operating hydrocyclones to have sets of spigots of various sizes.

2.3.2 Pressure, Feed Concentration, Solids Density, and Slurry Viscosity

It has been explained how hydrocyclone design can affect hydrocyclone separation performance. However, operation of hydrocyclone is also very contingent on some operational variables. Likewise, most of these variables are correlated with each other. Some of variables have been introduced in the previous section about efficiency.

Several scientists (Kelsall, 1953, Yoshioka and Hotta, 1955, Rietema, 1961b, Bradley, 1965) have discussed the main influence of feed flow, pressure drop, feed solid concentration, solid and liquid density on hydrocyclone performance and will be summarized as follows.

A rise in feed flow rate will decrease cut size and increase the efficiency by increasing water split to overflow. Pressure drop will also be increased at higher flow rates. If the amount of feed reporting to underflow is above 10%, the capacity will also rise slightly as the amount of feed reporting to underflow will increase.

Feed pressure gives a negative correlation with cut size. Increasing feed pressure will lead to reduced cut size. It should be noted that in practice the pressure drop is basically applied instead of feed pressure, because feed pressure is less significant if there is any remaining pressure on the outlet. It is important to make sure that the hydrocyclone products exit into atmospheric pressure, so the application of feed inlet pressure becomes relevant.

The solids concentration of feed has a more complex influence on separation performance. A high concentration of solid in feed will cause a higher underflow which is susceptible to overloading or roping condition. The rotating movement of the slurry will also be interfered by a high solids concentration, so a higher pressure drop will be needed to achieve the same tangential velocity. Accordingly, the capacity can be increased slightly but can lead to overloaded underflow.

Solids density has a significant influence on separation efficiency. In investigating density effect, it is generally presented in the form of solid and medium liquid density difference. According to Stokes' Law, denser minerals will undergo a weaker separation, hence a lower cut size. The effect

is even more significant (with higher power factor) in larger diameter hydrocyclones. Mixture of solids in slurry affects the slurry density, hence it also influence the separation.

Slurry viscosity in previous time was difficult to be measured in industrial practice. Approaches to estimate viscosity effect were done from measurement of liquid medium viscosity or inferred from solid concentration. Since on-line viscometers have been invented, a few studies (Kawatra et al., 1996b, Kawatra et al., 1996a) showed that slurry viscosity is not only solid percentage and liquid medium dependant, but also affected by temperature of slurry. He suggested that as viscosity goes up, separation size will be higher. In his proposed cut size model, the power factor of viscosity is 0.35 (Kawatra et al., 1996a). Another finding from his experiment is that viscosity is not significant to separation sharpness but slightly affect water recovery.

2.4 Effect of Inclination on Hydrocyclone

When the hydrocyclone was initially invented by Bretney (1891), the concept of separation (purification) process was employing centrifugal force while influence of gravitational force was excluded. With this idea in mind, there was no orientation limitation in constructing hydrocyclone whether it vertical, horizontal, inclined downwards, inclined upwards, or even upside down. Processing plants were had been installing hydrocyclones orientation to adapt to their own operational practical needs, for instance sampling condition or limitation of construction area.

The consideration of evaluating orientation is initially driven by the need for self-draining of hydrocyclone. When a hydrocyclone is to be stopped, whether for plant maintenance or unit reparation, it will need to allow self-acting drain in order to prevent fractions of slurry deposit inside hydrocyclone body and change the inside dimension of the cyclone, affecting its overall performance. According to Svarovsky (1984), a small angle of minimal 5^{o} from the lowest line down to horizontal line is enough to provide automatic draining.

It was generally believed that gravity had to have some effects on hydrocyclone operation, especially on large diameter ones, since particles entrapped in short-circuit flow (section 2.2.3) will decline. However, there was no thorough examination of this effect, until in the late 1980's several investigations of horizontally installed hydrocyclones being published simultaneously (Hochsheid, 1987, Orwe and Noreen, 1988, Johnstone and Rais, 1988).

Hochscheid (1987) from Krebs Engineer reported the improvement that he identified from installing horizontal hydrocyclone on three processing plants. The first investigation was conducted in Brazil in 1973. The 660 mm diameters Krebs hydrocyclone was run in a closed circuit with a rod mill,

processing apatite ores. The plant was having difficulties in working at high (62.4%) solid concentration slurry in order to maintain coarse overflow product of 12% coarser than 300μm. By changing the orientation from vertical to horizontal, it was hoped that overflow size could be higher without sacrificing the underflow become too dilute due to water addition. From a total of three tests, he concluded that circulating load can be significantly minimized with horizontal hydrocyclone operation. Therefore, higher feed tonnage was also shown, increased from 64 ton per hour in average up to 80.7 ton per hour, with the same pressure drop.

The second investigation was in 1981 (Hochsheid, 1987) at a lithium ore processing plant in North Carolina. Operating very high circulating load of 670% and relatively high feed solid concentration of 65%, spigot plugging was similarly occurred. Based on previous success in the Brazilian plant, the same idea was implemented. He concluded from the four tests that circulating load could be reduced substantially by setting the hydrocyclone parallel to horizon because the amount of water transporting a fraction of fine particles to coarse stream was lower, in response to less gravitational influence. However, no improvement on plant throughput was reported.

The similar outputs also gained from the last observation which was reported from a galena and sphalerite concentrator in Missouri (Hochsheid, 1987). Once again, spigot blockage of the hydrocyclones had become the issue since the grinding mill aimed to a coarse product with more than 50% finer than 75 micron. By installing the hydrocyclone horizontally, circulating load decreased followed by a slight raise in total throughput. Around a five per cent decrease on fine-end size fraction and ten per cent increase on coarse-end size fraction was also noticed on the underflow products, indicating sharper separation.

All of those three observations by Hochseid (1987) confirmed that installation of a horizontal hydrocyclone was beneficial for overall closed circuit performance, i.e. increasing of plant capacity and lowering circulating load. In the second and third reports, it was also mentioned the availability of application of larger diameter spigot with this new orientation arrangement, resulting in the elimination of the worrisome spigot plugging.

Orwe and Noreen (1988) published a comparison test work of horizontal hydrocyclone at Bougainville Copper Limited, Papua New Guinea. An arrangement in a cluster of 4-762 mm diameter hydrocyclones, closing on the primary ball mill, was done so they could be inclined 10-20 degrees less from horizontal. Variation of spigot and vortex finder combination was also performed. From the tests, it could be confirmed that applying horizontal orientation can give valuable

reductions of circulating load percentage as much as 30% compared with the standard vertical operation. With less circulating loads, upward trends on fresh feed tonnage were followed. Additionally, lower operating cost was also recorded due to less pump power required. With regard to classification efficiency, it was found that separation cut size decrease as the hydrocyclones put into horizontal. However, there was an inconsistency on classification sharpness.

In Indonesia, Johnstone and Rais (1988) investigated a two-year performance of two clusters of newly installed Krebs hydrocyclones which were inclined 45^{o}. The chalcopyrite ores for the clusters feed came from crusher circuit undersize product and from a considerable amount of 400% circulating load of the primary mills. Once again, the results showed a cutback of circulating load down to half, and consequently an increment of 10% of the circuit capacity was appraised from each mill circuit. The result also mentioned a small reduction of coarse particles on overflow products, which was then explicitly confirmed by putting more pressure.

Several years later, Asomah and Napier-Munn (1997) put angle of inclination as one of hydrocyclone operational variable and proposed the first ever model incorporating inclination. The observations on a 51 mm Mozley hydrocyclone and a 102 mm diameter Krebs hydrocyclone were done at the JKMRC facility and the second one on a larger 508 mm diameter Krebs hydrocyclone was conducted at the Mount Isa Mines.

In his thesis (Asomah, 1996), Asomah concluded that inclining hydrocyclone more than 45^{o} could give a substantial improvement on performance, marked by the water recovery reduction and increased underflow solids concentration, most notably on the larger diameter hydrocyclone. Cut size was also increased with inclination. It was found that feed solid concentration can substantially affect performance of inclined hydrocyclone. However, sharpness of separation seemed to be unaffected on larger hydrocylone.

By using 51 mm and 102 mm hydrocyclone, he managed to work at 135 inclinations using up to 60% solids concentration of limestone, while on larger hydrocyclone the feed concentrations were only 22% – 33% solids. This is an indication of operation limitation in Asomah's work with larger diameter hydrocyclone of not capable with higher solids concentration at 135 degrees. In addition, the experiment was performed at single pressure point.

Rong and Napier-Munn (2003) observed the influence of inclination on hydrocyclone performance using coal slurry. Observation of various angle inclinations from 0 to 180 degrees position with 30 degrees interval was conducted on 200 mm diameter hydrocyclone. Their work showed rather different response on separation sharpness, given in Table 2-1, compare with Asomah work (1996).

It was found that separation sharpness could be affected positively by increasing the degree of inclination below horizontal position, whereas semi-inverted positions would give deleterious influence on the sharpness of separation. It is interesting that varying inclination below horizontal position only affected separation size to a small degree.

Table 2-1 : The effect of inclination on several key performance parameters by Rong and Napier-Munn (2003)

Test no.	Angle of cyclone inclination (degree)	α	Flow ratio Rf	d_{50c} (mm)	Feed flowrate (tph)	% solids in U/F
JKCC - 1	0	4.837	22.18	0.053	26.96	47.0
JKCC - 2	30	4.565	18.89	0.050	26.37	50.5
JKCC - 3	60	5.621	16.34	0.053	26.32	54.3
JKCC - 4	90	8.418	12.74	0.054	24.97	59.4
JKCC - 5	120	3.710	12.58	0.077	26.00	63.7
JKCC - 6	150	3.014	12.04	0.095	24.59	62.2
JKCC - 7	180	3.212	13.38	0.092	25.41	62.4

Rong and Napier-Munn did not report any similar difficulty with Asomah's in executing hydrocyclone at semi-inverted positions. The reason might be because they applied diluted concentration feed, although such information was not found in the report. Another possible cause might be due to different characteristic of coal slurry.

Banisi and Deghan-Nayeri (2005) reported a significant 24.5% increase of cut size by varying angle of inclination and percentage of solid of feed. A rather small Krebs hydrocyclone with diameter of 75 mm was operated in various angles from 0 to 90^{o}, fed by copper bearing ores with P_{70} 75 micron at constantly low pressure drop. Even though it has been confirmed that the cut size arise as inclination increase, the trend was only shown at degree above 45^{o}. Additionally, recovery of feed water to underflow did reduce as inclination went up, but it was only shown by degree more than 67.5^{o}.

The most recent publication discussing hydrocyclone orientation was published by Vakamalla et al. (2014). Working with a silica feed input, he varied the slurry solid concentration and spigot diameter at several angles from 0 to 60 degrees on a 75mm hydrocyclone to see the influence of inclination on separation performance parameters such as water recovery to underflow, underflow solid percentage, cut size and sharpness of separation.

From his work, Vakamalla found that inclination gave reduction effect on amount of water recovered in the underflow. For lesser concentration slurry of 28.76% solid concentration, the trend was only shown when inclination above 45 degrees. Underflow solid percentages were increased beyond 45 degrees. The separation size increased with feed solid concentration, but showed unclear trend under the influence of inclination.

To conclude, while effects of inclination on hydrocyclone performance have been investigated by all these authors, only two previous projects have incorporated a high angle of inclination as a variable (Rong and Napier-Munn, 2003, Asomah, 1996) as their attention was on inclinations between vertical and horizontal. Asomah did not perform at feed concentration higher than 33% solids at 135 degrees, whereas Rong did not specify the concentration of the coal slurry he used. The effect of pressure has not been investigated in either project. The gaps between these studies imply hydrocyclone at semi-inverted positions needs further investigation due to limitation of data and different types of ores.

2.5 Hydrocyclone Empirical Models

Initially, hydrocyclone performance was quantified by the cut size value. Hence, the earlier models predicted the value of separation size which is efficiency curve related. From an efficiency point of view, water recovery and throughput-pressure drop relation are as important as separation size. Water recovery to underflow, as mentioned in the previous section, is one of the factor that affecting separation efficiency. It refers to its capability in bypassing fraction of particles out of hydrocyclone underflow without classified first.

2.5.1 Separation Size Models

Empirical models of hydrocyclone to predict hydrocyclone cut point have been proposed by some authors (Yoshioka and Hotta, 1955, Bradley, 1965, Rietema, 1961c, Lynch et al., 1975). Several older models like from Dahlstrom (1949 and 1954), Haas (1957), Matschke and Dahlstrom (1959). are reviewed by Bradley (1965) in his textbook.

Dahlstrom (1949, cited in Bradley, 1965) worked with different hydrocyclone diameter of smaller than 40 mm to produce the following cut size model:

$$d_{50} = \frac{87.2\,(D_o D_i)^{0.65}}{Q^{0.60}} \left(\frac{1}{\rho_s - \rho_l}\right)^{0.5} \tag{2.11}$$

where D_o and D_i are in inches, Q is in US gal/min, ρ_s and ρ_l are in g/cm^3. This equation is only valid to small diameter hydrocyclone with 10^o cone angle.

Yoshioka and Hotta (1955), working with 6 inches, 20^o cone angle hydrocyclone, proposed the following function from the obtained flow pattern from their experiment:

$$\boldsymbol{d_{50} = 6.3\, x10^{6} \left(\frac{\mu_{sl}}{\rho_s - \rho_l}\right)^{0.5} \frac{D_c^{0.1}\, D_i^{0.6}\, D_o^{0.8}}{Q^{0.5}}} \tag{2.12}$$

Haas (1957, cited in Bradley, 1965) worked with small diameter hydrocyclone to address the issue on the previous equation. He introduced fluid factor, $H^{0.5}$, and proposed a developed form of Yoshioka and Hotta formula into:

$$\boldsymbol{d_{50} = 5\, x\, 10^{3} \left(\frac{D_c\, \mu_{sl}}{H^{0.5}\, (\rho_s - \rho_l)}\right)^{0.5}} \tag{2.13}$$

All those earlier models above derived from the theoretical concept of balance between centrifugal and drag force, or equilibrium orbit theory, combined with empirical data. Bradley (1965) simplified those equations into a general form:

$$\boldsymbol{d_{50} = k \left[\frac{D_c^3\, \mu_{sl}}{Q\, (\rho_s - \rho_l)}\right]^{0.5}} \tag{2.14}$$

where Dc = Hydrocyclone diameter, in cm

Q = Feed flow rate, in cm3/s

μ_{sl} = slurry viscosity, in cP

ρ_s = solid density, in g/cm3

ρ_l = liquid density, in g/cm3

k = dimensional constant.

However, this equation is not widely used to apply in practice, mainly because of uncommon equilibrium orbit concept, usage of dilute slurries, and correction of bypassing fraction were not involved.

A model proposed by Lynch et al. (1975, cited in Rao et al., 1976) was used for scale-up purpose. The equation was derived from their previous work on 10.2, 15.2, 25.4, and 38.1cm Krebs hydrocyclones processing various feed size distributions. The equation is in the logarithmic form:

$$log_{10} d_{50c} = 0.0637 D_o - 0.0712 D_u + 0.0220 D_i + 0.0390 C_w - 0.0002 Q - 0.481 \quad (2.15)$$

where C_w = ratio of solid in feed slurry

D_o = overflow orifice inside diameter, in cm

D_u = underflow orifice inside diameter, in cm

D_i = inlet orifice inside diameter, in cm

Q = feed flow rate, in l/min

although the model was applied extensively by industries for a while, it was reported that the prediction results were not satisfying (Coelho and Medronho, 1992). Since the model is empirically derived within a certain range of conditions where it was developed, hence it is not recommended to use this model for a significantly different hydrocyclone geometry.

Plitt (1976) proposed a multi-purposed models that were developed by computational linear regression method using various design and operational variables. The model for cut separation is given by:

$$d_{50c} = \frac{50.5 D_c^{0.46} D_o^{1.21} D_i^{0.6} e^{0.063\phi}}{D_u^{0.71} h^{0.38} Q^{0.45} (\rho_s - \rho_l)^{0.5}} \quad (2.16)$$

and complemented by sharpness separation model as followed:

$$\alpha + 0.47 = 2.99 exp(-1.58 R_v)[D_c^2 H/Q]^{0.15} \quad (2.17)$$

where d_{50c} = separation size/cut-size, in μm

D_c = hydrocyclone diameter measured on the bottom vortex finder, in cm

D_o = inside diameter of vortex finder, in cm

D_i = inside diameter of inlet pipe, in cm

D_u = inside diameter of spigot, in cm

ϕ = volumetric solid fraction in solid, in %

h = free vortex height (distance between vortex finder bottom and spigot), in cm

ρ_s = solid density, in g/cm^3

ρ_l = liquid density, in g/cm^3

α = separation sharpness from Whiten efficiency curve parameter

R_v = feed volumetric recovery to underflow, in %

H = distance between spigot and vortex finder

Q = feed flow rate, in l/min.

The Plitt equation has been widely used in predicting separation size. In consequence, it has also been modified and corrected by other researchers to be a more accurate model (Coelho and Medronho, 1992, Nageswararao et al., 2004, Gupta and Yan, 2006, Andre Carlos Silva, 2012).

Nageswararao introduced his model in his thesis at the JKMRC (Nageswararao, 1978), then he developed it into a better predictive model (Nageswararao et al., 2004). By using data sets from his work on Krebs hydrocyclone using limestone suspended slurry, combined with database obtained from Lynch and Rao (Lynch and Rao, 1975), he produced the following dimensionless empirical model:

$$\frac{\boldsymbol{d_{50c}}}{\boldsymbol{D_c}} = \boldsymbol{K_{Do}}\, \boldsymbol{D_c^{-0.65}} \left(\frac{\boldsymbol{D_o}}{\boldsymbol{D_c}}\right)^{\boldsymbol{0.52}} \left(\frac{\boldsymbol{D_u}}{\boldsymbol{D_c}}\right)^{\boldsymbol{-0.5}} \left(\frac{\boldsymbol{D_i}}{\boldsymbol{D_c}}\right)^{\boldsymbol{0.2}} \left(\frac{\boldsymbol{L_c}}{\boldsymbol{D_c}}\right)^{\boldsymbol{0.2}} \left(\frac{\boldsymbol{P}}{\boldsymbol{\rho_p g D_c}}\right)^{\boldsymbol{-0.22}} \boldsymbol{\theta^{-0.24}} \boldsymbol{\lambda^{0.93}} \qquad (2.18)$$

with D_c ,D_o, D_u, and D_i are in meter, d_{50c} in micron, and

L_c = cylinder height, in m

θ = cone angle, in degrees

P = inlet feed pressure, in kPa

ρ_p = feed slurry density, in ton/m^3

g = gravity acceleration, 9.81 m/s^2

λ = hindered settling factor, with $\lambda = \phi/(1-\phi)^3$

Even though Nagesawarao model was successful enough in industrial application either on plant optimisation or on design scale-up, there is a limitation on fitting the model constant, K_{D0}, especially on simulating feed density lower than 30% (Kojovic, 1988). A very wide range of feed size is also a common problem for this model (Napier-Munn et al., 1996).

Arterburn (1982) proposed a method for selecting proper hydrocyclones size and number for the design of comminution circuit. He characterized standard hydrocyclone geometry for a typical Krebs hydrocyclone, followed by a certain correction factors, and set the cut size as:

$$\boldsymbol{d_{50c}} = \frac{\boldsymbol{11.93\, D_c^{0.66}}}{\boldsymbol{\Delta P^{0.28}\, (\rho_s - \rho_l)^{0.5}\, (1 - 1.89\phi)^{1.43}}} \qquad (2.19)$$

where ΔP is pressure drop in kPa, d_{50c} in micron, D_c in cm, and the rest symbols are defined in either equation 2.16 or 2.17.

Asomah and Napier-Munn (1997) developed a hydrocyclone model generated from experiments at the JKMRC and Mount Isa Mines (MIM) by utilising hydrocyclone inclination, *i* , for the first time

as one of the model parameters. They conducted the modelling by using JKSimMet simulator on 117 sets of data, and additionally validated by another hundreds data sets available from JKTech and other previous workers (Rao, 1966, Nageswararao, 1978, Castro, 1990). The proposed model as followed:

$$d_{50c} = D_c^{0.229}\left(\frac{P_{40}}{D_o}\right)^{-0.457}\left(\frac{D_o}{D_u}\right)^{0.948}\left(1 - V_s^{\left(1-\frac{i}{180}\right)}\right)^{-2.941} x\,(Rep)^{-0.155}\,\theta^{0.719}\,e^{-1.392\frac{i}{180}}\,B1 \quad (2.20)$$

They also introduced separation function model, alpha, as:

$$\alpha = D_c^{-0.148}\left(\frac{D_o}{D_c}\right)^{1.046}\left(\frac{D_u}{D_c}\right)^{-0.161}\left(\frac{\mu_{sl}}{\mu_l}\right)^{-0.854}\left(\frac{\rho_s - \rho_p}{\rho_s}\right)^{-2.182} x\,Rep^{-0.107}\,\theta^{0.429}\,e^{\left(-0.094\frac{i}{180}\right)}\,B3 \quad (2.21)$$

where Rep is Reynold Number, P_{40} is 40% passing size of feed, V_s is volumetric solids fraction of feed, μ_{sl} and μ_l are slurry and water viscosity, B1 and B3 are model constant parameters for cut size and alpha respectively, and the rest symbols are defined in either equation 2.17 or 2.18.

Lately, Narasimha et al. (2014) developed a semi-mechanistic hydrocyclone model which combining the approach from historical and experimental data of hydrocyclone performance and dimensionless approach from computational fluid dynamic (CFD) data inputs. He collected a numerous historical datasets, including Asomah's dataset, in addition to his own experimental work to validate the model. The equation is as followed:

$$\frac{d_{50c}}{D_c} = K_D\,Re^{-0.436}\left(\frac{D_o}{D_c}\right)^{1.093}\left(\frac{D_u}{D_c}\right)^{-1}\left(\frac{D_i}{D_c}\right)^{-0.936}\left(\frac{L_c}{D_c}\right)^{0.187}\left(\frac{1}{tan(\theta)}\right)^{-0.1988} \left(\frac{(1-\phi)^2}{10^{(1.82\,\phi)}}\right)^{-0.703}\left(cos\left(\frac{i}{2}\right)\right)^{-1.034}\left(\frac{\rho_s - \rho_l}{\rho_l}\right)^{-0.217} \quad (2.22)$$

where K_D is cut size constant parameter.

2.5.2 Water recovery or volume split model

The importance of flow split of feed water to underflow in assessing separation efficiency has been discussed in previous section. Feed water recovery to underflow, symbolized with R_f, is also closely related to volume split, *S*, solid feed recovery to underflow, R_s, and volumetric slurry feed to underflow, R_v. The relationships between those four are shown as:

$$R_f = \frac{R_v - R_s V}{1 - V} = \frac{Underflow\ water\ flowrate}{Feed\ water\ flowrate} \tag{2.23}$$

$$R_v = \frac{Underflow\ slurry\ volumetric\ flowrate}{Feed\ slurry\ volumetric\ flowrate} \tag{2.24}$$

$$R_s = \frac{Solid\ underflow\ flowrate}{Solid\ feed\ flowrate} \tag{2.25}$$

$$S = \frac{Underflow\ volumetric\ flowrate}{Overflow\ volumetric\ flowrate} \tag{2.26}$$

where V is volumetric solid fraction in the feed. Thus,

$$R_v = \frac{S}{1 + S} \tag{2.27}$$

where $R_v \approx R_f$ when dilute slurry is treated.

Yoshioka and Hotta (1955), working on 7.6 and 15.2cm hydrocyclones with D_u/D_o ratio ranging from 0.3 to 0.8, proposed the volume recovery model as:

$$1 - R_v = \frac{0.95}{(D_u/D_o)^4 + 1} \tag{2.28}$$

Bradley (1965) incorporated throughput and dimensionless parameter of hydrocyclone geometries for volume split equation:

$$S = 2.3\, Q^{-0.75} \left(\frac{D_u}{D_o}\right)^{1.75} \tag{2.29}$$

where Q = feed flowrate (m^3/s)

D_u/D_o = Ratio of spigot and vortex finder diameter.

Lynch and Rao (1975) suggested a linear relationship for water recovery to underflow, as it is influenced by feed water flowrate, *WF*, and spigot diameter, D_u:

$$R_f = K1 \frac{D_u}{WF} - K2 \frac{1}{WF} + K3 \tag{2.30}$$

K1, K2, and K3 are constants.

Along with cut size model, Plitt (1976) also stated a predictive model for volume split, *S*, from his computational regression. After slight modification (Flintoff et al., 1987), the model becomes:

$$S = \frac{F4\ 18.62\ \rho_p^{0.24} \left[\frac{D_u}{D_o}\right]^{3.31} (D_u^2 + D_o^2)^{0.36}\ h^{0.54}\ exp(0.0054\phi)}{D_c^{1.11}\ P^{0.24}} \tag{2.31}$$

where ρ_p = feed slurry density, in kg/l

P = pressure drop inside hydrocyclone, in kPa

h = distance between spigot and vortex finder, in cm

F4 = Plitt calibration factor, default value by 1

then water recovery to underflow, R_f, can be calculated by equation 2.23.

A model for water recovery to underflow was proposed by Nageswarararo (1978). The model is dependent on feed size distribution, as well as vortex finder length and diameter, which are included on the constants, K_{wo}. The model is then developed by the same author (Nageswararao et al., 2004), finally given as:

$$R_f = K_{wo} \left(\frac{P}{\rho_p g\ D_c}\right)^{-0.53} \left(\frac{D_o}{D_c}\right)^{-1.19} \left(\frac{D_u}{D_c}\right)^{2.4} \left(\frac{D_i}{D_c}\right)^{-0.5} \left(\frac{L_c}{D_c}\right)^{0.22} \theta^{-0.24}\ \lambda^{0.27} \tag{2.32}$$

where definitions and symbols are the same with equation 2.18.

Asomah and Napier-Munn (1997) developed the first water recovery model which incorporates angle of inclination, *i*, as a variable. The model also takes slurry viscosity into the equation as experimental results in Asomah thesis (1996) showed a raise in water recovery when viscosity increase. The water recovery model is given as:

$$R_f = D_c^{0.471} \left(\frac{P_{40}}{D_o}\right)^{0.214} \left(\frac{D_o}{D_u}\right)^{-1.806} \left(\frac{L_c}{D_c}\right)^{0.287} (1 - V_s)^{-0.825} \\ x\ (Rep)^{-0.175}\ \theta^{-0.478}\ e^{-1.357\frac{i}{180}}\ B2 \tag{2.33}$$

where B2 is the constant parameters for water recovery model and viscosity influence is represented by Reynolds number (*Rep*), P_{40}, and V_s.

Narasimha (2014) proposed another dimensionless model for water recovery from CFD simulations refined with dataset from wide range of laboratory and industrial operation, including inclined hydrocyclone. The model is given as:

$$R_f = K_w \left(\frac{D_o}{D_c}\right)^{-1.06787} \left(\frac{D_u}{D_c}\right)^{2.2062} \left(\frac{V_t^2}{0.5\ D_c\ g}\right)^{-0.20472} \left(\frac{L_c}{D_c}\right)^{2.424} \left(\frac{1}{tan(\theta/2)}\right)^{0.829} \\ \left(\frac{\mu_{sl}}{\mu_l}\right)^{-0.7118} \left(\frac{(1-\phi)^2}{10^{(1.82\,\phi)}}\right)^{-0.8843} \left(cos\left(\frac{i}{2}\right)\right)^{1.793} \left(\frac{\rho_s - \rho_l}{\rho_l}\right)^{0.523} \tag{2.34}$$

where K_w is water recovery constant parameter.

2.5.3 Throughput and pressure model

The relationship between throughput and pressure drop is "interdependent" (Svarovsky, 1984). An increase in pressure drop will give a proportional raise on throughput in a square root function:

$$\boldsymbol{Q} \propto \sqrt{\boldsymbol{P}} \tag{2.35}$$

Napier-Munn et al., (1996) expressed hydrocyclone throughput as a function of pressure drop and hydrocyclone diameter in the following formula:

$$\boldsymbol{Q = 0.0095\sqrt{P}\,D_c^2} \tag{2.36}$$

He argued that equation 2.36 have given satisfactory results when pressure is measured accurately.

In industrial practice, the complexity of the plant operation treating various kinds of slurry and the wide range of hydrocyclone designs have interfered with this basic correlation. Consequently, hydrocyclone capacity is no longer pressure drop and hydrocyclone diameter dependent only. Several researchers have proposed their empirical models to predict the hydrocyclone capacity by incorporating other variables (Plitt, 1976, Flintoff et al., 1987, Nageswararao, 1978, Svarovsky, 1984).

Flintoff and Plitt (1987) modified Plitt's original throughput model (Plitt, 1976), which was produced from experimental data using computational linear regression technique, and suggested the modified predictive model for hydrocyclone throughput as:

$$\boldsymbol{Q^{1.78} = \frac{P\,D_c^{0.37}\,D_i^{0.94}\,H^{0.26}\,(D_u^2 + D_o^2)^{0.87}}{1.88\;exp(0.0055V_p)\;F3}} \tag{2.37}$$

where F3 is calibration factor with default value of 1.

Another throughput model is developed by Nageswararao (1978) by using Krebs hydrocyclone:

$$\boldsymbol{Q = K_{q0}\,D_c^{1.9}\left(\frac{P}{\rho_p}\right)^{0.5}\left(\frac{D_o}{D_c}\right)^{0.68}\left(\frac{D_i}{D_c}\right)^{0.45}\theta^{-0.1}\left(\frac{L_c}{D_c}\right)^{0.20}} \tag{2.38}$$

where Q unit is in m^3/h.

Svarovsky (1984) produced hydrocyclone throughput model by using combination of mathematical derivation of dimensionless group models. The resulted model is as followed:

$$Q^{2+n_p} = \frac{\Delta P\, \pi^2\, D_c^4}{8\, \rho_s\, K_p} \left(\frac{\pi\, D_c\, \mu}{4\, \rho_s}\right)^{n_p} \tag{2.39}$$

where n_p and K_p are hydrocyclone geometrical empirical constants.

Along with cut size, water recovery, and alpha models, Asomah and Napier-Munn (1997) generated the following equation for throughput prediction:

$$Q_f = D_c^{0.749} \left(\frac{(D_i D_o)^{1.538}\, L_c^{0.455}\, P}{\rho_p\, (1 - V_s)^{0.435}\, A^{0.246}\, e^{-0.113\frac{\theta}{180}}}\right)^{0.5} B5 \tag{2.40}$$

where B5 is constant parameter for throughput model. Another constant parameter, B4, is used when equation 2.40 is reorganized into the pressure model.

Narasimha's empirical model for hydrocyclone throughput is given in the following equation:

$$Q = K_{Q0} \left(\frac{D_i}{D_c}\right)^{0.45} \left(\frac{D_u}{D_c}\right)^{0.037} D_c^2 \sqrt{\frac{P}{\rho_p}} \left(\frac{D_o}{D_c}\right)^{1.099} \left(\frac{L_c}{D_c}\right)^{0.3} \left(\frac{1}{tan(\theta/2)}\right)^{0.405} \left(\frac{(1-\phi)^2}{10^{(1.82\,\phi)}}\right)^{-0.048} \left(cos\left(\frac{i}{2}\right)\right)^{-0.092} \tag{2.41}$$

where K_{Q0} is throughput constant parameter.

2.5.4 Model Fitting and the JKSimMet Simulator

All those prediction models reviewed in this section have incorporated the main variables in hydrocyclone that are very significant to the performance parameters i.e. d_{50c}, water recovery, throughput, and alpha. These main variables include both design variables (for example hydrocyclone diameter, hydrocyclone length or height, vortex finder and spigot diameter, inlet diameter, and cone angle) and operation variables (pressure, angle of inclination, feed concentration, slurry density and viscosity). There are still many other variables left out from those models because either their individual significances are minor compare to the main variables or they cannot be quantified. These other variables for instance particles shape, particle density distribution, vortex finder length, etc. Nevertheless, the gravity of their importance becomes higher if their influences are accumulated. The most influential factor is feed characteristic over the others.

Accordingly, each model usually will have a constant parameter introduced into the model to substitute those miscellaneous variables as a single component. In Narasimha/Mainza model, those constant parameters are KD0 for cut size model, KW1 for water recovery model, KQ0 for

throughput model, and KAlpha0 for alpha model. In Asomah model, there are B1 for cut size model and B2 for water recovery models. In both model, these constant parameters mainly represent feed characteristic above the other factors.

These constant parameters in most cases are different for each hydrocyclone operation condition. Thus, to estimates hydrocyclone performance using those models, model fitting step is required. Existing computer software can assist users to do the iteration calculation in fitting a model.

JKSimMet is a simulator software package that allows users to do most metallurgical calculation of mineral comminution system. In addition to material can metallurgical balance tools, it also has the model fitting feature that contains a number of hydrocyclone prediction models generated from numerous empirical database of mineral processing operation.

Several hydrocyclone models embedded in JKSimMet are for instance Plitt's model (1976) and Nagesawararao's model (1978), but these models do not have angle of inclination as predictor. The very first model that incorporate angle of inclination into variable and put separation sharpness (alpha) prediction was Asomah model (1997). Narasimha/Mainza's model is currently the only hydrocyclone model available on JKSimMet which take inclination angle into account though simulation of semi-inverted operation was not encouraged.

In JKSimMet simulator, Narasimha/Mainza prediction models in Equation 2.23, Equation 2.34, and Equation 2.41, along with a sharpness of separation model have been refined with larger dataset. The final form of his models are as followed:

$$\frac{d_{50c}}{D_c} = K_{D0}\, Re^{-0.5} \left(\frac{D_o}{D_c}\right)^{1.207} \left(\frac{D_u}{D_c}\right)^{-0.921} \left(\frac{D_i}{D_c}\right)^{-0.75} \left(\frac{L_c}{D_c}\right)^{0.272} \left(\frac{\rho_s - \rho_l}{\rho_l}\right)^{-0.244} x\, \lambda^{-0.657} tan\left(\frac{\frac{\pi}{180}\theta}{2}\right)^{0.139} cos\left(\frac{\frac{\pi}{180}i}{2}\right)^{-1.05} \tag{2.42}$$

$$R_f = K_{W0} \left(\frac{D_o}{D_c}\right)^{-0.835} \left(\frac{D_u}{D_c}\right)^{2.19} \left(\frac{L_c}{D_c}\right)^{1.937} \left(\frac{V_t^2}{0.5\, D_c\, g}\right)^{-0.259} \left(\frac{\rho_s - \rho_l}{\rho_l}\right)^{0.462} x\, \lambda^{-0.93}\, \mu_r^{-0.792} \left(tan\left(\frac{\frac{\pi}{180}\theta}{2}\right)\right)^{-0.649} \left(cos\left(\frac{\frac{\pi}{180}i}{2}\right)\right)^{1.765} \tag{2.43}$$

$$Q = K_{Q0}\left(\frac{D_i}{D_c}\right)^{0.45}\left(\frac{D_u}{D_c}\right)^{0.06} D_c^2\sqrt{\frac{P}{\rho_{sl}}}\left(\frac{D_o}{D_c}\right)^{1.25}\left(\frac{L_c}{D_c}\right)^{0.33}\left(\frac{(1-\phi)^2}{10^{(1.82\,\phi)}}\right)^{-0.047} x\left(cos\left(\frac{\frac{\pi}{180}i}{2}\right)\right)^{-0.090}\left(tan\left(\frac{\frac{\pi}{180}\theta}{2}\right)\right)^{-0.405} \quad (2.44)$$

$$\alpha = K_{\alpha 0}\left(\frac{D_o}{D_c}\right)^{0.191}\left(\frac{D_u}{D_c}\right)^{-0.467}\left(\frac{L_c}{D_c}\right)^{-0.233}\left(\frac{V_t^2}{0.5\,D_c\,g}\right)^{0.012}\left(\frac{\rho_s-\rho_l}{\rho_l}\right)^{-1.67} x\,\lambda^{0.739}\,\mu_r^{-0.112}\,tan\left(\frac{\frac{\pi}{180}\theta}{2}\right)^{-0.018}\left(cos\left(\frac{\frac{\pi}{180}i}{2}\right)\right)^{0.751} \quad (2.45)$$

Where

$$\lambda = \text{hindered settling factor} = \frac{(1-\phi)^2}{10^{(1.82\,\phi)}} \quad (2.46)$$

$$\mu_r = \text{viscosity model} = \left(1-\left(\frac{\phi}{0.622}\right)\right)^{-1.55} f_{38}^{0.39} \quad (2.47)$$

$$Re = \text{Reynolds number} = \frac{V_i\,D_c\,\rho_p}{\mu_r} \quad (2.48)$$

and

$$V_t = 4.5\,V_i\left(\frac{D_i}{D_c}\right)^{1.13} \quad (2.49)$$

CHAPTER 3 : Preliminary Experiment with 40% and 25% Feed Solids

In the previous chapter, earlier work by several authors has been reviewed to signify the importance of inclination on performance of a hydrocyclone. Even though these studies show its advantage in performance compared with conventional vertical hydrocyclones, most of them were limited to operation with the cone below horizontal position. Investigations on high inclination operation (above horizontal) were actually included in a small portion by Asomah (1996) and Rong and Napier-Munn (2003). However, Asomah did not specifically expose this area in detail as previously mentioned in Chapter 2. Rong and Napier Munn did experiment with his proposed novel hydrocyclone design to classify coal slurries instead of minerals. Conclusions from both projects on sharpness of cut showed no clear trend.

The Asomah semi-inverted hydrocyclone test work considered only a very narrow range of operating pressure, with only single low pressure operation using half a meter hydrocyclone. The effect of different mineral density on high angle separation has not been observed. Moreover, current empircal hydrocyclone models do not engage angle higher than 90 degrees in their validity range.

This chapter will discuss the initial stage of the experiments investigation. Variation of inclinations and pressure drop were applied to ascertain how those parameters impact on classification. Two types of feed slurry of different concentration, 40% solids and 25% solids, were used for the test work.

3.1 Experiment with 40% Solids Feed Concentration

At an earlier stage of this work, a standard JKMRC hydrocyclone with 250 mm diameter was tested on moderate to high solids slurry systems. A slurry system of 40% concentration silica by weight was initially prepared. Originally this experiment was meant to be the part of main experiment, which will be presented on the next chapter; however, the hydrocyclone met its operational limitation when slurry was fed on high inclination. Nevertheless, a couple of sample set has successfully been taken during a short period to enable quick analysis.

3.1.1 Experimental condition

The schematic picture of standard JKMRC hydrocyclone with 250 mm diameter employed in this experiment was shown in Figure 3-1.

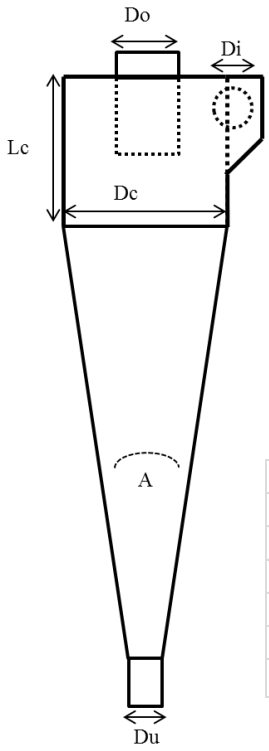

Legends:		
Body diameter, Dc	250	mm
Cylindrical body length, Lc	250	mm
Inlet diameter, Di	72	mm
Vortex finder diameter, Do	90	mm
Spigot diameter, Du	70	mm
Cone angle, A	10	degree (^{o})

Figure 3-1: Schematic picture of 250 mm JKMRC hydrocyclone dimensions

The hydrocyclone was installed on a test rig at the JKMRC Pilot Plant. The schematic diagram of this rig is given by Figure 3-2. The rig has a 3-inch variable speed pump to supply high pressurized feed into the hydrocyclone. The pump speed was adjusted until the pressure gauge shows the target operating pressure. The by-pass valve was fully closed during experiment, it was only open during the changing of hydrocyclone position (without stopping the pump).

Slurry was pumped through a pipe which has metal rods inside to provide a proper mixing for the feed. Feed samples were taken from the feed stream through a valve which gate was controlled by a pressurised switch. The valve was located on the top of the feed line such that allowed it to alternate the moving feed stream directly when the gate was open. To collect a sample, the valve was opened for several seconds to let the flow stabilises before grab sample was taken. This should be sufficient to provide a good quality feed sample.

The capability assists hydrocyclone operation at any angle from vertical position up to 180 degrees upwards. Hydrocylone inclination angle is defined by Figure 3-3.

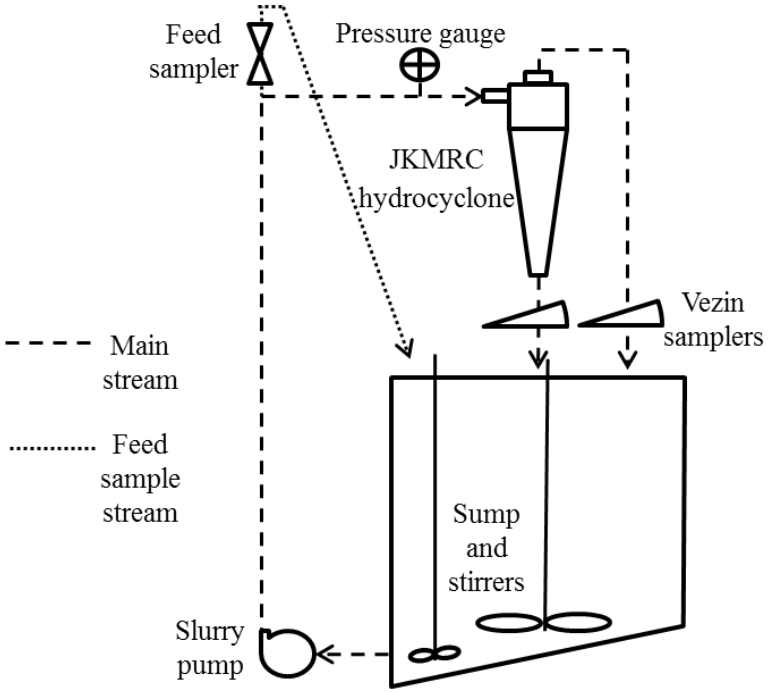

Figure 3-2: Schematic diagram of hydrocyclone rig facility at JKMRC Pilot Plant

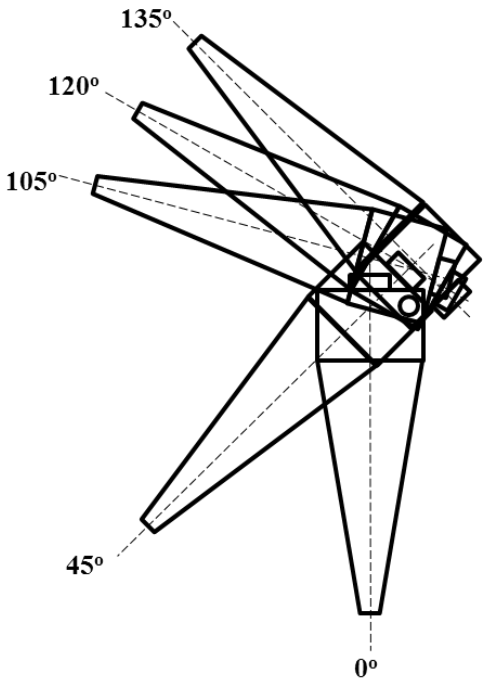

Figure 3-3: Schematic illustration of hydrocyclone inclination angle

The hydrocyclone test rig was equipped with additional devices in order to catch the underflow and overflow streams during any inclined operation. A metal catch box and a cylindrical "cap" were fitted to underflow and overflow orifices respectively, have been designed and manufactured by JKMRC workshop. These boxes have two roles; firstly to pass stream products to the Vezin samplers, and secondly to let both flow present as they leave the hydrocyclone. This especially helps visual observation on underflow discharge condition during operation to avoid roping.

Feed material used in this experiment was silica slurry. Commercial fine-grade silica was used as feed material. Before the test work, a representative sample of silica was collected from the bulk materials using rotary splitter and screened down to 20 micron sieve. The size distribution result is presented in Table 3-1.

Table 3-1: Fine grade silica size distribution

Sieve size (micron)	% weight retain
180	4.33
150	2.92
125	4.01
106	5.01
90	5.97
75	6.11
63	8.57
53	7.38
45	5.47
38	7.15
20	13.91
-20	29.17

As much as 375 kilograms of silica were introduced into the sump which was already filled with approximately 560 kg water to establish almost a ton of approximately 40% solids of slurry system in the sump. Stirrers were activated during silica introduction to prevent any particle settlement in the bottom of the sump.

In this initial stage of experiment, it was discovered that operating pressure region was strictly limited. Only three sample sets had been successfully collected in 100 kPa and 110 kPa pressure regime, while the later came with a replicate. Also, there was significant and rapid pressure fluctuation. During sampling at 100 kPa the pressure was varied between 95 kPa and 105 kPa. Similarly, pressure rapidly fluctuated around 105 kPa and 115 kPa during 110 kPa sampling.

Moreover, the rig system could not accommodate pressure lower than 95 kPa, which resulted in sudden flow collapse. System could not also achieve higher pressure region due to pump capacity.

Overflow and underflow samples were collected through the Vezin sampler and a feed sample was collected through a valve next to the hydrocyclone feed inlet.

Three samples representing each stream (feed, overflow, and underflow) were collected in buckets. Sub-samples were then collected from each sample by rotary divider and filtered.

Sub-sample weight was measured prior to sieves sizing. Sizes less than 20 micron were removed first through wet screening to avoid blocking during subsequent dry screening. The oversize fraction was then oven dried overnight and was screened the next day. The weight of each size fraction was then measured, thus retained percentage and cumulative passing percentage value for each size fraction were generated.

3.1.2 Experimental Data

The data collected comprised sample weights and sample solids concentrations (Table 3-2) and size analysis (Table 3-3) in raw data form.

Table 3-2: Sample raw data for operation at 135 degrees with 40% solids slurry

Stream	110 kPa			110 kPa (Replica)			100 kPa		
	Wet (kg)	**Dry (kg)**	**% Solids**	**Wet (kg)**	**Dry (kg)**	**% Solids**	**Wet (kg)**	**Dry (kg)**	**% Solids**
Feed	6.42	2.68	41.71	11.92	4.90	41.10	11.96	4.85	40.58
Overflow	31.32	9.48	30.26	3.82*	1.20*	31.33	30.98	10.04	32.40
Underflow	10.64	7.77	73.03	11.12	8.03	72.25	8.48	6.20	73.08

**overflow wet sample size was reduced using slurry rotary splitter*

Data in Table 3-2 and Table 3-3 were then processed through mass balancing and model fitting modes in the JKSimMet simulation software package.

Through mass balancing, the value of each data was brought closer to the most trusted measurement so that input and output would have self-consistency. Consequently, we would have adjusted values that were self-consistent but they still estimated the true value.

Table 3-3: Raw size analysis for operations at 135 degrees with 40% solids slurry

Sieve size (µm)	% weight retained								
	110 kPa			110 kPa (Replica)			100 kPa		
	Feed	O/F	U/F	Feed	O/F	U/F	Feed	O/F	U/F
180	3.45	0.00	6.92	3.78	0.01	7.76	3.45	0.10	8.56
150	2.79	0.00	5.96	2.91	0.02	6.00	2.53	0.07	6.44
125	4.07	0.03	9.12	3.77	0.04	8.80	3.50	0.31	11.24
106	4.91	0.16	10.87	5.27	0.28	11.79	4.93	0.78	12.56
90	6.11	0.69	14.17	5.93	0.55	14.34	5.66	1.55	13.51
75	6.25	1.58	10.95	6.23	0.80	11.20	6.15	3.31	9,50
63	8.33	4.55	12.15	8.53	4.74	11.81	8.37	7.76	9.71
53	5.88	5.46	5.73	5.83	6.25	5.38	5.98	6.56	4.53
45	5.77	6.08	4.44	5.30	6.64	4.16	5.60	6.03	3.32
38	6.47	8.12	4.25	6.72	8.33	4.05	6.90	7.58	3.66
20	14.79	22.07	6.25	14.75	18.69	5.99	16.92	25.31	6.00
pan	31.18	51.27	9.19	30.99	53.66	8.82	30.01	40.65	10.96
% solids	41.71	30.26	73.03	41.10	31.33	72.25	40.58	32.40	73.08

Narasimha/Mainza model was utilised for model fitting in the JKSimMet simulator as this model incorporates angle of inclination as one of the operating variable. This way, the data would not only mass balanced but also specific to the equipment and operating conditions.

3.1.3 Results and Discussion

Feed and product streams size results, F_{80} and $P_{80,}$ are summarised in Table 3-4.

Table 3-4 : F_{80} and P_{80} for operation at 135^{o} applying 40% feed solids slurry

Pressure (kPa)	Feed F_{80} (micron)	Overflow P_{80} (micron)	Underflow P_{80} (micron)
100	91.1	51.9	140
110	94.6	43.1	130
110 (Replica)	96.4	42.2	130

At a semi-inverted position of 135 degrees, both overflow and underflow product sizes were increased by pressure variation as indicated by Table 3-4. With only 10 kPa difference, the P_{80} of the overflow increased from 43.1 micron at 110 kPa to 51.9 micron at 100 kPa. This was

accompanied by underflow as P_{80} of 130 micron increased up to 140 micron. Replication at 110 kPa showed consistent results.

There results suggested that when a hydrocyclone was used at high inclination higher pressure would produce a finer overflow product. An increase in underflow product size is possibly due to feed size variation rather than pressure. With higher pressure, particles would have more momentum to reach underflow as the gravity would oppose the axial flow inside hydrocyclone body. The amount of slurry appearing in the coarse product would also be more and less appeared in fine product. This reduction of amount of solids reporting to underflow was shown in Table 3-5. This also explained the increasing trend of the cut size, d_{50c}.

Table 3-5 : Hydrocyclone performance parameters applying 40% feed solids slurry at 135 degree operation

Pressure (kPa)	Performance parameters			Solids recovery to Underflow (%)
	d_{50c} (µm)	R_f (%)	α	
100	78.2	9.5	4.5	36.01
110	61.2	12.3	4.3	46.41
110 (Replica)	60.3	12.4	5.2	47.06

According to conventional practice, operating a hydrocyclone with lower pressure would increase amount of water reporting to coarse product. However at 135^{o} inclination from vertical, the opposite trend occurred; amount of water reporting to underflow decreased at lower pressure (see Table 3-5). This might be explained by the tendency inside hydrocyclone operating at this orientation which allows gravity to drag more water to the fine product. This resulted in lower water recovery to underflow. Thus, the fine fraction which was entrained in the water that originally went to coarse product also decreased as the pressure dropped.

Classification curves are shown in Figure 3-4, Figure 3-5, and Figure 3-6. There was good agreement between balanced and fitted data on the graphs though there was a misfit on fine fractions particularly on replicate curve, where the software overestimated the fitted values from the balanced data. This could cause bias to the higher alpha value of 5.2 over the 4.3 from the first result. However, those sharpness values were still reasonably high for a typical hydrocyclone classification of a single component.

Because of very limited data in this stage, these indications can be misleading to the wrong conclusion. Therefore further investigation with more datasets will be delivered in the next few chapters.

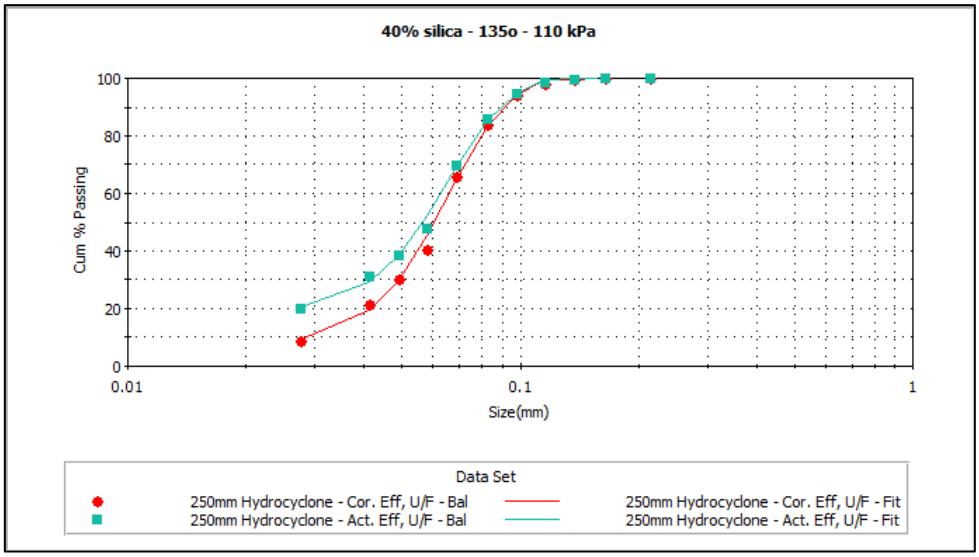

Figure 3-4: Efficiency curves at 135 degrees inclination applying 40% feed solids silica slurry at 110 kPa

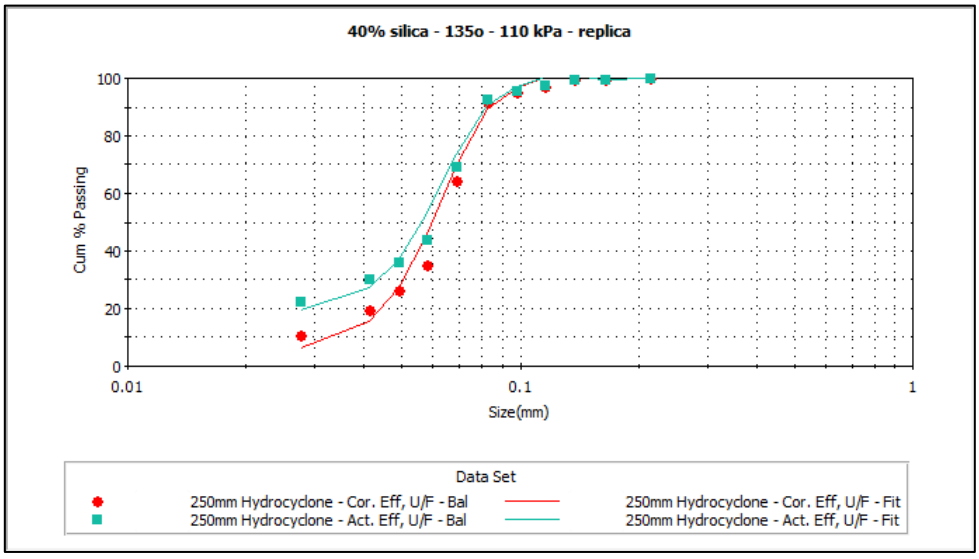

Figure 3-5: Efficiency curves at 135 degrees inclination applying 40% feed solids slurry at 110 kPa (Replica)

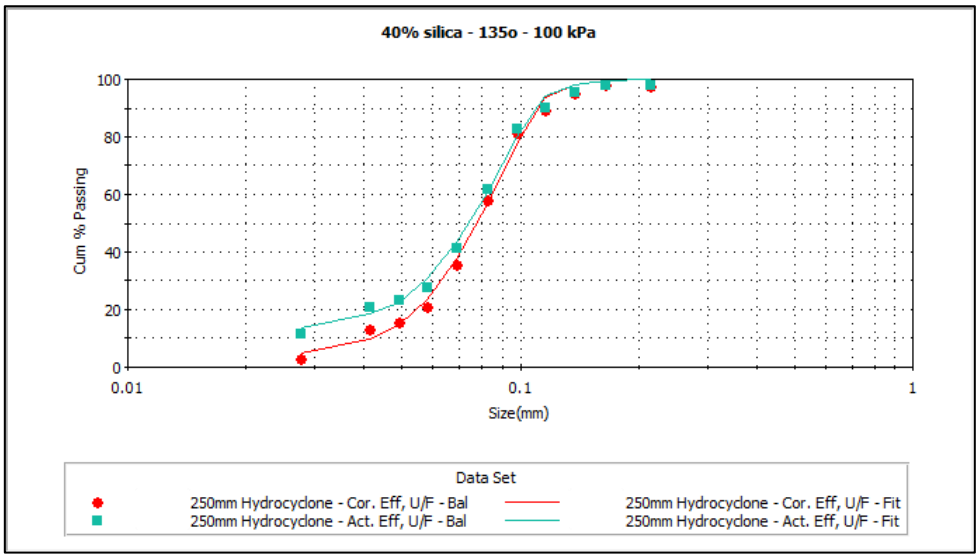

Figure 3-6: Efficiency curves at 135 degrees inclination applying 40% feed solids slurry at 100 kPa

3.2 Experiment with 25% Feed Solids Concentration

As previously mentioned in sub-section 3.1.1, further operation using the 40% solids slurry could not be performed due to limited operating pressure. To make use of the silica material in the sump, it was then decided to continue with less concentration slurry and see if the current hydrocyclone configuration could still produce meaningful results. The slurry was diluted to a moderate concentration of 25% solids by weight.

3.2.1 Experiment condition

The same hydrocyclone was utilised in this stage of experiment. Hydrocyclone inclinations were varied from 120^{o}, 105^{o}, 45^{o}, and 0^{o} as illustrated by Figure 3-3. An angle of 135^{o} was intended to be tested but sample collection could not be performed. It is believed the limitation at 135 degrees might be caused by pressure loss from opening feed sampler valve. A feed sampler valve was located close to the hydrocyclone inlet, it was possible that feed sampling release a significant amount of dynamic pressure the slurry. This pressure loss could initiate the slurry to have less momentum to reach underflow exit, in addition to the high friction of hydrocyclone cone wall. Another possible explanation might be spigot blockage. At 135 degrees, the amount of feed water reporting to underflow exit was too low, not to mention the long cone impeding the water transport. These could leads to significant increase of solids concentration close to spigot discharge causing blockage.

There was no significant fluctuation of pressure observed with 25% solids, unlike 40% solids slurry. The pressure fluctuation indicates an unstable operation, probably rapid change between blocking and roping conditions.

To investigate pressure influence on semi-inverted hydrocyclone, three different pressures of 80 kPa, 100 kPa, and 120 kPa were chosen. However, the feasible operating range between semi-inverted operations and operation below horizontal did not fall exactly in the same region. For the interest of the study to still have three operating pressures, one additional pressure of 60 kPa was included to the experiment. The summary of operating range is presented by Table 3-6. The sampling method is grab sample for feed and Vezin sampler for product streams, the same with the previous experiment with 40% solids concentration mention in sub-section 3.1.1. A rotary sub-sampler for slurry was introduced in the sample preparations

Table 3-6: Operating condition of experiment with 25% solids concentration slurry.

Inclinations	60 kPa	80 kPa	100 kPa	120 kPa
0 degree	✓	✓	✓	-
45 degrees	✓	✓	✓	-
105 degrees	-	✓	✓	✓
120 degrees	-	✓	✓	✓

Application of low concentration slurry results in finer cut sizes. Hence sieves sizing could not reach fractions finer than 20 micron while some overflow product would have P_{80} less than 20 micron. A cyclosizer was used for sizing material below 38 micron.

3.2.2 Experimental data

Data collected from this experiment were solids concentration of each stream and size analysis in raw data form. A pair of sub-samples was collected instead of single sub-sample to check the variability of the slurry splitting. Sample solids concentration data were given by Table 3-7. Complete size analysis results were presented in Appendix A.1.

Through the same process, size distributions and solids percentage for all three streams were mass balanced and model fitted in JKSimMet to produce their closest estimated values to the true values. The balanced result and fitted results were then compared in graph. One example of balanced and fitted result of stream size distribution is given by Figure 3-7.

Table 3-7: Solids percentage data for all streams from 25% feed solids slurry operation

Inclination: 0°				
Sample	**60 kPa**	**80 kPa**	**100 kPa**	
	%solids	**%solids**	**%solids 1**	**%solids 2**
Feed	30.1	28.9	27.5	27.7
Overflow	11.6	10.3	9.8	9.9
Underflow	53.6	54.0	54.6	54.1
Inclination: 45°				
Sample	**60 kPa**	**80 kPa**	**100 kPa**	
	%solids	**%solids**	**%solids 1**	**%solids 2**
Feed	25.1	26.2	24.4	24.4
Overflow	8.8	8.6	8.5	8.5
Underflow	50.4	49.5	50.8	53.1
Inclination: 105°				

Sample	**80 kPa**		**100 kPa**		**120 kPa**	
	%solids 1	**%solids 2**	**%solids 1**	**%solids 2**	**%solids 1**	**%solids 2**
Feed	25.3	24.2	25.3	25.3	24.8	25.2
Overflow	9.5	10.1	9.1	9.0	8.8	8.9
Underflow	63.0	63.5	63.8	63.9	65.0	64.8
Inclination: 120°						

Sample	**80 kPa**	**100 kPa**		**120 kPa**	
	%solids	**%solids 1**	**%solids 2**	**%solids 1**	**%solids 2**
Feed	23.9	25.1	24.3	24.8	25.9
Overflow	10.9	10.1	10.1	9.7	9.5
Underflow	69.0	70.5	70.2	71.7	71.4

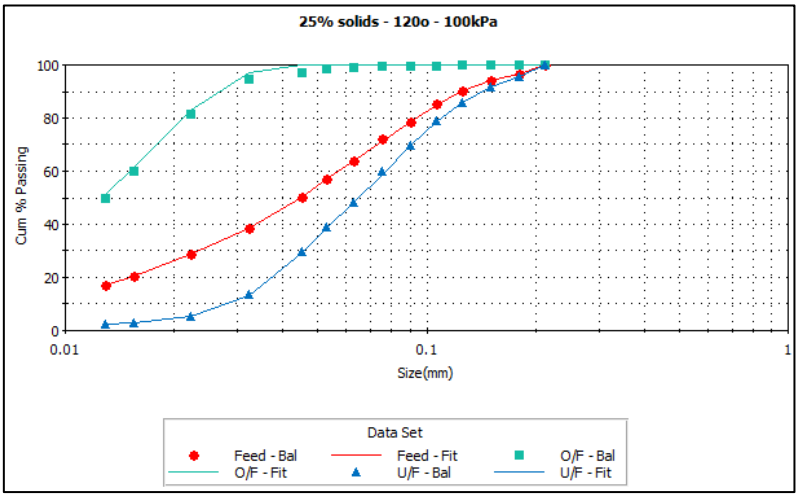

Figure 3-7: Feed and product size distributions of experiment with 25% solids concentration at 120 degrees and 100 kPa operation

3.2.3 Results and Discussion

3.2.3.1 Feed stability

From raw data provided by Table 3-7, the solids concentrations of all the feeds were consistent for most operation from 120^{o} down to 45^{o} at range from 23.8% to 26.2% but then slightly rose to 27.4% – 28.9% solids when vertically operated. This can be explained by the fact that there was insufficient amount of slurry left in the sump, thus some water and silica were added. This material added caused the solids concentration to alter.

The silica feeds were constant at all operating variables as indicated by Figure 3-8. The graph showed that the experiment was in stable condition when sampling campaigns were performed. No significant change in feed size also showed that silica particles were not ground easily by the circulating slurry pump and stirrers.

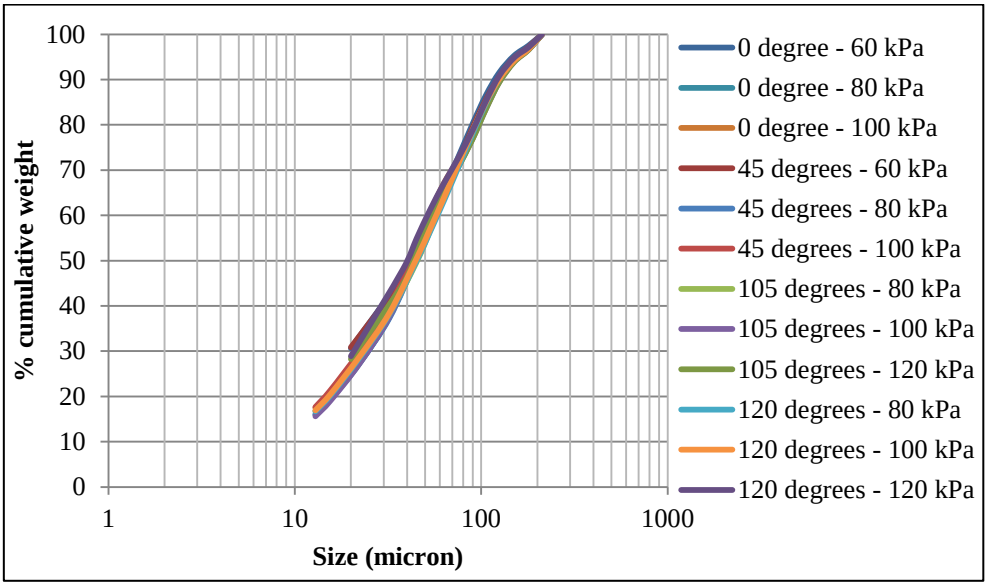

Figure 3-8: Feed size distributions at all operating conditions with 25% solids silica

3.2.3.2 Hydrocylone Performance versus Inclination

The hydrocyclone efficiency parameters are summarised in Table 3-8. The results trend are illustrated in Figure 3-9, Figure 3-10, and Figure 3-11. Efficiency curves for all cases were presented in Appendix A.7.

Table 3-8 : Efficiency parameters on various inclinations for 25% solids concentration slurry

inclinations	d_{50c} (micron)				Water recovery to U/F (%)				Alpha			
	60 kPa	80 kPa	100 kPa	120 kPa	60 kPa	80 kPa	100 kPa	120 kPa	60 kPa	80 kPa	100 kPa	120 kPa
0°	20.7	21.0	20.6	-	27.6	28.0	25.0	-	1.5	1.3	2.5	-
45°	20.3	20.4	21.2	-	23.7	29.4	23.7	-	1.3	2.6	2.4	-
105°	-	24.8	23.2	22.6	-	14.5	14.9	13.0	-	4.3	4.7	3.5
120°	-	29.6	26.8	25.5	-	10.0	9.8	9.8	-	5.0	5.3	4.1

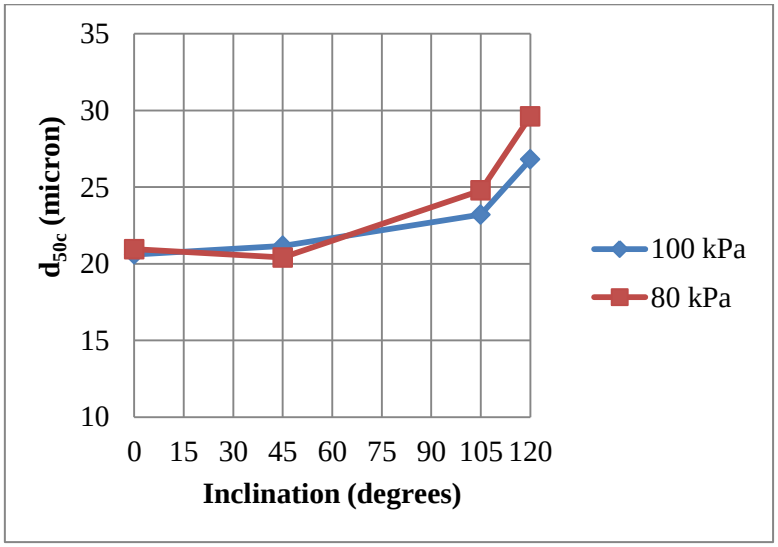

Figure 3-9 : Cut size versus inclinations at 80 kPa and 100 kPa with 25% solids silica

From Figure 3-9 it can be observed that corrected separation size, d_{50c}, was remained constant at around 20 micron both at 0 degree and 45 degrees inclinations. Improvements on cut size are shown at both 80 kPa and 100 kPa when hydrocyclone was inclined to 105 degrees. At 120 degrees, cut size is 10 micron coarser or increased by 50% from vertical operation.

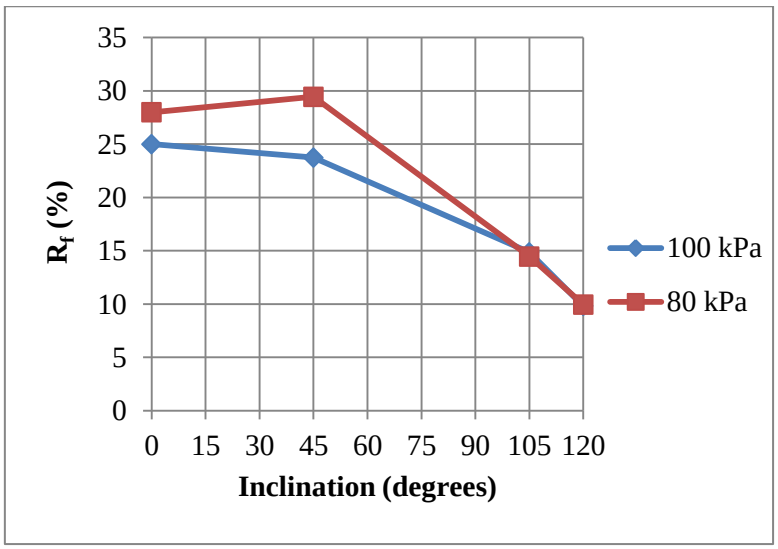

Figure 3-10 : Water recovery trends with 25% feed solids versus inclination

Figure 3-10 shows a large reduction in amount of water reporting to underflow when inclination went beyond horizontal. Semi-inverted positions significantly reduced water recovery by 40 – 50 per cents.

This water recovery to underflow behaviour affects the underflow solids percentages as indicated by Figure 3-11. Underflow solids percentage upsurges in consequence with the reduction of water recovery to underflow at semi-inverted orientation.

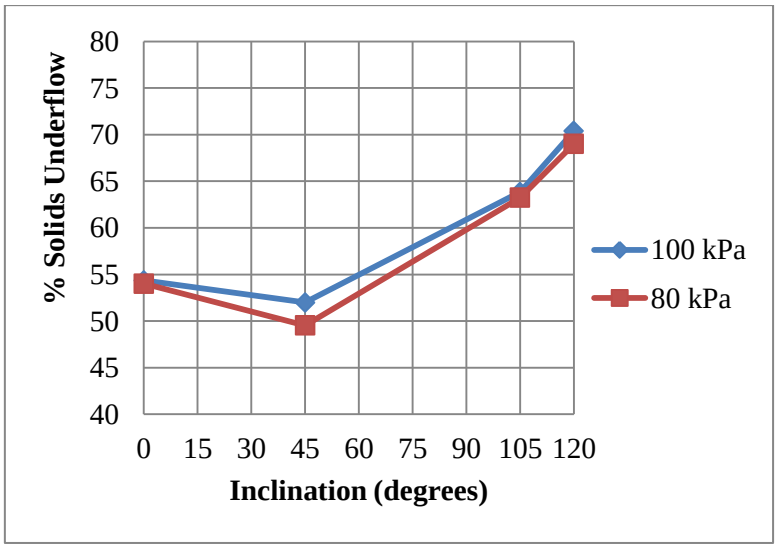

Figure 3-11 : Solids percentage of underflow at various angles with two pressure levels

On the contrary, water recovery does not influence overflow solids percentage as shown by Figure 3-12. The reason for this might be that overflow concentration was already low enough (around 90% is water), therefore additional water sent to overflow at semi-inverted angle was negligible.

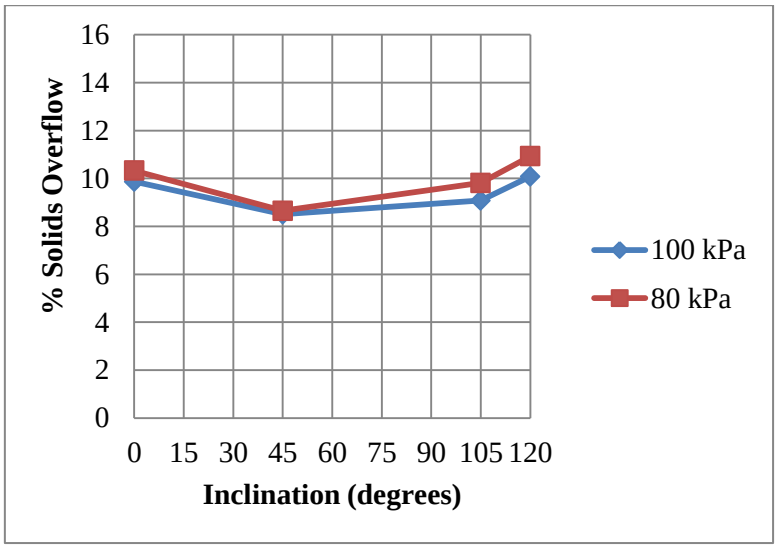

Figure 3-12 : Solids percentage of overflow at various angles with two pressure levels

There is some indication of sharper classification when semi-inverted hydrocyclone employed, as shown in Figure 3-13. From the classification curves presented in Appendix A.7, vertical hydrocyclone cuts too fine, causing less accurate fitting result. Hence, the alpha value at vertical operation is low. Inclined operation and semi-inverted operation cut sizes are in coarser and the fitting results are quite good.

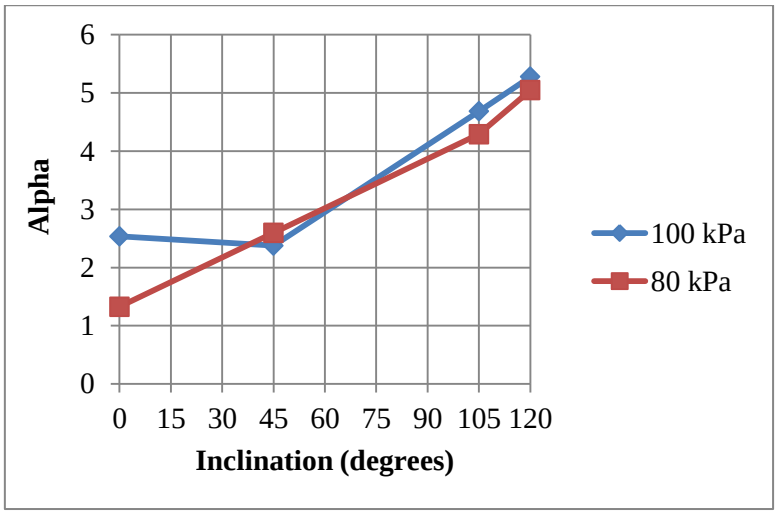

Figure 3-13: Alpha trends for hydrocyclone applying 25% feed solids concentration at four inclinations and two pressures

3.2.3.3 Hydrocyclone Performance versus Pressure

The influence of pressure on cut size at semi-inverted operation is significant as indicated in Figure 3-14. At 105^{o} and 120 degrees, increasing feed pressure would depress cut size, which agrees the conventional relationship. However, the effect of pressure on cut size is insignificant at 0 degree and 45 degrees positions. The possible explanation might be that the feed solids concentration on vertical operation is 3 to 5% higher (see Table 3-7). Another possible explanation is that the cut size values on both positions was too fine (around 20 microns) so further decrease of cut size by increasing the pressure could not be detected by the sizing methods which were used.

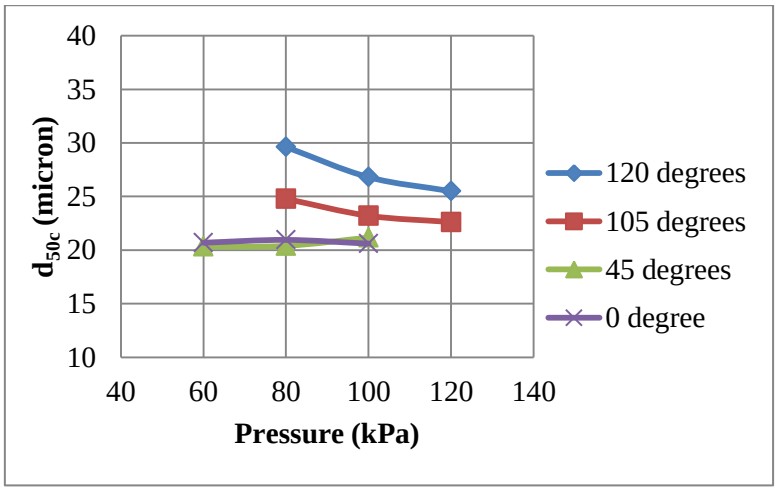

Figure 3-14: Pressure to cut size relationships on all four hydrocyclone inclinations for 25% solids concentration slurry

It is shown by Figure 3-15 that water recovery to underflow is inversely affected by pressure at vertical position. This response confirmed the response of normal hydrocyclone operation. At 45 degrees, the effect of pressure on water recovery is not clearly determined. At this angle, the water recovery hits the peak of 30% at 80 kPa and decrease to 23% at 60 kPa and 100 kPa. At 105 degrees and 120 degrees, the effect of pressure on water recovery to underflow is not present. This indicates semi-inverted positions hydrocyclone is not dependent to pressure.

From Figure 3-16, at 105 degrees and 120 degrees there are tendencies of sharpness reduction when operating pressure reaches 120 kPa. Sharpness is improved with higher pressure on vertical and 45 degrees operations. This indicates that sharpness response to pressure on semi-inverted positions oppose to vertical and inclined hydrocyclone operation.

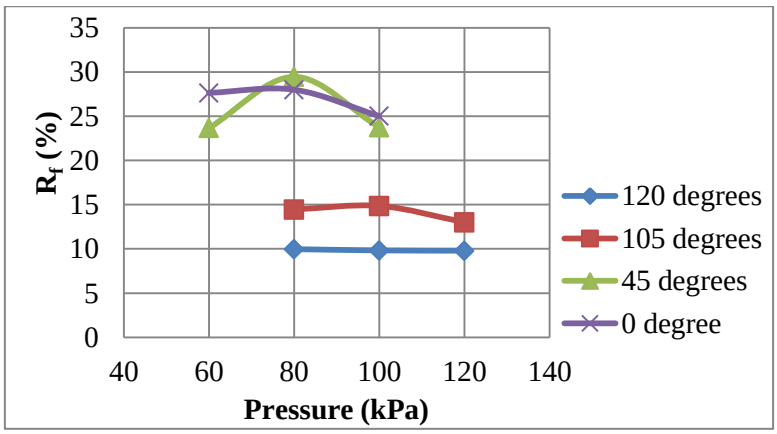

Figure 3-15: Pressure to water recovery relationships on all four inclinations for 25% solids concentration slurry

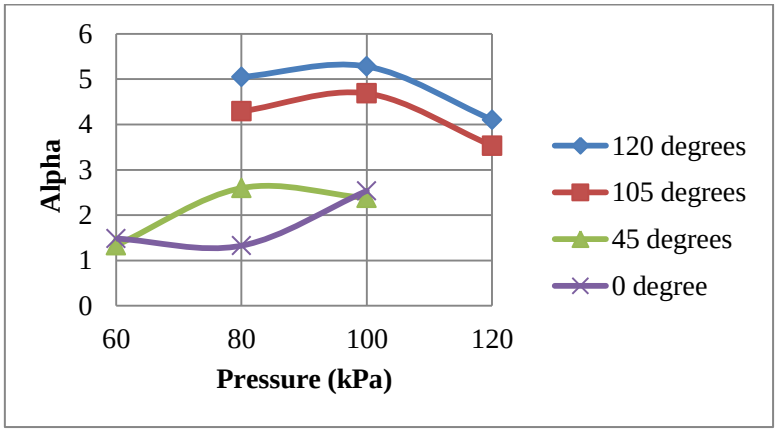

Figure 3-16: Pressure to separation sharpness relationships on all four inclinations

3.2.4 Conclusion and a Possible Way Forward

Hydrocyclone operation at 40% and 25% silica concentration slurry at various angles and at a certain unequal pressure drops have been considered. It was indicated that using 250 mm diameter hydrocyclone operated at semi-inverted position can advance hydrocyclone efficiency performance by reducing water recovery to underflow by almost half. Cut size increases as inclination goes higher while alpha is also promoted compare to vertical and 45 degrees inclination operations.

In addition, this experiment has explored the influence of pressure for semi-inverted hydrocyclone operation. From this preliminary experiment with 40% and 25% feed solids concentration, higher pressure would result in cut size and water recovery to underflow reduction, while on the contrary indication of sharper separation was shown.

Through this preliminary experiment, the JKMRC hydrocyclone with 250 mm diameter could not accommodate operation at 135 degrees applying 40% solids and 25% solids concentration slurry. It is believed that the reason of incapability of the JKMRC hydrocyclone is due to the frictional force from the cone wall was sufficient to impede the slurry transport. That is, the slurry lost its kinetic energy before reaching the spigot discharge. Asomah's (1996) accomplishment working with 33% solids concentration at 135 degrees with cone angle of 20^{o} indicates that a large hydrocyclone could run higher feed concentration with wider cone angle.

Therefore, an idea to modify the hydrocyclone cone used in this experiment to a wider cone angle was proposed. The wider cone also reduces the gravitational potential energy to the overflow. Details of modification will be given in the next chapter.

CHAPTER 4 : Experiment of 40% Solids Slurry with Modified Cone

As concluded in Chapter 3, hydrocyclone operation at semi-inverted angles especially at 135 degrees with high solids concentration slurry was not possible using the standard JKMRC hydrocyclone. This chapter describes a modification of the hydrocyclone which was proposed and tested.

Discussed in this chapter are the results of hydrocyclone work with 40% solids concentration slurry, including the range of operating condition, and followed by discussion of trends of classification performance in terms of cut size, water recovery to underflow, and sharpness of separation under the influence of inclinations beyond horizontal.

4.1 Cone Modification

The standard JKMRC 250 mm hydrocyclone which previously used in preliminary work could not be used at semi-inverted position (135 degrees) due to flow limitation. This might be related to the force balance within hydrocyclone internal body (see Chapter 2). When the hydrocyclone point upwards, fluid force and gravity force both drag towards overflow stream. At 135 degrees, the resultant force towards the overflow end was too high. As a result, the hydrocyclone either stopped discharging or discharging only insignificant amount of underflow.

A necessary adjustment to the standard JKMRC hydrocyclone was required to improve the hydrocyclone capability working with higher concentration slurries. An idea was proposed to change the cone angle to 15^{o}; the standard one was 10^{o}.

The hydrocyclone cone has important role in prolonging retention time available for particle settlement. With a wider cone angle at the same desired spigot diameter, the hydrocyclone will have shorter length which improves chances for slurry to exit from underflow duct. However, if cone angle becomes too wide, hydrocyclone might promptly discharge product before the required retention time achieved, which could cost separation efficiency. The shorter hydrocyclone also values gravitational potential energy to be overcome by the underflow.

Shortening the cone does increase the possibility of separation inefficiency on heavy density particles due to shorter separation time inside the hydrocyclone. However this effect cannot be

quantified and compared as the experiment with mixed-density minerals was only performed on shorter cone.

The standard hydrocyclone bottom body consists of three parts; upper cone, lower cone, and the spigot with total length of 1.4 meters. The upper and lower cones were replaced by the proposed cone design. The schematic drawing and detail of dimensions of original and new cone are given by Figure 4-1.

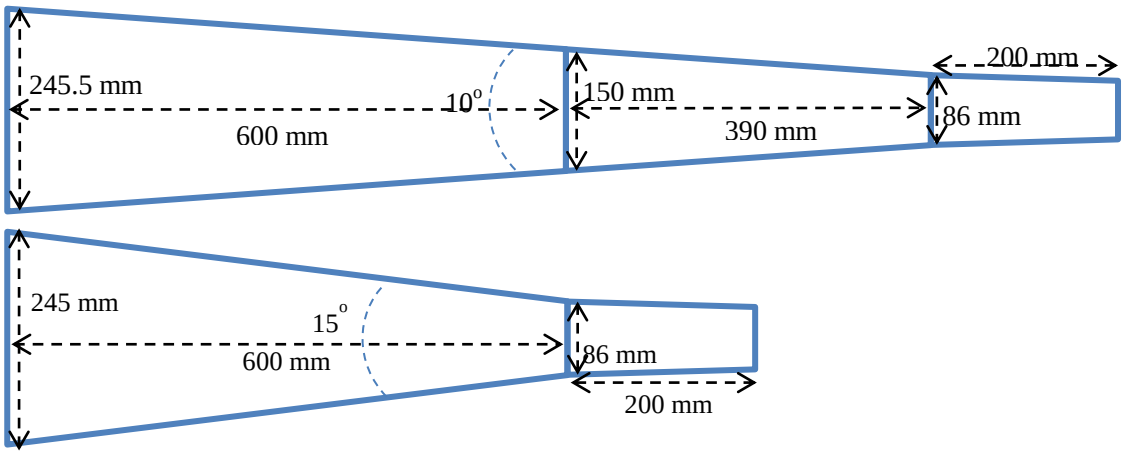

Figure 4-1: Standard (top) and new (bottom) cone schematic dimensions

The JKMRC workshop has constructed the new cone which was made from polyvinyl chloride (PVC). The modified JKMRC hydrocyclone construction has a 15° cone attached to the cylinder body on the top and the spigot on the bottom end. The spigot angle was not changed.

4.2 Experimental Setup

A new cone was installed within the hydrocyclone as described in previous section. The complete rig system has been described in Subsection 3.1.1.

A 40% solids concentration slurry was prepared by adding a calculated amount of silica into the rig sump, already filled with water, until the concentration reached 40% solids. The silica material was the same silica powder used on preliminary experiment (Chapter 3). The viscosity of slurry was also measured separately to test the feed consistency. The measurement was done using Rheomat RM180 which was installed in a rig apparatus specifically constructed in JKMRC (Figure 4-2). The

viscosity rig was constructed specifically for slurry to avoid particles settling and ensure homogenized mixing.

Figure 4-2: Rheomat RM180 installation on viscosity rig at JKMRC

4.3 Results and Discussion of Experiment with 40% Solids Feed

4.3.1 Operating condition range

One of the primary control systems of hydrocyclone operation is by observations of shape of underflow discharge (Neesse et al., 2004). This has been a necessity in hydrocyclone practice since the old days to determine whether hydrocyclone is performing well or not. Visual observation is the easiest and straight forward way to conduct the observation.

Table 4-1 provides the summary of visual observations of the hydrocyclone applying 40% silica solids concentration slurry. According to the results in this table, the vertical hydrocyclone could operate even at low pressure to produce both underflow and overflow stream and had no trouble in moderate and high pressure. However, the hydrocyclone at semi-inverted positions requires higher pressure as inclination goes higher. Operation at 120^{o} and 50 kPa has an underflow stream, whereas at the same pressure at 135^{o} there was no underflow stream. These results suggest that semi-inverted operation of hydrocyclone has different operating range.

Table 4-1: Observation on hydrocyclone discharges applying 40% solids silica slurry

Inclination (degrees)	Pressure (kPa)	Observed Discharge
0	25	No overflow
	30	Overflow starts running
	80	Spray underflow
	120	Spray underflow
105	80	Spray underflow
	140	Spray underflow
120	50	Very small flow of underflow
	80	Small flow of underflow
	125	Not available to observe
135	70	No underflow
	80	Very small flow of underflow
	100	At the edge of roping appearance
	140	Nice spray

4.3.2 Trend Results and Discussion

4.3.2.1 Feed stability

The first point of analysis in this section was the examination of solids concentration of feed and the F_{80} values. The data are given by Table 4-2. The data are presented according to the sequence of sampling.

Table 4-2: Feed solids concentration and F_{80} of experiments with 40% solids silica

Operating Condition	Feed % solids	F80 (micron)
0^o - 100 kPa	42.6	94.7
0^o - 100 kPa (II)	41.9	95.3
0^o - 120 kPa	42.9	95.1
0^o - 80 kPa	42.0	93.6
135^o - 80 kPa	42.5	89.8
135^o - 100 kPa	41.9	90.0
135^o - 120 kPa	41.9	90.4
120^o - 120 kPa	41.6	89.4
120^o - 120 kPa (II)	41.4	91.1
120^o - 100 kPa	41.7	90.2
120^o - 80 kPa	42.1	91.3
105^o - 120 kPa	42.0	89.9
105^o - 100 kPa	42.1	90.8
105^o - 80 kPa	42.7	93.4
105^o - 80 kPa (II)	43.6	94.3

From Table 4-2, it can be seen that the feed solids percentage is stable throughout sampling campaign at around 42% solids by weight (21% solids by volume). To overcome material loss due to sequence of samplings, more silica and water were added to the system during the 120^o – 120 kPa operation but it did not seem to affect solids concentration in the system. However, towards the end of experiment the feed solids percentage was increasing. The reason for this might be due to malfunctioning overflow tube causing some water and fine particles loss.

Around a 5 micron variation in the feed size was also recorded as Table 4-2 shows. The possible explanation for this inconsistency is that some of the coarse-grains might have settled and clung in the bottom of the sump, since the semi-inverted tests were performed several days after the vertical tests.

Three sampling repeats were done and all the repeats show very small deviations on solids concentration and F_{80} (0.507 and 0.467 for 0^o – 100 kPa, 0.195 and 1.206 for 120^o – 120 kPa, and 0.621 and 0.690 for 105^o – 80 kPa). This indicates good confidence in the results.

The viscosity test results for 40% solids silica slurry is given by Table 4-3. The results were generated at a single shear rate of one thousand per second. This table reveals that the viscosity decreased slowly with temperature, but the difference is negligible at the maximum experiment temperature of 43^oC. Slurry temperature during the experiment was between 29^oC and 43^oC.

Table 4-3: Viscosity measurement on 40% solids silica slurry

Temperature (^oC)	Torque (mN.m)	Shear stress, τ (Pa)	Viscosity (cP)
28.3	1.167	46.6	46
32.2	1.135	45.3	45
36.3	1.130	44.9	45
37.9	1.104	44.0	44

Based on results on feed concentration, feed size F_{80}, and viscosity tests, it can therefore be assumed that the feed properties were relatively constant, with a few anomalous points which have been marked with caution.

4.3.2.2 Pressure – Flowrate Relationship

Pressure – flowrate relationship for different hydrocyclone positions is presented in Figure 4-3. The graph shows flowrate response to operating pressure of semi-inverted positions is similar with the vertical operation. Their trends agree with the previously established pressure – flowrate relationship on normal hydrocyclone operation, that at a given slurry condition and fixed hydrocyclone dimension, flowrate and pressure will give a fixed relationship (Bradley, 1965, Svarovsky, 1984). This suggests that the dominant pressure drop occurs on the feed flows through the smallest section of the feed inlet.

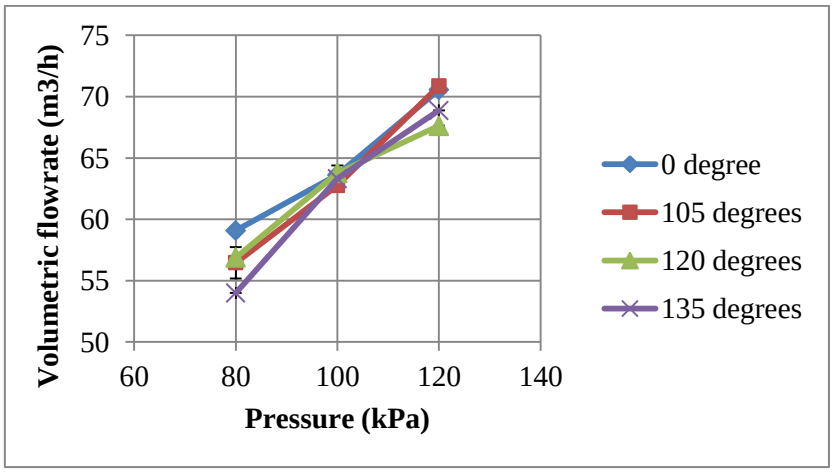

Figure 4-3: Flowrate response to pressure for 40% solids silica feed

4.3.2.3 Water Recovery, Cut Size, and Separation Sharpness

Water recovery responses to inclinations and pressure at semi-inverted operation are presented in Figure 4-4. Strong evidences of effective reduction of water recovery to underflow were found at semi-inverted position. It drops from around 20% at vertical position to around 10% at 105^{o} and 120^{o}. The most significant result is that at 135 degrees water recoveries are reduced to 5%. Further reduction to 3% was achieved by lowering pressure to 80 kPa. At this operating condition, the appearance of underflow stream was similar to roping (see Table 4-1), but alpha was still high as pointed out later in this section.

This reduction of water recovery to underflow was followed by the increasing of solids percentage of underflow at semi-inverted inclinations as shown in Table 4-4. At 135 degrees operating at 80 kPa, the underflow concentration was almost 80% solids. The overflow concentration increased gradually with inclinations. At 135 degrees, the overflow solids concentration was closed to the feed concentration.

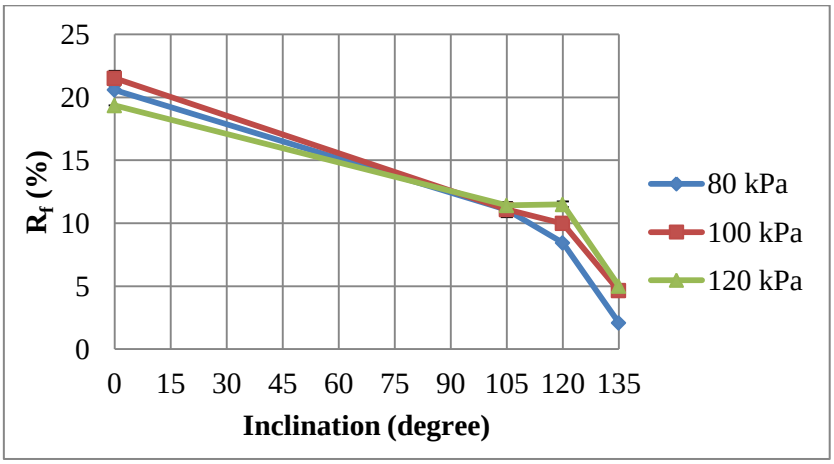

Figure 4-4: Water recovery versus inclinations for 40% solids silica feed

Error bars are available for conditions that have repeats. Those are 0.577 for 0^{o} – 100 kPa, 0.225 for 120^{o} – 120 kPa, and 0.597 for 105^{o} – 80 kPa. Most of the errors are so small that the bars are not visible. This is also applied to plot diagrams in all chapters.

Table 4-4: Solids percentage data for all streams from 40% solids silica experiment

Inclination : 0 degree				
Stream	**80 kPa**	**100 kPa**		**120 kPa**
	% Solids	**% Solids 1**	**% Solids 2**	**% Solids**
Feed	42.0	42.6	41.9	42.9
O/F	28.6	29.1	28.4	30.3
U/F	66.3	65.8	66.0	67.5

Inclination : 105 degrees				
Stream	**80 kPa**		**100 kPa**	**120 kPa**
	% Solids 1	**% Solids 2**	**% Solids**	**% Solids**
Feed	42.7	43.6	42.1	42.0
O/F	32.6	33.1	31.2	30.0
U/F	74.6	74.5	74.5	75.2

Inclination : 120 degrees				
Stream	**80 kPa**	**100 kPa**	**120 kPa**	
	% Solids	**% Solids**	**% Solids 1**	**% Solids 2**
Feed	42.1	41.8	41.6	41.4
O/F	33.1	31.6	31.5	30.8
U/F	76.6	75.1	72.5	73.3

Inclination : 135 degrees			
Stream	**80 kPa**	**100 kPa**	**120 kPa**
	% Solids	**% Solids**	**% Solids**
Feed	42.5	41.9	41.9
O/F	40.2	37.4	37.4
U/F	79.3	76.6	75.3

The water recovery responses to pressures at all inclinations are presented in Figure 4-5. At vertical operation, water recovery to underflow tends to decline as pressure increases. This result confirms normal behaviour on conventional hydrocyclone. On the contrary, there are tendencies of increasing water reporting to underflow as pressure increases at semi-inverted operations. This might be explained by the changing of force balance within semi-inverted body. At semi-inverted positions, the gravity force will drive water towards the overflow outlet. In consequence, operation at low inlet pressure will reduce amount of water passing through underflow discharge thus reducing water recovery, and vice versa.

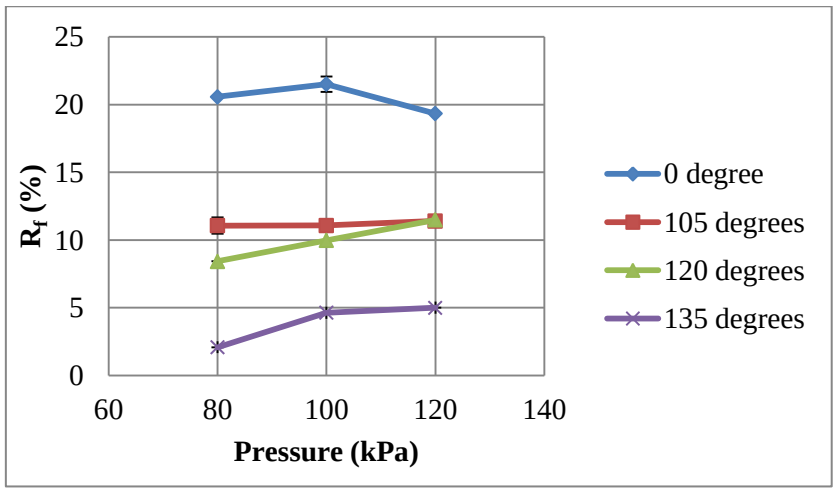

Figure 4-5: Water recovery to underflow versus pressure for 40% solids silica feed

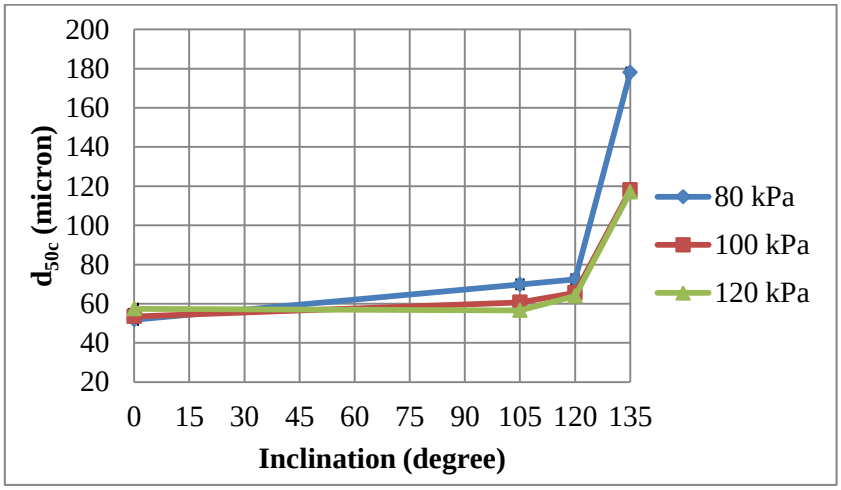

Figure 4-6: Corrected cut sizes response to inclinations for 40% solids silica feed

Figure 4-6 provides information of how inclination affects corrected cut size, d_{50c}. As shown in the graph, it can be generally concluded that semi-inverted hydrocyclone cut coarser than vertical hydrocyclone. Generally these results agree with the previous reports by Asomah (1996) and Rong and Napier-Munn (2003). The increasing cut size is more pronounce at low pressure of 80 kPa. At 120 kPa cut size is remain steady from vertical to 105 degrees before increase at higher inclinations.

The most surprising finding in Figure 4-6 is separation become very coarse at 135 degrees. At this angle, cut sizes are 2.5 times higher at 80 kPa and two times higher at 120 kPa compare to cut sizes on vertical position. This can be explained by the significant drop of solids recovery to underflow as shown in Figure 4-7. Only 10 to 20 per cent of feed solids appear on the underflow at 135 degrees,

result in very high solids concentration underflow product and overflow product closed to feed concentration (see Table 4-4). Consequently, cut size becomes very coarse.

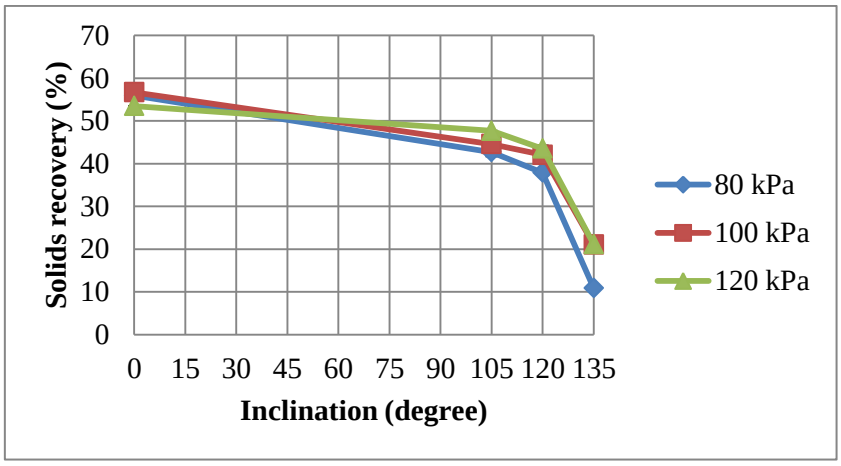

Figure 4-7: Solids recovery to underflow response to inclinations for 40% solids silica feed

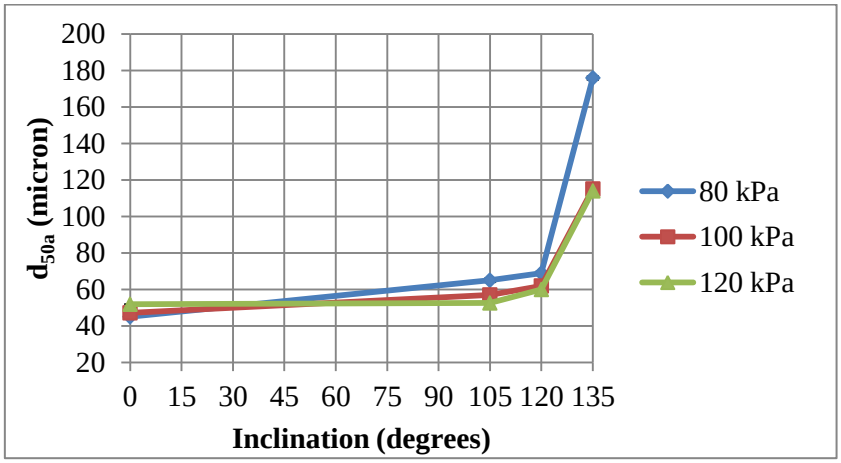

Figure 4-8: Actual cut sizes response to inclinations for 40% solids silica feed

The change in water recovery in fact does not affect actual classification. From Figure 4-8, the actual cut size trends are very similar with the corrected cut size results (Figure 4-6). Thus, it can be argued that the increasing effect of cut size on semi-inverted hydrocyclone operation was not due to change in water recovery. Semi-inverted operation is in fact affecting the actual classification of solids particle within hydrocyclone body.

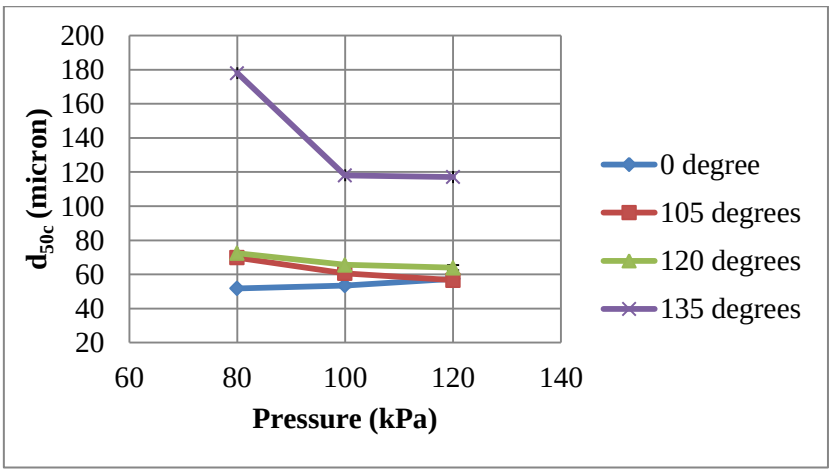

Figure 4-9: Corrected cut sizes response to pressure for 40% solids silica feed

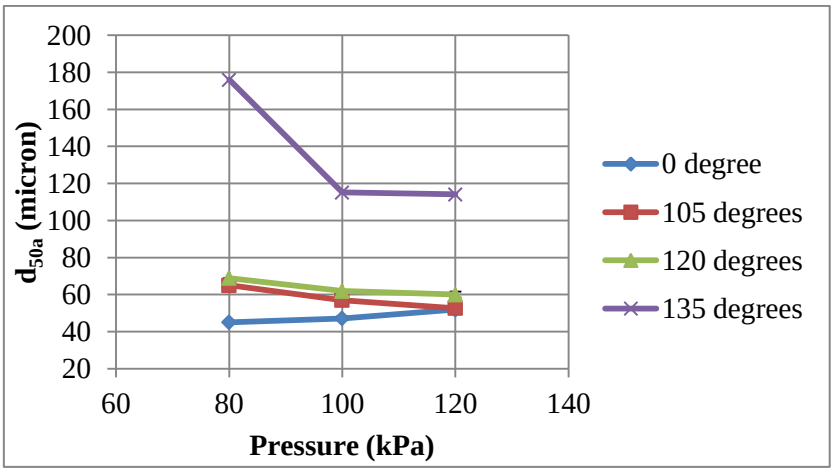

Figure 4-10: Actual cut sizes response to pressures for 40% solids silica feed

The graph in Figure 4-9 and Figure 4-10 show overviews of pressure influence to corrected and actual cut size on three semi-inverted positions. From the figures, it can be seen that cut size decreases with higher pressure. This result indicates cut size response towards pressure follows conventional hydrocyclone behaviour. Both graphs also reveal pressure influence on cut size is more pronounce at semi-inverted operation compared to vertical operation.

Analysis on alpha or efficiency parameter responding to inclination at semi-inverted operation is given in Figure 4-11. The chart reveals that compare to vertical operation, semi-inverted operated hydrocyclone has slightly lower alpha values, but alpha around 4 still indicates good separation. Some error bars indicates the results of the repeats give narrow standard deviations (0.05 for 0^o – 100 kPa, 0.17 for 105^o – 80 kPa, and 0.28 for 120^o – 120kPa).

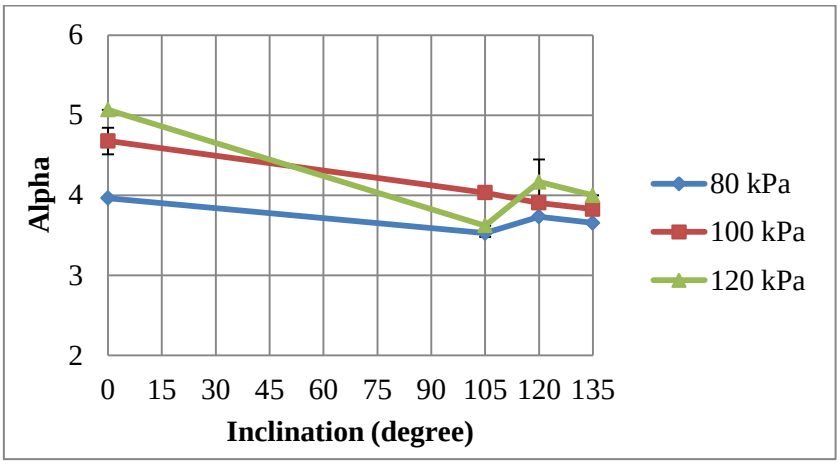

Figure 4-11: Sharpness of separation versus inclination for 40% solids silica feed

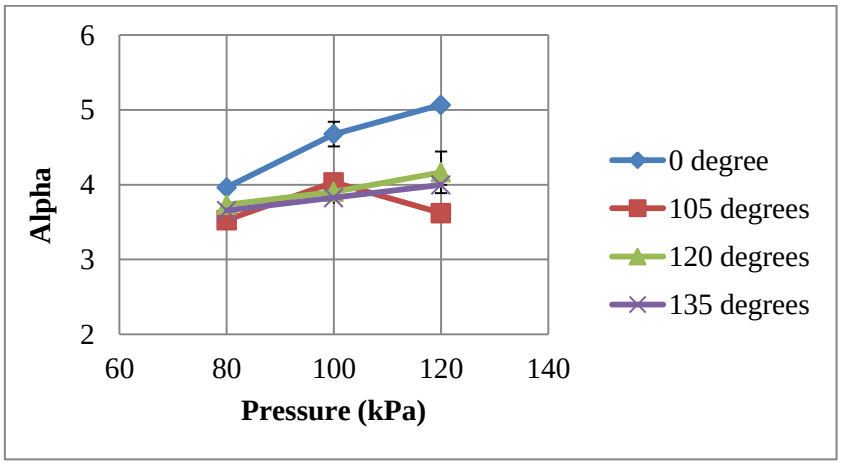

Figure 4-12: Sharpness of separation response to pressure for 40% solids silica feed

The response of separation sharpness to pressure on each inclination is given by Figure 4-12. No major difference on alpha was observed at the three semi-inverted angles, but gradual increase on alpha was shown at vertical position. These finding suggest that sharpness of separation of the tested hydrocyclone is not as pressure sensitive at semi-inverted operations as it is in vertical operation.

4.4 Conclusions

Through this experiment, the installation of the new cone has proven that the shorter, wider cone allowed the hydrocylone to perform at semi-inverted position, with maximum angle of 135 degree from vertical.

It has been identified in this chapter that with 40% feed solids concentration the semi-inverted hydrocyclone could increase cut size significantly and could achieve a very low water recovery to underflow, while it did not alter the separation sharpness. The underflow solids concentrations significantly increased with inclinations while the overflow solids concentration at 135 degrees almost has the same concentration with feed. This finding complements and conforms with the previous works on inclined hydrocyclone below horizontal positions.

The second major finding was the demonstration of pressure influence on cut size, water recovery, and separation sharpness at semi-inverted hydrocyclone. Water recovery slightly increases with pressure. On the contrary, cut size decreases with pressure and it is most significant at 135 degrees while at vertical operation cut size is less affected by pressure. Efficiency of separation is not pressure sensitive at semi-inverted positions. It has to be noted that these conclusions are only valid for the 250mm hydrocyclone and silica slurry which was tested.

CHAPTER 5 : Experiment with 50% Solids Feed Slurry with Modified Cone

The previous chapter has extensively discussed how the semi-inverted hydrocyclone performs under several operating pressure and semi-inverted positions compared with conventional vertical operation at a moderate feed concentration. It has also been reported in the previous chapter that the new cone with wide angle has successfully extended the semi-inverted operating range.

In this chapter, a further step of investigation on semi-inverted hydrocyclone is discussed. The theme central to this chapter will be the application of higher solids concentration of feed slurry. The previous experiments have been limited to single component feed concentration of 40%, this study will extend investigation on different feed solids concentration.

Feed solids concentration is another important variable that has long been accepted as being critical to hydrocyclone separation (Bradley, 1965, Braun, 1990, Asomah, 1996, Kuang et al., 2012). Feed solids concentration effect to conventional hydrocyclone performance has been reviewed in Chapter 2 although no information on semi-inverted operation was found.

Although extensive researches on feed solids concentration have been carried out, most of those studies have only focussed on its influence on angle below horizontal and vertical position. No previous study has given sufficient consideration on feed solids influence on semi-inverted hydrocyclone except Asomah's thesis (1996). Moreover, Asomah's 500 mm hydrocyclone has been limited with maximum solids percentage of 33% solids at 135 degrees.

It is still unknown whether a moderate size hydrocyclone with 250 mm diameter could respond in a similar manner to Asomah's finding. Additionally, there was lack of information on high feed solids concentration (40 to 50% solids) influence at semi-inverted angles (105 to 135 degrees) on separation performance. Therefore, this chapter will try to fill in these gaps to give better understanding on semi-inverted hydrocyclone operational limits.

5.1 Experimental Setup

The experiment was done in exactly the same hydrocyclone rig as the 40% solids slurry. All the equipment, materials, and methods were also the same (see sub-section 3.1.1 in Chapter 3).

The only difference was the concentration level of solids within the slurry system. The targeted slurry system was 50% solids. Since this experiment was adjoined with experiment with 40% solids concentration, there was slurry leftover inside the sump with concentration around 42 – 43 % solids.

To reach a sufficient material inside the rig system with solids concentration of 50%, additional silica and water were added.

5.2 Results and Discussion: Experiment with 50% Solids Feed

5.2.1 Operating Condition

Visual observation on discharge was done in the first place. The observation was necessary to test whether semi-inverted hydrocyclone that have been supported with the new cone could also perform normally on 50% solids. The shape of underflow discharge was used as an indicator of operation. The results are presented in Table 5-1.

Table 5-1: Observation on hydrocyclone discharges applying 50% solids silica slurry

inclination (degrees)	Pressure (kPa)	Observed underflow discharge
135	60	start flowing
	80	roping appearance
	85	at the edge of roping appearance
	120	spray
	140	nice spray

It could be seen from the Table 5-1 that at 135 degrees from vertical, hydrocyclone started to work well at pressure more than 85 kPa since lower pressure could only produce underflow of similar appearance to roping. The operation of 140 kPa was optimal as it gave stable spray discharge.

Compared to operation with 40% solids concentration in Chapter 4 (see Table 4-1), these conditions indicate that higher pressure region is preferable at 135 degrees with 50% solids concentration.

This roping-like discharge condition of the semi-inverted hydrocyclone is not initiated by the same mechanism with conventional hydrocyclone. While for the conventional hydrocyclone roping is caused by feeding over capacity of spigot discharge, the appearance of roping on semi-inverted hydrocyclone was probably initiated by insufficient amount of water report to spigot discharge. This

affected the fluid force of the slurry to reach the spigot discharge. Therefore, the intensity of the discharge was low compared with the roping condition on conventional vertical hydrocyclone.

5.2.2 Trend Results and Discussion

5.2.2.1 Feed stability

The solids percentage and particle size passing 80% of feed stream by sampling sequence is given by Table 5-2. This information can be used to see how feed characteristic changed through the sampling campaign. It is apparent that there were decreases of feed solids concentration and feed size through the experiments. The first was when angle during vertical operations and the second was when hydrocyclone was turned to angle of 105 degrees.

Table 5-2: Feed solids concentration and F_{80} of experiments with 50% silica slurry

Operating condition	Feed % Solids	F_{80} (micron)
0^o - 120 kPa	50.3	111.4
0^o - 100 kPa	49.7	105.8
0^o - 80 kPa	48.7	96.5
135^o - 140 kPa	48.8	93.7
135^o - 120 kPa	48.7	94.2
135^o - 120 kPa (II)	48.6	94.0
135^o - 100 kPa	48.7	93.8
120^o - 120 kPa	48.7	93.6
120^o - 120 kPa (II)	49.0	94.4
120^o - 100 kPa	48.9	94.0
120^o - 80 kPa	48.8	94.1
105^o - 120 kPa	47.2	84.3
105^o - 100 kPa	47.4	85.0
105^o - 80 kPa	47.7	84.9

The reason for the change of feed concentration was a stirrer malfunctioning reported at the beginning of vertical hydrocyclone testing. Lack of stirring actions might have caused some coarse particles settled in the bottom of the sump progressively. This is marked by gradual reduction of F_{80} (blue line). The stirrers were back in use at 135 degrees operation.

At 105 degrees, the feed solids percentage dropped 2 to 3 per cent. This may be due to loss of underflow product when the rubber line disengaged for several second right before sampling was performed. The stream was containing more than 70% solids, hence the solids percentage inside the system decreased.

5.2.2.2 Pressure – Flowrate Relationship

The flowrate – pressure relationship on vertical and semi-inverted angles are illustrated by Figure 5-1. From the figure, it can be said that the volumetric throughput of hydrocyclone increases with operating pressure, and this applied to both vertical and semi-inverted inclinations. The trend is similar with the data provided by Figure 4-3 in the previous case with 40% slurry concentration. These results conform with conventional hydrocyclone operation.

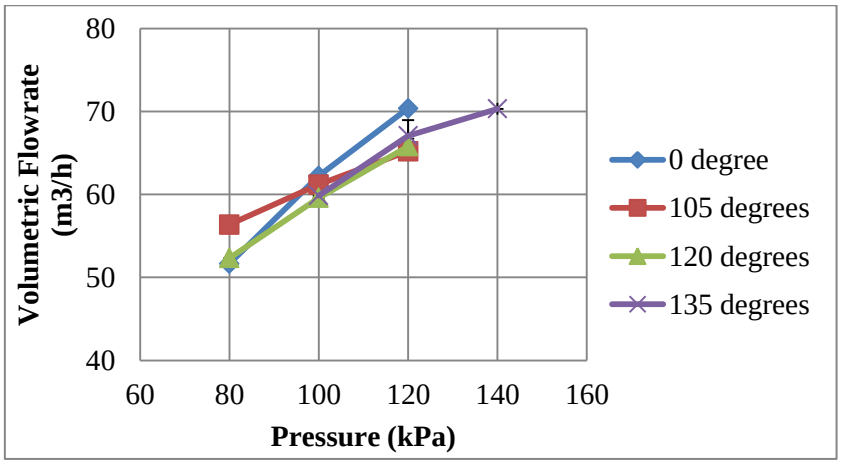

Figure 5-1: Feed flowrate vs operating pressure for 50% silica feed

5.2.2.3 Water Recovery, Cut Size and Separation Sharpness

Water recovery to underflow declines as hydrocyclone put into semi-inverted position as summarised in Figure 5-2. At 80 kPa, water recovery drops significantly from 35% at vertical position to 12% at semi-inverted operations. At higher operating pressure, similar reductions were also observed. In other words, changing hydrocyclone orientation from vertical to semi-inverted could reduce water recovery to underflow by a minimum of 50%. With steady water recovery around a 11% at all semi-inverted operations, the underflow and overflow solids concentrations were relatively unaffected as given in Table 5-3.

With standard deviation 0.35 for 135^{o} – 120 kPa and 0.10 for 120^{o} – 120 kPa, the error bars are not visible in the Figure 5-2. Deviations is also not visible for the rest diagrams as repeats indicate very small deviations.

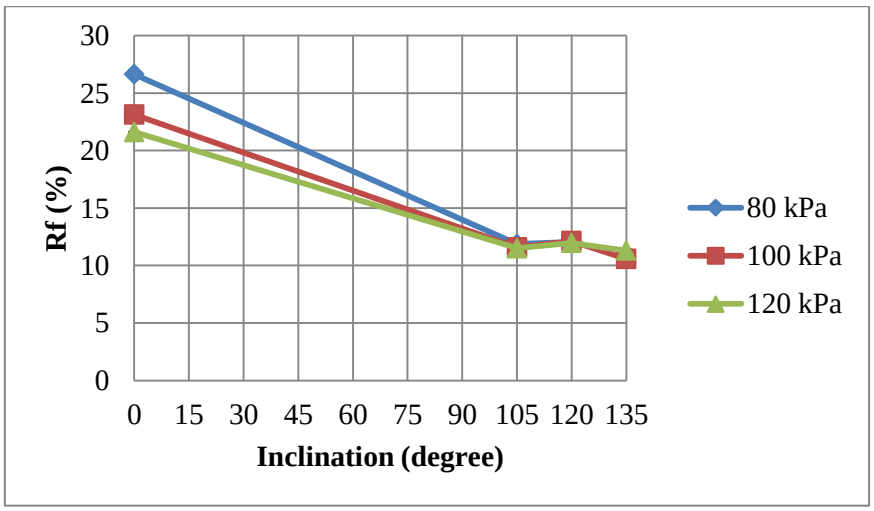

Figure 5-2: Water recovery to underflow versus inclinations for 50% silica feed

Table 5-3: Solids percentage data for all streams from 50% solids silica experiment

Inclination : 0 degree			
Stream	**80 kPa**	**100 kPa**	**120 kPa**
	% Solids	**% Solids**	**% Solids**
Feed	48.7	49.8	50.3
O/F	36.8	38.2	39.5
U/F	65.1	69.0	69.8

Inclination : 105 degree			
Stream	**80 kPa**	**100 kPa**	**120 kPa**
	% Solids	**% Solids**	**% Solids**
Feed	47.7	47.4	47.2
O/F	40.5	40.4	40.3
U/F	72.4	72.3	72.1

Inclination : 120 degree				
Stream	**80 kPa**	**100 kPa**	**120 kPa**	
	% Solids	**% Solids**	**% Solids 1**	**% Solids 2**
Feed	48.8	48.9	48.7	49.0
O/F	41.6	41.1	40.7	40.6
U/F	73.1	74.0	74.1	75.4

Inclination : 135 degree				
Stream	**100 kPa**	**120 kPa**		**140 kPa**
	% Solids	**% Solids 1**	**% Solids 2**	**% Solids**
Feed	48.7	48.8	48.6	48.8
O/F	41.8	41.5	41.3	41.3
U/F	74.4	74.1	73.9	73.3

There was no significant difference of water recovery between the three semi-inverted angles. Compared with operation with 40% silica in the previous chapter, water recovery could not be further reduced at 135 degrees. This indicates that 10% water recovery to underflow is a possible constraint when semi-inverted hydrocyclone operating with 50% silica concentration.

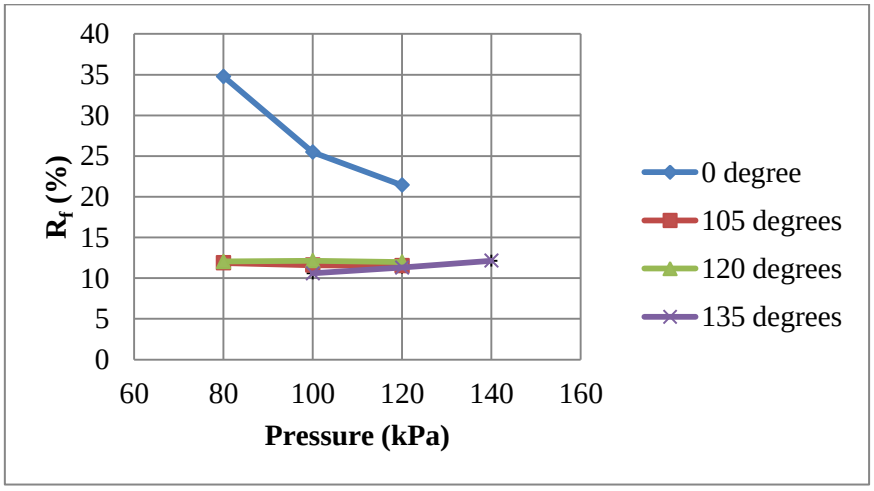

Figure 5-3: Water recovery to underflow response to pressure for 50% silica feed

Influence of pressure on water recovery to underflow is given by Figure 5-3. The figure reveals that at all three semi-inverted inclinations water recovery are constant. This finding disagrees with conventional vertical operation, where increase in pressure decrease water recovery to underflow if all other variables are kept constant. This result also suggest that a physical constraint is occurring at semi-inverted operations with 50% solids feed.

Information at 135 degrees at 80 kPa was unavailable since operation at that condition produced underflow discharge similar to roping as previously explained in Section 5.2.1. One pressure point of 140 kPa was performed to complete three pressure levels at 135 degrees.

Figure 5-4 presents interactions between corrected cut size (d_{50c}) and inclination under various pressures. From the graph, corrected cut size increases as inclination increases at all operating pressures. More pronounce response is given by the lowest pressure operation of 80 kPa.

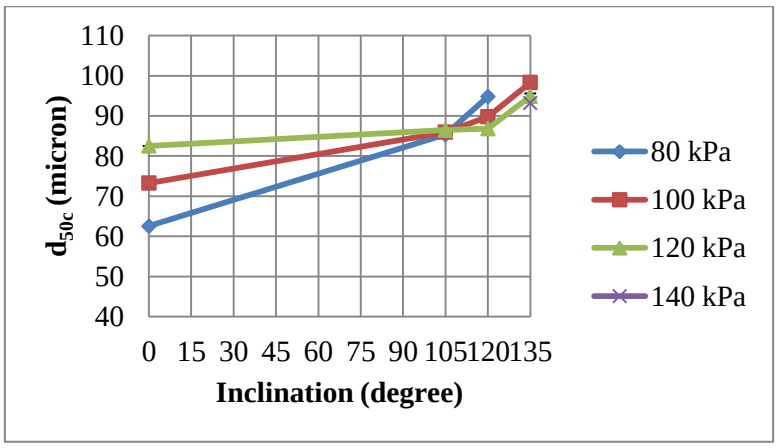

Figure 5-4: Corrected cut sizes response to inclinations for 50% silica feed

There is no extreme jump of cut size at 135 degrees as was observed with 40% solids silica feed (see Chapter 4). This can be explained with the fact that with 50% solids concentration (25% – 27% solids by volume), the amount of solids reporting to underflow were 32% – 35% on 100 kPa – 140 kPa operating pressure, while compared to 10% – 21% on 80 kPa – 120 kPa operating pressure with 40% solids concentration (or 21% solids by volume). To put into words, with 50% solids feed, operation at 135 degrees were able to deliver more solids to underflow product compared with operation with 40% solids feed at the same angle. Consequently, cut size rises significantly.

This change in corrected cut size, however, might not be entirely due to the change on amount of water reporting to underflow. Semi-inverted operation is in fact influential on actual classification which is denoted by actual cut size, d_{50a}. This is illustrated in Figure 5-5. As shown by the graph, actual cut size increases with inclination. Similarly with corrected ones, the magnitude of cut size rise was the highest at the lowest pressure.

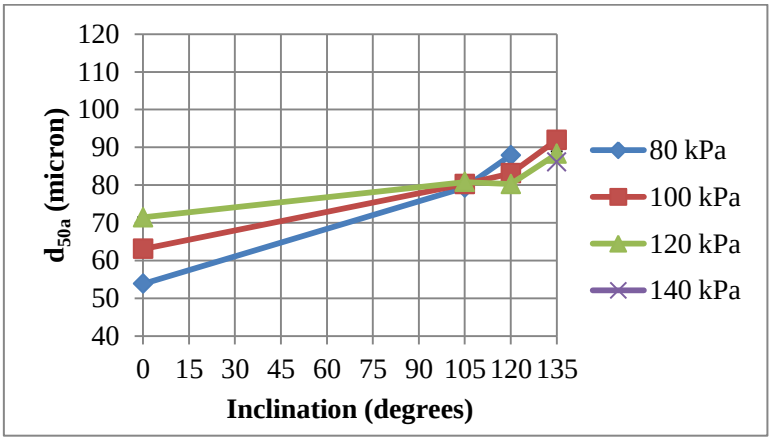

Figure 5-5: Actual cut sizes response to inclinations for 50% silica feed

The pressure influence on corrected and actual cut size is shown in Figure 5-6 and Figure 5-7. At vertical operation, cut size increases with pressure, which contradicts the behaviour of conventional hydrocyclone. Reason for this is substantial variation on the feed size caused by malfunctioning sump stirrers as mentioned in subsection 5.2.2.1.

At semi-inverted operations, pressure was found to cause a reduction on both corrected and actual cut sizes, most apparent on 120 degrees and 135 degrees. This result agrees with conventional hydrocyclone behaviour.

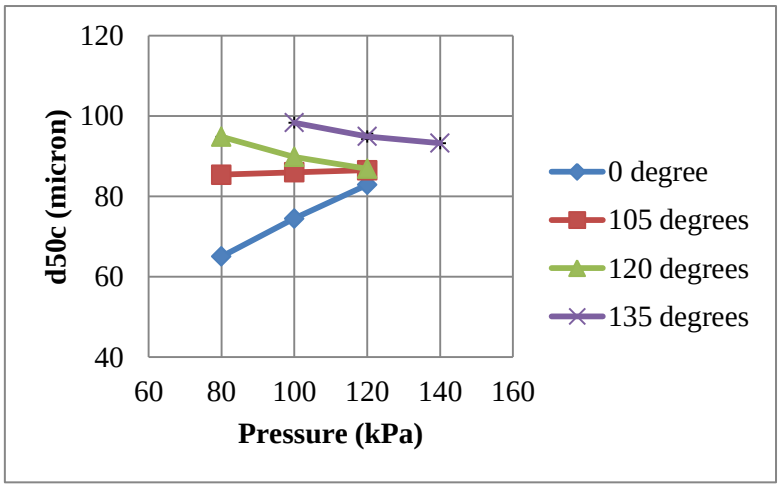

Figure 5-6: Corrected cut sizes response to pressures for 50% silica feed

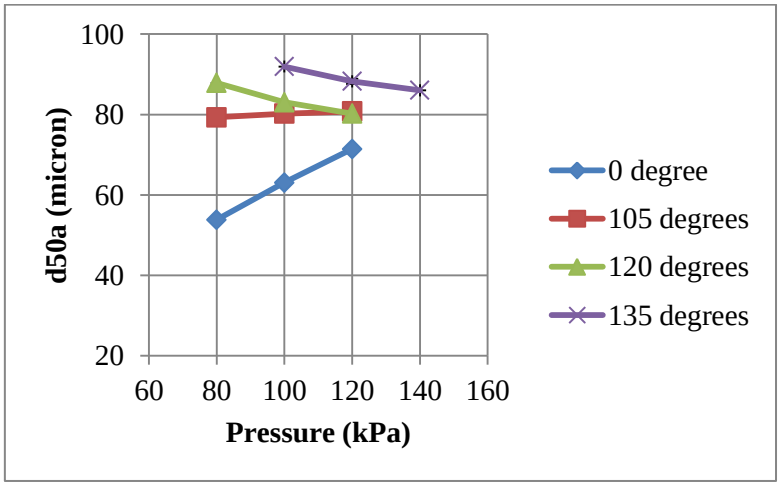

Figure 5-7: Actual cut sizes response to pressures for 50% silica feed

Analysis of separation sharpness for operation with 50% solids concentration slurry is presented in Figure 5-8. From the chart, it can be seen that semi-inverted angles reduce sharpness at low pressure but not for moderate and high pressure. At 120 degrees and 135 degrees angle, sharpness drops slightly. However, the benefit of having very low water recovery to underflow (Figure 5-2) overcomes this minor disadvantage.

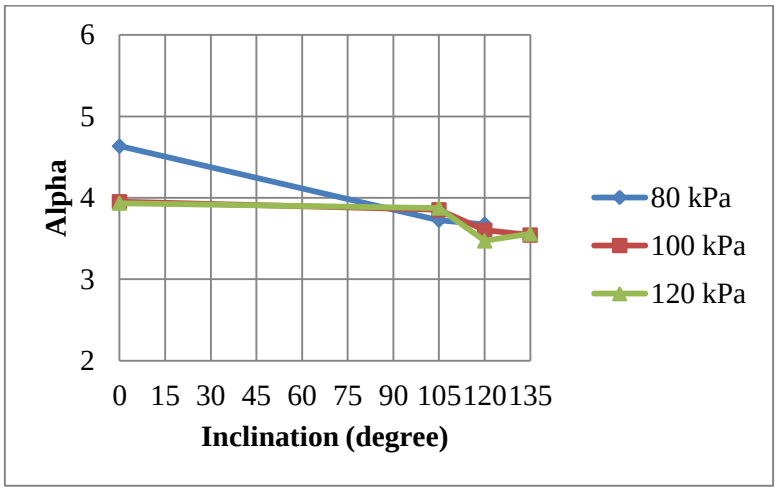

Figure 5-8: Sharpness of separation versus inclination for 50% silica feed

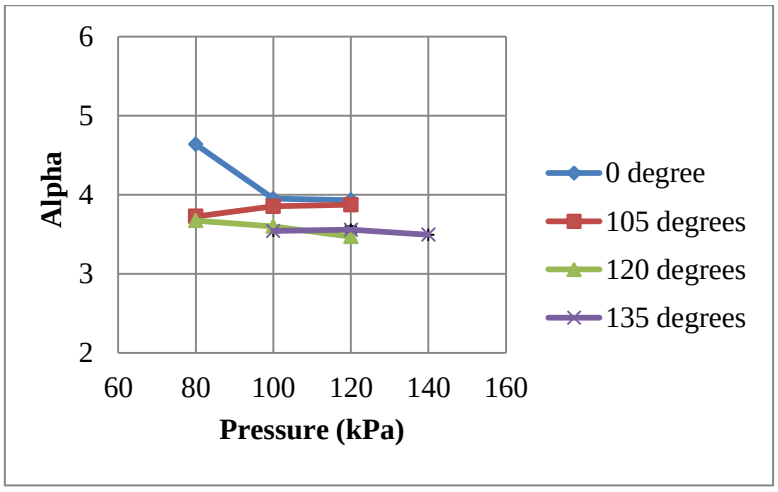

Figure 5-9: Separation sharpness response to pressure for 50% silica feed

In relationship with pressure, Figure 5-9 presents sharpness of separation is almost constant at all inclinations. Even though there seems a slight decrease of alpha with increasing operating pressure at vertical operation, the result might be biased with the overestimation of the fitted curve as can be seen in Appendix A.7.

5.3 Conclusions

In this chapter, the assessment of semi-inverted hydrocyclone applying higher feed solids concentration of 50% solids at various operating pressure have been discussed.

From the results, it has been shown that inclination can increase both actual and corrected cut size even at higher solids concentration. Even though, there was no extreme jump of cut size at 135 degrees as previously found at 40% solids. Solids recovery to underflow is higher with 50% solids feed, thus preventing a very coarse cut at 135 degrees.

Water recovery to underflow was reduced significantly at semi-inverted positions compared with the vertical position, but the results do not seem to have any difference between the three semi-inverted inclinations, suggesting a physical limit has been reached. Consequently, the underflow and the overflow solids concentration remained almost unaffected at semi-inverted operations. Sharpness is slightly diminished with inclinations but the alpha values are still reasonably high, indicating stable separation.

One of important findings in this investigation is the effect of pressure on semi-inverted hydrocyclone performance. It was found that pressure is inversely related with cut size at semi-inverted operation, while the result at vertical operation is biased with feed variation. There is no influence of pressure on water recovery to underflow and sharpness at semi-inverted angles.

CHAPTER 6 : Experiment of 40% Solids Mixed Density Slurry with Modified Cone

Previous studies have established the importance of feed density on hydrocyclone performance (see Chapter 2). However, researches to date have provided very little information about the influence of density variation on semi-inverted hydrocyclone operation. This study aims to investigate the classification performance of semi-inverted hydrocyclone with different slurry density from the previous experiments. Furthermore, an investigation of asymmetrical air core was also conducted. Therefore, this chapter provides new insights into understanding on semi-inverted hydrocyclone operations under different feed conditions, particularly with feed contain mineral of different density.

6.1 Experimental Setup

This experiment was prepared in continuation of previous work of 40% solids and 50% solids silica slurry. The majority of the experimental setups have been described in Chapter 3, while the new modified cone utilised in this experiment is explained in Chapter 4.

Table 6-1: Particle size distribution of magnetite

Sieve size (micron)	% weight retain
150	0.32
125	0.40
106	0.80
90	1.07
75	1.76
63	2.87
53	5.51
45	9.74
38	14.76
-38	62.79

In order to vary solids density from the previous silica experiment, a slurry containing 40% solids of a silica-magnetite mixture was prepared. The magnetite has 80% of particles passing 42 microns. The magnetite size distribution used in this experiment is given by Table 6-1.

Magnetite was added into the slurry with magnetite to silica ratio of 20:80. Typical specific gravity (SG) for silica is 2.7 and for magnetite is 5.2. The overall solids mixed density is approximately 3.2. The targeted volumetric concentration is 17.5%, slightly less than 40% weight silica case which is 19.8%. The change is assumed to be insignificant to the result.

6.2 Results and Discussion of Experiment with 40% Solids Mixed Density Feed

6.2.1 Operating Condition Range

The operating condition was examined prior to sampling campaign. The result of the observation is summarised by Table 6-2.

Table 6-2: Observation on hydrocyclone discharges applying 40% solids mixture slurry

Inclination (degrees)	Pressure (kPa)	Observed discharge
105	40	Small flow
	80	Spray
	100	Spray
	120	Spray
120	50	Small flow
	80	At the edge of roping appearance
	100	Spray
	125	Spray
135	50	Small flow of underflow
	100	Roping appearance
	120	Nice spray

From Table 6-2, it can be argued that at semi-inverted hydrocyclone needs a higher operating pressure to achieve normal operating condition. This is indicated by the fact that underflow discharge condition shows roping-like appearance at 100 kPa. Only when pressure is set to 120 kPa

the underflow produced spraying discharge. At 120 degrees, underflow is still in a transition state between roping-like appearance and spraying at 80 kPa. At lower inclination of 105 degrees, the same pressure level can produce spraying underflow discharge. Additionally, compare to observation on operation with 40% solids silica slurry (chapter 4), operation at 135 degrees with 40% silica-magnetite starts at slightly higher pressure.

The results suggest that semi-inverted angle of 105 degrees can be operated at low operating pressure while higher angle operations (120 degrees and 135 degrees) could only be benefited at high pressure regions.

6.2.2 Trend Results and Discussion

6.2.2.1 Feed Stability

Feed solids concentration and feed size for the experiment with mixed feed are summarized in Table 6-3. The feed solids concentration was consistent around 43% solids by weight (19.5% solids by volume) through the whole experiments although the value was slightly over the targeted 40% solids by weight (17.5% solids by volume). This is similar to the case with 40% silica. It is possible that during material preparation the amount of water added to the sump was less due to measurement error, therefore the achieved solids concentrations were a little over the target of 40%.

Table 6-3: Feed characteristic during experiment with 40% solids mixture slurry

Operating Condition	Feed % Solids	F_{80} (micron)
0^o - 80 kPa	43.3	87.1
0^o - 100 kPa	43.0	86.4
0^o - 100 kPa (II)	42.9	83.9
0^o - 120 kPa	43.1	88.3
135^o - 120 kPa	43.1	81.2
135^o - 120 kPa (II)	42.8	80.9
135^o - 140 kPa	42.9	82.3
135^o - 100 kPa	43.3	81.8
120^o - 80 kPa	43.0	83.6
120^o - 100 kPa	43.3	84.7
120^o - 100 kPa (II)	43.4	84.7
120^o- 120 kPa	42.8	83.9
105^o - 80 kPa	42.7	84.5
105^o - 80 kPa (II)	42.9	83.5
105^o - 100 kPa	42.7	83.9
105^o - 120 kPa	43.6	85.4

There was some indication of feed size reduction at initial the beginning of the experiments. A possible explanation for this might be that some coarse magnetite particles were being ground by the pump impeller. Magnetite is more susceptible to this unwanted grinding than because it is softer. After the experiment at 135 degrees, there was no further variation in the feed size.

The viscosity of slurry shows a gradual decrease as its temperature rises as shown in Table 6-4. The temperature of slurry during the experiment was between 26.2^{o}C and 36.4^{o}C. This decreasing trend with temperature characteristic confirms with normal behaviour of slurry.

Table 6-4: Viscosity measurement on 40% solids mixture slurry

Temperature (^{o}C)	Torque, M (mN.m)	Shear stress, τ (Pa)	Calc. Viscosity, η (Pa.s)
27.8	1.20	48.5	49
30.5	1.19	47.9	48
32.5	1.15	46.0	46
32.8	1.14	45.3	45

6.2.2.2 Pressure – Flowrate Relationship

The relationship of pressure and slurry flowrate applying 40% solids mixture slurry is established in Figure 6-1. Pressure increases with flowrate at each inclination. The result is also comparable with previous results on 40% solids and 50% solids silica cases (Figure 4-3 and Figure 5-1). These suggest semi-inverted hydrocyclone does not alter the previously well-established relationship between pressure and flowrate for normal (vertical) hydrocyclone.

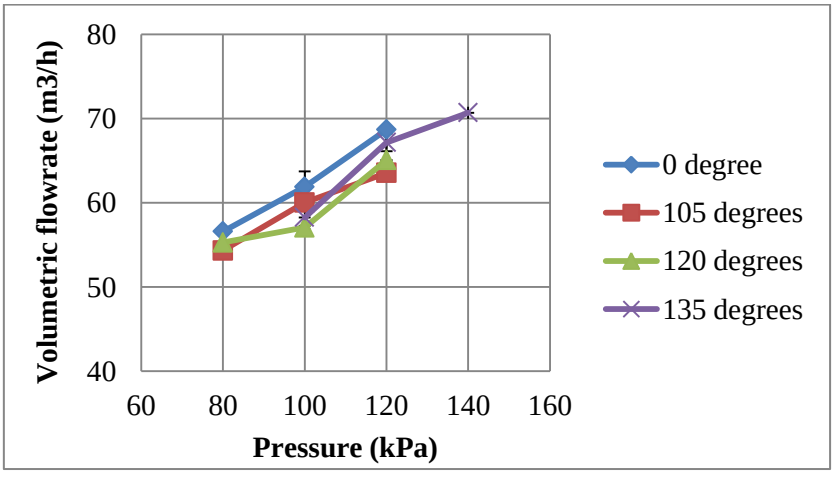

Figure 6-1: Pressure versus flowrate at various inclinations applying 40% silica-magnetite slurry

6.2.2.3 Water Recovery, Cut Size, and Sharpness of Separation

The results for water recovery, R_f, are shown in Figure 6-2. From the figure, it is shown that the semi-inverted hydrocyclone can greatly reduce water recovery to underflow. At 105 degrees, water recovery is reduced by half of that for zero degree operation. The reduction to only 5% is observed when semi-inverted hydrocyclone is turned to 135 degrees.

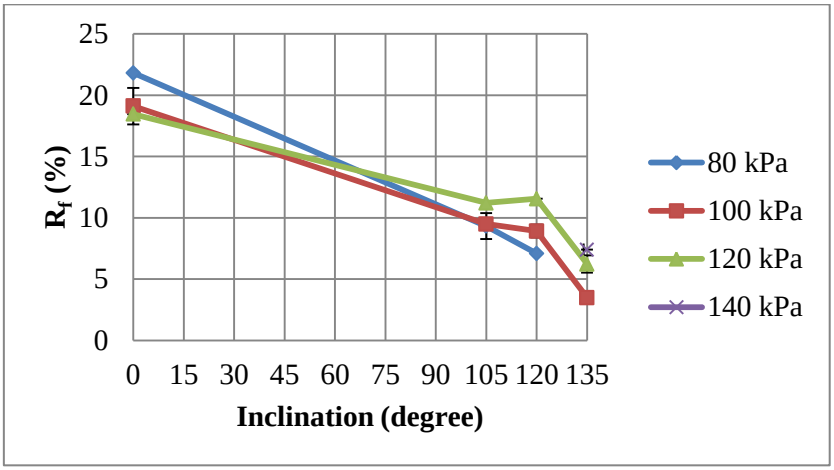

Figure 6-2: Water recovery to underflow versus inclinations on various pressures for 40% solids mixture slurry

The trends in Figure 6-2 are also similar with water recovery results using the 40% solids silica in Chapter 4 (Figure 4-4). This indicates that different solids density does not affect the water recovery response for a semi-inverted hydrocyclone. It may be possible that with real ores, which usually have certain range of particle densities, is applied to the same semi-inverted hydrocyclone under the same operating conditions, a similar low water recovery response will be produced.

Although deviations from repeats which are signified by error bars in Figure 6-2 and other diagrams in the rest of the chapter are slightly higher than those in chapter 4 and chapter 5, they still provide good confidence to the results.

Figure 6-3 shows that at vertical operation, water recovery gradually decreases with pressure, which confirms normal response for a conventional hydrocyclone. On the contrary, at semi-inverted operations, the water recovery to underflow increases with pressure. This indicates the energy balance for a semi-inverted hydrocyclone has shifted compared with vertical operation. For vertical operation, with low pressure operation, gravity will lead more water to report to the underflow. In semi-inverted operations, low pressure operation will let gravity drag water towards the overflow outlet, reducing water recovery to underflow. This result is similar to the results of additional experiments applying water only, as presented in Appendix B:.

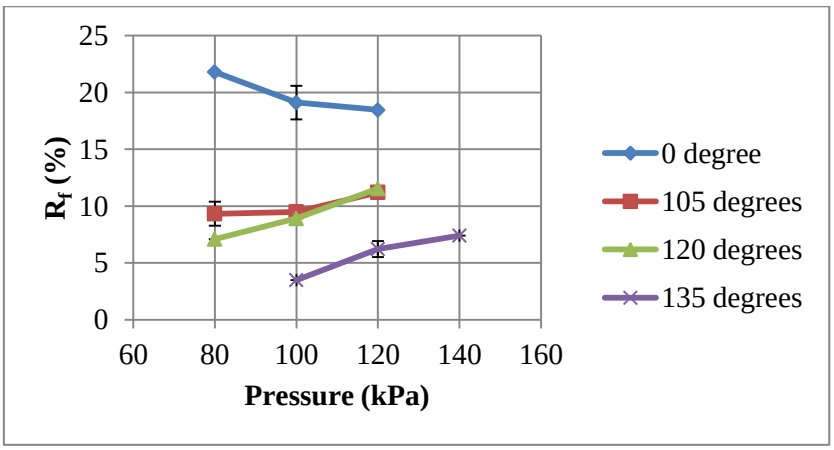

Figure 6-3: Water recovery to underflow versus pressure on various inclinations for 40% solids mixture slurry

Table 6-5: Solids percentage data for all streams from 40% solids silica-magnetite experiment

Inclination : 0 degree				
Stream	**80 kPa**	**100 kPa**		**120 kPa**
	% Solids	**% Solids 1**	**% Solids 2**	**% Solids**
Feed	42.7	43.0	42.9	43.1
O/F	29.9	28.7	30.7	30.3
U/F	66.3	68.2	68.2	68.8
Inclination : 105 degree				
Stream	**80 kPa**		**100 kPa**	**120 kPa**
	% Solids 1	**% Solids 2**	**% Solids**	**% Solids**
Feed	42.7	42.9	42.7	43.6
O/F	33.7	34.4	33.6	31.4
U/F	76.5	73.6	75.1	76.5
Inclination : 120 degree				
Stream	**80 kPa**	**100 kPa**		**120 kPa**
	% Solids	**% Solids 1**	**% Solids 2**	**% Solids**
Feed	43.0	43.3	43.4	42.8
O/F	36.5	34.7	34.7	33.9
U/F	75.6	76.4	75.5	71.9
Inclination : 135 degree				
Stream	**100 kPa**	**120 kPa**		**140 kPa**
	% Solids	**% Solids 1**	**% Solids 2**	**% Solids**
Feed	43.3	43.1	42.8	42.9
O/F	40.1	35.6	36.3	35.1
U/F	77.1	78.3	78.5	77.2

The smaller water recovery that is achieved at higher inclination has leaded to the increasing of underflow and overflow product solids concentration as highlighted in Table 6-5. This result is similar with the result with the 40% silica feed in Chapter 4.

The water recovery responses to inclination and pressure with the 40% mixture minerals in Figure 6-2 and Figure 6-3 give similar trends with the experiment with 40% silica (see Figure 4-4 and Figure 4-5 in Chapter 4). This suggests that solids density is not significant to the water recovery response on semi-inverted hydrocyclone.

From the information given in Figure 6-3, the water recovery can be reduced substantially at low pressure operation by turning the hydrocyclone to semi-inverted inclination. Operatios at low pressure with the semi-inverted hydrocyclone will not only reduce water recovery to underflow but also increase cut size.

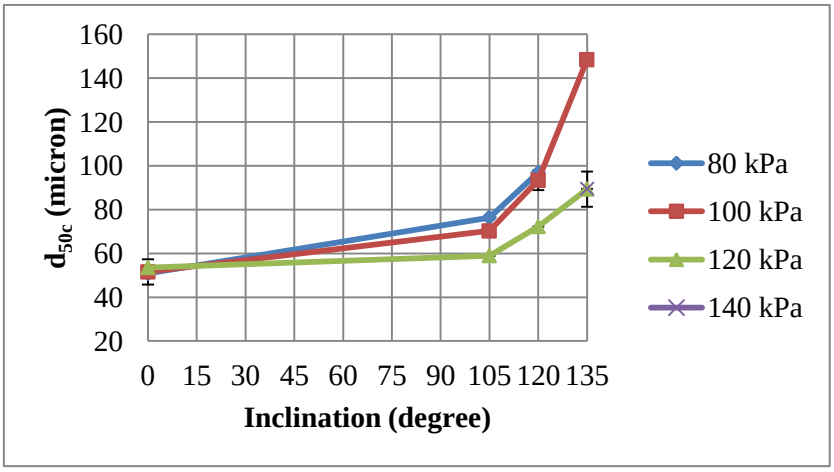

Figure 6-4: Corrected cut size versus inclination on various pressures for 40% solids silica-magnetite slurry

This change in water recovery to underflow with semi-inverted operations might also affect cut size of separation. The influence of inclination on corrected cut size for 40% solids slurry with mixed minerals is presented in Figure 6-4. The corrected cut size rises with an increase in inclination. Semi-inverted operation at 135 degrees produces the coarsest cut size at three times that of vertical operation. The result at 80 kPa was not available since there was very small flow of underflow discharge with appearance similar to roping.

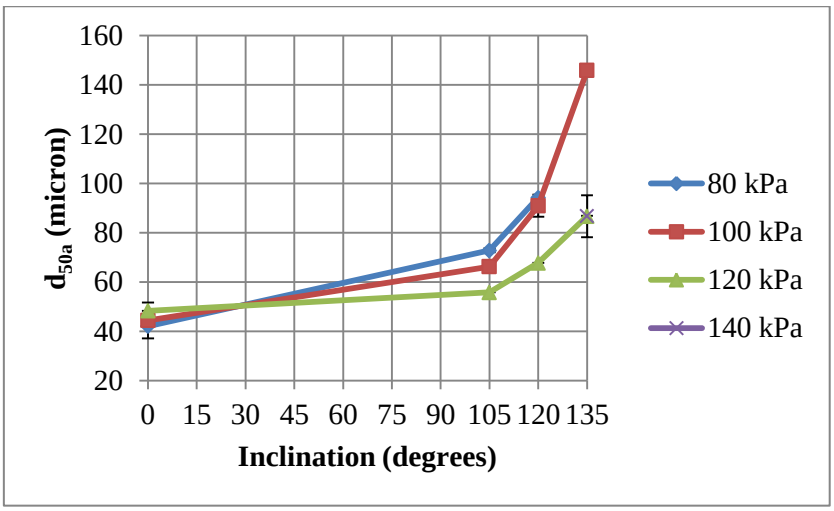

Figure 6-5: Actual cut size versus inclination on various pressures for 40% solids silica-magnetite slurry.

The response of actual cut size is similar to the corrected values as shown in Figure 6-5. This result suggests semi-inverted operation is significant to true classification. From the graph, actual cut sizes at 120 degrees – 80 kPa and at 135 degrees – 120 kPa are twice of the cut size in vertical operation. This suggests that a coarse cut size can be achieved with lower pressure by adjusting inclinations at semi-inverted position.

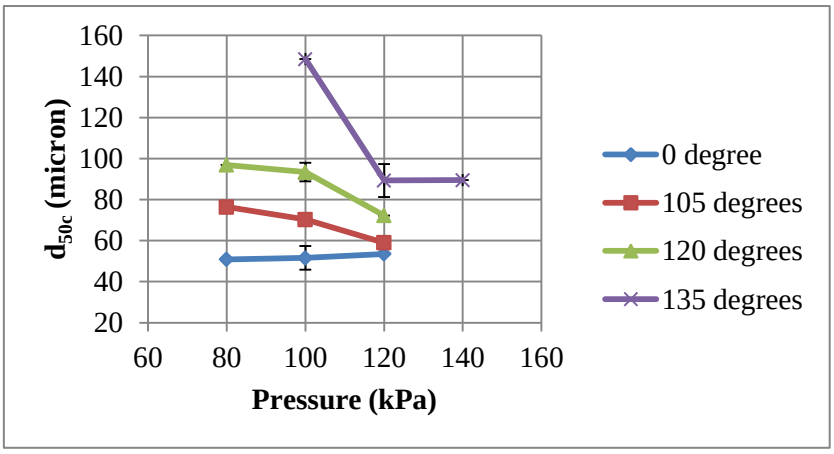

Figure 6-6: Corrected cut sizes versus pressure on various inclinations for 40% solids mixture slurry

Trends of corrected and actual cut size towards pressure are shown by Figure 6-6 and Figure 6-7. Both graphs respond similarly. The impact of pressure on cut size is more apparent at 135 degrees compared to other positions. This result shows that semi-inverted hydrocyclone follows general

inverse terms between pressure and size of separation. However at vertical operation, both corrected and actual cut size are not dependent much on pressure.

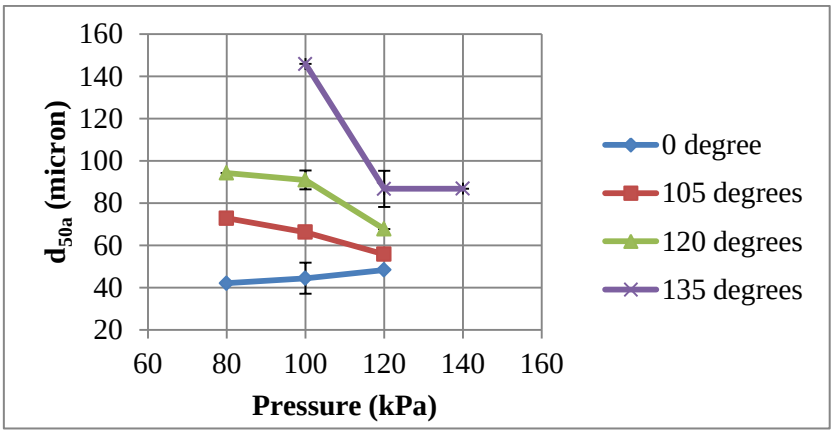

Figure 6-7: Actual cut sizes versus pressure on various inclinations for 40% solids mixture slurry

There is no significant change of separation efficiency, represented by alpha or sharpness of classification curve, in association with inclination as illustrated in Figure 6-8. Nevertheless, it can be concluded from the graph that classification efficiency at semi-inverted positions is still high, while the advantage of low water recovery to underflow can still be achieved.

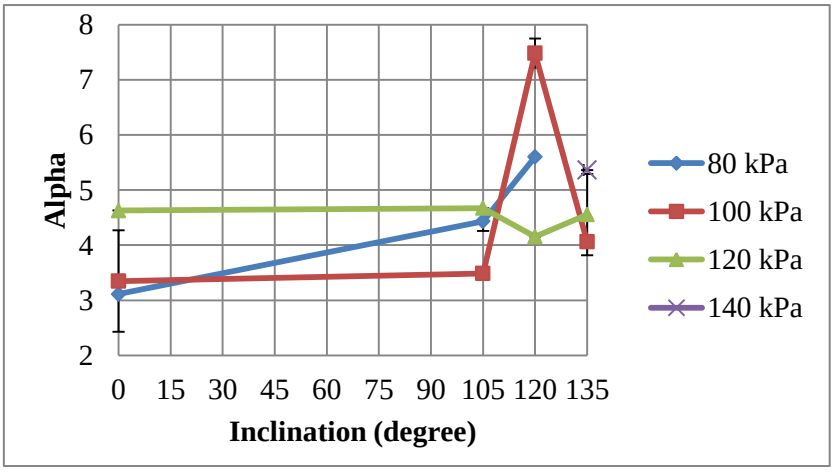

Figure 6-8: Sharpness of separation versus inclination on various pressures for 40% solids mixture slurry

The effect of pressure on sharpness in semi-inverted operation shown in Figure 6-9 is also unclear because of the nature of the alpha parameter. Possible sharper separation with increase of pressure

is shown on 0 degree and 135 degrees operation, but the trend on 105 degrees and 120 degrees is undefined. As magnetite and silica are expected to cut at different sizes in normal, vertical hydrocyclone, treating the mixture as a single component may be contributed these results.

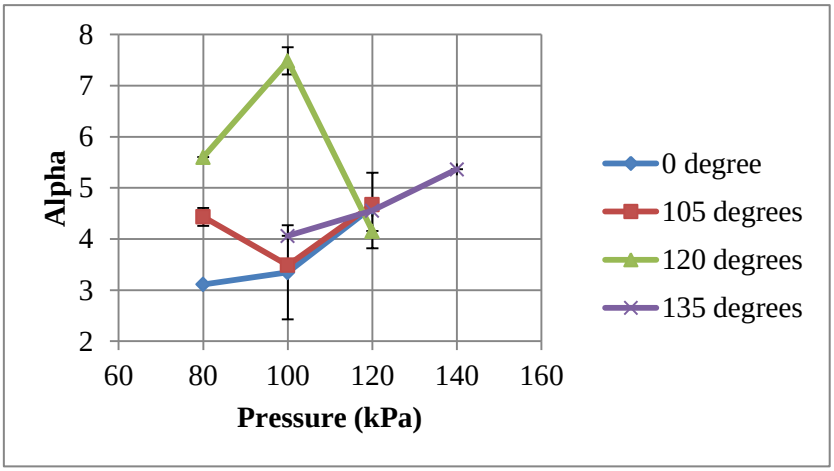

Figure 6-9: Sharpness of separation versus various pressure on various inclinations for 40% solids mixture slurry

A sudden jump of alpha at 120 degrees – 100 kPa might as well be random experimental scatter. Otherwise, an alpha value of 7 could be seen to be as sharp as an alpha of 4 as illustrated by Figure 6-10. The first graph on the top is the curve from 120 degrees – 100 kPa case with alpha parameter of 7.5, whereas similar curve on the bottom is produced from 120 degrees – 120 kPa case with alpha parameter of 4.2. These graphs also suggest that a single alpha does not provide a good fit at size finer than 70 microns.

.

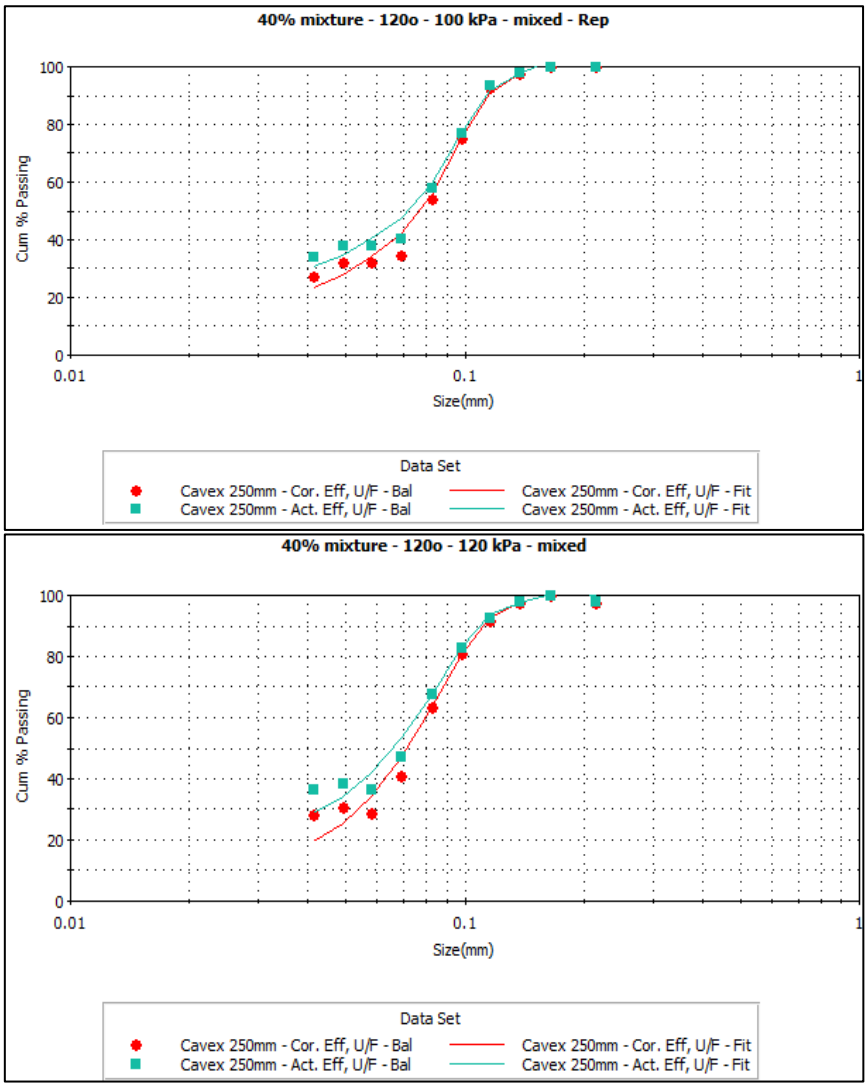

Figure 6-10: Classification curve of hydrocyclone operated at 120 degrees at 100 kPa and 120 kPa applying 40% solids mixture slurry.

6.3 Conclusions

An investigation of semi-inverted operation of hydrocyclone and a comparison with vertical one has been done for a mixture of silica and magnetite at 40% solids concentration.

Optimum range of operating pressure for semi-inverted hydrocyclone increases higher as inclination gets higher. At the same concentration level, the results suggest that the optimum operating pressure range is very similar to 40% silica feed case. Nevertheless, the minimum pressure to produce spray discharge at 135 degrees on silica-magnetite slurry is slightly higher.

From these experiments, it is concluded that as inclination goes higher, cut size will increase and water recovery to underflow will decrease greatly, especially at 135 degrees from vertical.

Separation efficiency or sharpness of classification curve, however, remained approximately constant. This experiment has successfully managed to work with higher solids concentration and at various pressures, which agrees and expands the range that Asomah was able to investigate (1996).

It is established in this study that pressure is a more critical variable at semi-inverted operation compared with vertical operations. Cut size is inversely affected by pressure and this is more evident as inclination gets higher. It has to be noted that water recovery is increased with pressure for semi-inverted operation. This contradicts the pressure – water recovery relationship expected for a vertical hydrocyclone.

CHAPTER 7 : Model Evaluation

As pointed out in the literature review, most of the hydrocyclone models reviewed in Chapter 2 do not consider inclination as a model parameter except some of the latest models proposed by Asomah (1997) and Narasimha et al. (2014). Moreover, the Narasimha/Mainza model, which the only model in JKSimMet that incorporates inclination as a model variable, does not envisage predictions with inclination above 90 degrees since this mode of operation is outside the range of its database.

The results provided in Chapter 4 to Chapter 6 were produced from experimental data processed and fitted to the Naramsimha/Mainza model in JKSimMet simulator. The model constant parameters were also fitted for all cases. Because results of semi-inverted cases stand upon an "unconfirmed" area that the model cannot actually predict, it is worthwhile to investigate whether those experimental results match with the model prediction without having to refit the constant parameters. By this comparison, the existing model capability to predict semi-inverted hydrocyclone performance could be assessed.

In addition, the same experiment results are also compared with prediction results from Asomah model. Although this model has only been developed based on single pressure operation for each diameter of hydrocyclone and maximum 30% feed solids concentration, a comparison study might help to understand the semi-inverted hydrocyclone better.

7.1 Model Calibration

7.1.1 Narasimha/Mainza Model Calibration

Each experiment case in the vertical position was selected as a base case for parameter estimated and was then used to predict results of semi-inverted operations. The idea was to apply the Narasimha/Mainza model constant parameters (KD0, KW1, and KAlpha0) from vertical case to all other semi-inverted cases to predict their cut size, water recovery, and alpha. K-constant parameters will take into account other undefined variables, with feed characteristics as the most dominant factor. Thus feeds can be assumed to be the same for all conditions.

The mean values from all vertical operations are taken to represent each feed. The results are summarised in Table 7-1.

Table 7-1: Narasimha/Mainza model K-parameters values of all vertical operation

Feed	Operation case	KD0	KW1	KAlpha0	KQ0
40% silica	0^o - 80 kPa	0.0214	0.95	20.9	345
	0^o - 100 kPa	0.0229	1.01	25.8	330
	0^o - 100 kPa	0.0230	1.00	23.9	335
	0^o - 120 kPa	0.0253	0.94	27.5	337
	mean	**0.0231**	**0.97**	**24.5**	**336**
	standard dev.	0.0016	0.037	2.84	6
50% silica	0^o - 80 kPa*	0.0172	1.17	34.4	322
	0^o - 100 kPa*	0.0223	0.95	29.0	336
	0^o - 120 kPa	**0.0268**	**0.85**	**28.6**	**340**
	mean	0.0221	0.99	30.7	332
	standard dev.	0.00482	0.163	3.25	9.6
40% silica – magnetite	0^o - 80 kPa	0.0243	0.95	22.3	339
	0^o - 100 kPa	0.0239	0.91	19.1	324
	0^o - 100 kPa	0.0284	0.84	28.3	338
	0^o - 120 kPa	0.0283	0.89	32.9	336
	mean	**0.0263**	**0.90**	**25.6**	**334**
	standard dev.	0.0025	0.043	6.13	6.75

*)Suspected incorrect numbers due to sump stirrers malfunction during experiments

An exception on 50% silica cases (will discuss later) has been highlighted. As previously explained in Chapter 5 Subsection 5.2.2.1, there was a malfunction of sump stirrers during experiment at vertical operation that altered feed characteristic. Operation at 120 kPa was performed first, so K-parameters of this operating condition were used as representatives, with an assumption of minimum particle settlement. K-parameters at 80 kPa and 100 kPa were neglected.

The mean K-parameters were then re-applied to all vertical cases. Comparisons between experimental values and model predictions among all vertical operations are given by Figure 7-3, Figure 7-2, and Figure 7-3. The error bars show the impact from the K-parameters standard deviation in Table 7-1.

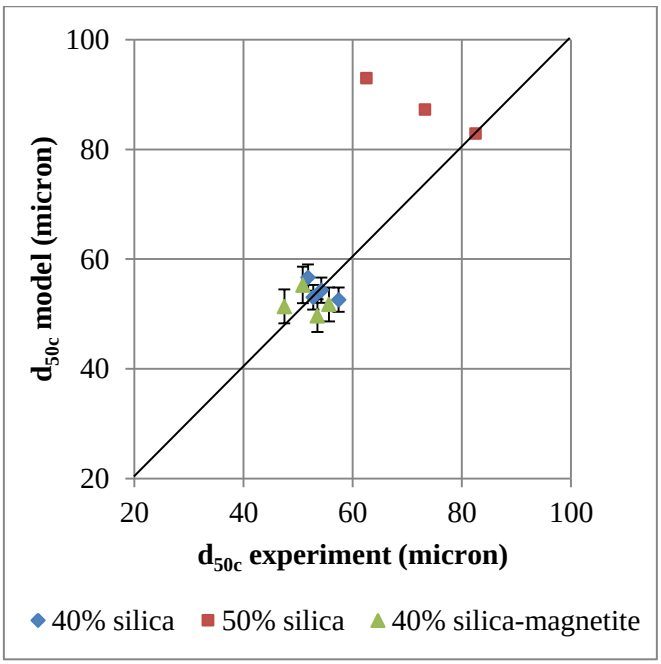

Figure 7-1: Narasimha model prediction vs. experiment of cut size at vertical operation

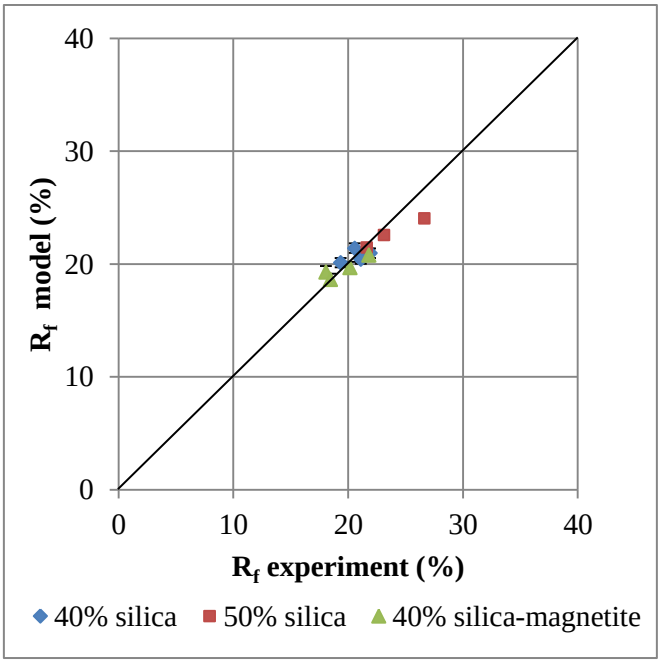

Figure 7-2: Narasimha model prediction vs. experiment of water recovery at vertical operation

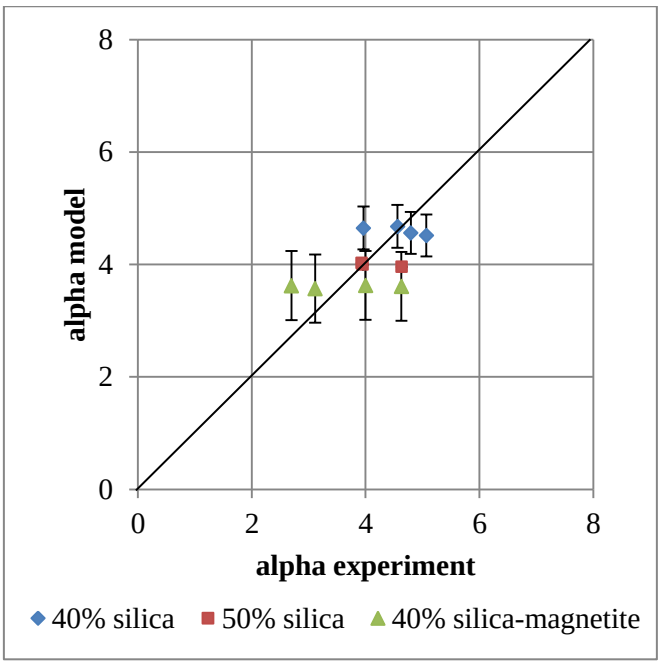

Figure 7-3: Narasimha/Mainza model prediction vs. experiment results at vertical operation

Figure 7-3 indicates the model predictions for cut size are quite well matched with the experimental results for 40% silica and 40% silica-magnetite. However, for 50% solids the model response mismatched the experiment results. As has been explained in Chapter 5, variation in the feed size at vertical operation causes the cut size to disagree with the model prediction. This feed variation is also indicated by larger standard deviation of the KD0 mean values compared to other feed cases shown in Table 7-1Table 7-1.

Figure 7-2 and Figure 7-3 compare model prediction results with experimental results for water recovery and alpha at vertical operations respectively. The water recovery results show much better fits than the cut size prediction. Alpha model also works fine with 40% and 50% silica feed but it does not exactly fit with 40% silica-magnetite feed as might be expected.

These results show Narasimha/Mainza model works well for vertical operation. All the K-parameters in Table 7-1 are also within 95% confidence level of two standard deviations, suggesting that they are not statistically different. Therefore, the mean values in Table 7-1 can reasonably be applied to calculate d_{50c}, water recover, and alpha for semi-inverted cases. The calculation was done in Excel worksheet.

7.1.2 Asomah Model Calibration

With slightly different approach, constant parameters for Asomah models were also calibrated from vertical operations. In calibrating Narasimha/Mainza model, the constant parameters were produced from JKSimMet simulator. Since Asomah model is not embedded in the software, its constant parameters were recalculated in an Excel worksheet. The results for each vertical test are given in Table 7-2.

Table 7-2: Asomah model B-parameters values of all vertical operation

Feed	Operation case	B1	B2	B3
40% silica	0^o - 80 kPa	0.155	5.75	9.0
	0^o - 100 kPa	0.171	6.50	10.7
	0^o - 100 kPa	0.166	6.41	10.3
	0^o - 120 kPa	0.180	5.86	11.5
	mean	**0.168**	**6.13**	**10.4**
	standard dev.	0.010	0.38	1.05
50% silica	0^o - 80 kPa*	0.158	7.12	9.6
	0^o - 100 kPa*	0.191	6.09	8.7
	0^o - 120 kPa	**0.218**	**5.69**	**8.8**
	mean	0.189	6.30	9.0
	standard dev.	0.030	0.74	0.49
40% silica – magnetite	0^o - 80 kPa	0.168	7.00	8.7
	0^o - 100 kPa	0.158	6.64	7.6
	0^o - 100 kPa	0.180	6.07	11.4
	0^o - 120 kPa	0.178	6.24	13.3
	mean	**0.171**	**6.49**	**10.3**
	standard dev.	0.010	0.42	2.59

The mean values of B1, B2, and B3 for each feed cases are then adopted by the model to predict cut size, water recovery, and alpha for vertical operations. Plotting results of Asomah model predictions against experiment results are presented in Figure 7-4, Figure 7-5, and Figure 7-6.

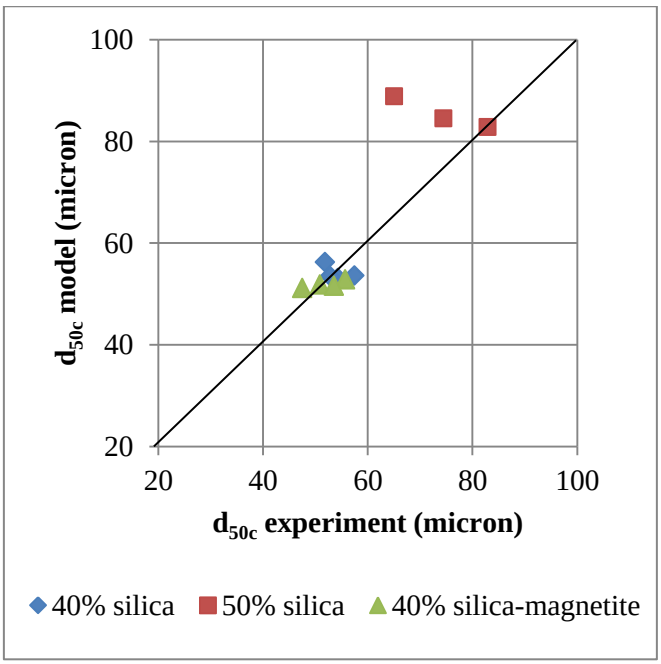

Figure 7-4: Asomah model prediction vs. experiment of cut size at vertical operation

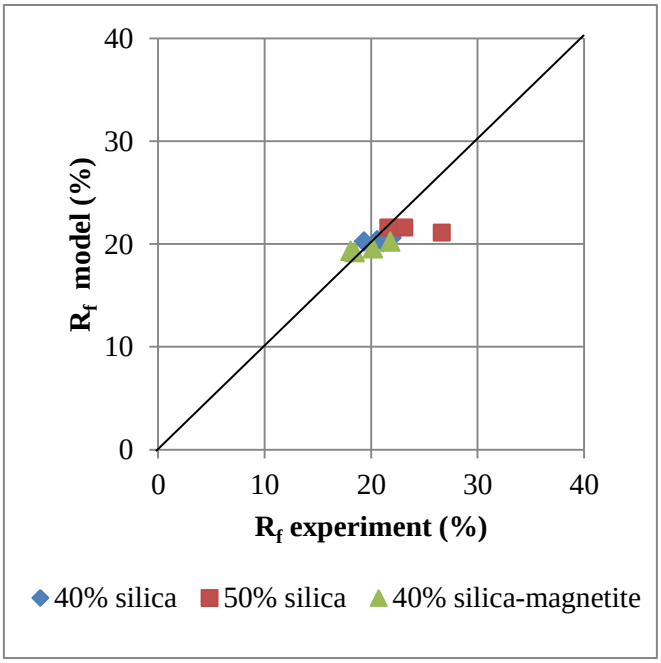

Figure 7-5: Asomah model prediction vs. experiment of water recovery at vertical operation

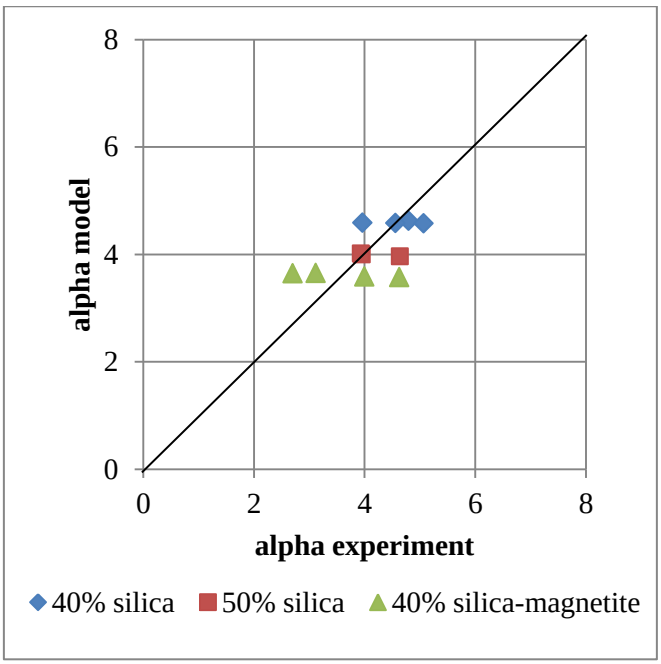

Figure 7-6: Asomah model prediction vs. experiment results at vertical operation

Asomah model works fine in predicting cut size and water recovery as illustrated by Figure 7-4 and Figure 7-5, except scatters from 50% silica feed cases marked by red dots. Same with Narasimha/Mainza results, these scatters came from experimental errors due to stirrers malfunction. Asomah model do not fit alpha well as shown by Figure 7-6.

7.2 Comparison Results with Narasimha/Mainza Model

7.2.1 40% Solids Silica Feed

The compared results between experimental results and models prediction results on cut size, water recovery to underflow, and separation sharpness are given in Figure 7-7, Figure 7-8 and Figure 7-9 respectively. Model prediction results were produced by using the average values of K-parameters in vertical operations provided in Table 7-1.

Figure 7-7 shows the cut size model follows the trend of the experimental result though the model overestimates cut sizes at semi-inverted operations. There is one outlier in the figure coming from 135 degrees operation running at 80 kPa. The experiment cut size reach 178 micron, while model predicts around 28 micron less. This can be explained by the extreme low water recovery (three percent) and low solid recovery (ten per cent). This might lead to the very coarse cut size.

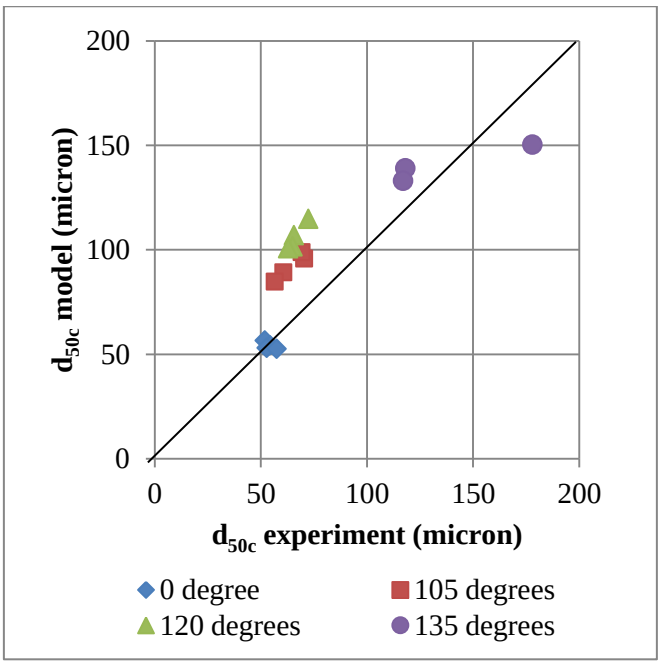

Figure 7-7: Narasimha/Mainza model predictions vs. experiment for cut size with 40% silica feed

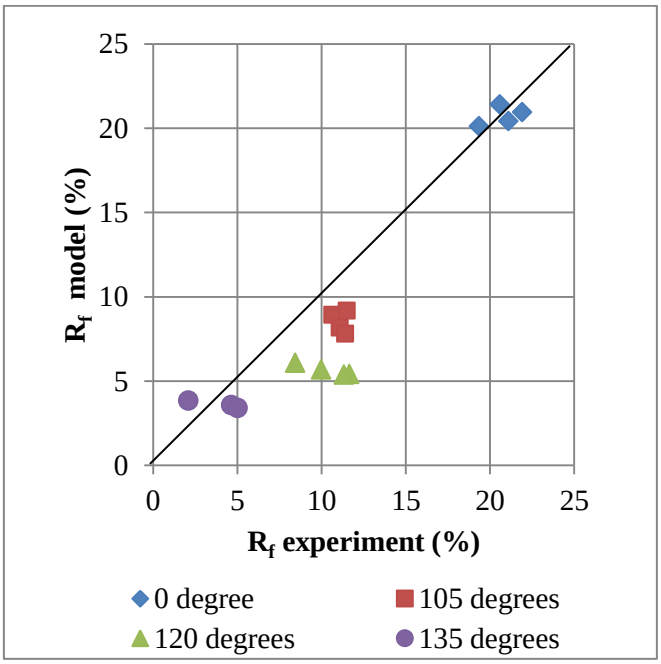

Figure 7-8: Narasimha/Mainza model predictions vs. experiment for water recovery with 40% silica feed

Figure 7-8 reveals that the water recovery model predictions match the trends of the experimental result with a little exception. Although the model underestimates water recovery values at 105 and

120 degrees in comparison with experiment results, overall comparison shows the model predictions seem to be of the same order as the experiments.

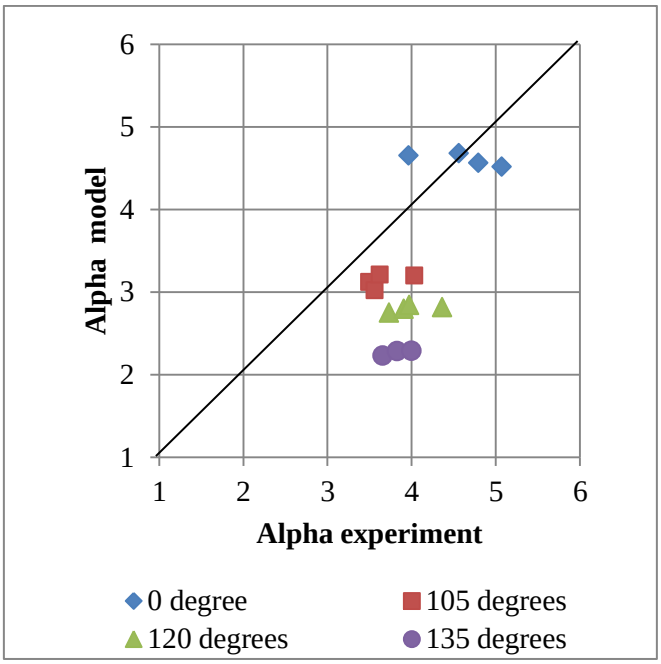

Figure 7-9: Narasimha/Mainza model predictions vs. experiment for alpha with 40% silica feed

Figure 7-9 shows that the Narasimha/Mainza efficiency model does not work very well for semi-inverted operation. The model predicts alpha to become lower with inclinations, while experimental alpha were consistent at around 4.

7.2.2 50% Solids Silica Feed

Instead of using the average values of K-parameters, the model prediction results were calculated by applying the K-parameters of vertical operation at 120 degrees (see Table 7-1).

A comparison of corrected cut size between model prediction and experiment for 50% solids silica is given Figure 7-10. This result is slightly different with 40% silica feed (Figure 7-7) where the model result on semi-inverted cases has closer fits to the experimental result. With 50% silica feed, semi-inverted inclinations give less impact on cut size. This might be related with a becoming actives water recovery to underflow.

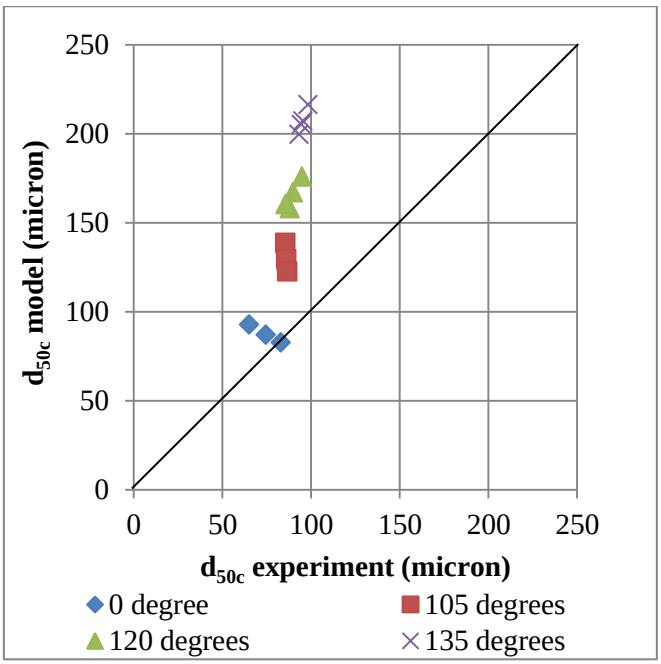

Figure 7-10: Narasimha/Mainza model predictions vs. experiment for cut size with 40% silica feed

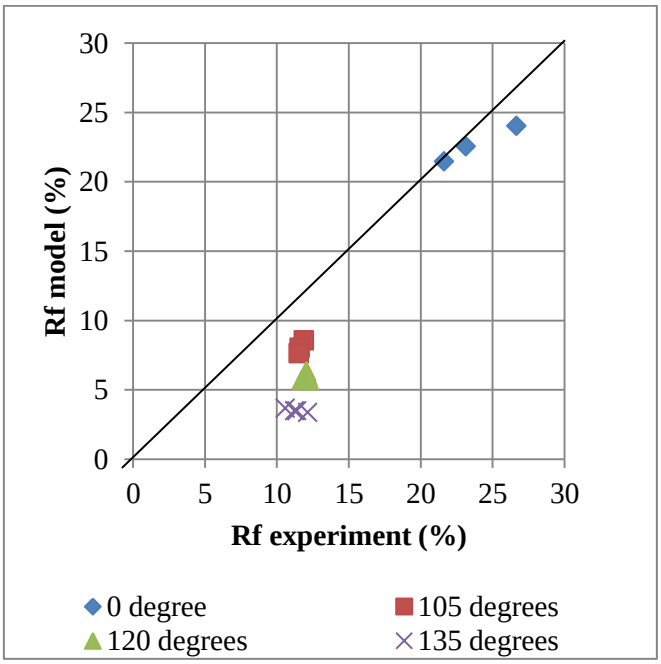

Figure 7-11: Narasimha/Mainza model predictions vs. experiment for water recovery with 40% silica feed

The experimental results of water recovery stop at around 10% at all semi-inverted inclinations while the model continues to predict lower water recovery with inclinations as shown Figure 7-11. As has been highlighted in Chapter 5, there is some indication of a physical constraint at semi-

inverted operation with 50% feed concentration. This might be due to a viscosity constraint as the solids percentage increase with inclination (see Table 5-3) and the shear rates in the underflow are low compared with the vertical operation. The Narasihma/Mainza model is lack of information of this constraint. Therefore, it could not predict water recovery accurately.

In Figure 7-12, constant experimental alpha of around 4 suggested more efficient separation compare to the model prediction which predicts alpha impairment with inclination.

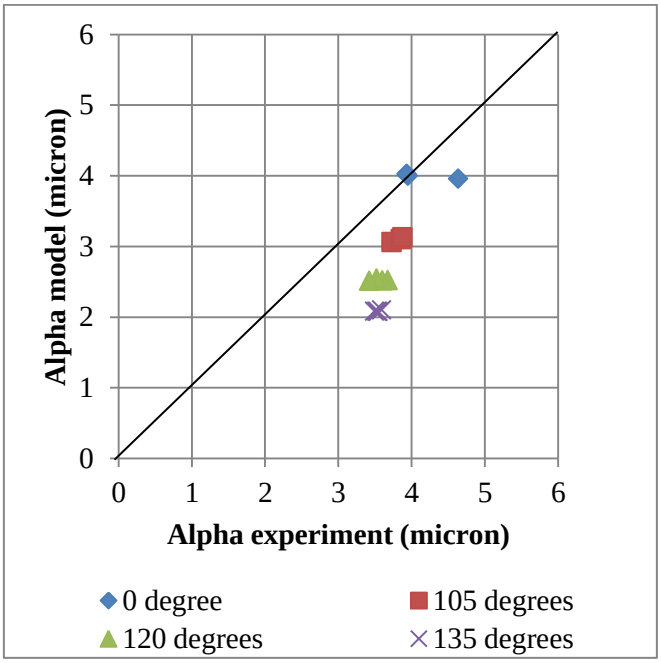

Figure 7-12: Narasimha/Mainza model predictions vs. experiment for alpha with 40% silica feed

7.2.3 40% Solid Silica-Magnetite Feed

The model prediction results (using the average fits of K-parameters in Table 7-1) with 40% silica-magnetite feed are provided in Figure 7-13, Figure 7-14 and Figure 7-15. Consistent with the two previous cases on single component feed, Narasimha/Mainza cut size model is able to follow the increase in experimental cut size although slightly overestimating as shown in Figure 7-13. The fitting is very similar to the 40% silica case (see Figure 7-7), which also has a good fit. This suggests that Narasimha/Mainza cut size model works better for 40% solids concentration rather than with 50% solids.

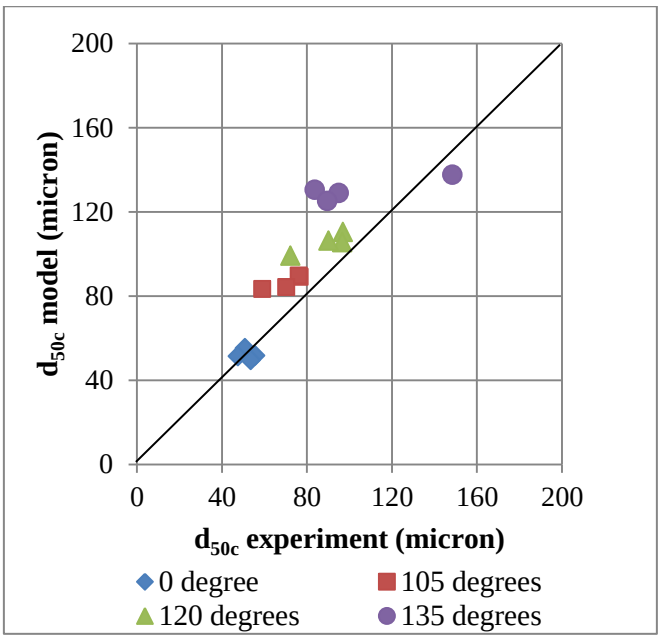

Figure 7-13: Narasimha/Mainza model predictions vs. experiment for cut size with 40% silica-magnetite feed

A good agreement between model and experiment results is also given by water recovery as shown by Figure 7-14. As inclination higher at semi-inverted positions, both model and experiment show a reduction of water recovery to underflow, although the model does not predict the differences coming from pressure variation like the experiment results show.

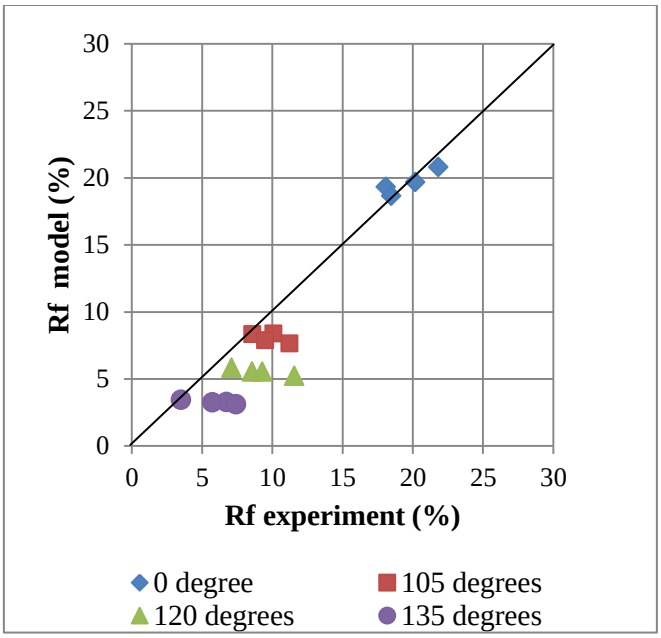

Figure 7-14: Narasimha/Mainza model predictions vs. experiment for water recovery with 40% silica-magnetite feed

The Narasimha/Mainza model, however, does not seem to fit the experimental alpha as illustrated in Figure 7-15. The experiments show good efficiency with alpha higher than 3.5 at all semi-inverted positions while the model predicts lower alpha values of around 2. The outliers at 120 degrees reaching alpha of 7.5 can be misleading as it might come from experimental random error.

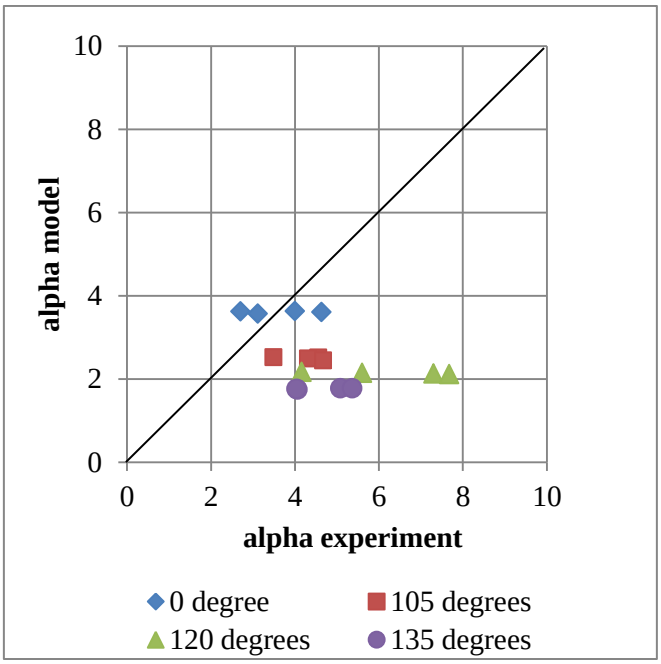

Figure 7-15: Narasimha/Mainza model predictions vs. experiment for alpha with 40% silica-magnetite feed

7.2.4 Narasimha/Mainza Constant Parameters Results

The experimental fitted K-parameters for all operating conditions are plotted against inclination and the results are provided in Figure 7-16 for KD0 and KW1 and Figure 7-17 for KAlpha0. The KD0 generally decreases with inclination for the three feed cases, but it suddenly raise at 135 degrees for 40% solids silica and mixture feeds. Opposite to KD0, KW1 increases with inclination in most cases and drops at 135 degrees. There seems to be a turning point for KD0 and KW1 at 135 degrees that cause them to decline. K-parameters trends for 40% silica-magnetite feed are a bit unclear but generally similar to trends for 40% silica trends.

The trends of KAlpha0 against inclination are given in Figure 7-17. It can be said that KAlpha0 increase progressively with inclination up to 135 degrees for all feeds.

These results suggest that Narasimha/Mainza model may be suitable for further development, which would include semi-inverted operations into its parameters.

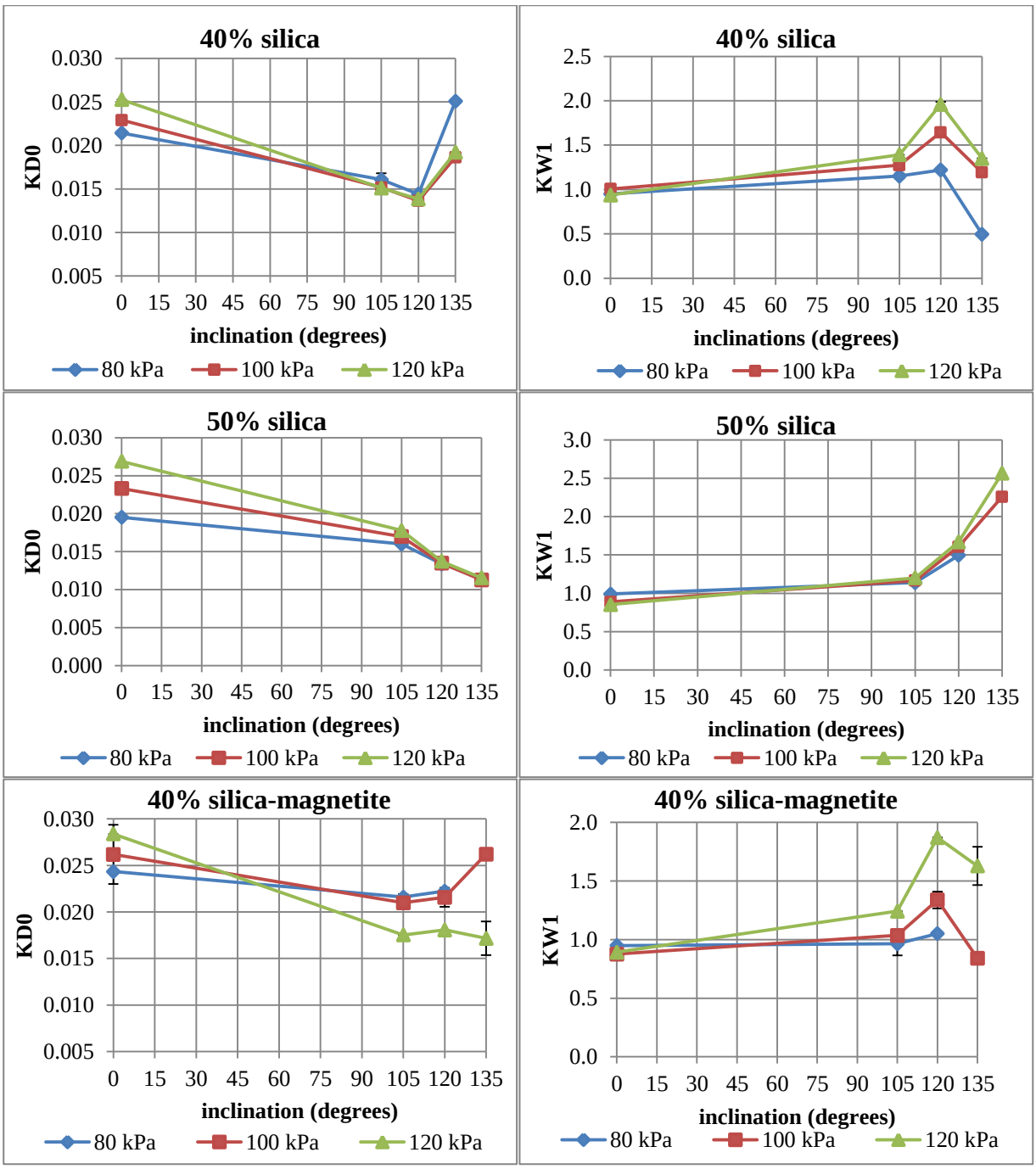

Figure 7-16: KD0 (left) and KW1 (right) responses to inclination for all feed cases

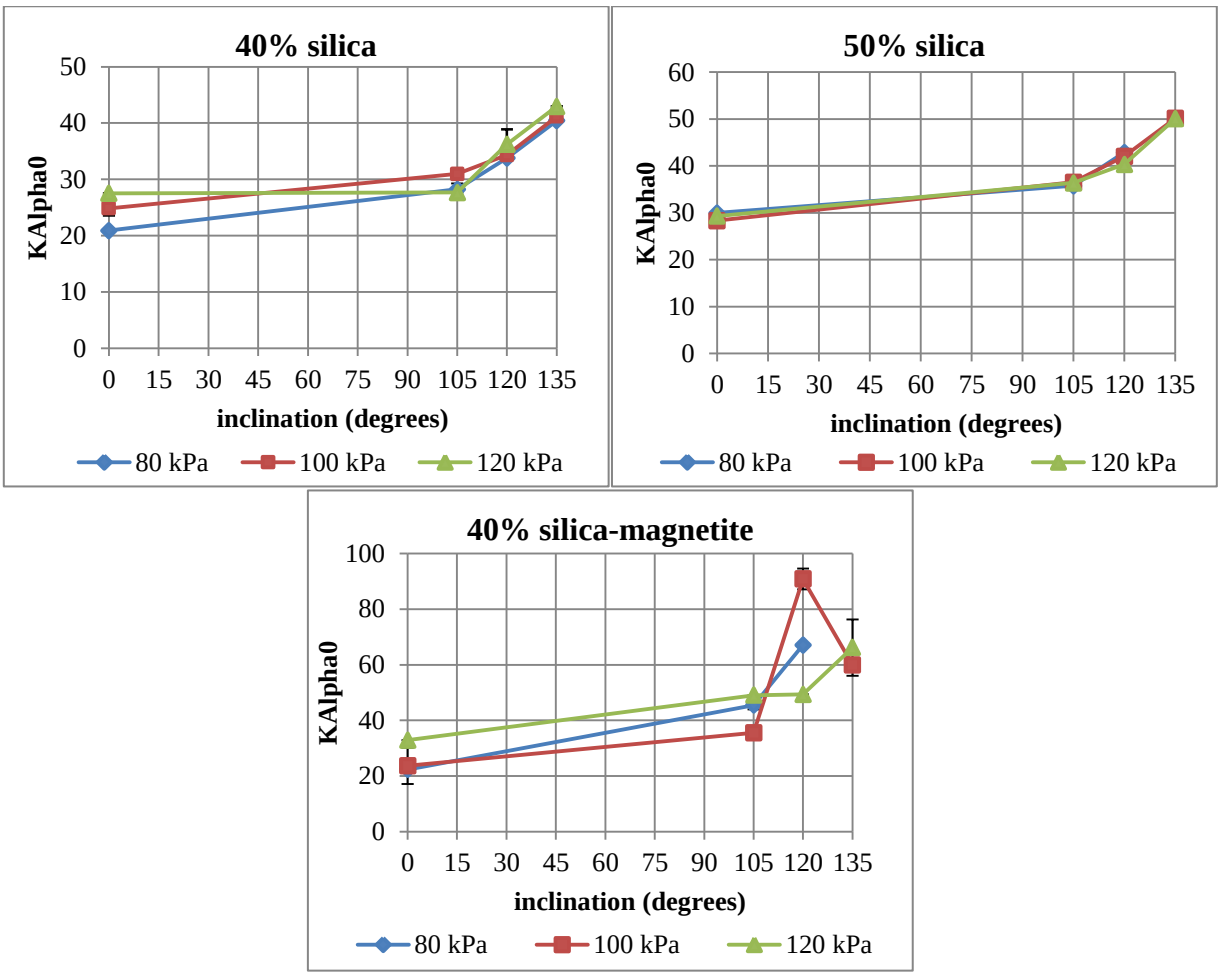

Figure 7-17: Kalpha0 response to inclination for all feed cases

7.3 Comparison Results with Asomah Model

7.3.1 Asomah Model Prediction vs. Experimental Result

A corrected cut size comparison between Asomah model prediction results and experimental results for 40% silica, 50% silica, and 40% silica-magnetite feeds are given in Figure 7-18. By using the average value of B1 at vertical operations (Table 7-2), the Asomah model overestimates cut size at all semi-inverted operations for all three feeds. Model predictions are three to five times coarser than experiment results for 135 degrees operations. Though the overestimations are larger, the Asomah cut size model predictions show similar trends to the Narasimha/Mainza model (Figure 7-7, Figure 7-10 and Figure 7-13).

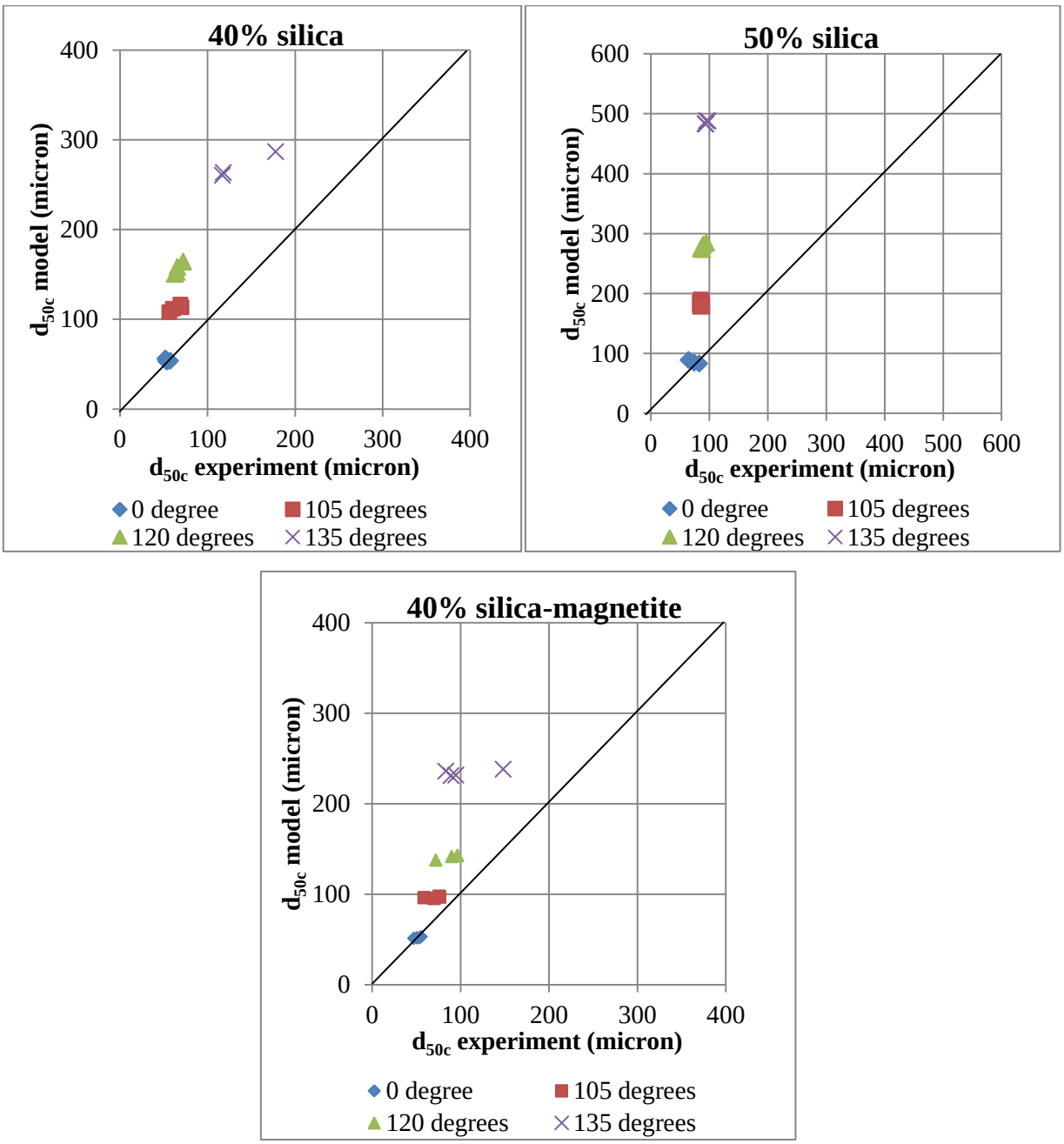

Figure 7-18: Asomah model predictions vs. experiment for cut size with all feed cases

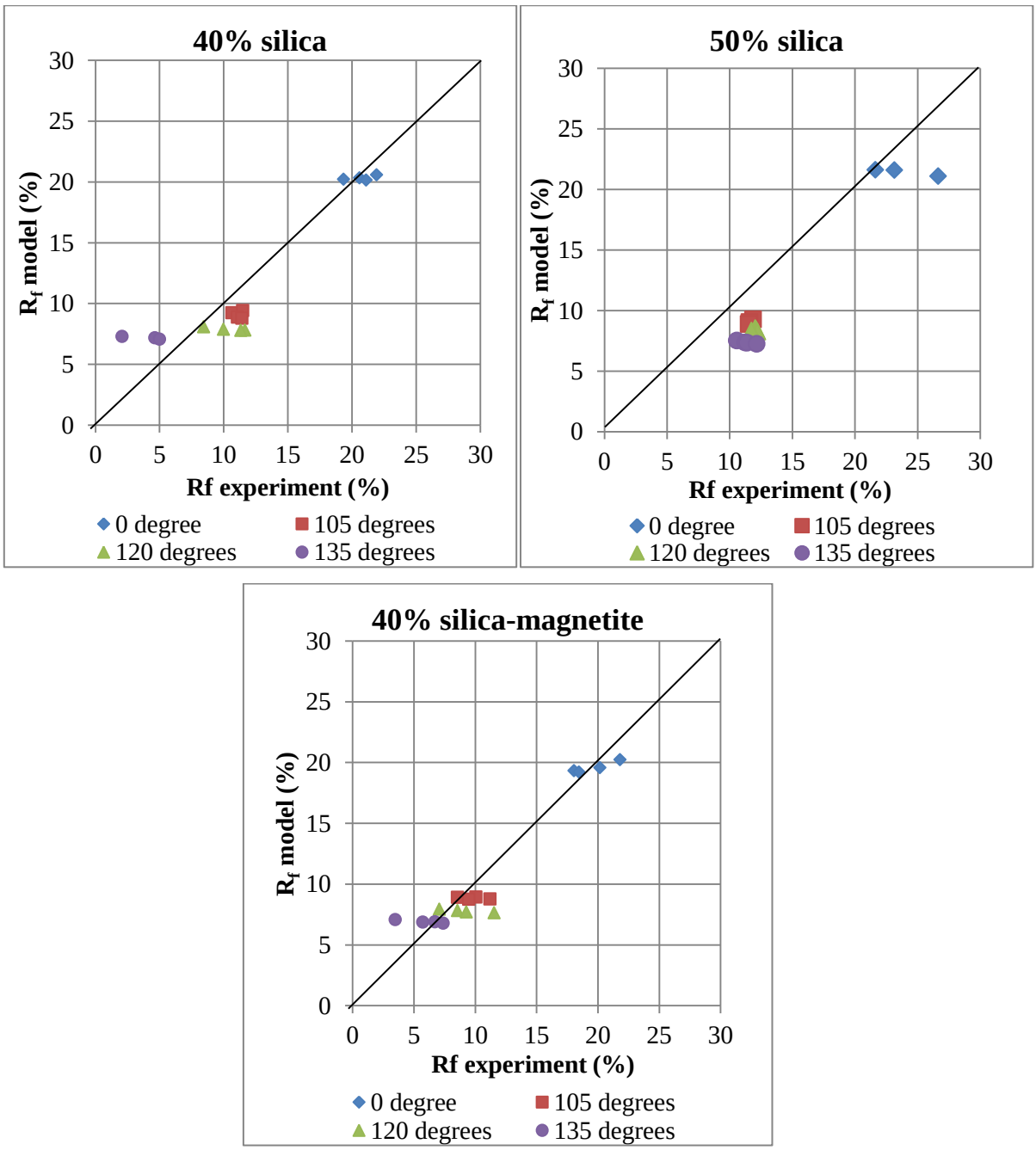

Figure 7-19: Asomah model prediction vs. experiment for water recovery with all feed cases

Comparison results of water recovery, R_f, are shown in Figure 7-19. Asomah model predictions tend to stop at around 7% at 135 degrees, while experimental results can go as low as 2 to 3 per cent for 40% silica and 40% silica-magnetite feeds. Similar with the Narasimha/Mainza model, the Asomah model does not seem able to predict the experimental constraint for 50% silica feed case.

Figure 7-20 shows Asomah model prediction result against experimental results. The fits of alpha are surprisingly better than Narasimha/Mainza model predictions except for 40% silica-magnetite mixture feed (see Figure 7-9, Figure 7-12, and Figure 7-15).

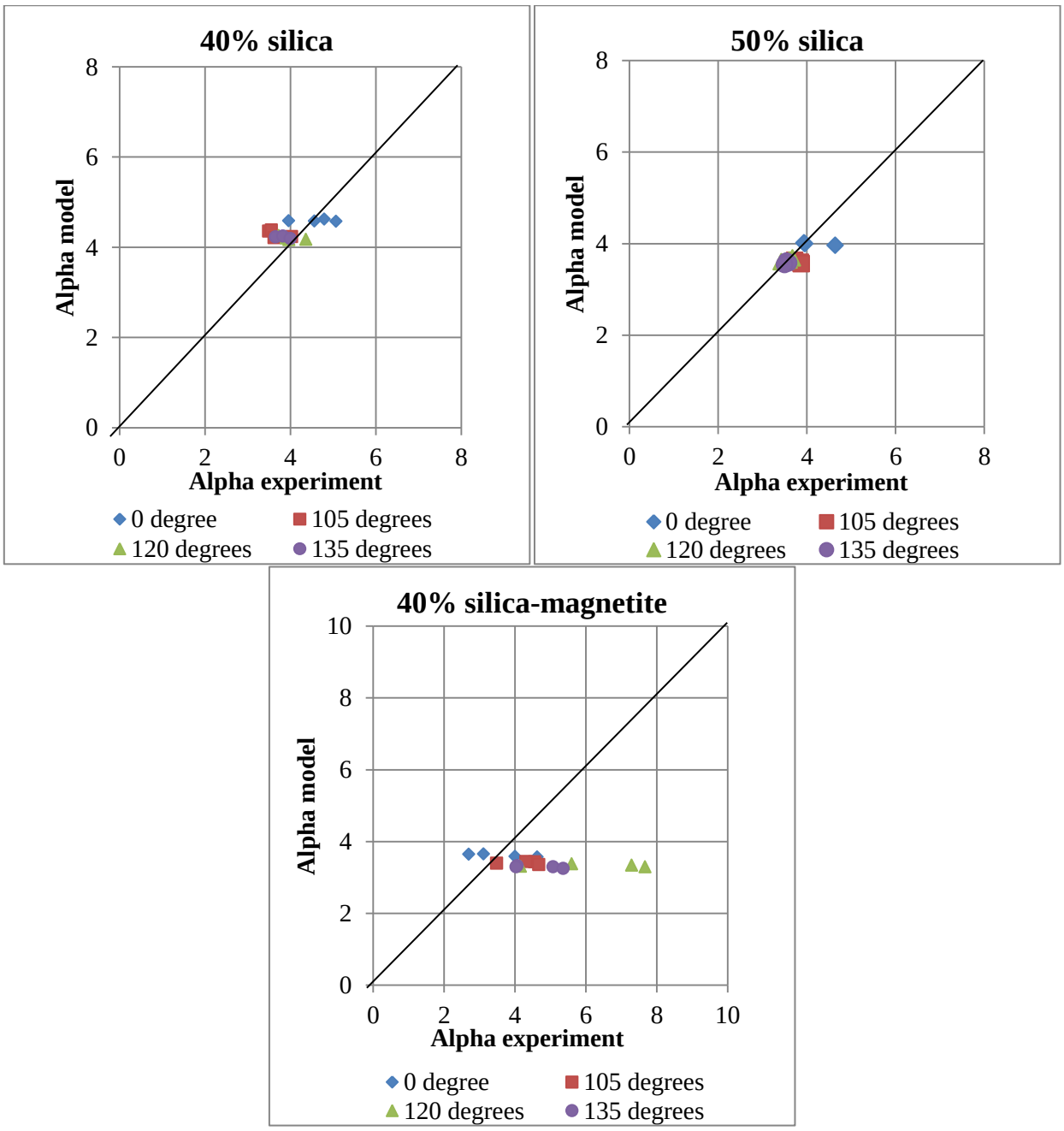

Figure 7-20: Asomah model predictions vs. experiment for alpha with all feed cases

7.3.2 Asomah Constant Parameters Results

The trends of Asomah model constant parameters, B1 and B2, responding to inclination are given in Figure 7-21. As can be illustrated on three graphs on the left constant parameter for cut size, B1, constantly drop at semi-inverted inclinations although a small pick up was indicated with 40% silica. The right graphs show the water recovery constant, B2, slightly increase at semi-inverted positions and drop suddenly at 135 degrees. These results trend are comparable with Narasimha/Mainza result trends (Figure 7-16)

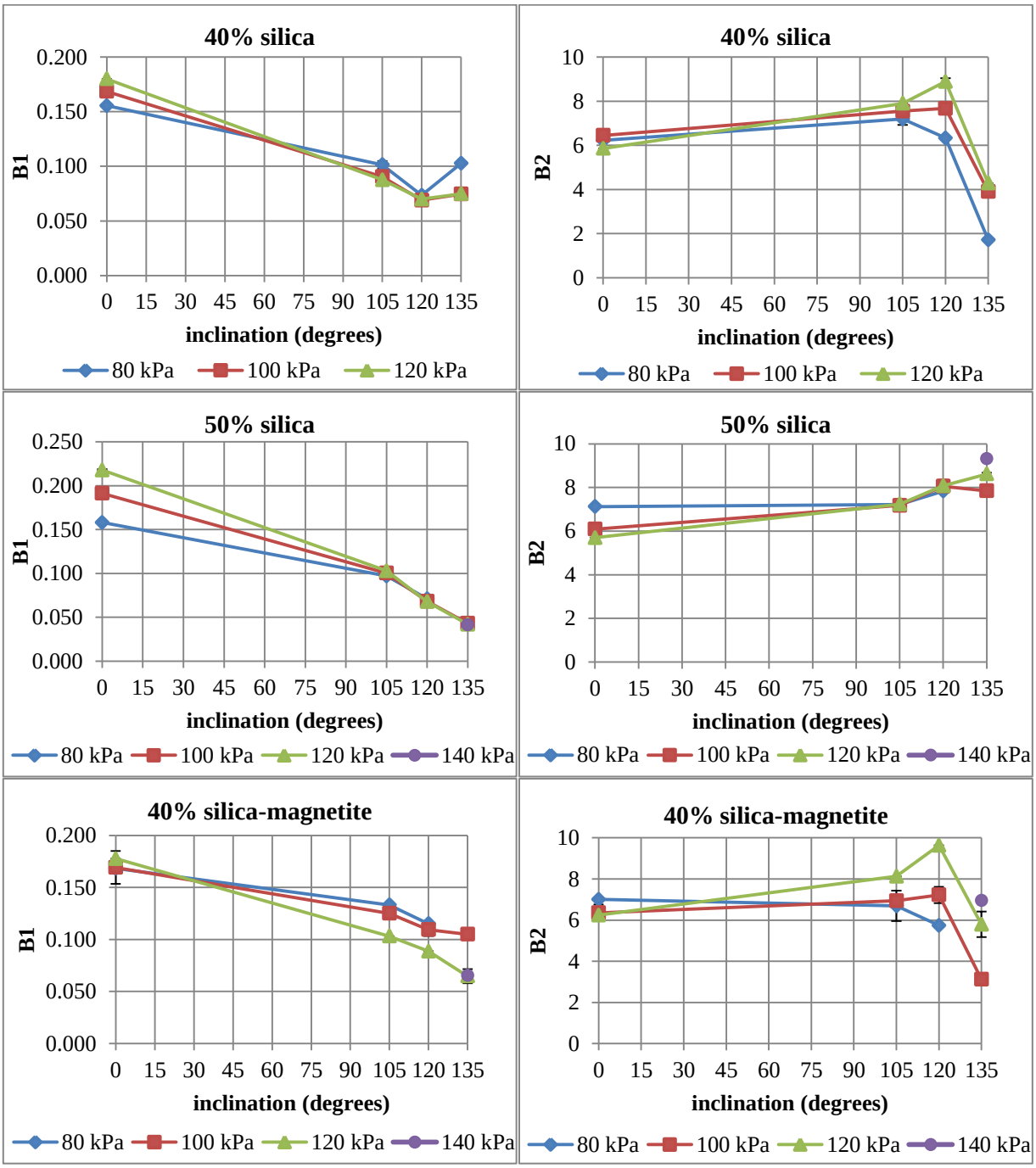

Figure 7-21: constant parameters B1 (left) and B2 (right) responses to inclination

7.4 Conclusions

The Narasimha/Mainza model has been used to predict hydrocyclone performance when operating at semi-inverted inclinations in terms of corrected cut size (d_{50c}), water recovery to underflow (R_f), and sharpness of separation (alpha) after it has been calibrated using tests data from vertical operation. The results have been compared with the experimental results from Chapter 4, Chapter 5, and Chapter 6.

The Narasimha/Mainza model has a consistent trend of slightly overestimating cut size and underestimating water recovery compared with the experimental results. Model prediction with 50% silica feed give less satisfying fitting to experimental results rather than fitting of 40% silica and 40% silica-magnetite feed cases. This is because water recovery to underflow reached its minimum with 50% silica feed, while model does not provide any warning of this constraint.

Semi-inverted inclination seems not to affect alpha, or to have little influence at the very least. This could not be accurately predicted by Narasimha/Mainza.

The Asomah model overestimates cut size even more than the Narasimha/Mainza model does. It also overestimates water recovery at vertical operations and apparently cannot predict lower than 7% at semi-inverted inclinations. This happened to all three feeds.

The Asomah model comparison with experimental results was less accurate than Narasimha/Mainza model is due the experiment results are produced in JKSimMet using Narasimha/Mainza model. It can be argued that Asomah model could work better if the model constant parameters were refitted using the experiment results.

The constant parameters responses to inclination from both models have comparable trends. These are good indications that semi-inverted conditions can be embedded into predictive model.

To conclude this chapter, it can be said that to some extent the Narasimha/Mainza model predictions are of the same order as the experimental results. Therefore it can be argued that the Narasimha/Mainza semi-empirical model has the potential to be further developed and applied to semi-inverted operation simulation, but this will require more experimental work and some of this work should be carried out using larger diameter hydrocyclones.

CHAPTER 8 : Novel Vortex Finder

As pointed out in Chapter 2, Vakamalla et al. (2014) found through a CFD investigation that hydrocyclone inclined below horizontal change the flow pattern and air core profile due to the decline of pressure drop inside the hydrocyclone body. However, their observation was only up to 60 degrees from vertical and there is no further information especially for semi-inverted hydrocyclone operation. A CFD simulation carried out by Weerasekara (private communication, 2016) as part of this project showed asymmetrical traces for simulated particles.

A better separation performance might therefore be achieved if the asymmetric flow pattern is matched with a specific design of vortex finder. To test whether the asymmetric flow pattern responds differently at semi-inverted positions, an additional experiment was performed using a novel asymmetrical vortex finder.

This is best illustrated by Figure 8-1. The air core (and particle flow) is possibly elliptical and at a lower position under the influence of gravity. This might allow unclassified coarse fraction to slip through the original vortex finder. The novel vortex finder with its offset design may fit the asymmetric air core and preventing the coarse fraction by-passing to overflow.

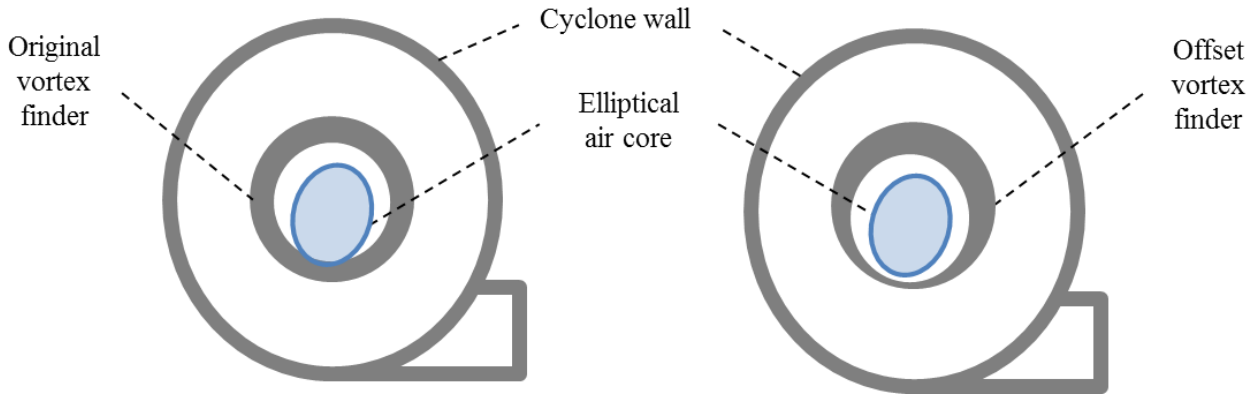

Figure 8-1: Simplistic illustration of air core capture by original vortex finder (left) and novel vortex finder with an offset centre (right) in semi-inverted operation

This novel vortex finder was manufactured by JKMRC workshop. The diameter and the length of the new vortex finder are the same as the standard one, while the centre of radius is shifted 10 mm away from the true centre.

The novel vortex finder was first set at a possible position to catch as much of an elliptical pattern as possible (Figure 8-1). One secondary position was tested with 40% silica-magnetite feed, by rotating the novel vortex finder 90 degrees clockwise from the first position. This additional position is aimed to test if there is any real difference in the performance of the novel vortex finder.

8.1 Experimental Results

A total of eleven sample sets were taken with the novel vortex finder. The differences in classification performance parameters between novel and original vortex finder are summarized in Table 8-1 and are illustrated into graphs from Figure 8-2 to Figure 8-6.

Table 8-1: Summary of comparison between original and novel vortex finder at 0^o, 120^o, and 135^o

Operating conditions (inclination-pressure-feed)	d_{50c} (micron)		d_{50a} (micron)		R_f (%)		Alpha	
	Original VF	Novel VF	Original VF	Novel VF	Original VF	Novel VF	Original VF	Novel VF
0^o - 120kPa - 40% silica	57.4	50.8	47.8	45.2	19.3	21.1	5.1	5.0
0^o - 120 kPa - 50% silica	82.5	85.4	71.1	74.9	21.4	19.6	3.9	3.9
0^o - 100 kPa - 40% mixture	51.6	48.7	44.4	41.4	19.1	20.6	3.3	3.5
120^o - 120 kPa - 40% silica	64.0	64.7	61.2	60.5	11.5	12.3	4.2	4.3
120^o - 120 kPa - 50% silica	86.9	79.8	80.3	74.1	12.0	12.2	3.5	3.8
135^o - 100 kPa - 40% silica	118.1	91.3	115.1	87.2	4.6	8.1	3.8	3.9
135^o - 120 kPa - 40% silica	117.1	81.5	114.1	74.0	5.0	9.2	4.0	3.9
135^o - 120 kPa - 50% silica	94.9	85.1	88.3	78.8	11.3	11.4	3.6	3.4
135^o - 100 kPa - 40% mixture	148.5	126.8	145.9	124.8	3.5	4.2	4.1	5.4
135^o - 120 kPa - 40% mixture	89.3	99.9	86.7	97.1	6.2	6.3	4.6	4.7
135^o - 120 kPa - 40% mixture with Novel VF Position 2*	89.3	91.54	86.74	88.5	6.22	7.03	4.56	4.58

*)Position 1 is offset at the lowest position as illustrated by Figure 8-1. Position 2 is offset rotated 90 degrees clockwise from Position 1.

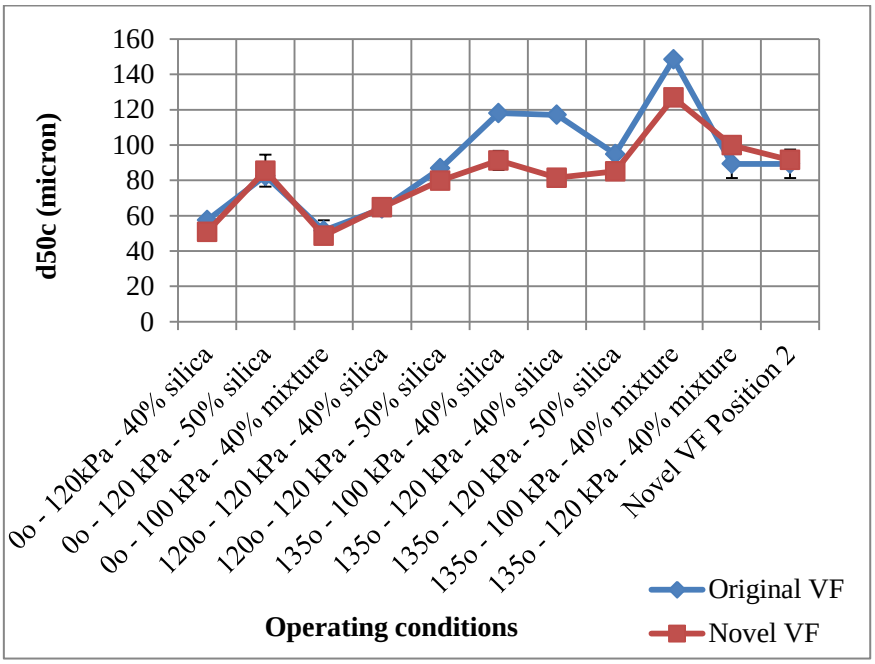

Figure 8-2: Corrected cut size comparison between the two vortex finder

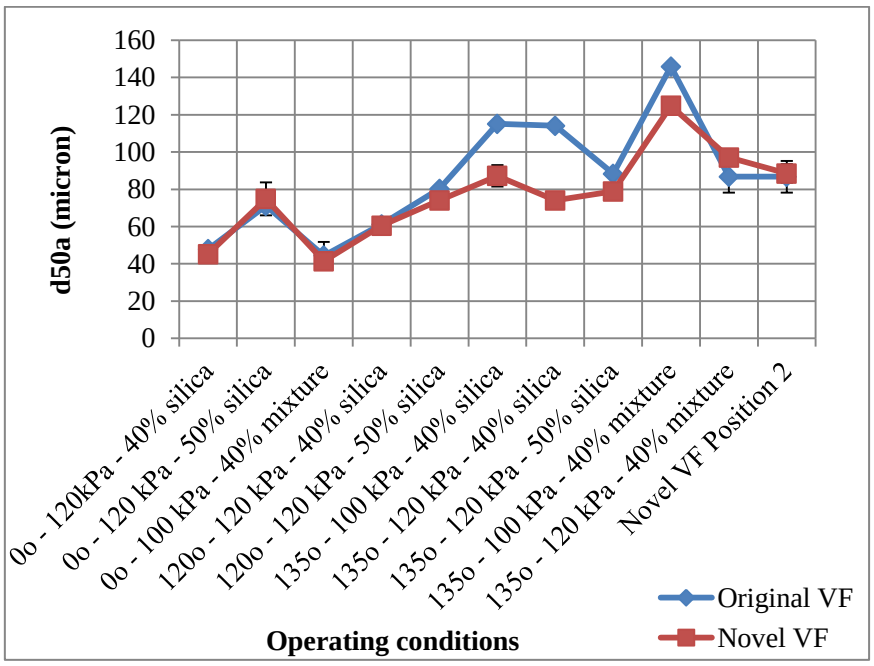

Figure 8-3: Actual cut size comparison between the two vortex finder

From Figure 8-2, it can be seen that cut size reduction by novel vortex finder was found at all three feed types. Significant differences are visible at 135 degrees at 100 kPa and 120 kPa operation with 40% silica feed. Finer cut sizes were also produced with 50% silica and 40% silica-magnetite feed

at semi-inverted operations by changing to the novel vortex finder. The novel vortex finder did not affect cut size at vertical operation. It is also found that the secondary position of novel vortex finder did not influence cut size with original vortex finder.

Identical responses are also given by actual cuts as shown in Figure 8-3. At semi-inverted operation, particle flow pattern moves in elliptical orbits due to the influence of gravity. It is possible that the novel vortex finder has accommodated the particle movement, reducing coarse material short-circuiting to overflow product. Therefore, the actual cut size decreases. This indicates that changing to novel vortex finder from the original one does impact true classification. This result also suggests that changing cut size while in operation might be potentially performed by using the novel vortex finder, without much effect on water recovery and alpha.

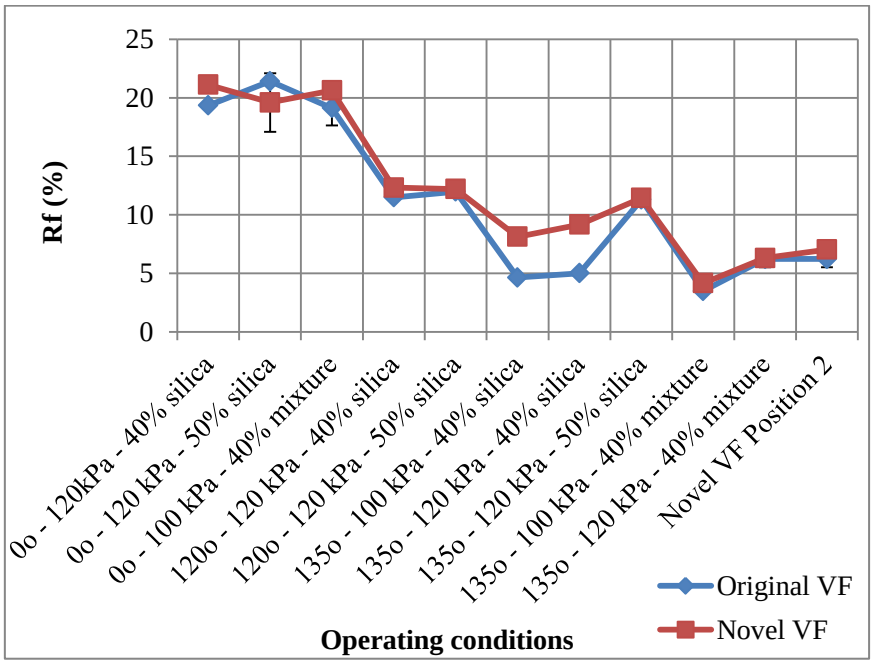

Figure 8-4: Water recovery comparison between the two vortex finders

Figure 8-4 shows the comparisons of water recovery responds on several operating conditions between the two tested vortex finders. The large gaps between the two vortex finders at 135 degrees – 100 kPa and 135 degrees – 120 kPa with 40% silica are also featured in the water recovery responses (Figure 8-4). Although the novel vortex finder worked less efficiently by sending more water to underflow on these two conditions, corrected cut sizes still have these differences (Figure 8-2). Thus, the reduction of water recovery at these two particular conditions did not affect the separation.

Figure 8-4 also shows that the novel vortex finder did not affect water recovery to underflow almost at each operating condition, including at vertical operation and when the secondary position of novel vortex finder was applied. There is no clear understanding of this unaffected water recovery, but the solids concentration of stream products may give some indication.

Table 8-2: Product solids percentages at 135^o with 40% silica feed at 0^o, 120^o, and 135^o

Operating conditions	%Solids OF		%Solids UF	
	Original VF	Novel VF	Original VF	Novel VF
0^o - 120kPa - 40% silica	30.3	26.5	67.5	67.5
0^o - 120 kPa - 50% silica	39.4	39.4	69.9	70.4
0^o - 100 kPa - 40% mixture	29.7	29.3	68.2	68.0
120^o - 120 kPa - 40% silica	31.2	29.2	72.9	74.0
120^o - 120 kPa - 50% silica	40.6	38.0	72.9	73.6
135^o - 100 kPa - 40% silica	37.4	33.2	76.6	75.6
135^o - 120 kPa - 40% silica	37.4	32.0	75.3	75.4
135^o - 120 kPa - 50% silica	41.4	38.6	74.0	73.8
135^o - 100 kPa - 40% mixture	40.1	38.5	77.1	77.9
135^o - 120 kPa - 40% mixture	35.9	36.0	78.4	76.3
135^o - 120 kPa - 40% mixture Novel VF Position 2*	35.9	35.6	78.4	76.6

*)Position 1 is offset at the lowest position as illustrated by Figure 8-1. Position 2 is offset rotated 90 degrees clockwise from Position 1.

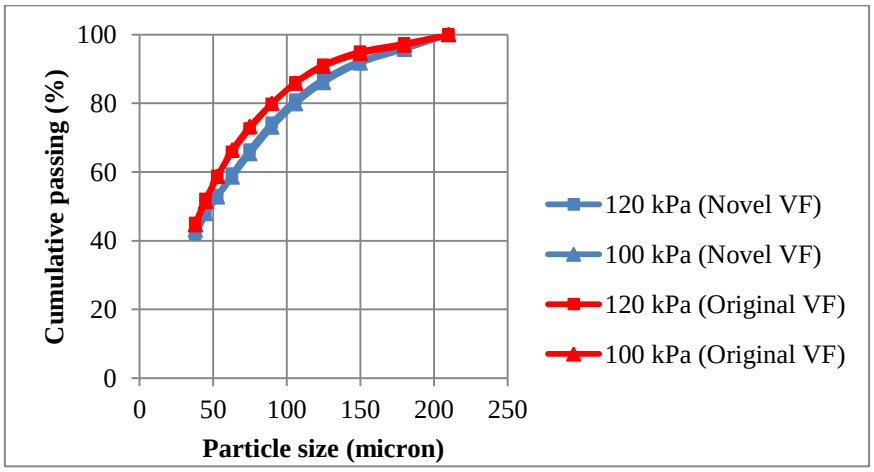

Figure 8-5: Feed size distribution at 135 degrees with 40% silica

From Table 8-2, the novel vortex finder at 135 degrees at 100 kPa and 120 kPa with 40% silica reduce solids percentage of overflow product around 5%. This might explain the significant reduction in cut size and water recovery. Another possible explanation is that there was variability in the feed characteristics. As shown by Figure 8-5, the feed size distributions between original vortex finder and novel vortex finder are a little different. The F_{80} for the experiment with the novel vortex finder was around 15 microns coarser than for the original vortex finder. Thus, it can be argued that significant cut size and water recovery differences at 135 degrees with 40% silica could also be initiated by feed size variability.

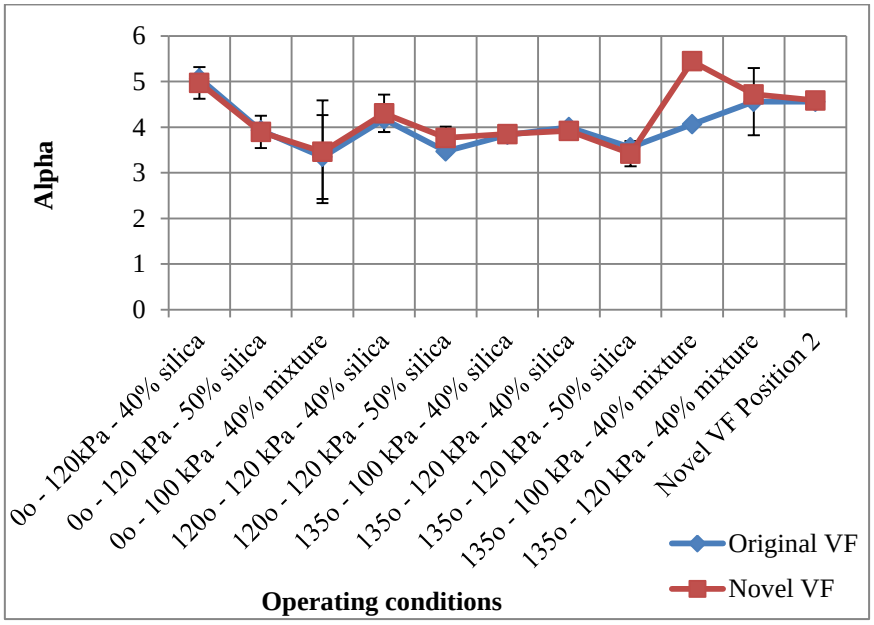

Figure 8-6: Comparison of original and novel vortex finder on sharpness of separation

From Figure 8-6, changing original vortex finder to the novel one did not improve separation sharpness. It was expected that vortex finder with the offset centre could improve alpha by limiting the amount of any possible short-circuiting material when operated in semi-inverted operation. At 135 degrees 100 kPa operation with 40% silica-magnetite mixture, alpha high value with novel vortex finder can be misleading since the classification curve does not quite differ with original vortex finder (see Appendix A.7)

However, there are some indications of separation improvement from their classification curves. For instance, Figure 8-7 provides classification curves for original and novel vortex finders at 135 degrees applying 40% silica feed at 120 kPa. The novel vortex finder curve shows less

misplacement of coarse particles compared with the original vortex finder. Also, the novel vortex finder produces a sharper separation at the fine end, although the alpha function does not fit well with the experimental values. Even though sharpness could be slightly improved with the novel vortex finder, the original vortex finder produced a lower water recovery to underflow.

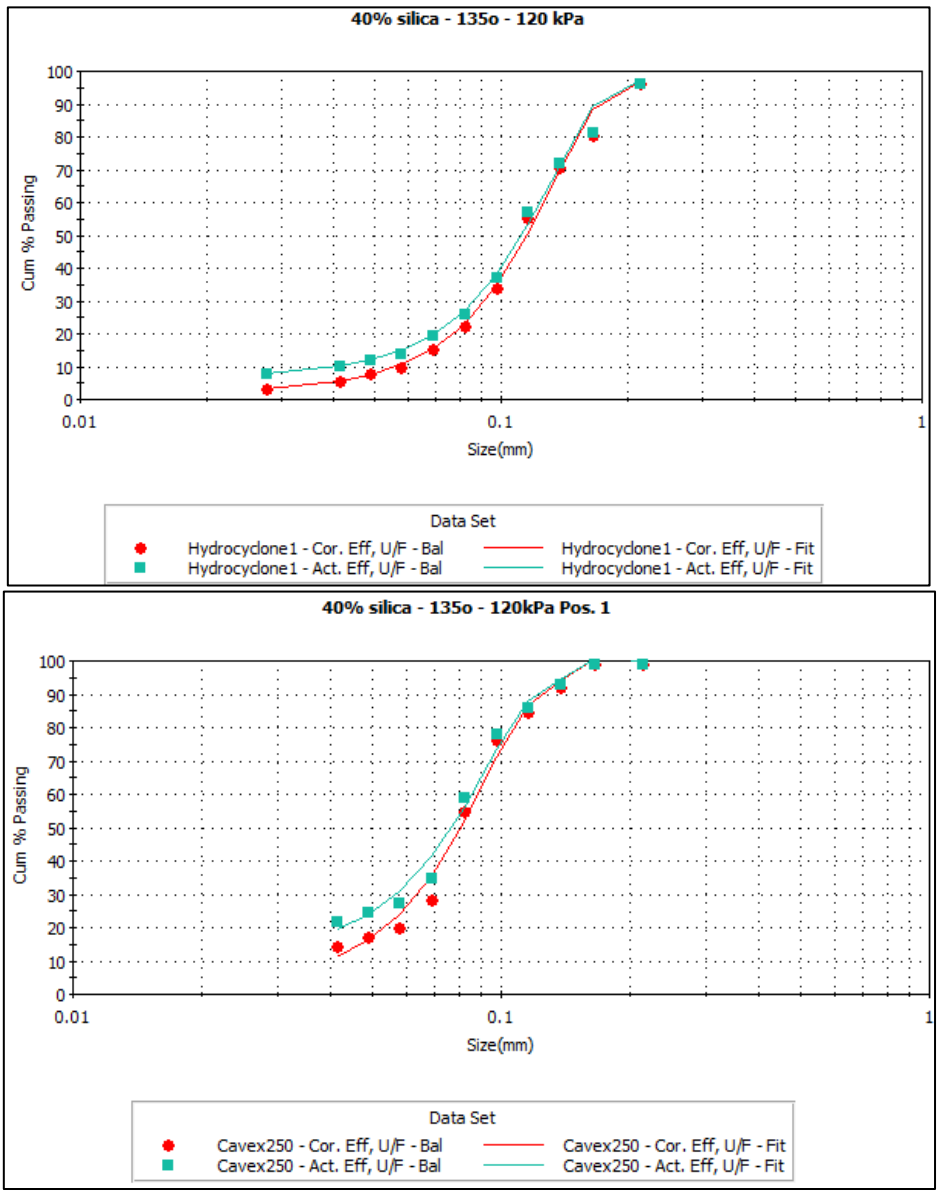

Figure 8-7: Classification curves at 135^{o} – 120 kPa with 40% silica feed using original vortex finder (top) and novel vortex finder (bottom)

Through a simulation analysis using JK-MDK (JK-Model Development Kit), the experimental data was processed to produce the separation performance specific for each mineral component. That is, for silica and magnetite. The results are given in Table 8-3.

As can be seen in Table 8-3, there is a significant change in cut size using the novel vortex finder at 135 degrees operation. At 100 kPa operation, mixtures and individual components have lower cut sizes while sharpness is maintained. At 120 kPa, lower cut size is shown by magnetite, yet alpha is steady. Less reduction of cut size given by secondary position of novel vortex finder might signify less impact made by the offset vortex finder. These results are an indication of the existence of asymmetrical particles orbits within the semi-inverted hydrocyclone that were captured by application of the novel vortex finder.

At vertical operation, cut size for magnetite particles increase by using the novel vortex finder, while overall mixture and silica cut size do not change. It is possible that magnetite particles are misplaced or short-circuited to the overflow by the novel vortex finder, result in cut size increase.

Table 8-3: Cut size responses comparison between standard and novel vortex finder using the JK-MDK for data analysis

Inclination (degrees)	Pressure (kPa)	Vortex Finder	Silica-magnetite mixture			Silica only		Magnetite only	
			d50c (µm)	alpha	Rf (%)	d50c (µm)	alpha	d50c (µm)	alpha
0	100	standard	47	2.3	20	51	2.6	17	0
0	100	standard	54	2.8	18	62	6.2	10	0.9
0	100	Position 1	48	2.9	21	60	5.4	27	10.5
0	100	Position 1	47	2.9	20	53	3.5	33	2.7
135	100	standard	148	3.2	4	156	4.2	61	3.4
135	100	Position 1	123	3.1	4	130	4.3	53	3
135	120	standard	82	2.8	7	90	5.4	46	2.2
135	120	standard	92	2.9	6	98	5.2	67	2.4
135	120	Position 1	97	2.9	6	100	4.4	42	2.8
135	120	Position 2*	87	3	7	92	5.9	39	2.2
135	120	Position 2*	88	2.7	7	95	4.7	39	1.6

*)Position 1 is offset at the position as illustrated by Figure 8-1. Position 2 is offset rotated 90 degrees clockwise from Position 1.

8.2 Conclusions

Although there is no sufficient datasets for conclusion, there are some indications which require further research. There is indication that asymmetric flow pattern affect separation inside the semi-inverted hydrocyclone, particularly at 135 degrees operations. Corrected and actual cut size is

decreased slightly with application of the novel vortex finder which suggests short-circuiting of coarse particles to overflow is reduced.

It is apparent that the application of the novel vortex finder did not affect water recovery very much at most experiment conditions. Alpha seems not to be affected by the novel vortex finder, but sharper separation at both fine and coarse ends was notable on the classification curves with 40% silica feed at 135 degrees operation.

The secondary position of novel vortex finder, which is 45 degrees rotated from the initial position, did not influence hydrocyclone performance. Cut size, water recovery, and alpha are identical with the original vortex finder. This also supports that the possible existence of elliptical flow pattern which successfully captured by the offset design of novel vortex in the initial position.

Although those findings have supported the existence of asymmetrical flow pattern and also a shift in the separation zone during semi-inverted operation, data are still limited to a few tests. An extensive investigation on this subject, possibly include numerically intensive work or visual imaging technique, is needed to further explore this hypothesis.

CHAPTER 9 : Conclusions and Recommendations

9.1 Conclusions

Comprehensive test work using a semi-inverted hydrocyclone (inclination beyond horizontal) has been done in JKMRC pilot plant using the 250 mm diameter JKMRC modified hydrocyclone. The aim of the study is to understand influence of semi-inverted positions on hydrocyclone performance concerning water recovery to underflow, corrected and actual cut size, and sharpness of separation. Experiments were also performed at various operating pressure levels. Three different types of feed were applied.

Unlike previous work in this area, considerable attention was given to establishing ranges of possible operation.

The major findings about semi-inverted hydrocyclone performance from this study are summarised as follow:

- By changing cone angle from 10^{o} to 15^{o}, the range of semi-inverted hydrocyclone operation can be extended to higher feed solids concentrations of up to 50% solids at 135 degrees. This is an area of operation which was not possible in Asomah's work (1996). Optimum operation (without appearance similar to roping) of semi-inverted operation with 40% feed solids concentration can be achieved at lower feed pressure range compared with 50% feed solids.
- Water recovery to underflow can be significantly reduced by using a semi-inverted hydrocyclone. Consistent reductions of water recovery down to only 3 – 5 % have been achieved at 135 degrees with 40% silica and 40% silica-magnetite feeds. With 50% silica feed, minimum water recovery that can be achieved is 10% at 135 degrees. This is an indication of a performance constraint with higher feed solids concentration.
- The change in water recovery by semi-inverted hydrocyclone does not influence actual classification. Cut size, both corrected and actual, is increased as inclinations go higher for all feed types, which confirms previous investigations of the inclination effect on cut size (Asomah, 1996, Rong and Napier-Munn, 2003, Banisi and Deghan-Nayeri, 2005, Vakamalla et al., 2014). With 40% silica and 40% silica-magnetite feeds, cut sizes at 135 degrees are two to three times those of the vertical operation.

- There are several signs of less sharp separation at semi-inverted inclinations compared with vertical operation treating 40% silica and 50% silica feeds, yet alphas are still maintained at around 4. Even though some operations at 135 degrees (typically at lower pressure) showed a discharge appearance similar to roping, sharpness does not collapse. To some point, this result agrees with Rong and Napier-Munn (2003) and disagrees with Asomah (1996). Additionally, sharpness is not pressure sensitive at semi-inverted operation.
- At semi-inverted operation cut size decreases with pressure and its influence is significant at higher inclination, while at vertical operation cut size is much more stable towards pressure. It can be argued that operation at semi-inverted positions is more pressure sensitive to cut size than at vertical operation.
- Pressure and water recovery relationship at semi-inverted positions generally contradicts with conventional vertical operation. Increases in pressure achieved slightly higher water recovery in experiment with 40% silica and 40% silica-magnetite. However, water recovery at semi-inverted positions was unaffected by pressure in experiment with 50% silica feed.

In addition to performance assessment, existing hydrocyclone models were evaluated by comparing model predictions with experiment results. Parameters for these models were obtained from average results for vertical operation with similar feed. The conclusion results are as follow:

- The Narasimha/Mainza model overestimates cut size and underestimates water recovery for semi-inverted hydrocyclone compared with experimental result, yet they follow similar trends. Though it is rather succesful in estimating 5% water recovery at 135 degrees operation on 40% silica and 40% silica-magnetite cases, it fails to predict the water recovery constraint for the 50% silica feed experiment. Alpha predictions was also poor since the experimental alpha are unaffected at semi-inverted operations while the model predicts a decline.
- The Asomah model overestimates cut size to a greater extent than the Narasimha/Mainza model for semi-inverted positions. Water recovery prediction at vertical position also does not fit well. The model also unable to predict water recoveries lower than 7% at 135 degrees on all feed conditions. There may be an implicit constant in the model.
- The Narasimha/Mainza K-parameters from the experiment and the Asomah B-parameters provide comparable trends to each other, which is a good sign for further model development incorporating semi-inverted conditions.

Lastly, asymmetric flow patterns within semi-inverted hydrocyclone were investigated through a limited series of tests using a novel vortex finder with an offset centre. The novel vortex finder has produced finer cut sizes particularly at the highest inclination of 135 degrees, though water recovery is arguably unaltered. Slightly sharper separation at the fine and coarse end of classification curves are signs of better separation, even though alpha function does not change. Rotating the offset closer to the central position gives a similar to the original vortex finder. These findings support the argument of the existence of elliptical flow pattern on semi-inverted hydrocyclone initiated by the offset gravity force, though further investigation is needed to confirm this.

9.2 Contribution to Knowledge

Several contributions to knowledge have been made by this study:

- This project reports a substantial investigation of the semi-inverted hydrocyclone operation. Fundamental behaviour of semi-inverted hydrocyclone under various pressure, feed concentration, and feed density have been well determined by this comprehensive study.
- This research has successfully extended semi-inverted hydrocyclone operation up to 50% solids feed concentration (for silica) at 135 degrees hydrocyclone operation with 250 mm diameter hydrocyclone, while previous research on inclined hydrocyclone was limited to maximum 33% solids concentration on 508 mm diameter hydrocyclone at the same angle.

9.3 Contribution to Sustainability

Mineral industry nowadays is striving to increase profitability while high grade ores are more difficult to find. The challenges from global perspective i.e. creating energy efficient and environmental friendly technology in processing minerals have never been as demanding as it is today. This research offers some important contributions to address these sustainability problems.

Semi-inverted hydrocyclone operation provides superior performance compared with vertical or inclined hydrocyclone below horizontal due to its ability in maintaining low water recovery to underflow while maintaining good separation sharpness. Maintaining low amount of feed water to underflow product implies a lower rate of overgrinding in a comminution circuit.

Extremely low water recovery can be further achieved with lower pressure operation, though it comes at the expense of a coarse separation size. If the target cut size can be adjusted for each

process requirement (ore type), an advantage of operating at lower grinding energy consumption and by pumping less pressure can be achieved as well.

9.4 Recommendations for future work

Even though semi-inverted 250 mm hydrocyclone has been investigated extensively in this study, further investigations are still needed to better understand the fundamentals of semi-inverted operated hydrocyclone. These are include:

- Investigation of larger diameter hydrocyclone operation in semi-inverted mode, and
- Investigation with a range of different solids concentrations and mineral densities of real ores.

Another concern is the need to develop better empirical predictive model(s) that can predict hydrocyclone in semi-inverted positions in addition to current existing models from Asomah and Narasimha/Mainza that have incorporated inclination angle into their parameters.

This thesis has better defined the zones of possible operation. However, this work should be extended to larger hydrocyclone diameter.

Additionally, the existence of asymmetrical, possibly elliptical, flow patterns inside semi-inverted hydrocyclones need to be further investigated. Fully numerically intensive investigation may help to clarify these questions.

List of References

ANDRE CARLOS SILVA, E. M. S. S., JAINER DIOGO VIEIRA MATOS 2012. A Modification in Plitt' for Hydrocyclone Simulation. *International Journal of Research and Reviews in Applied Sciences,* 13.

ARTERBURN, R. A. 1982. The sizing and selection of hydrocyclones. *Design and Installation of Comminution Circuits,* 1**,** 597-607.

ASOMAH, A. K. & NAPIER-MUNN, T. J. 1997. An empirical model of hydrocyclones incorporating angle of cyclone inclination. *Minerals Engineering,* 10**,** 339-347.

ASOMAH, I. 1996. *Improved models of hydrocyclones.* Dissertation/Thesis, University of Queensland.

BANISI, S. & DEGHAN-NAYERI, H. 2005. Effect of angle of hydrocyclone inclination on cut size. *Canadian Metallurgical Quarterly,* 44**,** 79-84.

BERGSTRÖM, J. & VOMHOFF, H. 2004. Velocity measurements in a cylindrical hydrocyclone operated with an opaque fiber suspension. *Minerals Engineering,* 17**,** 599-604.

BERGSTRÖM, J. & VOMHOFF, H. 2007. Experimental hydrocyclone flow field studies. *Separation and Purification Technology,* 53**,** 8-20.

BRADLEY, D. 1965. *The hydrocyclone,* Pergamon Press.

BRAUN, T. 1990. Influence of feed solids concentration on the performance of hydrocyclones. *Chemical engineering & technology,* 13**,** 15-20.

BRENNAN, M. 2006. CFD Simulations of Hydrocyclones with an Air Core: Comparison Between Large Eddy Simulations and a Second Moment Closure. *Chemical Engineering Research and Design,* 84**,** 495-505.

BRETNEY, E. 1891. bretney. Google Patents.

CASTRO, O. 1990. *An investigation of pulp rheology effects and their application to the dimensionless type hydrocyclone models.* Dissertation/Thesis.

CHANG, Y. F., ILEA, C. G., AASEN, Ø. L. & HOFFMANN, A. C. 2011. Particle flow in a hydrocyclone investigated by positron emission particle tracking. *Chemical Engineering Science,* 66**,** 4203-4211.

COELHO, M. A. Z. & MEDRONHO, R. A. 1992. An Evaluation of the Plitt and Lynch & Rao Models for the Hydrocyclones. *In:* SVAROVSKY, L. & THEW, M. T. (eds.) *Hydrocyclones.* Springer Netherlands.

COLLINS, A.-R. 2016. Classification of multi-component feeds in a hydrocyclone. The University of Queensland, Sustainable Minerals Institute.

CONCHA, F., BARRIENTOS, A., MONTERO, J. & SAMPAIO, R. 1996. Air core and roping in hydrocyclones. *International Journal of Mineral Processing,* 44–45**,** 743-749.

CULLIVAN, J. C., WILLIAMS, R. A., DYAKOWSKI, T. & CROSS, C. R. 2004. New understanding of a hydrocyclone flow field and separation mechanism from computational fluid dynamics. *Minerals Engineering,* 17**,** 651-660.

DUECK, J., FARGHALY, M. & NEESSE, T. 2014. The theoretical partition curve of the hydrocyclone. *Minerals Engineering,* 62**,** 25-30.

DYAKOWSKI, T. & WILLIAMS, R. A. 1993. Modelling turbulent flow within a small-diameter hydrocyclone. *Chemical Engineering Science,* 48**,** 1143-1152.

DYAKOWSKI, T. & WILLIAMS, R. A. 1995. Prediction of air-core size and shape in a hydrocyclone. *International Journal of Mineral Processing,* 43**,** 1-14.

FINCH, J. A. 1983. Modelling a fish-hook in hydrocyclone selectivity curves. *Powder Technology,* 36**,** 127-129.

FLINTOFF, B. C., PLITT, L. R. & TURAK, A. A. 1987. CYCLONE MODELLING: A REVIEW OF PRESENT TECHNOLOGY. *CIM Bulletin,* 80**,** 39-50.

GUPTA, A. & YAN, D. S. 2006. 12. Classification. *Mineral Processing Design and Operation - An Introduction.* Elsevier.

GUPTA, R., KAULASKAR, M. D., KUMAR, V., SRIPRIYA, R., MEIKAP, B. C. & CHAKRABORTY, S. 2008. Studies on the understanding mechanism of air core and vortex formation in a hydrocyclone. *Chemical Engineering Journal,* 144**,** 153-166.

HARARAH, M. A., ENDRES, E., DUECK, J., MINKOV, L. & NEESSE, T. 2010. Flow conditions in the air core of the hydrocyclone. *Minerals Engineering,* 23**,** 295-300.

HOCHSHEID, R. E. 1987. Horizontal cyclone in closed-circuit grinding. *Minerals Engineering*.

JOHNSTONE, R. H. & RAIS, S. A. 1988. Increased performance through flash flotation and cyclone optimization.

KAWATRA, S. K., BAKSHI, A. K. & RUSESKY, M. T. 1996a. The effect of slurry viscosity on hydrocyclone classification. *International Journal of Mineral Processing,* 48**,** 39-50.

KAWATRA, S. K., BAKSHI, A. K. & RUSESKY, M. T. 1996b. Effect of viscosity on the cut (d50) size of hydrocyclone classifiers. *Minerals Engineering,* 9**,** 881-891.

KELLY, E. G. 1991. The significance of by-pass in mineral separators. *Minerals Engineering,* 4**,** 1-7.

KELSALL, D. F. 1953. A further study of the hydraulic cyclone. *Chemical Engineering Science,* 2**,** 254-272.

KNOWLES, S. R., WOODS, D. R. & FEUERSTEIN, I. A. 1973. The velocity distribution within a hydrocyclone operating without an air core. *The Canadian Journal of Chemical Engineering,* 51**,** 263-271.

KOJOVIC, T. 1988. *The development and application of MODEL - an automated model builder for mineral processing.* Dissertation/Thesis.

KUANG, S. B., CHU, K. W., YU, A. B. & VINCE, A. 2012. Numerical study of liquid–gas–solid flow in classifying hydrocyclones: Effect of feed solids concentration. *Minerals Engineering,* 31**,** 17-31.

LILGE, E. O. 1962. Hydrocyclone fundamentals. *Trans. IMM,* 71**,** 285-337.

LYNCH, A. J. & RAO, T. C. 1975. Modelling and scale-up of hydrocyclone classifiers. *Proceedings XI International Mineral Processing Conference*.

LYNCH, A. J., RAO, T. C. & BAILEY, C. W. 1975. The influence of design and operating variables on the capacities of hydrocyclone classifiers. *International Journal of Mineral Processing,* 2**,** 29-37.

LYNCH, A. J., RAO, T. C. & PRISBREY, K. A. 1974. The influence of hydrocyclone diameter on reduced-efficiency curves. *International Journal of Mineral Processing,* 1**,** 173-181.

MILIN, L., HSIEH, K. T. & RAJAMANI, R. K. 1992. The leakage mechanisms in the hydrocyclone. *Minerals Engineering,* 5**,** 779-794.

MUSA, F. & MORRISON, R. 2009. A more sustainable approach to assessing comminution efficiency. *Minerals Engineering,* 22**,** 593-601.

NAGESWARARAO, K. 1978. *Further developments in the modelling and scale up of industrial hydrocyclones.* Dissertation/Thesis.

NAGESWARARAO, K. 1999. Normalisation of the efficiency curves of hydrocyclone classifiers. *Minerals Engineering,* 12**,** 107-118.

NAGESWARARAO, K., WISEMAN, D. M. & NAPIER-MUNN, T. J. 2004. Two empirical hydrocyclone models revisited. *Minerals Engineering,* 17**,** 671-687.

NAPIER-MUNN, T. J., MORRELL, S., MORRISON, R. D. & KOJOVIC, T. 1996. *Mineral comminution circuits: their operation and optimisation,* Indooroopilly, Qld, Julius Kruttschnitt Mineral Research Centre.

NARASIMHA, M., BRENNAN, M. & HOLTHAM, P. N. 2006. Large eddy simulation of hydrocyclone—prediction of air-core diameter and shape. *International Journal of Mineral Processing,* 80**,** 1-14.

NARASIMHA, M., MAINZA, A. N., HOLTHAM, P. N., POWELL, M. S. & BRENNAN, M. S. 2014. A semi-mechanistic model of hydrocyclones — Developed from industrial data and inputs from CFD. *International Journal of Mineral Processing,* 133**,** 1-12.

NEESSE, T. & DUECK, J. 2007. Air core formation in the hydrocyclone. *Minerals Engineering,* 20**,** 349-354.

NEESSE, T., SCHNEIDER, M., GOLYK, V. & TIEFEL, H. 2004. Measuring the operating state of the hydrocyclone. *Minerals Engineering,* 17**,** 697-703.

ORWE, D. & NOREEN, D. Horizontal cyclone plant trials at Bougainville. 1988 1988. 71-77.

PLITT, L. R. 1976. MATHEMATICAL MODEL OF THE HYDROCYCLONE CLASSIFIER. *CIM Bulletin,* 69**,** 114-123.

PLITT, L. R. & KAWATRA, S. K. 1979. Estimating the cut (d50) size of classifiers without product particle-size measurement. *International Journal of Mineral Processing,* 5**,** 369-378.

RAJAMANI, K. 1987. IMPROVEMENTS IN THE CLASSIFICATION EFFICIENCY OF A HYDROCYCLONE WITH AN IMPELLER INSTALLATION AROUND THE VORTEX-FINDER. *Particulate science and technology,* 5**,** 83-94.

RAO, T. C. 1966. *The characteristics of hydrocyclones: and their application as control units in comminution circuits.* Dissertation/Thesis.

RAO, T. C., NAGESWARARAO, K. & LYNCH, A. J. 1976. Influence of feed inlet diameter on the hydrocyclone behaviour. *International Journal of Mineral Processing,* 3**,** 357-363.

RIETEMA, K. 1961a. Performance and design of hydrocyclones—I: General considerations. *Chemical Engineering Science,* 15**,** 298-302.

RIETEMA, K. 1961b. Performance and design of hydrocyclones—II : Pressure drop in the hydrocyclone. *Chemical Engineering Science,* 15**,** 303-309.

RIETEMA, K. 1961c. Performance and design of hydrocyclones—III: Separating power of the hydrocyclone. *Chemical Engineering Science,* 15**,** 310-319.

RONG, R. & NAPIER-MUNN, T. J. 2003. Development of a More Efficient Classifying Cyclone. *Coal Preparation,* 23**,** 149-165.

SVAROVSKY, L. 1984. *Hydrocyclones,* London ; New York ; Sydney, Holt, Rinehart & Winston.

VAKAMALLA, T. R., KUMBHAR, K. S., GUJJULA, R. & MANGADODDY, N. 2014. Computational and experimental study of the effect of inclination on hydrocyclone performance. *Separation and Purification Technology,* 138**,** 104-117.

WILLS, B. A. 2006. 9. Classification. *Wills' Mineral Processing Technology - An Introduction to the Practical Aspects of Ore Treatment and Mineral Recovery (7th Edition).* Elsevier.

YALCIN, T., KAUKOLIN, E. & BYERS, A. 2003. Axial inlet cyclone for mineral processing applications. *Minerals Engineering,* 16**,** 1375-1381.

YOSHIOKA, N. & HOTTA, Y. 1955. Liquid Cyclone as a Hydraulic Classifier. *Kagaku kōgaku,* 19**,** 632-641.

ZHEN-BO, W., YI, M. & YOU-HAI, J. 2011. Simulation and experiment of flow field in axial-flow hydrocyclone. *Chemical Engineering Research and Design,* 89**,** 603-610.

APPENDICES

Appendix A: **Complete Experiment Data**

A.1. Summary of Experiment Data Chapter 3

Data sets for experiment with 25% silica feed using **original cone** used in Chapter 3:

Sieve size (µm)	Cumulative passing weight (%)		
	0° - 60 kPa		
	Feed	O/F	U/F
180	97.6	99.9	96.7
150	95.3	99.8	93.8
125	91.7	99.7	88.9
106	87.0	99.4	83.0
90	80.8	99.0	73.5
75	73.7	98.6	66.3
63	65.7	97.7	55.4
53	59.0	96.9	47.7
45	53.0	95.4	40.6
38	45.5	94.3	32.0
20	30.7	78.5	15.5
%Solids	30.1	11.6	53.6

Sieve size (µm)	Cumulative passing weight (%)					
	0° - 80 kPa			0° - 100 kPa		
	Feed	O/F	U/F	Feed	O/F	U/F
180	97.1	99.9	96.0	97.2	99.9	96.4
150	94.6	99.8	92.9	94.9	99.9	93.3
125	90.7	99.7	87.8	91.2	99.8	86.8
106	85.7	99.4	81.5	86.6	99.7	79.2
90	79.3	99.0	72.3	80.4	99.5	68.6
75	72.3	98.6	64.9	73.9	99.2	65.1
63	64.1	97.7	55.1	66.6	98.7	56.2
53	56.9	96.6	47.2	60.1	98.1	48.1
45	50.3	94.7	39.6	52.9	96.8	40.1
32	37.1	91.3	24.2	39.1	94.5	24.6
22	27.1	84.1	12.9	28.9	88.4	13.1
16	19.3	66.3	7.4	20.6	69.9	7.4
13	16.0	56.0	5.8	17.2	59.2	5.8
%Solids	28.9	10.3	54.0	27.6	9.9	54.4

Sieve size (µm)	Cumulative passing weight (%)		
	45° - 60 kPa		
	Feed	O/F	U/F
180	97.2	100.0	96.3
150	94.5	99.9	92.9
125	90.5	99.9	87.6
106	85.4	99.8	81.0
90	79.0	99.6	73.0
75	72.3	99.3	63.5
63	64.4	98.6	53.5
53	57.6	97.7	45.4
45	51.6	96.4	38.7
38	45.1	95.1	30.5
20	31.0	78.9	14.9
%Solids	25.1	8.8	50.4

Sieve size (µm)	Cumulative passing weight (%)					
	45° - 80 kPa			45° - 100 kPa		
	Feed	O/F	U/F	Feed	O/F	U/F
180	96.7	99.9	96.1	96.9	99.8	96.0
150	94.2	99.9	93.0	94.4	99.7	92.6
125	90.2	99.8	88.0	90.7	99.5	86.9
106	85.2	99.7	81.9	86.0	99.3	77.5
90	78.6	99.5	72.9	80.3	99.1	69.6
75	72.3	99.3	65.2	73.9	98.7	59.6
63	64.7	98.8	55.0	66.7	98.2	51.7
53	58.0	98.3	46.7	60.3	97.6	43.6
45	50.9	97.3	39.0	52.9	96.4	37.3
32	37.4	95.4	23.7	39.4	94.2	23.4
22	27.5	89.0	12.9	29.4	88.0	12.3
16	19.3	71.1	7.3	20.9	69.9	6.8
13	15.8	60.6	5.7	17.4	59.1	5.2
%Solids	26.2	8.6	49.5	24.4	8.5	52.0

Sieve size (µm)	Cumulative passing weight (%)					
	105° - 80 kPa			105° - 100 kPa		
	Feed	O/F	U/F	Feed	O/F	U/F
180	97.1	100.0	95.5	96.7	99.9	95.6
150	94.4	99.9	92.1	94.0	99.9	92.0
125	90.4	99.9	86.6	90.1	99.9	85.5
106	85.2	99.8	79.9	85.1	99.8	78.0
90	78.6	99.7	70.9	79.1	99.7	66.9
75	71.5	99.5	62.1	72.6	99.6	61.6
63	63.3	99.1	51.2	65.0	99.3	52.1
53	56.3	98.7	42.2	58.3	98.9	43.0
45	47.5	97.8	33.3	51.4	98.0	34.7
32	37.9	95.7	16.8	37.5	96.4	18.4
22	28.2	85.3	6.8	27.1	87.8	7.5
16	20.1	63.8	3.7	18.6	65.4	4.0
13	16.7	53.6	2.9	15.1	54.5	3.1
%Solids	24.8	9.8	63.2	25.3	9.1	63.8

Sieve size (µm)	Cumulative passing weight (%)		
	105° - 120 kPa		
	Feed	O/F	U/F
180	96.5	99.9	95.6
150	93.8	99.9	92.0
125	89.7	99.8	85.5
106	84.6	99.7	78.0
90	78.5	99.6	66.9
75	71.7	99.4	61.6
63	63.9	99.1	52.1
53	57.2	98.6	43.0
45	51.1	97.9	35.6
38	43.3	97.3	26.2
20	28.2	82.4	8.8
%Solids	25.0	8.9	64.9

Sieve size (µm)	Cumulative passing weight (%)					
	120° - 80 kPa			120° - 100 kPa		
	Feed	O/F	U/F	Feed	O/F	U/F
180	97.0	99.9	95.3	96.7	99.9	95.5
150	94.2	99.9	91.5	94.2	99.9	91.9
125	90.2	99.8	85.4	90.2	99.8	85.9
106	85.1	99.6	77.6	85.4	99.7	78.7
90	78.8	99.3	66.9	79.6	99.5	68.6
75	71.8	99.0	56.7	72.9	99.3	59.0
63	64.1	98.3	44.7	65.6	98.9	46.5
53	57.3	97.5	35.2	59.1	98.4	37.0
45	50.5	96.2	26.7	51.8	97.3	28.7
32	37.9	92.3	11.6	38.3	94.8	13.6
22	28.4	75.1	5.5	28.5	81.6	5.6
16	20.2	54.3	3.3	20.3	59.9	3.1
13	16.8	45.3	2.6	16.8	50.0	2.4
%Solids	23.9	10.9	69.0	24.7	10.1	70.4

Sieve size (µm)	Cumulative passing weight (%)		
	120° - 120 kPa		
	Feed	O/F	U/F
180	97.5	99.9	95.7
150	95.6	99.8	91.9
125	92.3	99.7	85.3
106	88.2	99.5	77.0
90	81.7	99.3	66.9
75	77.8	99.0	60.2
63	71.2	98.5	49.6
53	65.5	97.9	40.7
45	60.2	97.1	32.9
38	53.7	96.4	23.6
20	27.7	83.2	8.4
%Solids	25.3	9.6	71.5

A.2. Summary of Experiment Data Chapter 4

Data sets for experiment with 40% silica feed using **modified cone** used in Chapter 4:

Sieve size (µm)	Cumulative passing weight (%)											
	0° - 80 kPa			0° - 100 kPa			0° - 100 kPa (II)			0° - 120 kPa		
	Feed	O/F	U/F	Feed	O/F	U/F	Feed	O/F	U/F	Feed	O/F	U/F
180	97.0	99.3	94.5	96.5	99.8	94.6	96.5	99.8	94.6	95.7	99.9	94.4
150	94.1	99.1	90.1	93.9	99.7	90.2	93.9	99.7	90.2	92.8	99.5	89.8
125	90.5	98.9	82.8	89.8	99.6	82.8	89.8	99.6	82.8	88.7	99.0	82.3
106	85.8	98.5	74.1	84.7	99.2	73.6	84.7	99.2	73.6	83.7	98.5	72.3
90	80.1	98.0	60.3	78.0	98.7	60.7	78.0	98.7	60.7	77.8	97.9	59.5
75	73.8	97.2	52.8	72.8	98.1	52.3	72.8	98.1	52.3	71.7	97.1	47.8
63	64.7	94.9	39.8	64.5	95.9	37.8	64.5	95.9	37.8	63.1	94.4	35.6
53	59.2	91.7	31.4	57.2	91.9	29.6	57.2	91.9	29.6	55.7	88.1	27.2
45	53.1	86.0	25.4	51.2	85.8	24.4	51.2	85.8	24.4	50.2	82.0	22.7
38	46.4	77.7	20.5	44.1	77.2	19.7	44.1	77.2	19.7	43.1	72.0	18.0
20	28.3	51.3	12.1	29.2	52.3	12.0	29.2	52.3	12.0	29.2	49.4	11.1
%Solids	41.4	29.5	66.4	41.6	30.0	66.3	40.8	30.0	66.2	41.6	31.3	68.3

Sieve size (µm)	Cumulative passing weight (%)											
	105° - 80 kPa			105° - 80 kPa			105° - 100 kPa			105° - 120 kPa		
	Feed	O/F	U/F	Feed	O/F	U/F	Feed	O/F	U/F	Feed	O/F	U/F
180	96.9	99.5	92.5	96.3	99.6	92.8	97.0	99.5	93.5	96.8	99.4	94.1
150	93.7	99.5	86.5	93.5	99.5	85.7	94.2	99.4	88.3	94.1	99.3	88.2
125	89.9	99.1	76.0	89.5	99.0	77.0	90.6	99.2	79.8	90.2	99.1	81.0
106	85.2	98.4	63.5	84.3	98.4	65.5	86.1	98.8	69.0	85.4	98.7	71.4
90	79.3	96.9	50.7	78.1	97.0	52.6	80.7	97.9	54.9	79.8	98.0	59.8
75	72.9	93.9	40.8	72.3	94.0	40.8	74.6	96.7	46.1	74.3	96.7	47.5
63	63.4	85.8	30.0	64.1	86.2	31.2	65.9	92.8	33.7	66.6	92.9	33.0
53	58.0	80.1	23.8	57.5	79.6	24.3	60.8	86.9	26.3	60.1	88.4	27.4
45	51.8	72.9	19.2	50.6	72.6	19.6	54.3	79.8	20.0	53.9	81.8	21.4
38	45.5	65.7	15.6	44.9	65.8	16.0	47.9	72.3	16.6	47.5	73.7	16.9
20	29.7	46.4	9.3	29.2	45.8	9.8	31.4	49.2	9.3	30.1	50.3	9.3
%Solids	42.6	33.2	74.8	42.8	34.1	75.0	41.9	31.7	74.8	41.8	30.7	75.5

Sieve size (µm)	Cumulative passing weight (%)											
	120° - 80 kPa			120° - 100 kPa			120° - 120 kPa			120° - 120 kPa(II)		
	Feed	O/F	U/F	Feed	O/F	U/F	Feed	O/F	U/F	Feed	O/F	U/F
180	96.6	99.8	92.2	96.6	99.4	93.6	97.1	99.7	93.6	97.0	99.5	93.3
150	94.0	99.6	85.8	93.9	99.2	87.1	94.1	99.6	87.1	94.0	99.3	87.9
125	90.1	99.3	75.9	90.0	98.9	79.1	90.6	99.3	79.0	90.5	99.0	79.0
106	85.3	98.6	63.9	85.2	98.4	68.2	86.1	98.7	68.4	86.0	98.6	68.2
90	79.7	97.0	49.5	79.5	97.3	55.5	80.5	97.5	56.0	80.5	97.5	54.4
75	74.1	94.5	40.3	73.6	95.4	42.8	74.4	95.9	43.7	74.2	96.2	44.7
63	66.2	88.4	30.0	66.3	89.2	29.6	65.7	91.1	30.0	65.3	91.5	32.9
53	59.6	81.6	23.9	59.7	84.3	25.6	60.6	85.0	25.4	60.4	85.0	26.0
45	53.4	74.4	19.3	53.6	77.6	20.5	54.0	77.9	20.3	54.4	77.8	21.0
38	47.4	66.5	15.6	47.1	69.5	16.7	47.2	69.3	16.2	47.6	70.2	16.9
20	32.3	45.2	9.0	31.8	47.6	8.9	31.0	46.9	9.2	30.7	47.7	9.7
%Solids	41.9	33.4	77.0	41.8	31.9	75.6	42.2	31.5	72.7	41.3	31.2	73.7

Sieve size (μm)	Cumulative passing weight (%)								
	135° - 80 kPa			135° - 100 kPa			135° - 120 kPa		
	Feed	O/F	U/F	Feed	O/F	U/F	Feed	O/F	U/F
180	97.0	98.5	81.6	97.0	99.3	87.2	97.2	99.9	88.1
150	94.5	97.1	70.0	94.6	99.0	77.5	94.8	99.3	79.0
125	90.8	94.3	56.9	90.9	97.5	63.9	91.2	98.0	65.8
106	86.0	90.3	46.5	86.3	94.6	51.6	86.4	95.2	52.2
90	79.9	85.1	37.1	80.4	89.6	40.7	79.7	90.3	41.0
75	74.6	79.9	31.3	74.9	85.2	33.8	74.8	85.2	34.4
63	66.6	71.7	24.8	65.8	76.8	26.0	66.1	75.8	25.9
53	59.8	64.7	20.4	58.5	68.0	20.8	59.0	67.3	20.9
45	53.5	58.2	17.0	52.0	59.4	16.8	52.3	61.1	17.4
38	47.3	51.6	14.1	45.0	51.8	13.3	45.1	53.0	13.9
20	30.7	34.6	8.4	30.1	35.9	8.0	30.4	36.7	8.6
%Solids	41.7	40.5	79.2	41.8	39.6	75.7	41.9	37.0	75.3

A.3. Summary of Experiment Data Chapter 5

Data sets for experiment with 50% silica feed using **modified cone** used in Chapter 5:

Sieve size (μm)	Cumulative passing weight (%)									
	0° - 80 kPa			0° - 100 kPa			0° - 120 kPa			
	Feed	O/F	U/F	Feed	O/F	U/F	Feed	O/F	U/F	Reconstituted Feed*
180	95.8	100.0	93.6	95.8	99.9	92.5	95.8	99.9	90.8	95.4
150	91.2	99.9	88.2	91.2	99.8	85.6	91.2	99.8	82.7	91.1
125	85.3	99.8	80.5	85.3	99.4	74.8	85.3	99.2	70.5	84,8
106	78.3	99.4	71.6	78.3	98.3	63.5	78.3	97.6	58.5	77.8
90	70.7	98.6	59.6	70.7	96.4	50.6	70.7	94.3	46.4	70.4
75	63.8	96.3	47.9	63.8	92.4	41.9	63.8	88.8	37.7	62.9
63	56.5	90.6	38.5	56.5	85.4	33.4	56.5	82.1	31.0	56.7
53	51.0	84.5	32.8	51.0	78.3	28.0	51.0	75.6	26.6	50.8
45	45.5	76.5	27.8	45.5	70.8	24.0	45.5	67.0	22.6	45.0
38	39.6	68.7	23.7	39.6	62.7	20.0	39.6	57.5	18.7	38.8
20	26.2	47.8	15.4	26.2	39.5	12.2	26.2	38.6	13.2	26.1
%Solids	49.6	36.1	66.4	49.6	38.5	69.2	49.6	39.7	70.5	50.3

*reconstituted feed is calculated with JKSimMet Material Balance with using the compositions and relative flowrates of slurry through the Vezin samplers on the overflow and the underflow products.

Sieve size (µm)	Cumulative passing weight (%)								
	105° - 80 kPa			105° - 100 kPa			105° - 120 kPa		
	Feed	O/F	U/F	Feed	O/F	U/F	Feed	O/F	U/F
180	97.6	99.9	93.8	97.6	99.9	93.5	97.6	99.9	93.3
150	95.4	99.9	87.9	95.4	99.8	87.4	95.4	99.8	87.2
125	92.0	99.5	78.6	92.0	99.3	78.0	92.0	99.3	78.0
106	88.0	98.3	67.8	88.0	98.1	67.0	88.0	98.1	67.2
90	82.5	96.0	54.9	82.5	95.7	54.0	82.5	96.0	54.4
75	75.8	91.9	44.5	75.8	91.9	43.2	75.8	90.9	43.7
63	68.6	83.4	36.3	68.6	83.5	34.9	68.6	83.3	35.7
53	62.0	77.0	31.1	62.0	76.6	29.6	62.0	76.3	30.2
45	55.9	70.3	26.4	55.9	69.8	24.8	55.9	69.4	25.3
38	48.6	62.4	21.8	48.6	62.6	20.3	48.6	61.6	20.5
%Solids	47.2	40.9	72.9	47.2	40.8	72.0	47.2	40.5	71.9

Sieve size (µm)	Cumulative passing weight (%)											
	120° - 80 kPa			120° - 100 kPa			120° - 120 kPa			120° - 120 kPa (II)		
	Feed	O/F	U/F	Feed	O/F	U/F	Feed	O/F	U/F	Feed	O/F	U/F
180	96.7	100.0	90.9	96.7	100.0	91.8	96.7	100.0	91.3	96.7	99.9	92.1
150	93.8	99.9	82.7	93.8	99.9	84.1	93.8	99.9	83.7	93.8	99.9	84.9
125	89.5	99.0	71.5	89.5	99.1	73.1	89.5	99.3	73.1	89.5	99.2	73.8
106	84.7	97.0	60.5	84.7	97.5	61.2	84.7	97.9	62.1	84.7	97.7	62.9
90	78.4	93.4	49.1	78.4	94.3	49.7	78.4	94.7	50.6	78.4	94.8	50.0
75	71.5	87.7	40.6	71.5	88.8	41.1	71.5	89.2	42.1	71.5	89.5	41.2
63	64.3	80.6	32.2	64.3	81.3	32.4	64.3	81.4	33.2	64.3	82.3	32.0
53	57.4	73.5	27.1	57.4	74.4	27.2	57.4	74.6	27.7	57.4	75.6	27.0
45	51.5	66.4	23.1	51.5	67.5	23.1	51.5	67.6	23.2	51.5	68.4	22.8
38	45.0	58.5	18.9	45.0	59.6	19.3	45.0	59.8	19.0	45.0	60.6	19.2
%Solids	48.4	42.1	72.9	48.4	41.5	74.3	48.4	40.9	74.4	48.4	41.0	76.0

Sieve size (μm)	Cumulative passing weight (%)											
	135° - 100 kPa			135° - 120 kPa			135° - 120 kPa (II)			135° - 140 kPa		
	Feed	O/F	U/F	Feed	O/F	U/F	Feed	O/F	U/F	Feed	O/F	U/F
180	96.7	99.9	90.7	96.7	99.9	90.4	96.7	100.0	91.2	96.7	100.0	90.7
150	93.8	99.8	82.3	93.8	99.8	82.0	93.8	99.8	83.3	93.8	99.9	82.5
125	89.5	98.6	70.3	89.5	98.7	70.6	89.5	98.9	71.4	89.5	98.9	71.2
106	84.7	96.6	59.2	84.7	96.9	59.5	84.7	97.1	60.6	84.7	97.2	60.1
90	78.4	92.8	48.2	78.4	93.4	48.6	78.4	93.4	48.8	78.4	93.8	50.2
75	71.5	86.5	40.0	71.5	87.3	40.5	71.5	87.1	40.0	71.5	87.9	41.6
63	64.3	78.5	31.8	64.3	79.9	32.1	64.3	79.5	31.8	64.3	80.2	33.0
53	57.4	72.5	26.4	57.4	73.3	27.1	57.4	73.4	26.5	57.4	74.1	27.9
45	51.5	65.3	22.2	51.5	66.1	23.0	51.5	66.2	22.4	51.5	66.7	23.6
38	45.0	57.4	18.4	45.0	58.7	19.1	45.0	58.4	18.5	45.0	59.2	19.3
%Solids	48.4	42.2	74.5	48.4	41.8	74.4	48.4	41.5	73.8	48.4	41.6	73.4

A.4. Summary of Experiment Data Chapter 6

Data sets for experiment with 40% mixture silica-magnetite feed using **modified cone** used in Chapter 6:

sieves size (μm)	0° - 80 kPa								
	Mixture			Silica			Magnetite		
	Feed	O/F	U/F	Feed	O/F	U/F	Feed	O/F	U/F
180	96.1	100.0	93.3	96.5	100.0	93.8	94.5	100.0	91.9
150	93.4	100.0	88.5	93.4	100.0	88.1	93.3	100.0	89.9
125	90.2	99.8	82.9	90.4	99.8	81.1	89.5	100.0	87.9
106	86.1	99.5	75.7	85.6	99.5	71.9	87.9	99.6	86.0
90	81.0	99.0	66.4	79.6	99.0	60.4	86.0	99.5	82.9
75	74.8	98.0	55.9	72.4	97.9	47.4	83.5	99.3	79.3
63	68.4	94.2	46.4	65.2	93.9	36.3	80.2	98.9	74.4
53	61.6	89.2	38.6	58.1	88.8	28.3	74.5	97.9	67.0
45	54.6	82.6	31.4	51.4	81.9	22.7	66.6	95.2	55.3
38	50.7	76.9	27.3	47.7	76.1	20.0	61.8	92.1	47.5
20	30.5	51.9	12.9	25.4	51.7	6.8	49.4	55.9	29.8

%Solids	43.3	30.0	65.7

sieves size (μm)	0° - 100 kPa								
	Mixture			Silica			Magnetite		
	Feed	O/F	U/F	Feed	O/F	U/F	Feed	O/F	U/F
180	96.5	100.0	93.7	96.9	100.0	94.0	95.4	100.0	93.1
150	94.2	100.0	89.6	94.3	100.0	89.1	94.1	100.0	90.9
125	90.9	99.9	83.6	90.4	99.8	81.4	92.7	100.0	88.6
106	86.8	99.6	75.8	85.3	99.6	71.5	91.3	100.0	85.8
90	81.8	99.1	66.9	79.4	99.0	60.0	89.3	99.8	83.0
75	76.5	97.9	58.0	73.2	97.7	48.6	87.1	99.5	79.7
63	68.4	94.7	45.9	63.8	94.4	33.8	83.0	99.1	73.7
53	62.6	89.8	38.7	57.6	89.2	26.4	78.7	98.3	67.0
45	55.7	82.8	31.7	50.7	81.8	20.7	71.5	96.8	56.9
38	48.7	74.9	25.1	44.1	73.5	16.4	63.4	93.1	45.0
20	28.8	52.8	11.5	28.5	53.1	10.6	30.0	47.6	13.6

%Solids	42.6	30.0	67.6

sieves size (μm)	0o - 100 kPa (II)								
	Mixture			Silica			Magnetite		
	Feed	O/F	U/F	Feed	O/F	U/F	Feed	O/F	U/F
180	96.3	100.0	93.8	96.7	100.0	94.3	94.8	100.0	91.9
150	93.6	100.0	89.5	93.7	100.0	89.4	93.3	100.0	90.1
125	90.4	99.9	84.0	90.0	99.9	82.7	92.0	100.0	88.0
106	86.6	99.6	76.4	85.6	99.6	73.6	90.7	100.0	85.5
90	81.4	99.1	67.4	79.6	99.1	62.7	88.5	99.9	82.6
75	75.2	97.8	58.0	72.5	97.7	51.4	85.9	99.6	79.1
63	68.8	94.4	45.6	65.3	94.1	37.4	82.4	98.5	72.2
53	62.7	89.0	38.8	58.8	88.5	30.8	77.7	97.3	64.7
45	56.6	81.7	32.4	52.9	81.0	25.8	70.9	95.0	53.7
38	52.7	73.7	26.6	49.4	72.8	22.1	65.7	89.2	41.0
20	31.7	48.9	12.7	32.7	49.9	11.9	27.4	29.7	15.6

%Solids	43.6	30.4	67.9

sieves size (µm)	0° - 120 kPa								
	Mixture			Silica			Magnetite		
	Feed	O/F	U/F	Feed	O/F	U/F	Feed	O/F	U/F
180	96.7	100.0	94.0	96.9	100.0	94.3	95.8	100.0	93.0
150	94.1	99.9	89.8	93.9	99.9	89.4	94.6	99.9	91.1
125	90.8	99.7	83.8	90.1	99.7	82.0	93.3	99.7	89.1
106	86.8	99.4	75.4	85.3	99.3	71.6	92.1	99.6	86.4
90	80.4	99.0	64.6	77.8	98.9	58.5	89.7	99.4	82.6
75	73.7	98.1	54.2	70.0	97.9	46.0	86.9	99.2	78.3
63	66.8	94.3	43.1	62.3	93.4	33.4	82.8	99.1	71.7
53	61.1	88.9	36.5	56.3	87.0	26.9	78.2	98.8	64.7
45	54.5	82.6	30.2	49.9	79.6	22.2	71.0	98.5	53.5
38	50.6	77.6	25.6	46.1	73.9	19.2	66.7	97.8	44.6
20	31.0	52.4	11.7	31.1	49.2	11.1	30.6	69.9	13.5

%Solids	43.5	30.0	68.6

sieves size (µm)	105° - 80 kPa								
	Mixture			Silica			Magnetite		
	Feed	O/F	U/F	Feed	O/F	U/F	Feed	O/F	U/F
180	96.80	99.97	92.97	96.87	99.97	92.82	96.50	100.00	93.38
150	94.42	99.95	86.70	94.18	99.94	85.01	95.46	100.00	91.04
125	90.89	99.65	78.71	90.15	99.60	74.82	94.02	100.00	88.72
106	87.07	99.12	68.50	85.77	98.99	61.73	92.50	100.00	85.94
90	82.25	96.93	57.22	80.22	96.51	47.40	90.72	99.94	82.52
75	75.95	93.06	47.88	73.09	92.12	36.07	87.92	99.83	78.30
63	69.05	86.75	38.73	65.50	84.97	26.30	83.88	99.54	70.74
53	63.67	81.02	32.76	59.79	78.53	21.20	79.88	98.91	62.55
45	56.86	74.31	26.82	53.20	71.08	17.49	72.19	97.41	50.86
38	50.30	67.67	20.29	47.11	63.90	14.14	63.65	94.70	36.13

%Solids	42.7	33.8	76.2

sieves size (µm)	105° - 80 kPa (II)								
	Mixture			Silica			Magnetite		
	Feed	O/F	U/F	Feed	O/F	U/F	Feed	O/F	U/F
180	96.80	99.95	93.13	96.87	99.94	92.98	96.50	100.00	93.53
150	94.42	99.91	86.99	94.18	99.89	85.36	95.46	100.00	91.31
125	90.89	99.60	79.15	90.15	99.54	75.43	94.02	100.00	89.02
106	87.07	99.05	68.95	85.77	98.92	62.43	92.50	100.00	86.22
90	82.25	97.51	57.54	80.22	97.17	48.08	90.72	99.94	82.61
75	75.95	93.67	47.91	73.09	92.83	36.47	87.92	99.71	78.25
63	69.05	86.69	38.90	65.50	84.98	26.95	83.88	98.95	70.58
53	63.67	81.11	32.91	59.79	78.72	21.87	79.88	98.19	62.18
45	56.86	74.26	27.08	53.20	71.17	18.19	72.19	96.38	50.65
38	50.30	66.38	20.46	47.11	62.64	14.87	63.65	93.10	35.29

%Solids	42.7	34.7	73.4

sieves size (µm)	105° - 100 kPa								
	Mixture			Silica			Magnetite		
	Feed	O/F	U/F	Feed	O/F	U/F	Feed	O/F	U/F
180	96.80	99.88	93.44	96.87	99.86	93.17	96.50	100.00	94.13
150	94.42	99.80	87.31	94.18	99.77	85.47	95.46	100.00	91.96
125	90.89	99.58	79.67	90.15	99.52	75.65	94.02	100.00	89.82
106	87.07	99.37	69.57	85.77	99.28	62.58	92.50	100.00	87.22
90	82.25	97.54	57.92	80.22	97.19	47.62	90.72	99.95	83.94
75	75.95	94.13	47.92	73.09	93.31	35.20	87.92	99.79	80.04
63	69.05	88.53	37.68	65.50	86.92	24.02	83.88	99.53	72.19
53	63.67	83.00	31.08	59.79	80.63	18.36	79.88	99.22	63.21
45	56.86	76.28	25.46	53.20	73.07	14.64	72.19	98.29	52.77
38	50.30	68.98	18.62	47.11	65.02	11.04	63.65	96.12	37.75

%Solids	42.7	33.8	74.8

sieves size (µm)	105° - 120 kPa								
	Mixture			Silica			Magnetite		
	Feed	O/F	U/F	Feed	O/F	U/F	Feed	O/F	U/F
180	96.80	100.00	94.22	96.87	100.00	94.11	96.50	100.00	94.51
150	94.42	99.99	88.81	94.18	99.99	87.49	95.46	100.00	92.46
125	90.89	99.97	81.63	90.15	99.96	78.49	94.02	100.00	90.34
106	87.07	99.80	72.12	85.77	99.77	66.47	92.50	100.00	87.76
90	82.25	98.79	60.96	80.22	98.63	52.46	90.72	100.00	84.48
75	75.95	95.99	50.29	73.09	95.46	39.51	87.92	99.89	80.13
63	69.05	90.29	40.15	65.50	89.03	28.58	83.88	99.73	72.16
53	63.67	85.38	33.82	59.79	83.49	23.11	79.88	99.47	63.47
45	56.86	78.81	28.97	53.20	76.14	19.82	72.19	98.83	54.32
38	50.30	72.76	23.82	47.11	69.46	16.89	63.65	97.45	42.99

%Solids	42.7	33.1	75.8

sieves size (µm)	120° - 80 kPa								
	Mixture			Silica			Magnetite		
	Feed	O/F	U/F	Feed	O/F	U/F	Feed	O/F	U/F
180	96.66	99.99	89.55	96.90	99.99	89.59	95.60	100.00	89.43
150	94.37	99.98	81.37	94.35	99.97	79.57	94.47	100.00	86.30
125	91.03	99.51	71.69	90.63	99.44	67.49	92.80	100.00	83.16
106	87.04	98.08	62.34	86.10	97.83	55.90	91.21	100.00	79.94
90	82.30	95.26	51.78	80.76	94.67	43.44	89.14	99.84	74.56
75	76.89	90.55	43.66	74.70	89.39	34.87	86.58	99.57	67.66
63	69.10	82.29	37.08	66.22	80.21	28.88	81.87	98.45	59.50
53	63.42	76.53	30.97	60.32	73.87	24.51	77.20	97.18	48.63
45	57.48	70.49	24.18	54.57	67.38	20.91	70.39	94.62	33.10
38	51.55	63.86	20.61	49.08	60.67	19.25	62.49	88.65	24.33

%Solids	43.1	36.4	75.5

sieves size (μm)	120° - 100 kPa								
	Mixture			Silica			Magnetite		
	Feed	O/F	U/F	Feed	O/F	U/F	Feed	O/F	U/F
180	96.66	99.98	91.29	96.90	99.98	91.37	95.60	100.00	91.06
150	94.37	99.95	84.98	94.35	99.94	83.67	94.47	100.00	88.61
125	91.03	99.78	76.53	90.63	99.76	73.13	92.80	100.00	85.94
106	87.04	99.10	65.96	86.10	99.02	59.91	91.21	99.81	82.70
90	82.30	96.96	55.45	80.76	96.68	47.03	89.14	99.55	78.73
75	76.89	92.69	47.26	74.70	91.96	37.65	86.58	99.35	73.86
63	69.10	86.81	38.61	66.22	85.50	28.91	81.87	98.77	65.44
53	63.42	79.75	32.78	60.32	77.81	24.26	77.20	97.54	56.35
45	57.48	72.65	26.87	54.57	70.18	20.60	70.39	95.21	44.21
38	51.55	69.06	21.11	49.08	66.40	17.90	62.49	93.39	29.97

%Solids	43.1	34.8	76.5

sieves size (μm)	120° - 100 kPa (II)								
	Mixture			Silica			Magnetite		
	Feed	O/F	U/F	Feed	O/F	U/F	Feed	O/F	U/F
180	96.66	99.99	91.94	96.90	99.99	92.00	95.60	100.00	91.78
150	94.37	99.97	85.34	94.35	99.97	84.07	94.47	100.00	89.05
125	91.03	99.87	77.02	90.63	99.85	73.80	92.80	100.00	86.41
106	87.04	99.50	67.50	86.10	99.47	61.90	91.21	99.75	83.83
90	82.30	97.47	56.00	80.76	97.20	48.08	89.14	99.75	79.10
75	76.89	93.46	46.57	74.70	92.77	37.27	86.58	99.39	73.67
63	69.10	87.28	39.30	66.22	85.95	29.98	81.87	98.77	66.47
53	63.42	80.68	32.57	60.32	78.68	24.73	77.20	97.92	55.44
45	57.48	73.59	25.43	54.57	71.00	20.79	70.39	95.89	38.92
38	51.55	69.88	21.98	49.08	67.06	19.12	62.49	94.12	30.30

%Solids	43.1	34.8	76.5

sieves size (µm)	120° - 120 kPa								
	Mixture			Silica			Magnetite		
	Feed	O/F	U/F	Feed	O/F	U/F	Feed	O/F	U/F
180	96.66	99.93	92.56	96.90	99.95	92.53	95.60	99.70	92.65
150	94.37	99.89	87.08	94.35	99.91	85.86	94.47	99.70	90.58
125	91.03	99.81	79.04	90.63	99.83	75.89	92.80	99.64	88.11
106	87.04	99.26	68.94	86.10	99.23	63.30	91.21	99.58	85.16
90	82.30	97.90	57.94	80.76	97.72	49.77	89.14	99.52	81.42
75	76.89	95.08	48.68	74.70	94.61	38.92	86.58	99.39	76.76
63	69.10	88.45	39.15	66.22	87.31	29.04	81.87	98.97	68.23
53	63.42	82.37	33.54	60.32	80.66	24.48	77.20	98.12	59.59
45	57.48	76.68	27.85	54.57	74.45	20.81	70.39	97.22	48.09
38	51.55	70.05	21.91	49.08	67.36	17.89	62.49	94.85	33.45

%Solids	43.1	33.9	71.6

sieves size (µm)	135° - 100 kPa								
	Mixture			Silica			Magnetite		
	Feed	O/F	U/F	Feed	O/F	U/F	Feed	O/F	U/F
180	96.98	99.61	84.96	97.04	99.53	83.37	96.76	100.00	87.83
150	94.89	98.42	76.55	94.64	98.13	72.41	95.77	100.00	84.09
125	92.00	96.50	66.37	91.24	95.84	59.21	94.65	100.00	79.41
106	88.26	93.39	57.58	86.85	92.26	48.15	93.24	99.44	74.73
90	83.68	89.14	49.28	81.41	87.32	38.56	91.69	98.89	68.80
75	78.64	82.87	42.70	75.45	80.15	31.61	89.86	97.49	62.88
63	70.35	76.35	34.62	65.89	72.82	24.16	86.06	95.26	53.67
53	64.62	69.73	29.09	59.70	65.65	20.13	81.97	91.64	45.41
45	57.05	63.51	22.29	52.18	59.41	16.36	74.23	85.51	33.08
38	50.55	56.51	17.98	45.98	53.02	14.13	66.62	75.20	24.97

%Solids	43.0	40.4	76.7

sieves size (µm)	135° - 120 kPa								
	Mixture			Silica			Magnetite		
	Feed	O/F	U/F	Feed	O/F	U/F	Feed	O/F	U/F
180	96.98	99.90	91.48	97.04	99.88	90.72	96.76	100.00	93.12
150	94.89	99.85	85.34	94.64	99.82	82.69	95.77	100.00	91.01
125	92.00	99.51	76.03	91.24	99.47	70.29	94.65	99.72	88.34
106	88.26	98.58	65.39	86.85	98.34	56.20	93.24	99.72	85.09
90	83.68	96.37	55.05	81.41	95.73	42.82	91.69	99.44	81.26
75	78.64	92.80	47.26	75.45	91.52	33.36	89.86	98.87	77.06
63	70.35	85.30	38.99	65.89	82.74	24.62	86.06	97.46	69.79
53	64.62	79.37	32.91	59.70	75.80	19.63	81.97	96.34	61.38
45	57.05	72.56	25.73	52.18	68.09	15.43	74.23	93.80	47.80
38	50.55	65.21	18.98	45.98	60.02	12.13	66.62	89.86	33.65

%Solids	43.0	35.7	78.0

sieves size (µm)	135° - 120 kPa (II)								
	Mixture			Silica			Magnetite		
	Feed	O/F	U/F	Feed	O/F	U/F	Feed	O/F	U/F
180	96.98	99.85	90.82	97.04	99.83	90.11	96.76	100.00	92.48
150	94.89	99.76	83.47	94.64	99.72	80.76	95.77	100.00	89.79
125	92.00	99.27	73.46	91.24	99.17	67.73	94.65	99.93	86.86
106	88.26	97.93	63.67	86.85	97.65	54.86	93.24	99.75	84.25
90	83.68	94.96	51.69	81.41	94.23	40.09	91.69	99.64	78.75
75	78.64	89.85	43.62	75.45	88.38	31.04	89.86	99.17	73.01
63	70.35	82.02	36.14	65.89	79.42	24.03	86.06	98.60	64.42
53	64.62	76.03	30.03	59.70	72.68	19.62	81.97	97.38	54.33
45	57.05	69.42	23.04	52.18	65.41	16.09	74.23	95.01	39.28
38	50.55	63.88	19.27	45.98	59.62	14.24	66.62	90.98	31.01

%Solids	43.0	36.1	78.4

sieves size (µm)	135° - 140 kPa								
	Mixture			Silica			Magnetite		
	Feed	O/F	U/F	Feed	O/F	U/F	Feed	O/F	U/F
180	96.98	99.84	91.94	97.04	99.82	91.30	96.76	100.00	93.46
150	94.89	99.77	85.40	94.64	99.75	82.95	95.77	99.92	91.26
125	92.00	99.45	76.76	91.24	99.40	71.68	94.65	99.77	88.90
106	88.26	98.56	67.24	86.85	98.39	59.23	93.24	99.69	86.40
90	83.68	96.36	55.88	81.41	95.87	44.70	91.69	99.62	82.61
75	78.64	91.89	46.89	75.45	90.79	33.88	89.86	99.27	77.99
63	70.35	84.58	39.76	65.89	82.53	26.50	86.06	98.31	71.47
53	64.62	78.70	33.58	59.70	75.87	21.43	81.97	97.66	62.63
45	57.05	72.44	25.38	52.18	68.87	17.10	74.23	96.35	45.20
38	50.55	66.81	22.03	45.98	62.74	15.27	66.62	94.05	38.21

%Solids	43.0	35.0	77.9

A.5. Summary of Model Predictions

Narasimha/Mainza model predictions using calibrated K-parameters on 40% silica feed experiments used in Chapter 7 are as follow:

Operating condition		Narasimha Model Prediction			
Inclination (°)	Pressure (kPa)	d50c (micron)	Water split to U/F (%)	Alpha	Throughput (m3/h)
0	80	56.7	21.1	4.6	57.9
0	100	54.3	21.0	4.6	64.4
0	100	53.1	20.4	4.7	64.5
0	120	52.6	20.1	4.5	70.5
105	80	95.8	8.9	3.1	60.2
105	80	99.0	9.2	3.0	60.1
105	100	89.2	8.2	3.2	67.4
105	120	84.8	7.8	3.2	73.9
120	80	114.8	6.1	2.7	61.4
120	100	107.1	5.7	2.8	68.7
120	120	101.7	5.4	2.8	75.2
120	120	100.7	5.4	2.8	75.3
135	80	150.5	3.9	2.2	62.8
135	100	139.0	3.6	2.3	70.3
135	120	133.1	3.4	2.3	77.0

Narasimha/Mainza model predictions using calibrated K-parameters on 50% silica feed experiments used in Chapter 7 are as follow:

Operating condition		Narasimha Model Prediction			
Inclination (°)	Pressure (kPa)	d50c (micron)	Water recovery to U/F (%)	Alpha	Throughput (m3/h)
0	80	78.1	27.1	3.9	55.6
0	100	73.3	25.5	4.0	62.2
0	120	69.6	24.2	4.0	68.2
105	80	116.6	9.7	3.0	58.5
105	100	109.0	9.1	3.1	65.5
105	120	103.2	8.6	3.1	71.7
120	80	147.8	7.1	2.5	59.4
120	100	140.5	6.8	2.5	66.4
120	120	132.9	6.4	2.5	72.8
120	120	134.8	6.5	2.5	72.8
135	100	181.9	4.2	2.1	68.1
135	120	174.2	4.0	2.1	74.6
135	120	172.5	3.9	2.1	74.6
135	140	167.8	3.8	2.1	80.5

Narasimha/Mainza model predictions using calibrated K-parameters on 40% mixture silica-magnetite feed experiments used in Chapter 7 are as follow:

Operating condition		Narasimha Model Prediction			
Inclination (°)	Pressure (kPa)	d50c (micron)	Water recovery to U/F (%)	Alpha	Throughput (m3/h)
0	80	55.3	20.8	3.6	55.8
0	100	51.4	19.7	3.6	62.5
0	100	51.7	19.3	3.6	62.5
0	120	49.7	18.6	3.6	68.4
105	80	89.2	8.3	2.5	58.5
105	80	89.8	8.4	2.5	58.4
105	100	84.3	7.9	2.5	65.4
105	120	83.4	7.6	2.5	71.4
120	80	110.4	5.8	2.1	59.5
120	100	105.6	5.5	2.1	66.4
120	100	106.4	5.5	2.1	66.4
120	120	99.2	5.2	2.2	72.8
135	100	137.7	3.4	1.7	68.0
135	120	130.6	3.3	1.8	74.6
135	120	129.0	3.2	1.8	74.6
135	140	125.2	3.1	1.8	80.6

Narasimha/Mainza fitted K-parameters on 40% silica feed experiments presented in Chapter 7 are as follow:

Operating condition		Constant Parameters			
Inclination (°)	Pressure (kPa)	KD0	KW1	Kalpha0	KQ0
0	80	0.0214	0.95	20.9	345
0	100	0.0229	1.01	25.8	330
0	100	0.0230	1.00	23.9	335
0	120	0.0253	0.94	27.5	337
105	80	0.0166	1.13	27.5	320
105	80	0.0156	1.17	28.9	311
105	100	0.0152	1.27	31.0	313
105	120	0.0151	1.39	27.7	323
120	80	0.0144	1.22	33.8	311
120	100	0.0136	1.64	34.3	312
120	120	0.0140	1.98	38.1	302
120	120	0.0137	1.94	34.3	302
135	80	0.0251	0.50	40.4	289
135	100	0.0186	1.19	41.2	303
135	120	0.0192	1.35	43.0	301

Narasimha/Mainza fitted K-parameters on 50% silica feed experiments presented in Chapter 7 are as follow:

Operating condition		Constant Parameters			
Inclination (°)	Pressure (kPa)	KD0	KW1	Kalpha0	KQ0
0	80	0.0195	0.99	30.0	322
0	100	0.0233	0.89	28.3	335
0	120	0.0269	0.85	29.3	340
105	80	0.0160	1.14	35.8	318
105	100	0.0170	1.17	36.5	309
105	120	0.0178	1.20	36.4	300
120	80	0.0134	1.49	42.9	291
120	100	0.0135	1.61	42.1	296
120	120	0.0139	1.70	40.7	296
120	120	0.0135	1.64	40.0	302
135	100	0.0113	2.26	50.1	290
135	120	0.0117	2.57	49.8	303
135	120	0.0114	2.56	50.3	291
135	140	0.0116	2.82	49.4	288

Narasimha/Mainza fitted K-parameters on 40% mixture silica-magnetite feed experiments presented in Chapter 7 are as follow:

Operating condition		Constant Parameters				
Inclination (°)	**Pressure (kPa)**	**KD0**	**KW1**	**Kalpha0**	**KQ0**	**Beta**
0	80	0.0243	0.95	22.3	339	-0.14
0	100	0.0239	0.91	19.1	324	-0.15
0	100	0.0284	0.84	28.3	338	-0.29
0	120	0.0284	0.89	32.9	336	-0.37
105	80	0.0218	0.89	46.6	313	-0.34
105	80	0.0214	1.03	44.4	308	-0.19
105	100	0.0210	1.04	35.6	307	-0.05
105	120	0.0175	1.24	49.1	297	-7.22
120	80	0.0222	1.05	67.1	311	-0.31
120	100	0.0223	1.29	88.2	288	-0.55
120	100	0.0208	1.39	93.5	287	-0.57
120	120	0.0181	1.87	49.3	299	-0.19
135	100	0.0262	0.84	60.0	286	-0.13
135	120	0.0159	1.74	59.0	298	-0.22
135	120	0.0185	1.51	73.4	304	-0.29
135	140	0.0177	2.00	77.9	293	-0.45

A.6. Summary of Experiment Data with Novel Vortex

Data sets for experiment using novel vortex finder discussed in Chapter 8:

40% Silica Feed

Sieve size (μm)	Cumulative passing weight (%)											
	0° - 120 kPa P1			0° - 120 kPa P1 (II)			120° - 120 kPa P1			120° - 120 kPa P1 (II)		
	Feed	O/F	U/F	Feed	O/F	U/F	Feed	O/F	U/F	Feed	O/F	U/F
180	96.4	100.0	94.1	96.4	100.0	94.1	96.4	99.9	92.7	96.4	99.9	92.7
150	92.7	99.9	88.2	92.7	99.9	88.3	92.7	99.9	85.3	92.7	99.9	85.1
125	87.8	99.9	79.9	87.8	99.9	80.1	87.8	99.8	74.4	87.8	99.7	72.8
106	86.7	99.8	71.5	86.7	99.8	72.3	86.7	99.5	67.7	86.7	99.3	62.8
90	75.9	99.4	58.6	75.9	99.4	58.8	75.9	98.5	50.0	75.9	98.4	46.6
75	67.2	98.8	45.3	67.2	98.8	44.4	67.2	95.3	36.3	67.2	96.6	33.6
63	58.5	97.4	33.9	58.5	96.9	31.8	58.5	88.7	26.0	58.5	90.8	24.5
53	52.3	94.0	26.9	52.3	92.7	25.9	52.3	82.6	20.9	52.3	83.9	20.3
45	46.4	87.4	21.3	46.4	86.7	21.0	46.4	75.4	16.9	46.4	77.0	16.8
38	40.9	79.2	17.5	40.9	78.1	17.7	40.9	68.9	13.8	40.9	69.5	14.1
20	27.9	53.3	10.9	27.9	55.3	10.7						
%Solids	40.2	27.3	69.7	40.2	26.9	68.2	40.2	30.1	74.7	40.2	30.2	75.3

Sieve size (μm)	Cumulative passing weight (%)								
	135° - 100 kPa P1			135° - 100 kPa P1 (II)			135° - 120 kPa P1		
	Feed	O/F	U/F	Feed	O/F	U/F	Feed	O/F	U/F
180	96.4	100.0	89.0	96.4	99.9	89.5	96.4	99.9	91.0
150	92.7	99.8	77.6	92.7	99.8	78.5	92.7	99.9	81.3
125	87.8	98.5	63.1	87.8	99.0	63.8	87.8	99.2	66.6
106	86.7	96.5	53.8	86.7	97.4	55.2	86.7	97.9	60.1
90	75.9	92.6	37.9	75.9	92.9	38.1	75.9	95.4	40.9
75	67.2	86.9	29.0	67.2	87.2	28.3	67.2	91.1	30.3
63	58.5	78.5	22.9	58.5	80.0	22.0	58.5	82.9	22.8
53	52.3	71.9	18.7	52.3	74.4	18.2	52.3	75.9	18.9
45	46.4	65.2	15.3	46.4	68.3	14.9	46.4	68.8	15.6
38	40.9	58.0	12.8	40.9	62.8	12.3	40.9	60.9	13.1
%Solids	40.2	34.7	75.6	40.2	34.0	75.8	40.2	33.1	75.6

50% Silica Feed

Sieve size (µm)	Cumulative passing weight (%)					
	0° - 120 kPa P1			0° - 120 kPa P1 (II)		
	Feed	O/F	U/F	Feed	O/F	U/F
180	95.8	99.9	89.5	95.8	99.9	89.7
150	91.2	99.8	80.3	91.2	99.8	80.4
125	85.3	98.4	66.8	85.3	98.4	67.5
106	78.3	96.3	55.5	78.3	96.3	55.9
90	70.7	92.2	44.5	70.7	92.2	45.2
75	63.8	85.9	36.1	63.8	85.9	38.0
63	56.5	78.1	29.5	56.5	78.1	30.7
53	51.0	71.2	25.3	51.0	71.2	26.1
45	45.5	64.1	21.4	45.5	64.1	22.5
38	39.6	56.6	18.2	39.6	56.6	19.0
20	26.2	38.7	12.4	26.2	38.7	12.0
%Solids	49.6	40.6	71.3	49.6	38.3	70.1

Sieve size (µm)	Cumulative passing weight (%)											
	120° - 120 kPa P1			120° - 120 kPa P1 (II)			135° - 120 kPa P1			135° - 120 kPa P1 (II)		
	Feed	O/F	U/F	Feed	O/F	U/F	Feed	O/F	U/F	Feed	O/F	U/F
180	96.7	99.9	92.9	96.7	99.9	92.3	96.7	100.0	92.0	96.7	100.0	91.7
150	94.0	99.8	85.6	94.0	99.8	85.2	94.0	99.9	84.9	94.0	99.9	84.3
125	90.0	99.5	75.8	90.0	99.5	75.0	90.0	99.3	74.3	90.0	99.4	73.8
106	85.5	99.0	65.9	85.5	98.4	64.1	85.5	98.0	63.8	85.5	98.3	62.4
90	79.4	96.5	52.6	79.4	96.1	51.7	79.4	95.3	51.9	79.4	95.8	50.4
75	72.4	91.7	41.3	72.4	91.5	42.1	72.4	90.0	43.5	72.4	90.4	41.5
63	64.9	83.4	32.5	64.9	84.7	32.3	64.9	82.7	34.6	64.9	81.7	33.1
53	58.6	76.8	27.2	58.6	78.1	26.5	58.6	75.9	29.4	58.6	75.4	27.4
45	52.4	69.7	22.5	52.4	71.0	21.7	52.4	68.9	25.0	52.4	68.5	22.9
38	45.8	62.3	18.3	45.8	62.7	18.0	45.8	60.8	21.3	45.8	61.0	18.9
%Solids	46.3	38.5	73.9	46.3	38.7	73.9	46.3	39.0	75.4	46.3	39.0	74.2

40% Silica-Magnetite Feed

sieves size (µm)	0° - 100 kPa P1								
	Mixture			Silica			Magnetite		
	Feed	O/F	U/F	Feed	O/F	U/F	Feed	O/F	U/F
180	96.6	100.0	93.9	96.9	100.0	94.2	94.9	100.0	93.1
150	94.3	100.0	89.8	94.4	100.0	89.2	93.6	100.0	91.4
125	90.9	99.9	84.4	90.6	99.9	82.6	92.0	100.0	89.6
106	86.5	99.8	77.1	85.6	99.7	73.4	90.2	100.0	87.5
90	81.3	99.4	67.8	79.7	99.3	61.9	87.9	100.0	84.6
75	75.8	98.6	58.1	73.4	98.4	49.9	85.4	100.0	81.2
63	67.1	95.2	46.0	63.9	94.6	35.8	80.3	99.8	74.8
53	61.5	90.3	38.8	58.2	89.1	28.4	75.4	99.5	68.3
45	53.8	83.9	32.4	50.9	82.0	23.1	65.6	98.8	58.8
38	47.0	78.0	26.7	44.9	75.6	19.1	55.6	97.5	48.1
20	29.6	51.5	12.7	30.4	48.8	10.7	26.3	72.4	18.5

%Solids	43.2	29.6	67.9

sieves size (µm)	0° - 100 kPa P1 (II)								
	Mixture			Silica			Magnetite		
	Feed	O/F	U/F	Feed	O/F	U/F	Feed	O/F	U/F
180	96.6	99.9	94.3	96.9	99.9	94.5	94.9	100.0	93.5
150	94.3	99.9	90.4	94.4	99.8	89.9	93.6	100.0	91.8
125	90.9	99.7	84.6	90.6	99.7	82.9	92.0	99.7	89.4
106	86.5	99.4	77.2	85.6	99.4	73.7	90.2	99.4	87.2
90	81.3	98.9	68.5	79.7	98.9	62.9	87.9	98.9	84.3
75	75.8	98.1	59.4	73.4	98.1	51.9	85.4	98.3	81.0
63	67.1	96.0	47.1	63.9	95.7	37.5	80.3	97.8	74.7
53	61.5	92.3	39.5	58.2	91.5	29.7	75.4	96.6	67.7
45	53.8	85.5	32.0	50.9	83.7	23.5	65.6	95.5	56.4
38	47.0	77.9	25.5	44.9	74.9	19.1	55.6	93.9	43.6
20	29.6	49.7	10.7	30.4	46.6	9.6	26.3	66.5	13.7

%Solids	43.2	29.5	68.1

sieves size (µm)	135° - 100 kPa P1								
	Mixture			Silica			Magnetite		
	Feed	O/F	U/F	Feed	O/F	U/F	Feed	O/F	U/F
180	97.0	99.9	86.0	97.2	99.9	84.5	96.3	100.0	88.7
150	95.0	99.2	77.3	94.9	99.1	73.0	95.2	100.0	85.5
125	92.0	97.7	66.9	91.4	97.4	59.2	94.0	100.0	81.6
106	88.1	95.2	57.5	87.0	94.5	47.2	92.7	99.8	77.2
90	83.3	91.2	49.4	81.3	89.9	37.8	91.0	99.4	71.7
75	78.1	85.8	43.0	75.3	83.9	31.0	88.8	98.6	65.9
63	69.8	77.5	34.8	66.0	74.7	23.5	84.7	96.7	56.2
53	63.9	71.6	29.2	59.7	68.3	19.4	80.3	93.6	47.9
45	56.3	65.3	22.0	52.3	61.9	15.6	71.9	87.6	34.1
38	49.6	59.0	17.8	46.1	56.0	13.4	63.1	79.2	26.0

%Solids	42.4	38.9	77.9

sieves size (µm)	135° - 120 kPa P1								
	Mixture			Silica			Magnetite		
	Feed	O/F	U/F	Feed	O/F	U/F	Feed	O/F	U/F
180	97.0	99.9	89.5	97.2	99.9	88.2	96.3	100.0	91.9
150	95.0	99.8	82.3	94.9	99.8	78.6	95.2	100.0	89.4
125	92.0	99.0	72.3	91.4	98.9	64.9	94.0	99.7	86.3
106	88.1	97.4	61.9	87.0	97.1	50.9	92.7	99.1	82.7
90	83.3	94.4	52.9	81.3	93.6	39.4	91.0	98.2	78.5
75	78.1	90.1	46.1	75.3	88.7	31.5	88.8	97.3	73.8
63	69.8	82.6	38.6	66.0	79.9	24.0	84.7	96.4	66.0
53	63.9	76.6	32.5	59.7	73.0	19.5	80.3	95.5	57.1
45	56.3	69.0	25.8	52.3	64.5	16.1	71.9	91.9	44.2
38	49.6	61.8	19.3	46.1	57.1	13.0	63.1	85.9	31.3

%Solids	42.4	35.9	75.9

sieves size (μm)	135° - 120 kPa P2								
	Mixture			Silica			Magnetite		
	Feed	O/F	U/F	Feed	O/F	U/F	Feed	O/F	U/F
180	97.1	99.8	91.1	97.2	99.8	90.1	96.5	100.0	93.0
150	95.0	99.6	84.6	94.9	99.5	81.7	95.4	100.0	90.6
125	91.9	99.2	75.1	91.3	99.1	68.9	94.0	99.7	87.6
106	88.0	98.1	64.3	86.7	97.9	54.4	92.5	99.1	84.3
90	83.2	95.7	54.2	81.1	95.1	41.2	90.6	98.6	80.3
75	78.1	91.9	46.6	75.1	90.6	32.1	88.6	97.7	75.8
63	69.4	83.7	38.4	65.2	81.2	23.4	83.9	96.0	68.5
53	63.9	77.6	32.3	59.4	74.1	18.7	79.8	94.5	59.8
45	56.7	70.3	25.3	52.2	65.8	14.9	72.2	91.9	46.2
38	49.4	62.4	18.6	45.6	56.9	12.0	63.0	89.0	31.7

%Solids	42.8	35.6	76.4

sieves size (μm)	135° - 120 kPa P2 (II)								
	Mixture			Silica			Magnetite		
	Feed	O/F	U/F	Feed	O/F	U/F	Feed	O/F	U/F
180	97.1	100.0	92.3	97.2	99.9	91.9	96.5	100.0	93.3
150	95.0	99.9	85.2	94.9	99.9	82.8	95.4	100.0	90.8
125	91.9	99.2	75.0	91.3	99.1	69.5	94.0	100.0	87.7
106	88.0	98.0	63.7	86.7	97.7	54.9	92.5	99.7	84.0
90	83.2	94.8	54.2	81.1	94.0	43.0	90.6	99.3	80.0
75	78.1	90.0	45.5	75.1	88.5	33.0	88.6	98.7	74.2
63	69.4	82.4	38.4	65.2	79.8	26.2	83.9	98.0	66.5
53	63.9	76.6	31.9	59.4	73.1	21.5	79.8	97.0	55.9
45	56.7	70.2	25.6	52.2	66.1	18.1	72.2	94.3	43.0
38	49.4	64.3	20.7	45.6	59.8	15.8	63.0	90.7	31.8

%Solids	42.8	35.6	76.4

A.7. Classification Curves

Classification curves for preliminary experiment using **original cone** at 0 degree with 25% silica feed:

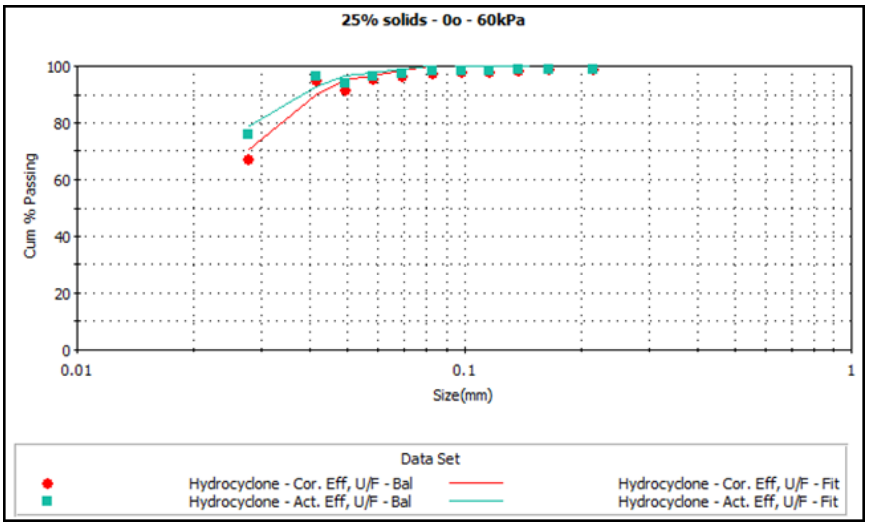

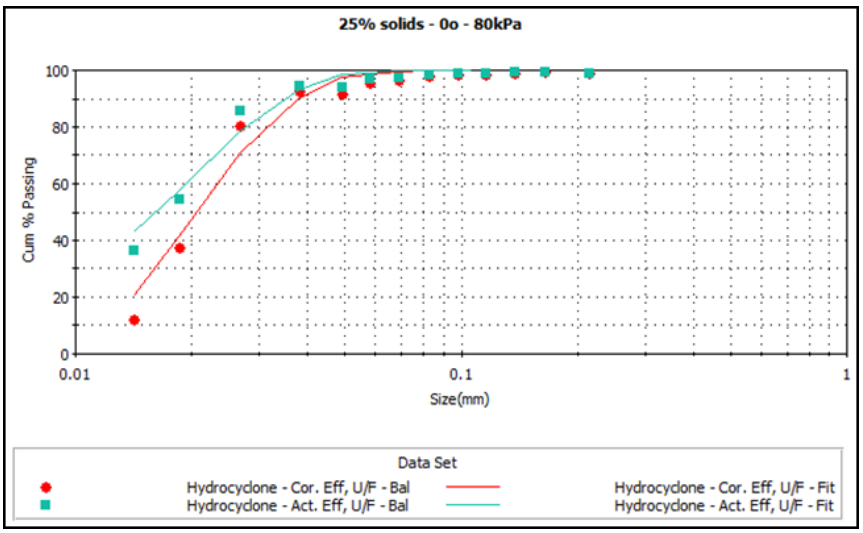

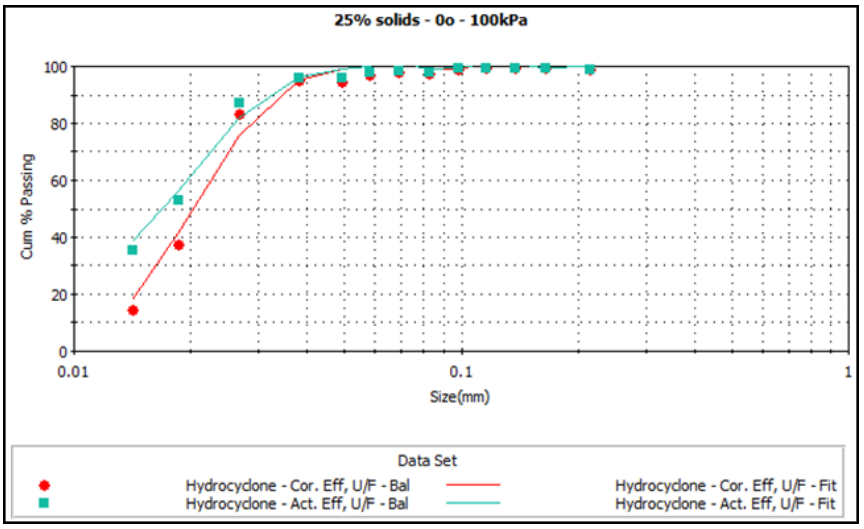

Classification curves for preliminary experiment using **original cone** at 45 degree with 25% silica feed:

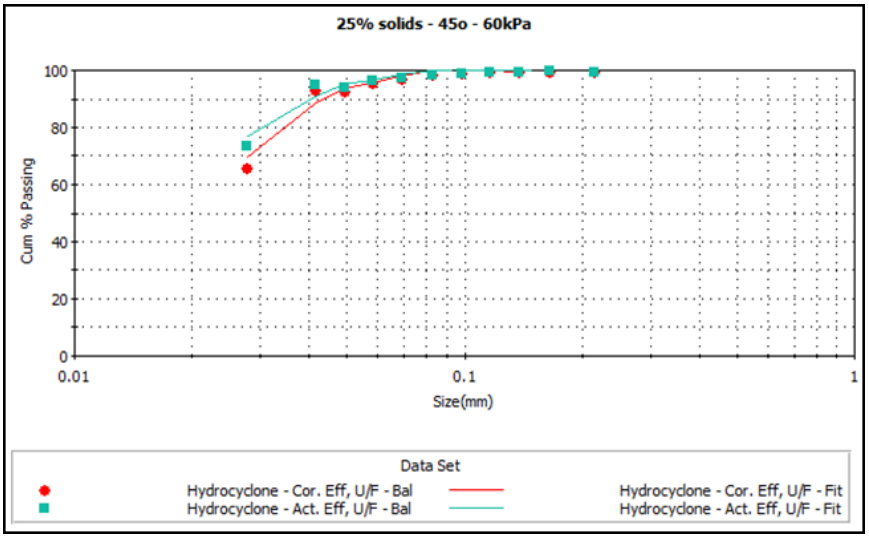

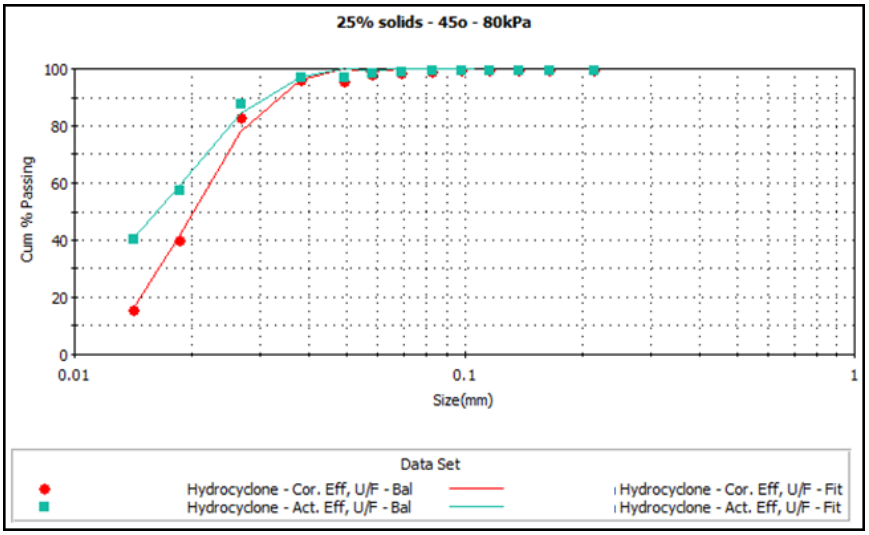

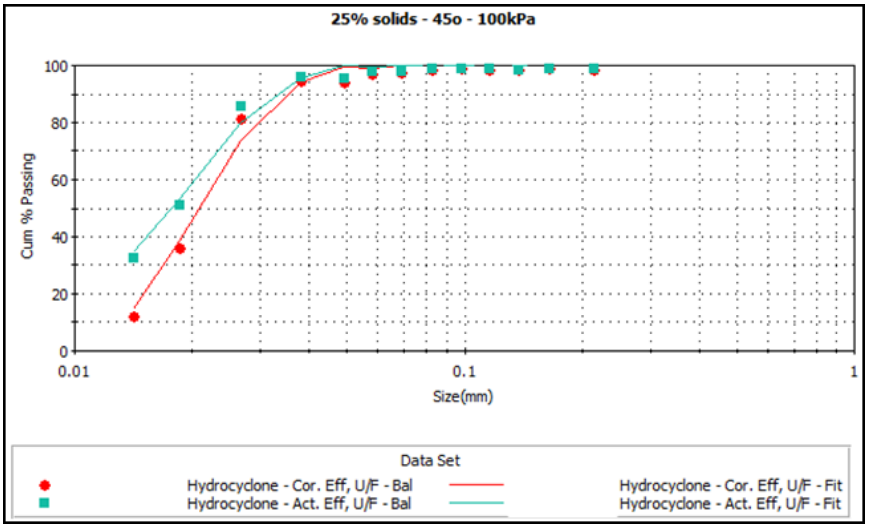

Classification curves for preliminary experiment using **original cone** at 105 degree with 25% silica feed:

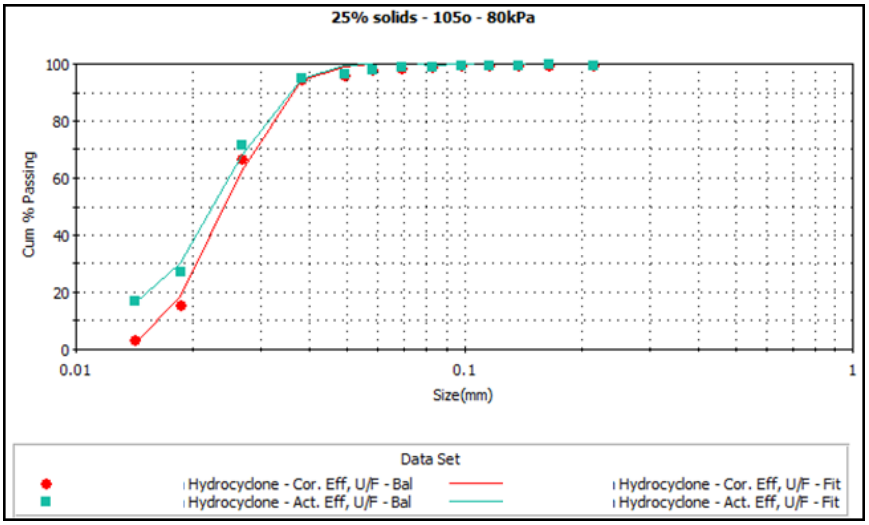

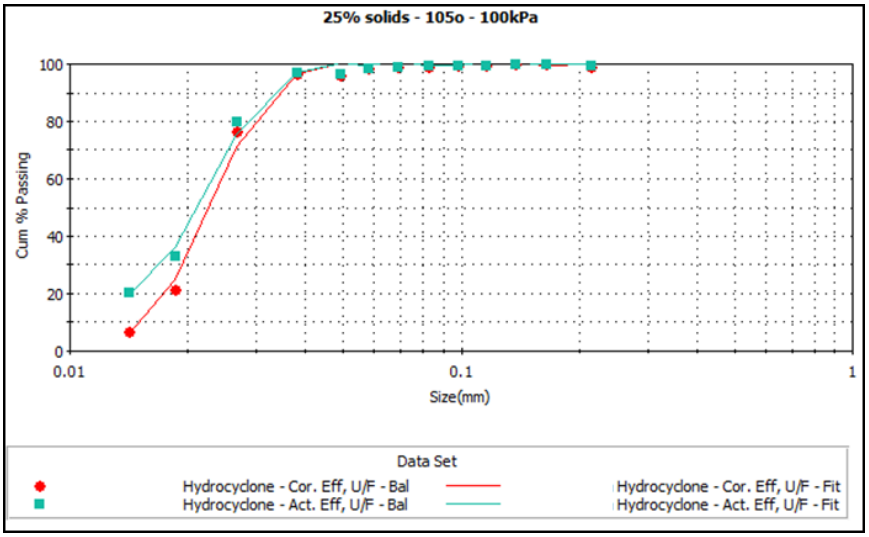

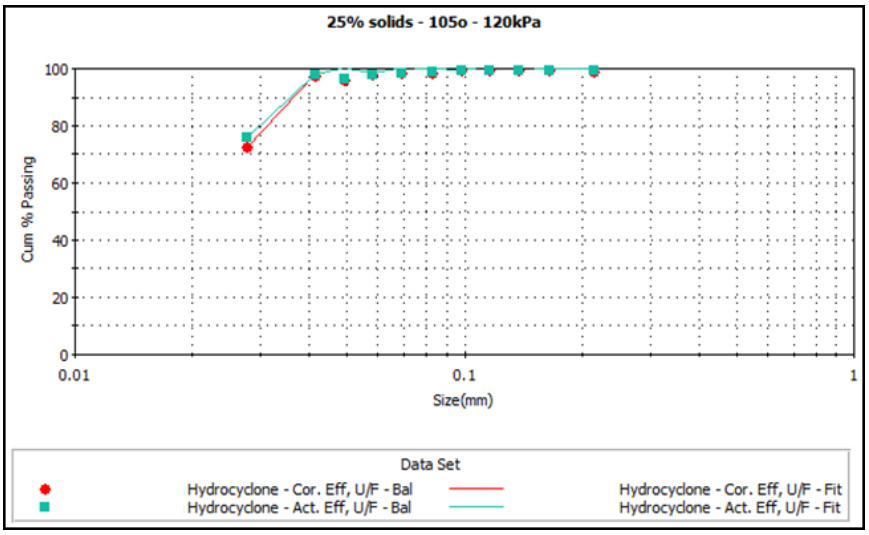

Classification curves for preliminary experiment using **original cone** at 120 degree with 25% silica feed:

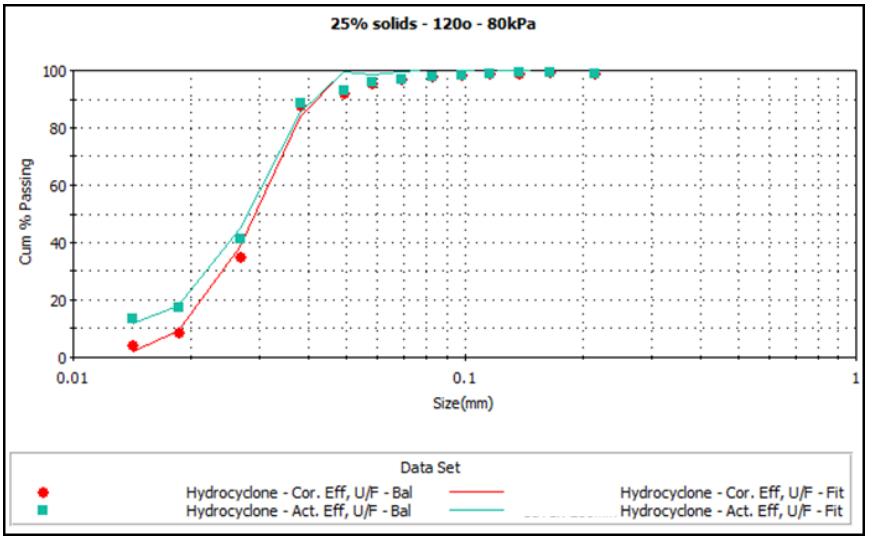

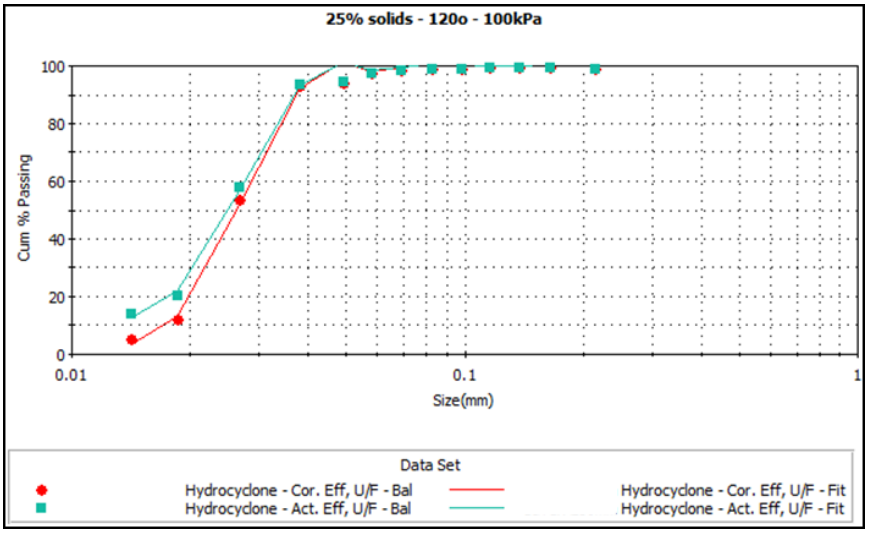

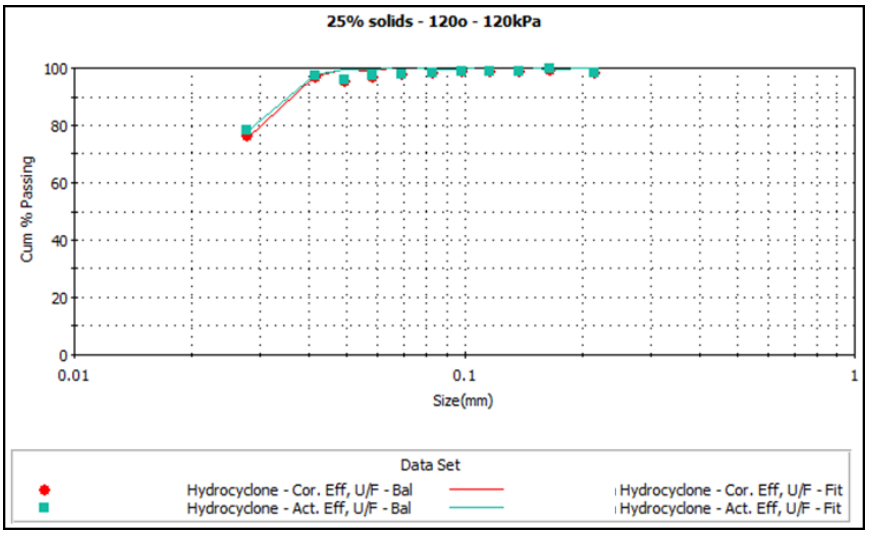

Classification curves for experiment using **modified cone** at 0 degree with 40% silica feed:

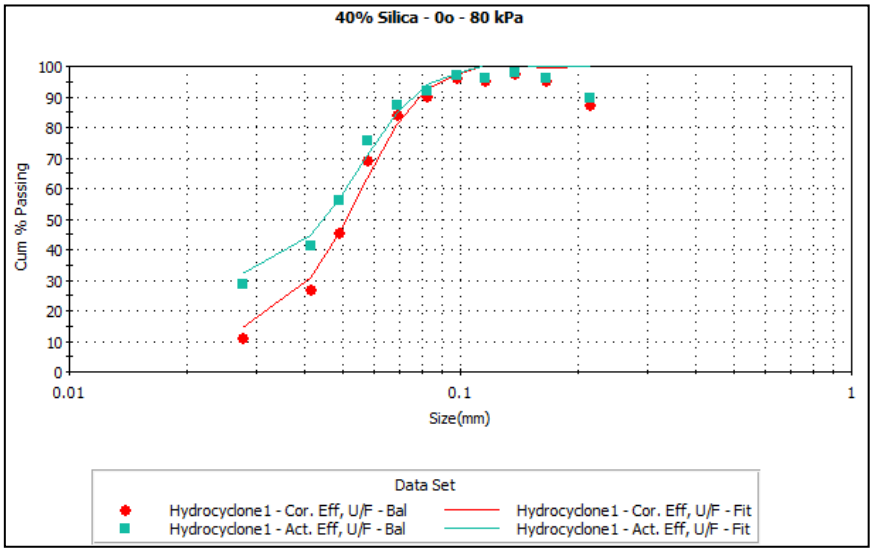

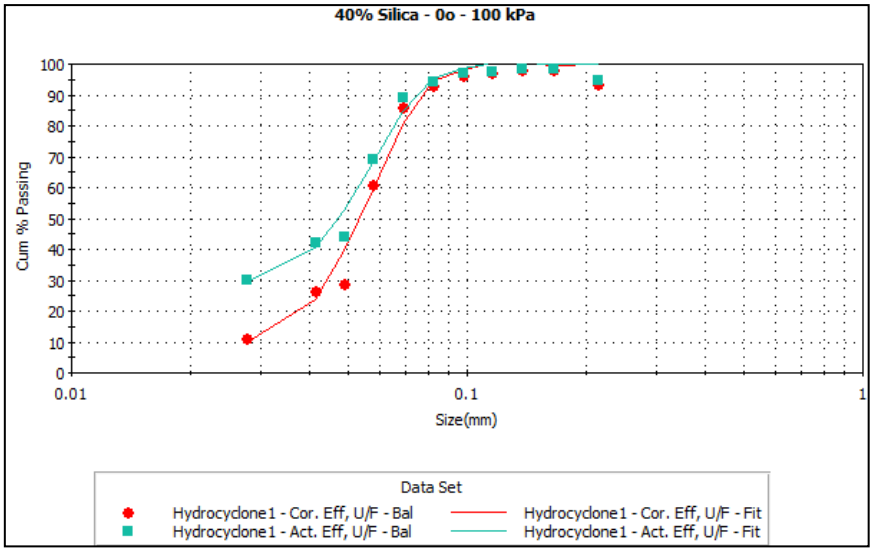

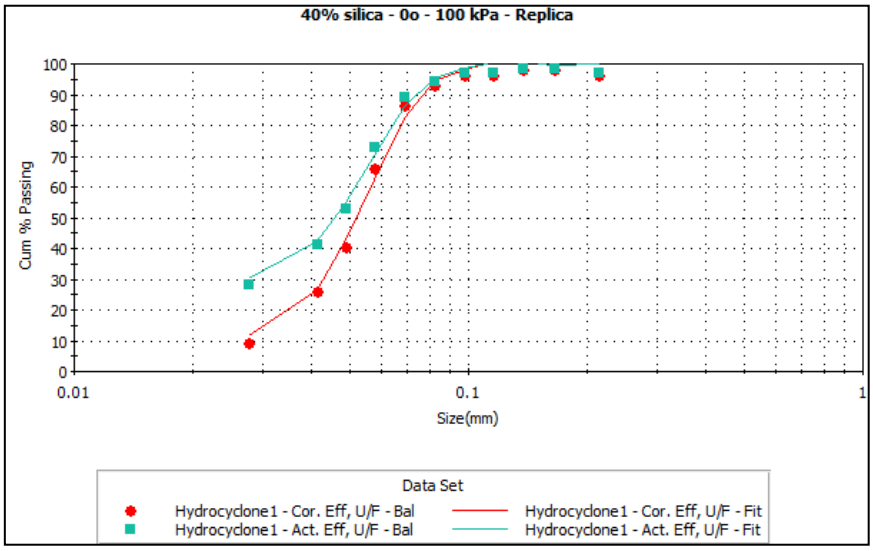

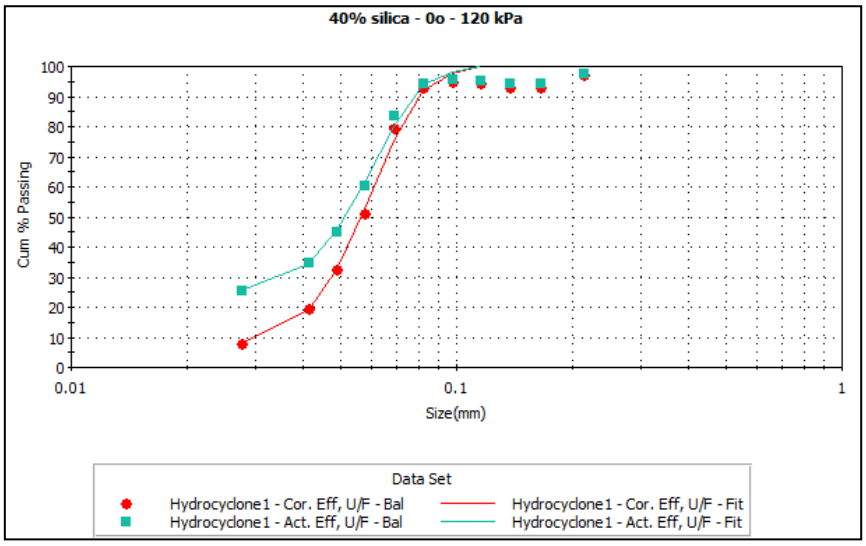
40% silica - 0o - 120 kPa
Cum % Passing
100
90
80
70
60
50
40
30
20
10
0
0.01
0.1
1
Size(mm)
Data Set
Hydrocyclone1 - Cor. Eff, U/F - Bal
Hydrocyclone1 - Act. Eff, U/F - Bal
Hydrocyclone1 - Cor. Eff, U/F - Fit
Hydrocyclone1 - Act. Eff, U/F - Fit

Classification curves for experiment using **modified cone** and **novel vortex finder** at 0 degree with 40% silica feed:

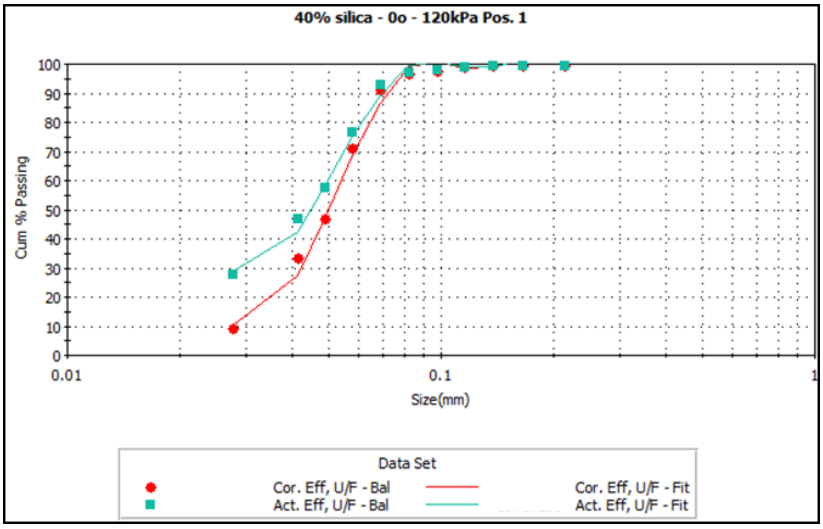

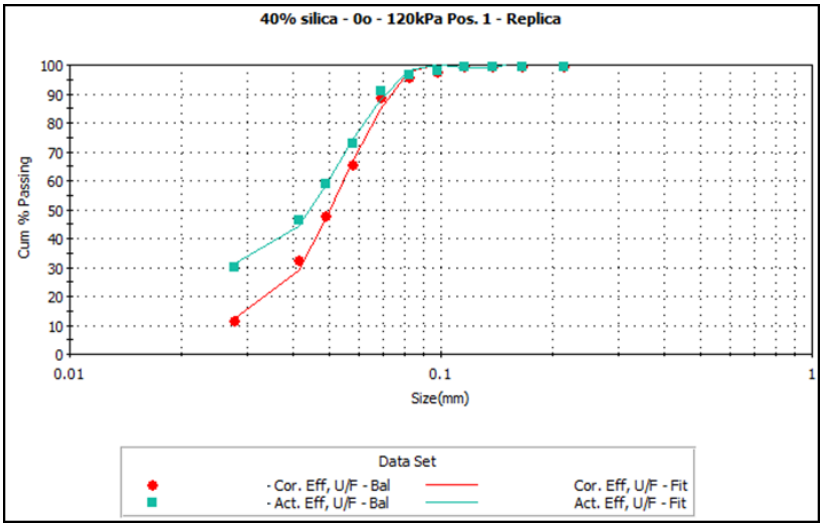

Classification curves for experiment using **modified cone** at 105 degree with 40% silica feed:

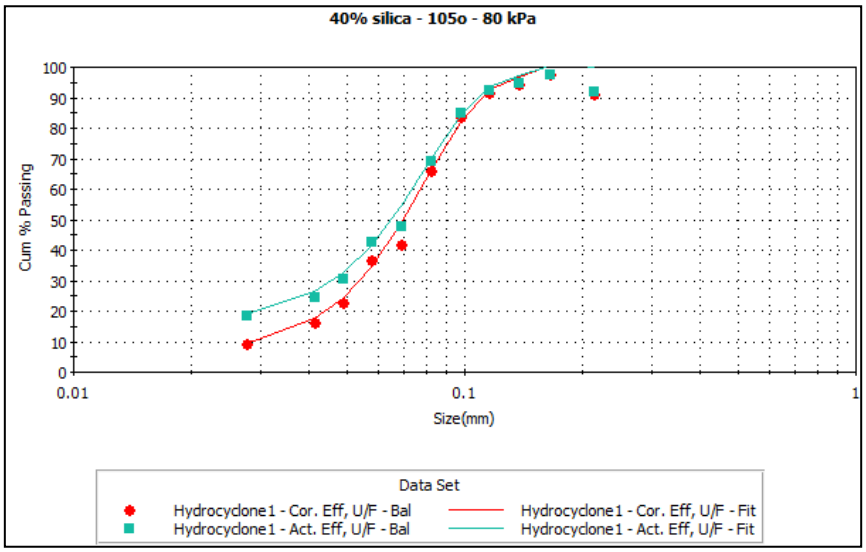

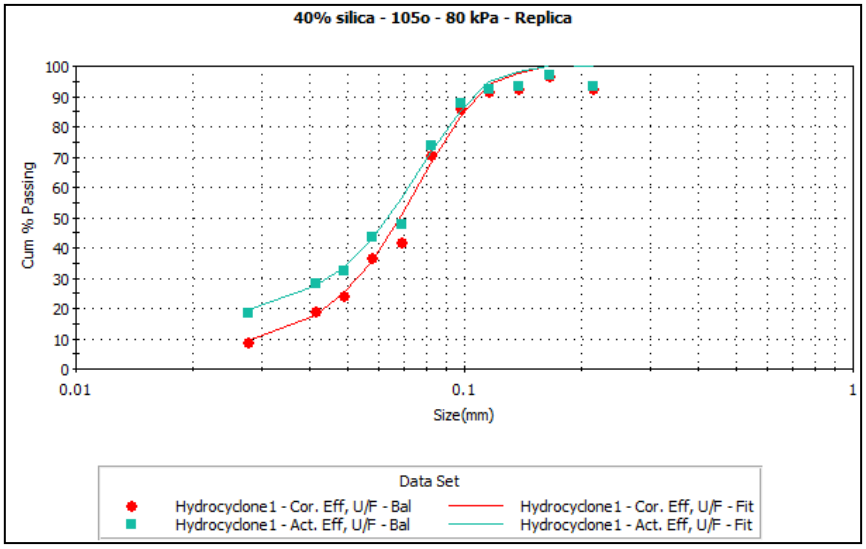

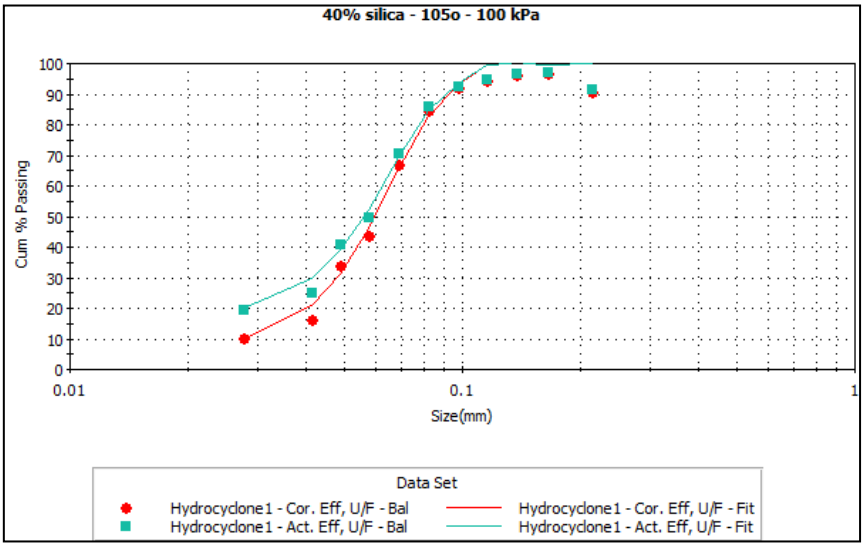

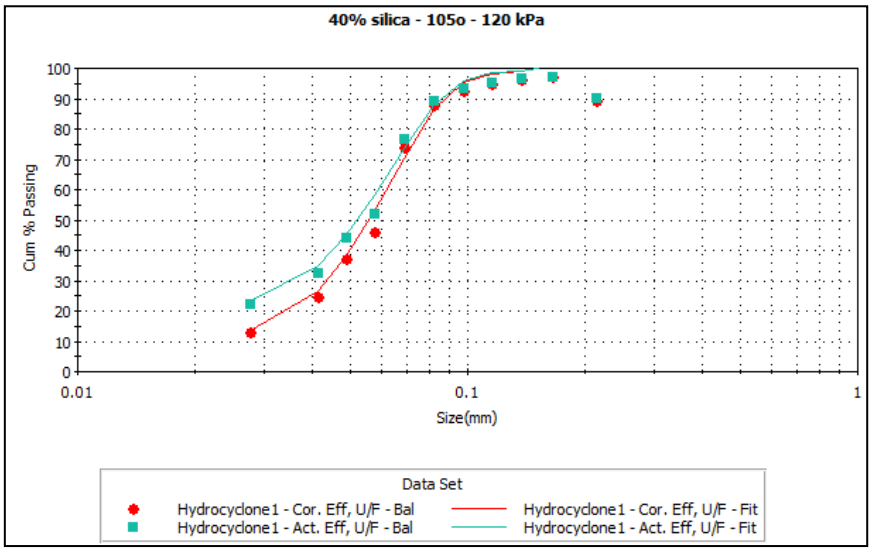
40% silica - 105o - 120 kPa
Cum % Passing
100
90
80
70
60
50
40
30
20
10
0
0.01
0.1
1
Size(mm)
Data Set
Hydrocyclone1 - Cor. Eff, U/F - Bal
Hydrocyclone1 - Act. Eff, U/F - Bal
Hydrocyclone1 - Cor. Eff, U/F - Fit
Hydrocyclone1 - Act. Eff, U/F - Fit

Classification curves for experiment using **modified cone** at 120 degree with 40% silica feed:

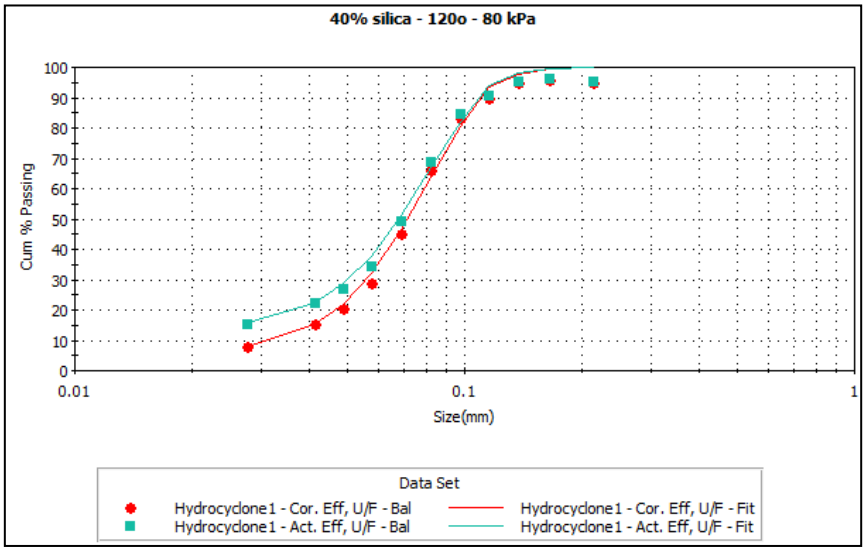

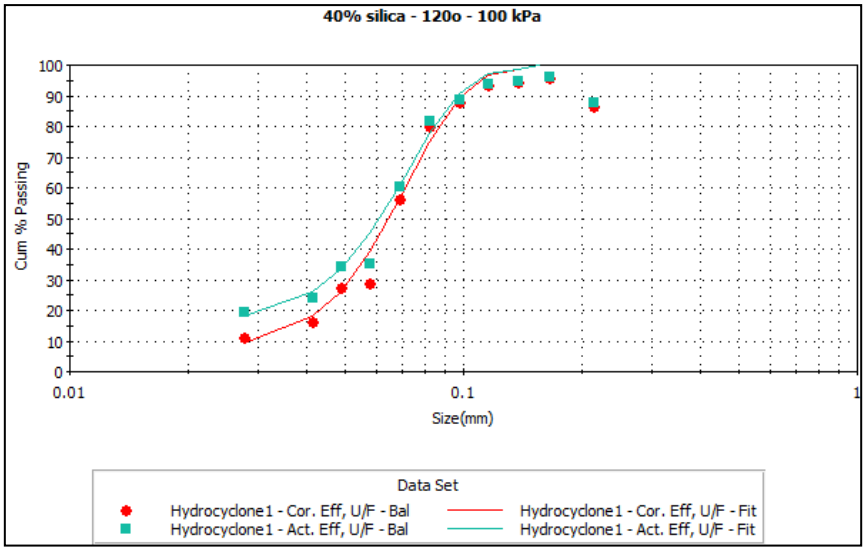

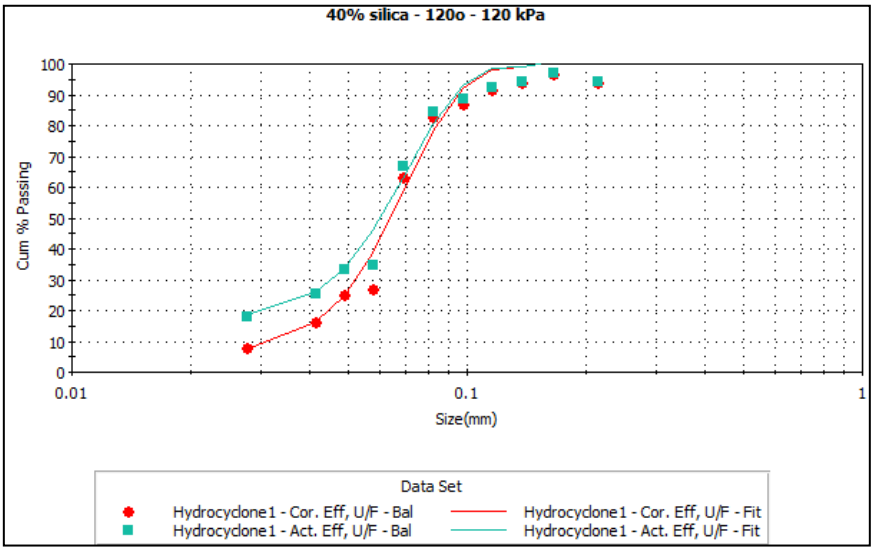

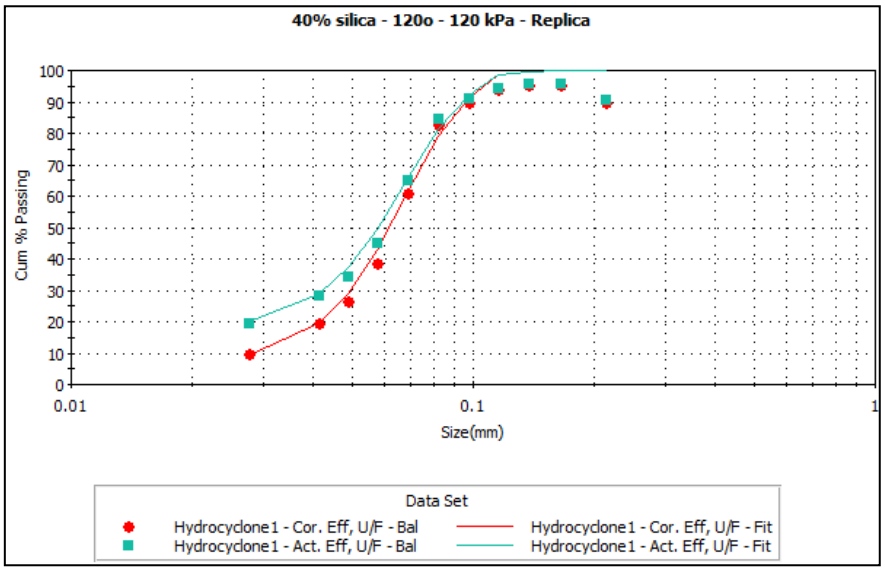
40% silica - 120o - 120 kPa - Replica
Cum % Passing
100
90
80
70
60
50
40
30
20
10
0
0.01
0.1
1
Size(mm)
Data Set
Hydrocyclone1 - Cor. Eff, U/F - Bal
Hydrocyclone1 - Act. Eff, U/F - Bal
Hydrocyclone1 - Cor. Eff, U/F - Fit
Hydrocyclone1 - Act. Eff, U/F - Fit

Classification curves for experiment using **modified cone** and **novel vortex finder** at 0 degree with 40% silica feed:

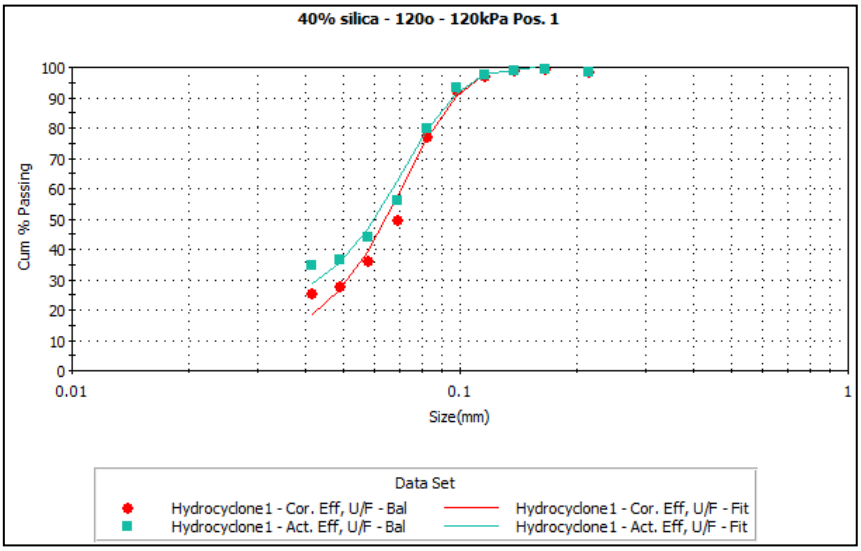

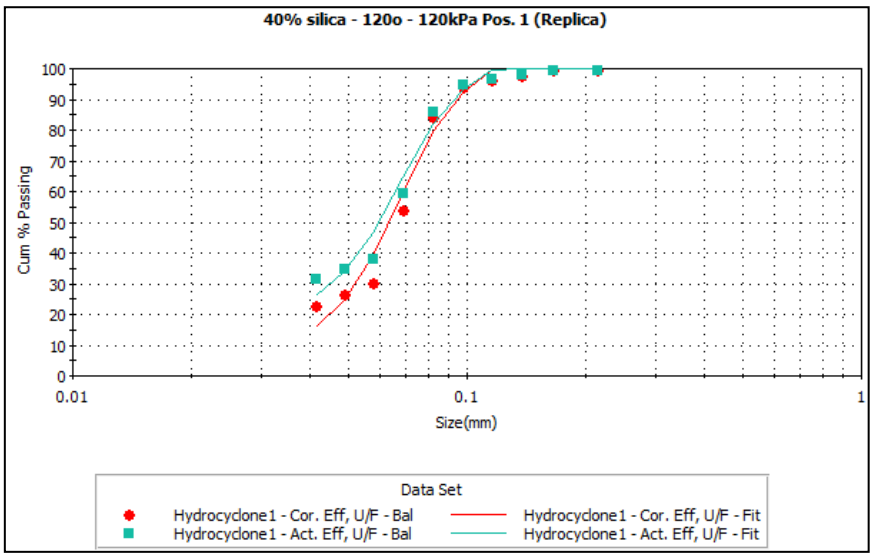

Classification curves for experiment using **modified cone** at 135 degree with 40% silica feed:

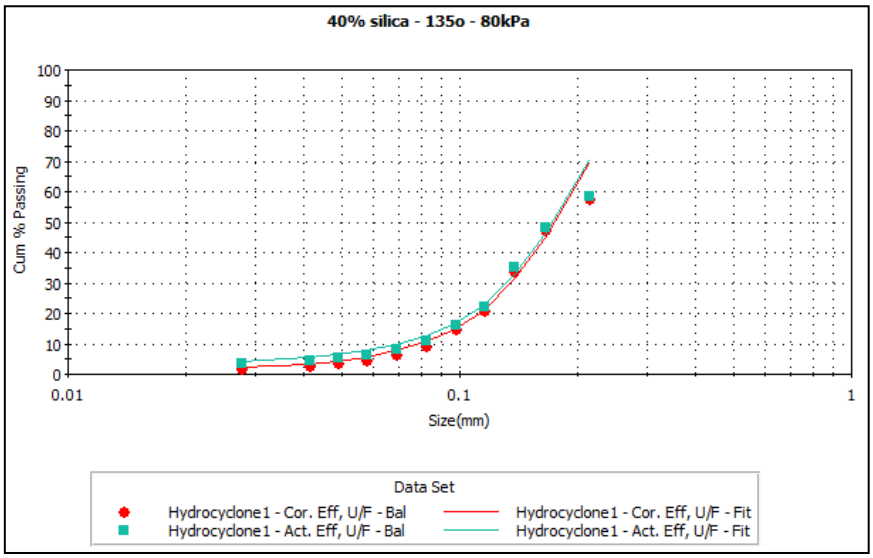

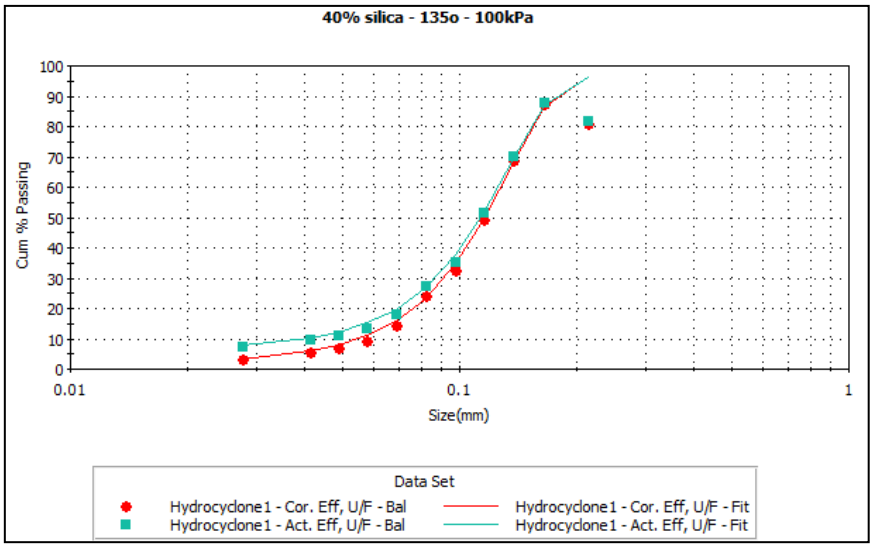

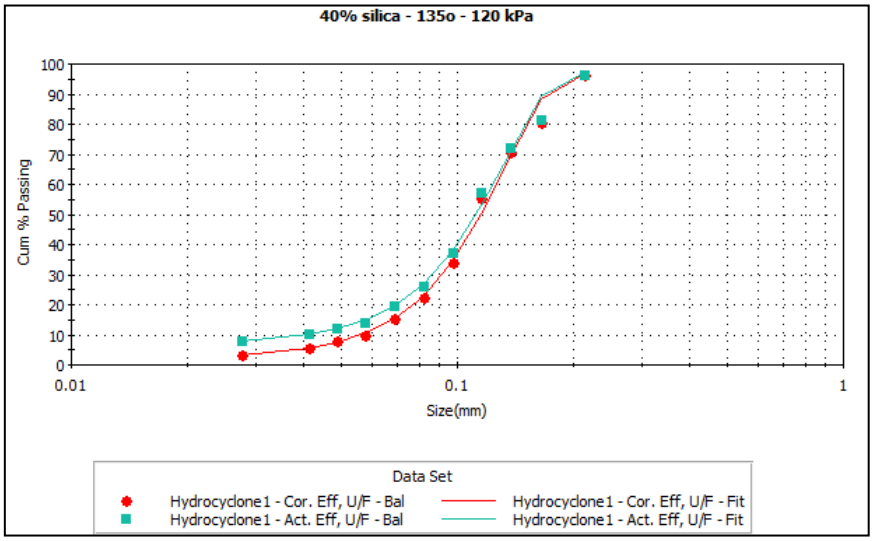

Classification curves for experiment using **modified cone** and **novel vortex finder** at 135 degree with 40% silica feed:

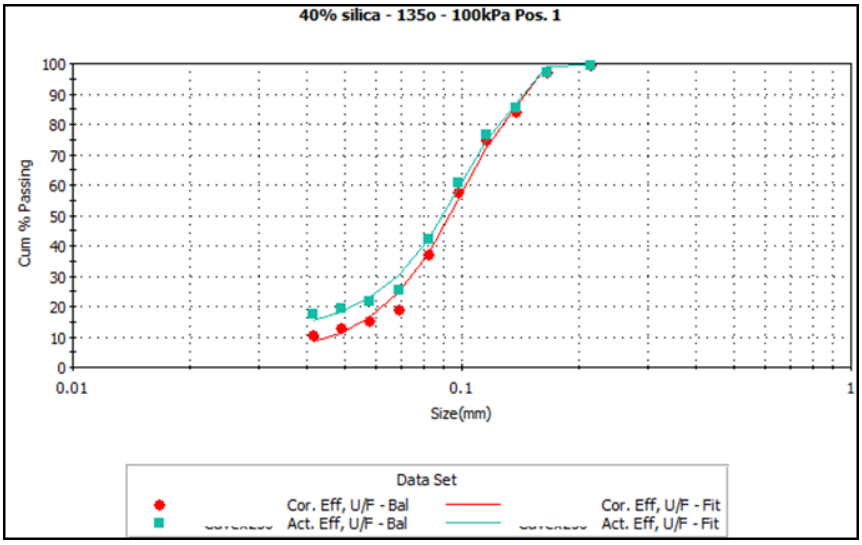

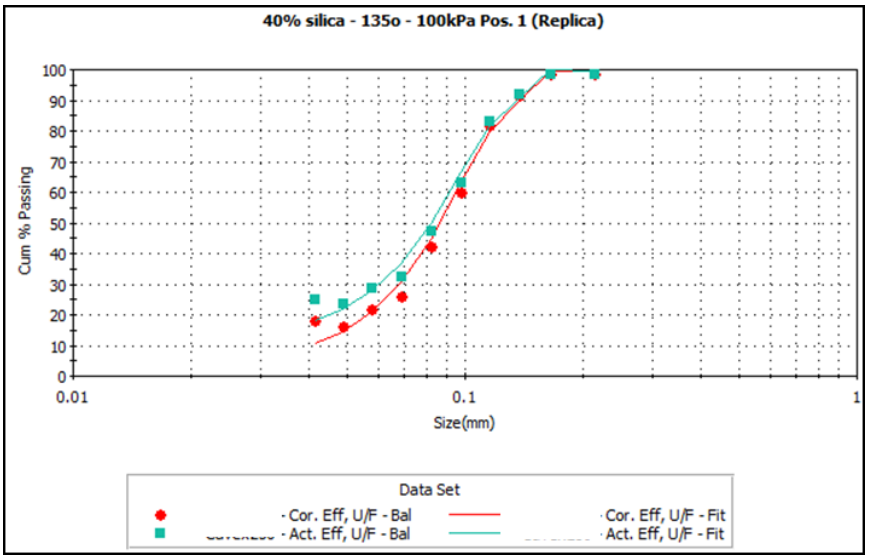

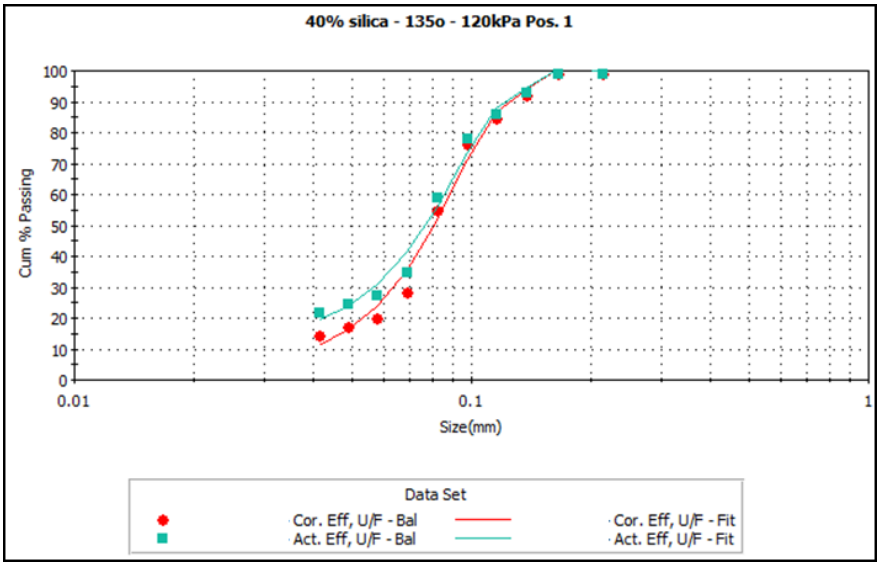

Classification curves for experiment using **modified cone** at 0 degree with 50% silica feed:

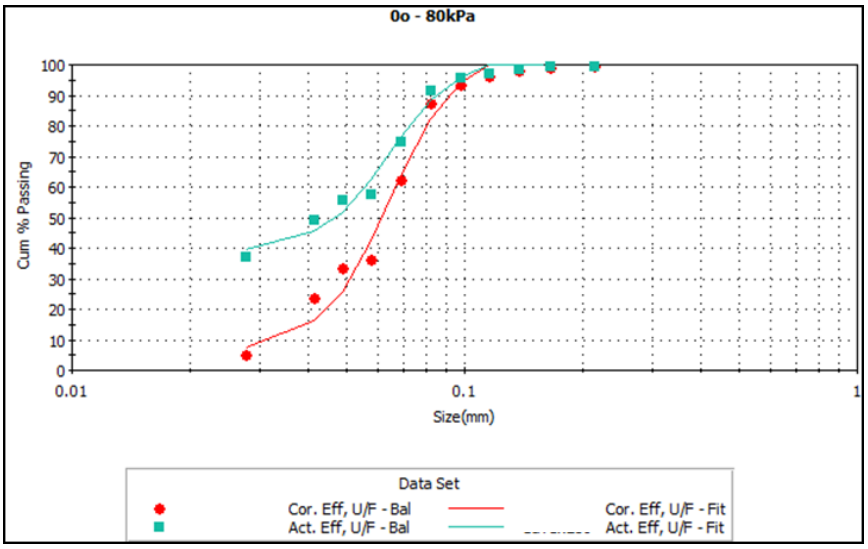

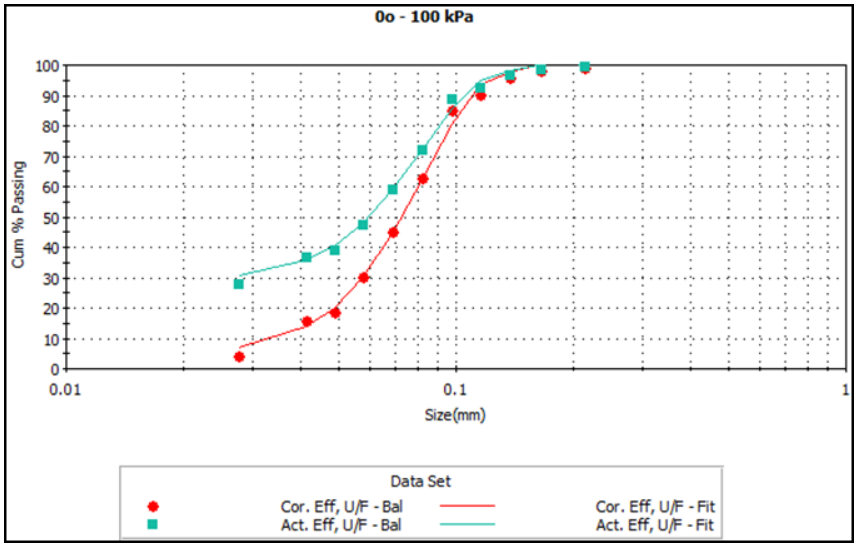

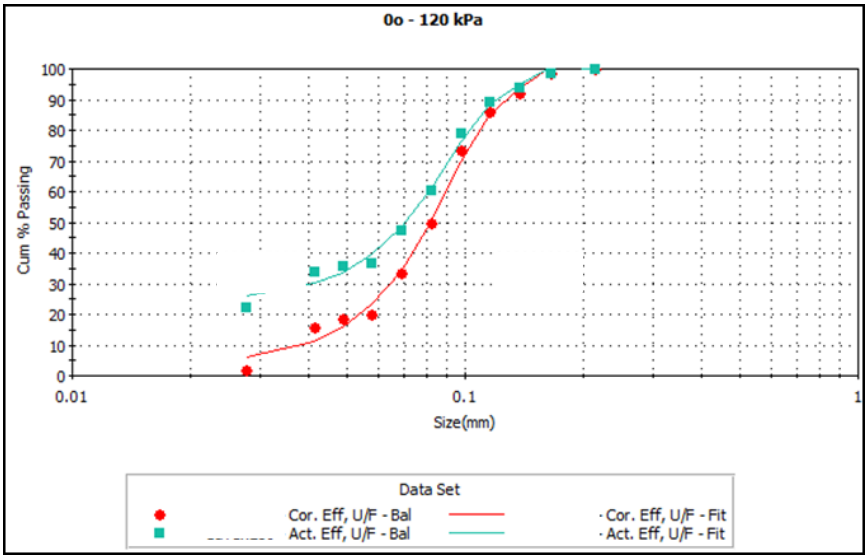

Classification curves for experiment using **modified cone** and **novel vortex finder** at 0 degree with 50% silica feed:

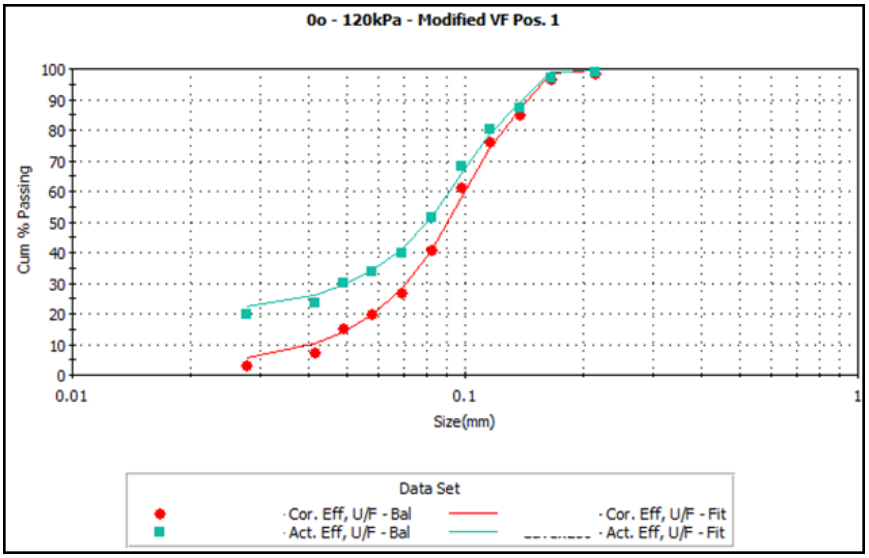

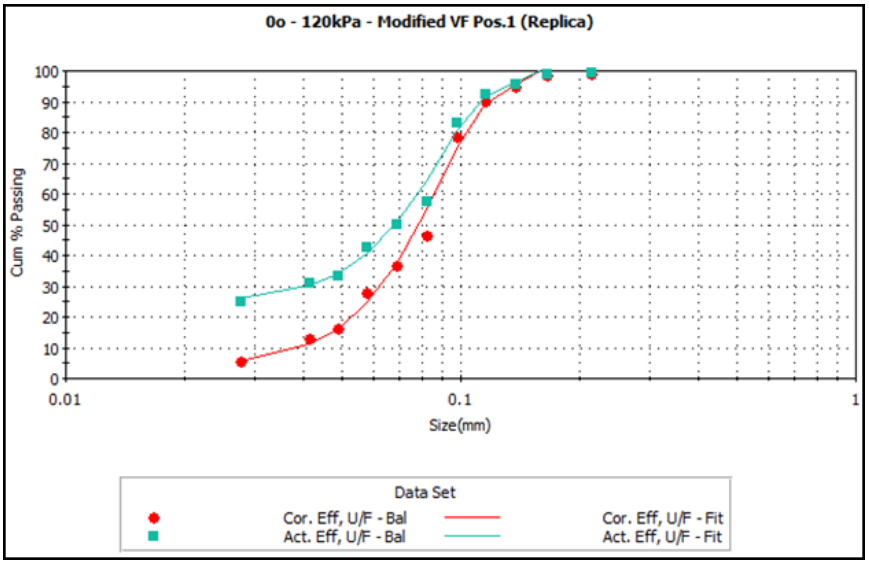

Classification curves for experiment using **modified cone** at 105 degree with 50% silica feed:

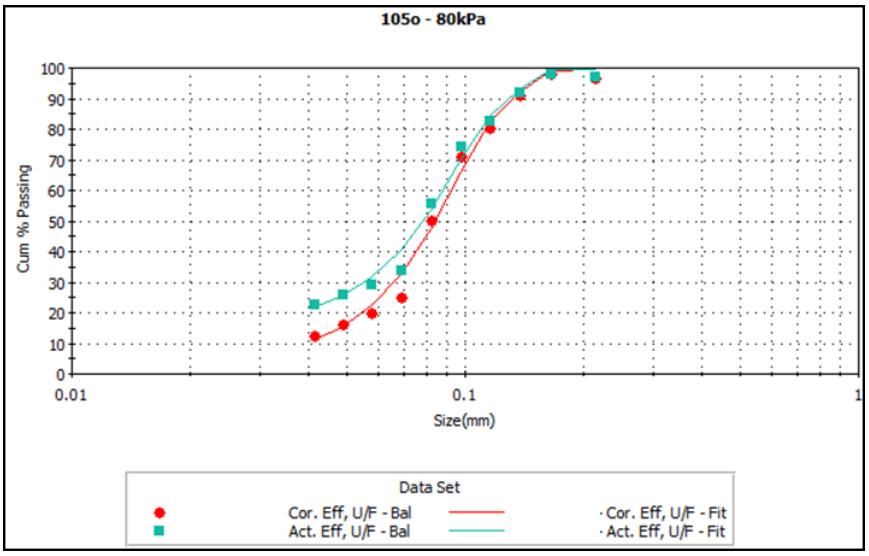

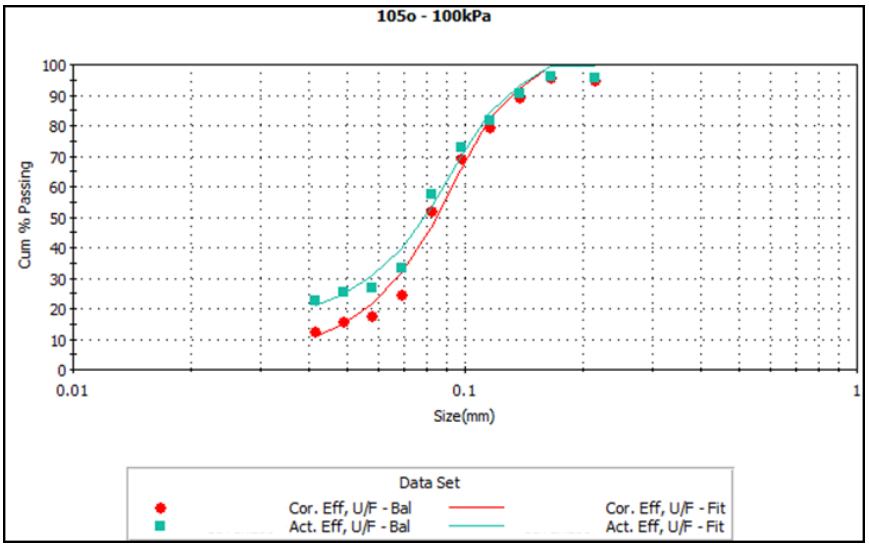

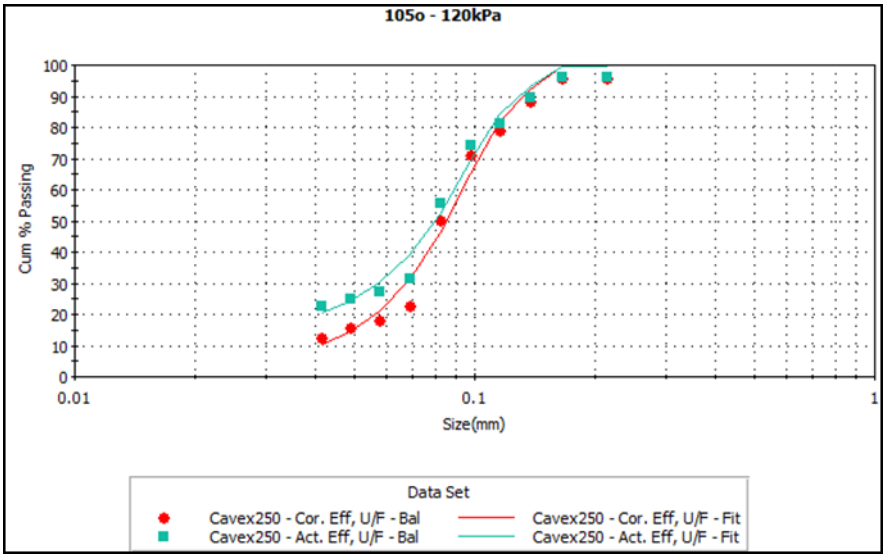

Classification curves for experiment using **modified cone** at 120 degree with 50% silica feed:

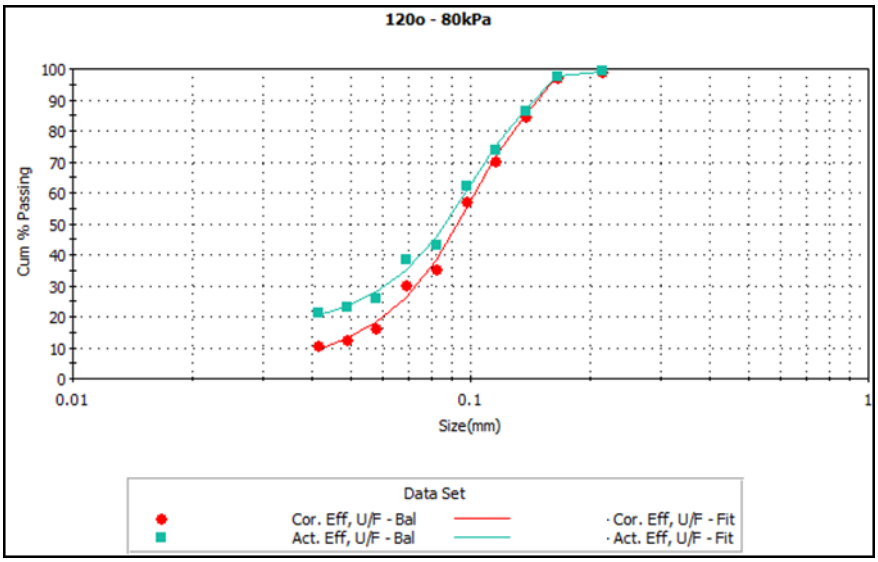

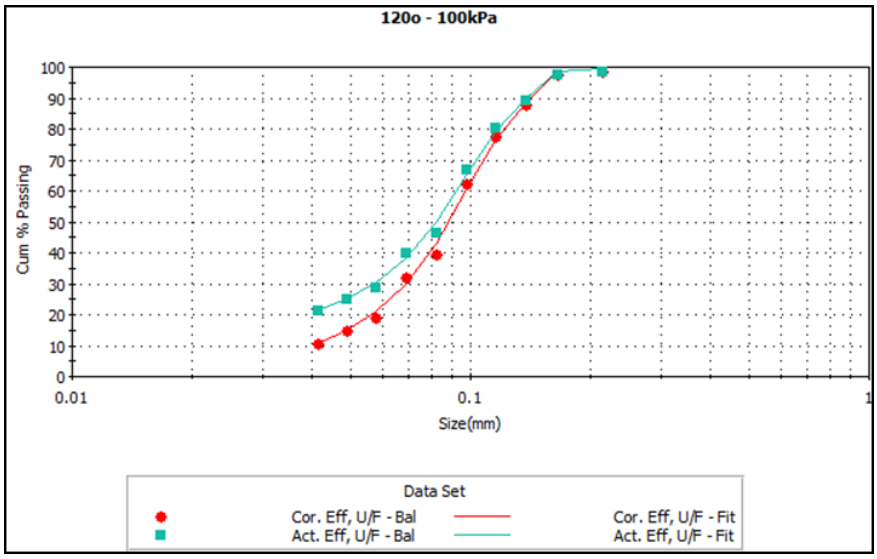

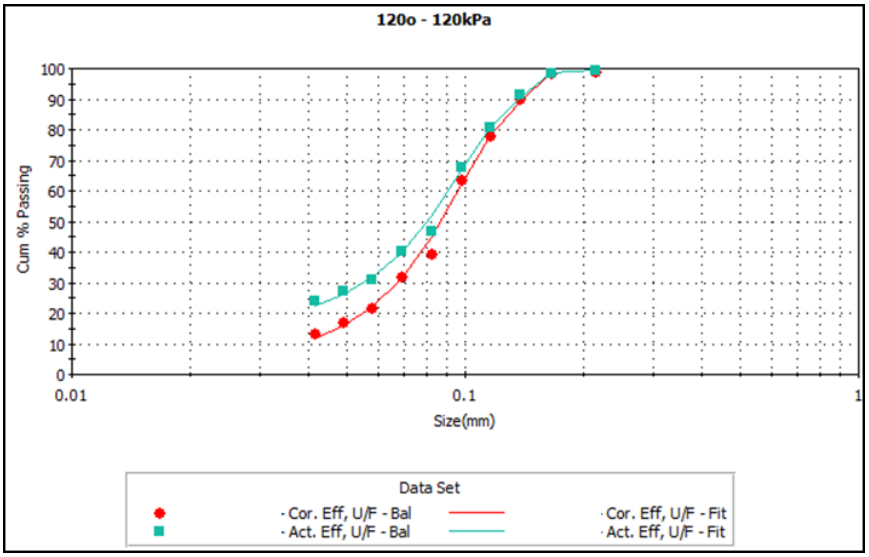

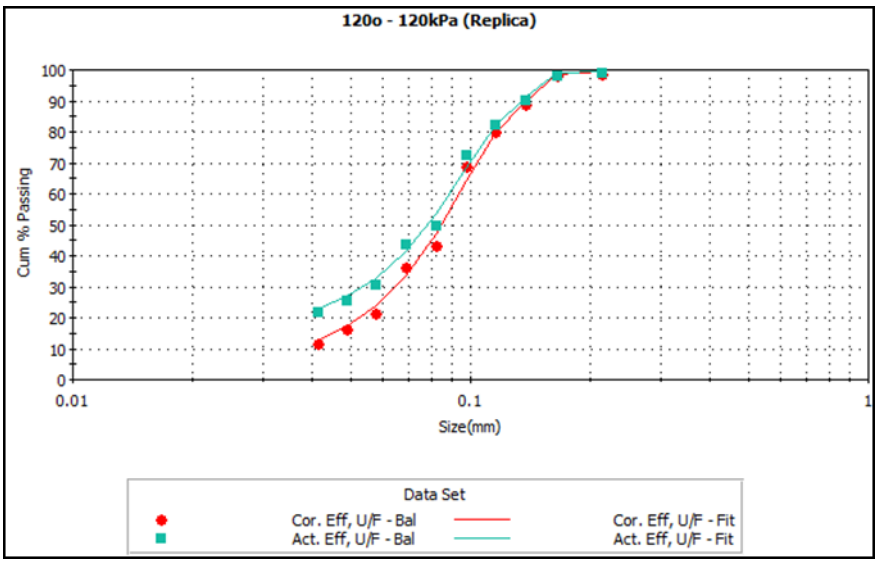
120o - 120kPa (Replica)
Cum % Passing
100
90
80
70
60
50
40
30
20
10
0
0.01
0.1
1
Size(mm)
Data Set
Cor. Eff, U/F - Bal
Act. Eff, U/F - Bal
Cor. Eff, U/F - Fit
Act. Eff, U/F - Fit

Classification curves for experiment using **modified cone** and **novel vortex finder** at 0 degree with 50% silica feed:

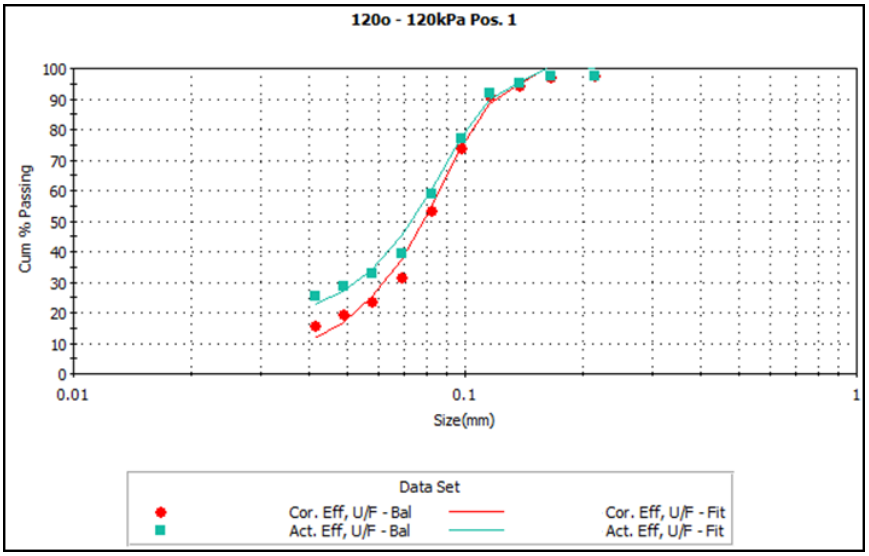

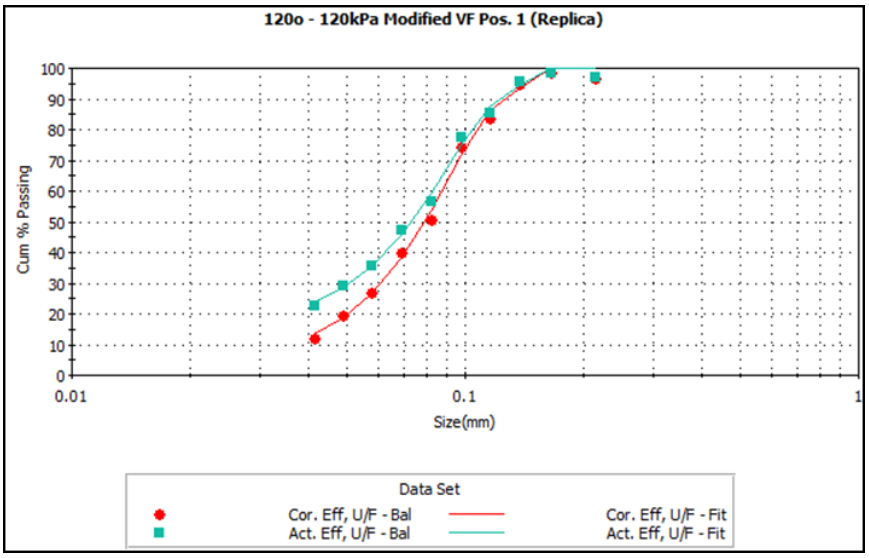

Classification curves for experiment using **modified cone** at 135 degree with 50% silica feed:

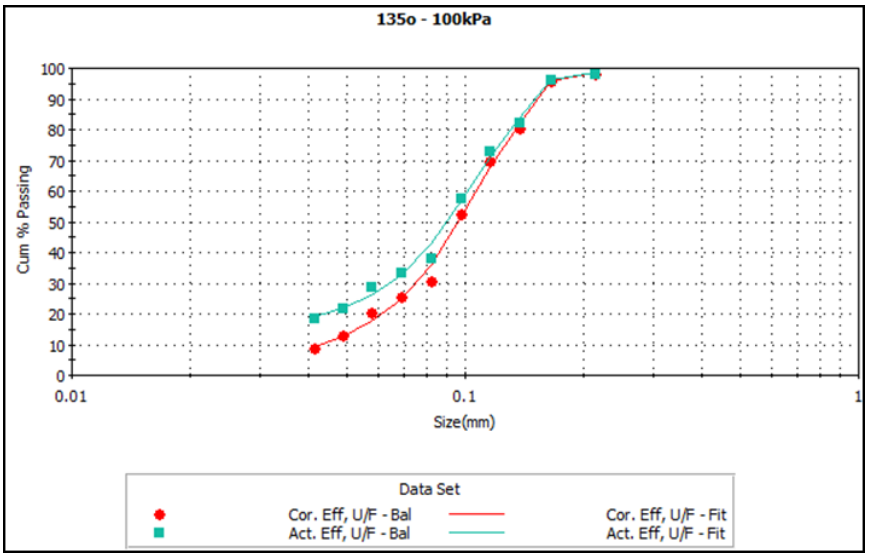

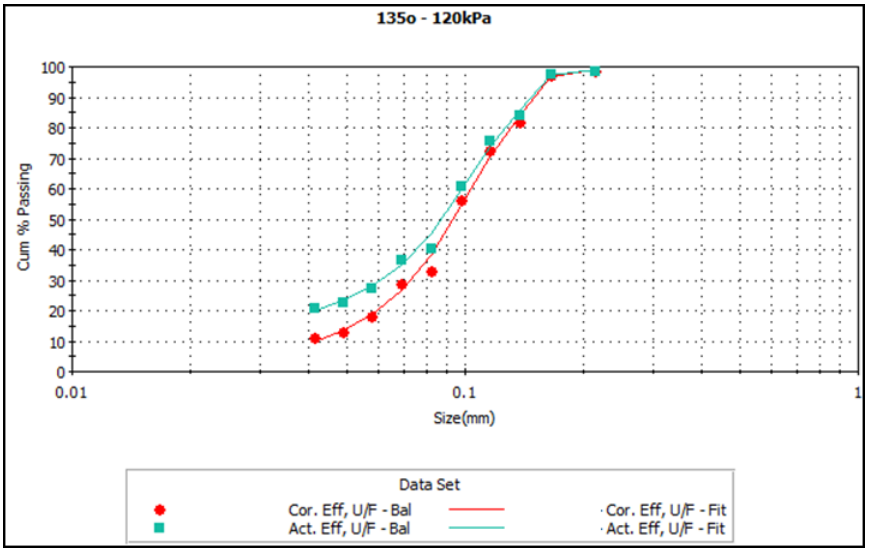

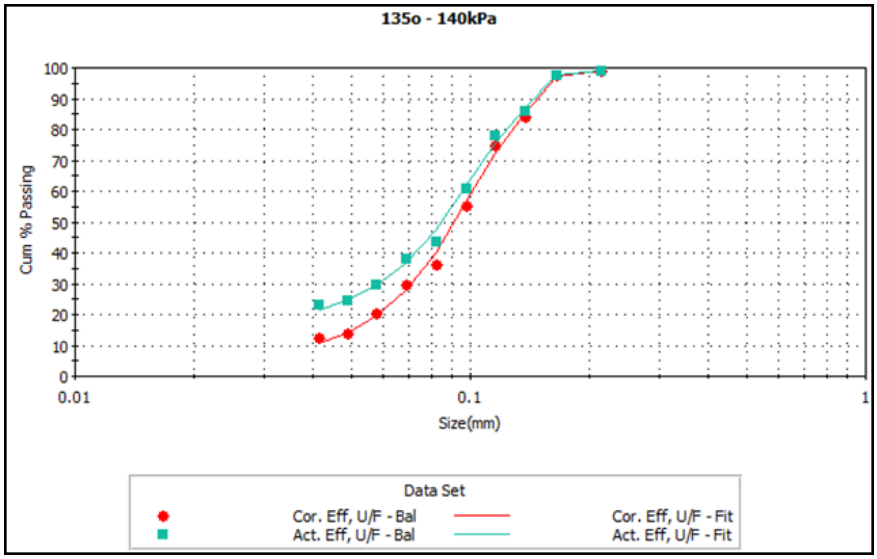

Classification curves for experiment using **modified cone** and **novel vortex finder** at 135 degree with 50% silica feed:

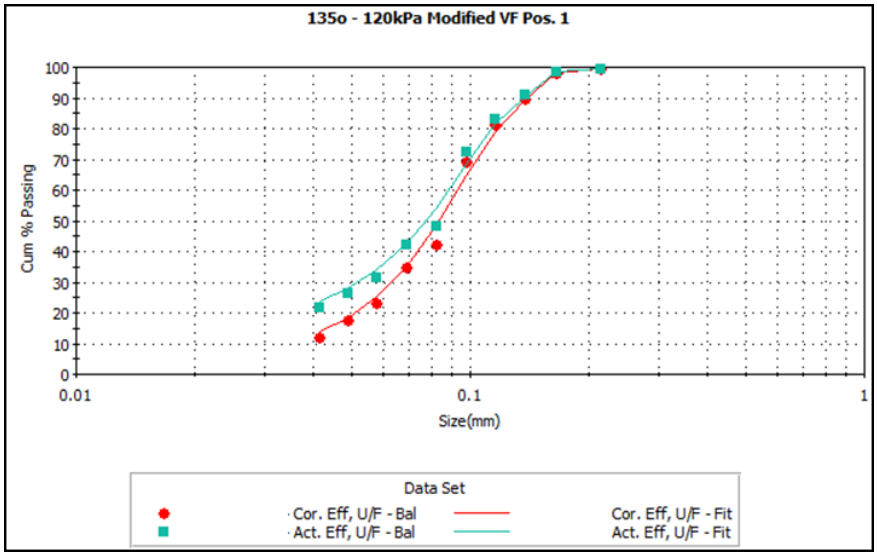

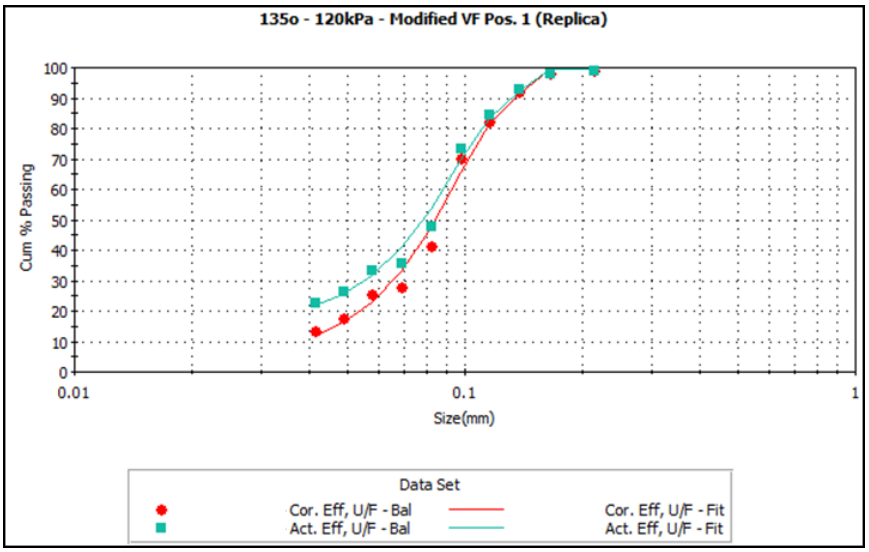

Classification curves for experiment using **modified cone** at 0 degree with 40% silica-magnetite mixture feed:

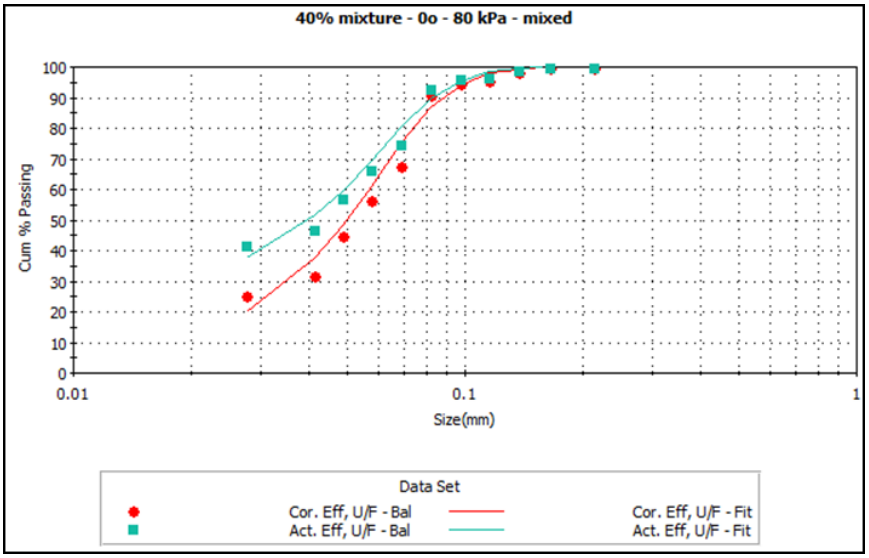

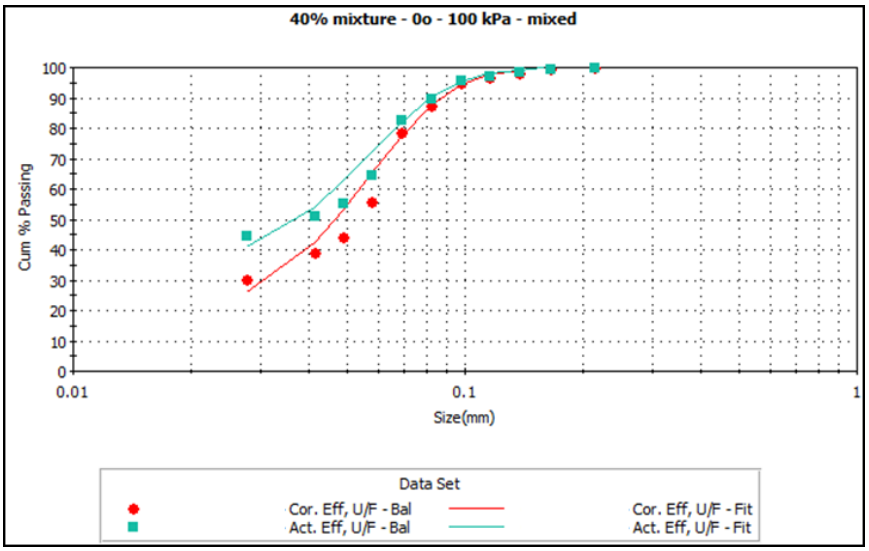

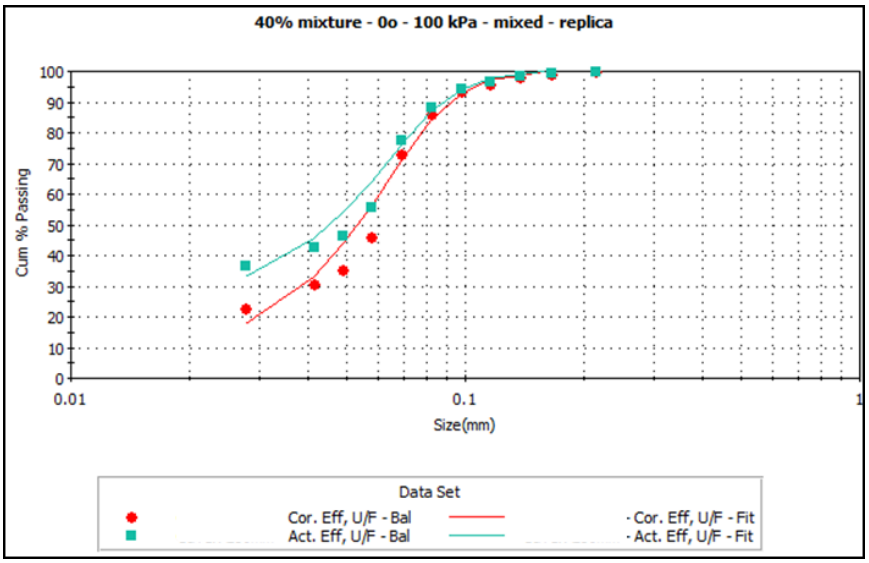

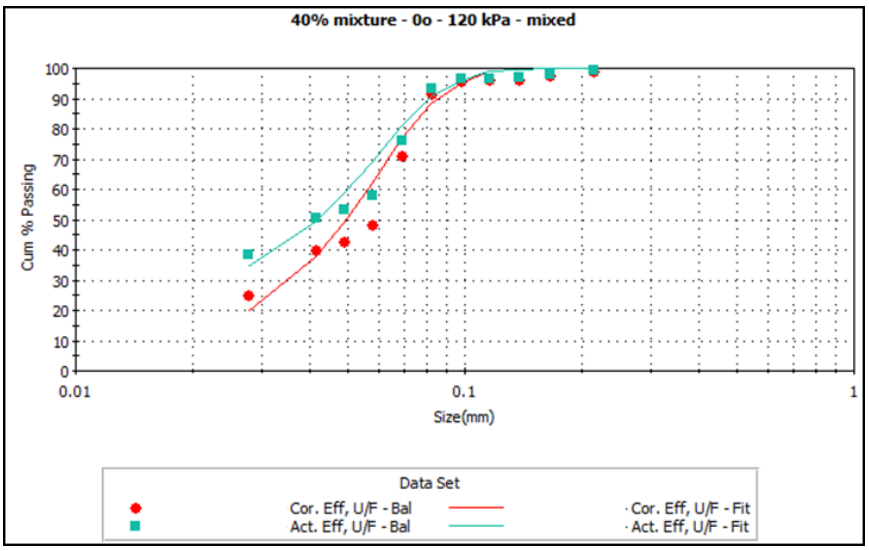
40% mixture - 0o - 120 kPa - mixed
Cum % Passing
100
90
80
70
60
50
40
30
20
10
0
0.01
0.1
1
Size(mm)
Data Set
Cor. Eff, U/F - Bal
Act. Eff, U/F - Bal
Cor. Eff, U/F - Fit
Act. Eff, U/F - Fit

Classification curves for experiment using **modified cone** and **novel vortex finder** at 0 degree with 40% silica-magnetite mixture feed:

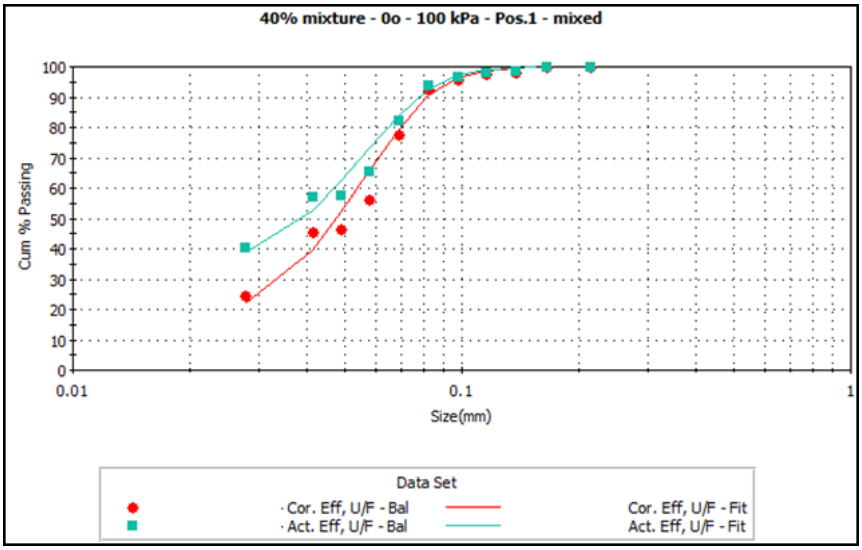

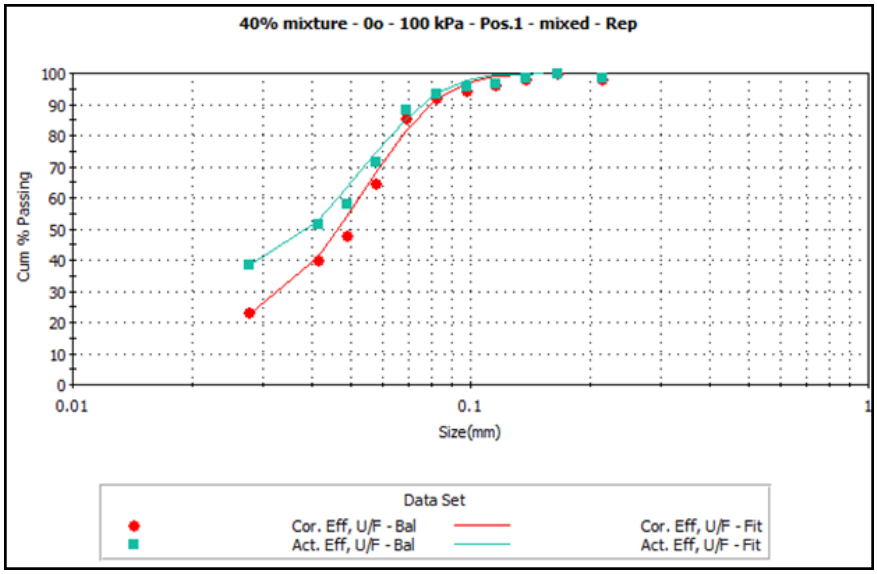

Classification curves for experiment using **modified cone** at 105 degree with 40% silica-magnetite mixture feed:

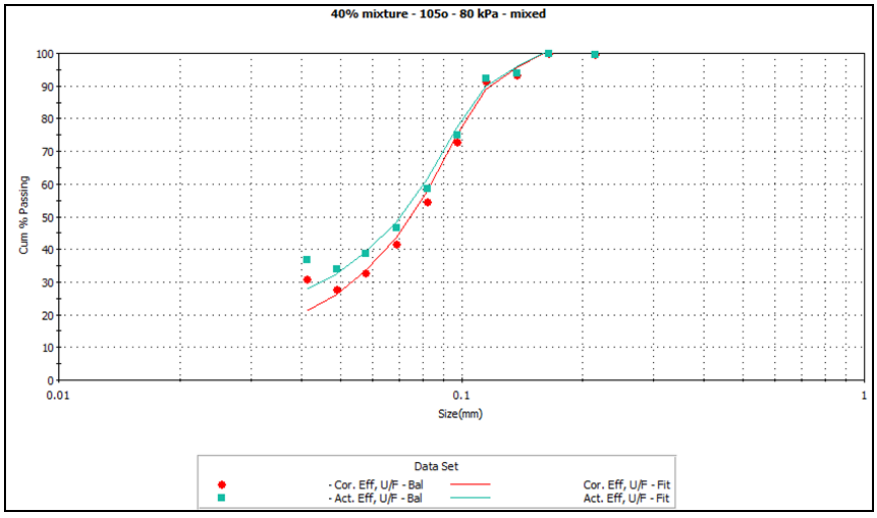

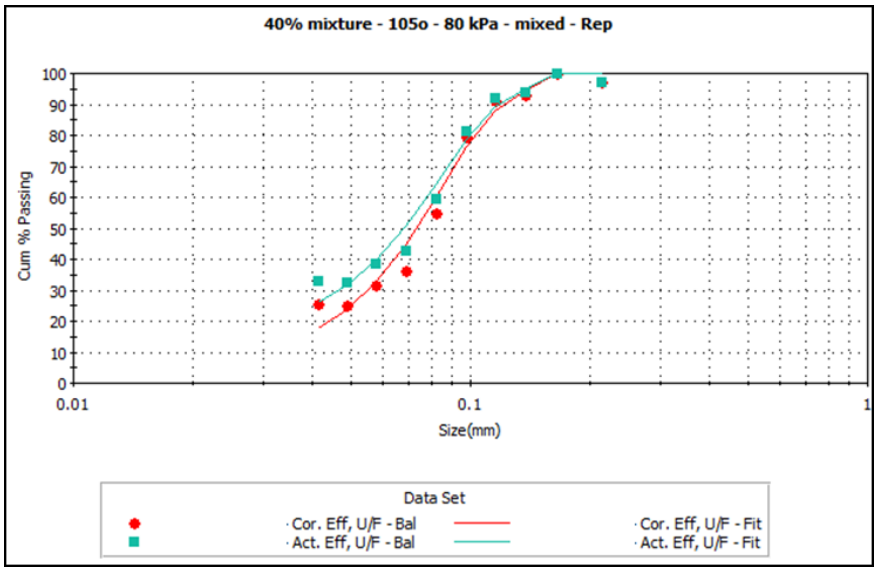

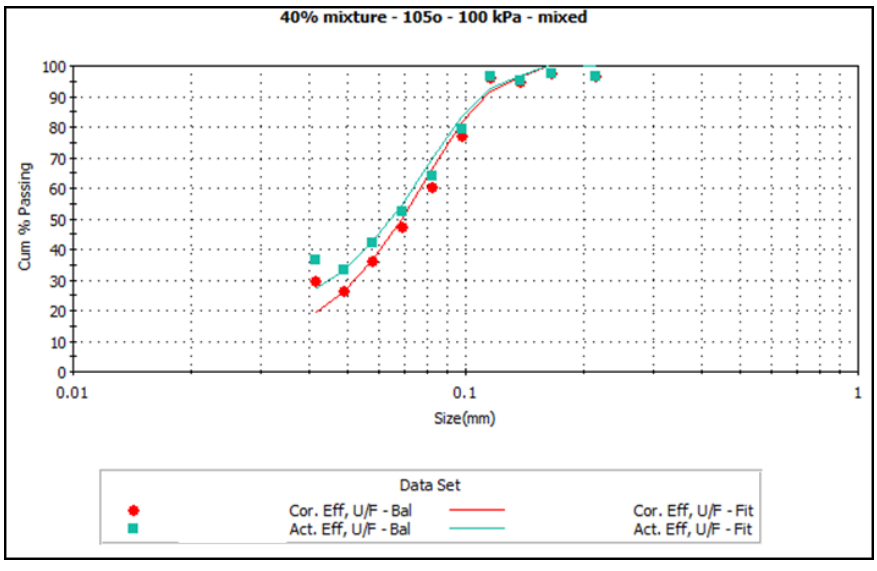

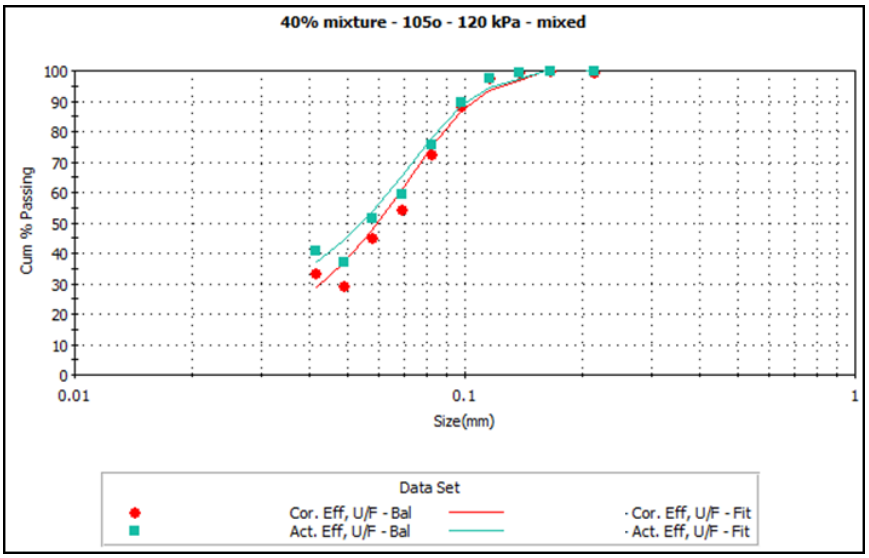
40% mixture - 105o - 120 kPa - mixed
Cum % Passing
100
90
80
70
60
50
40
30
20
10
0
0.01
0.1
1
Size(mm)
Data Set
Cor. Eff, U/F - Bal
Act. Eff, U/F - Bal
Cor. Eff, U/F - Fit
Act. Eff, U/F - Fit

Classification curves for experiment using **modified cone** at 120 degree with 40% silica-magnetite mixture feed:

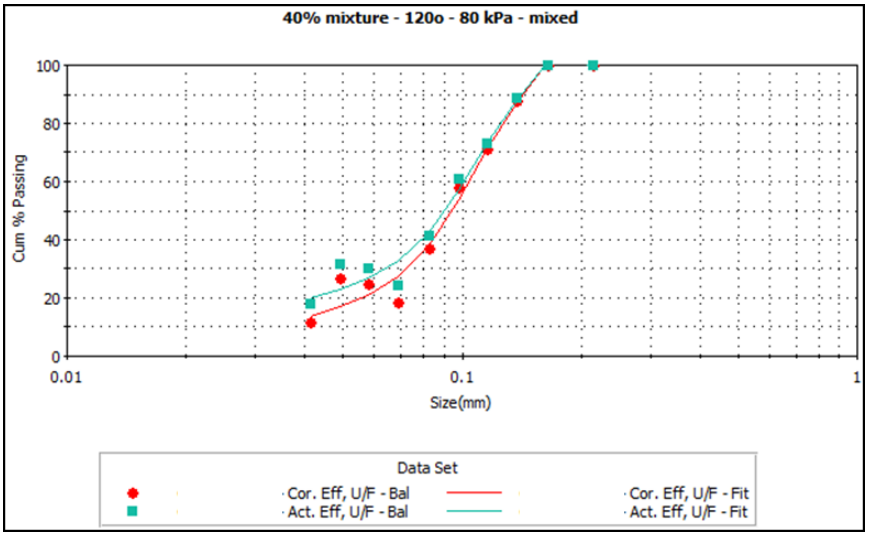

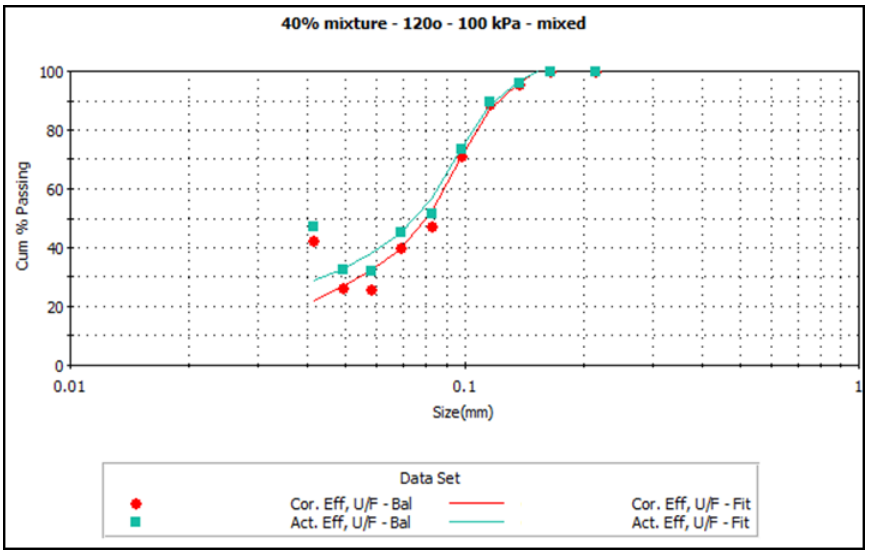

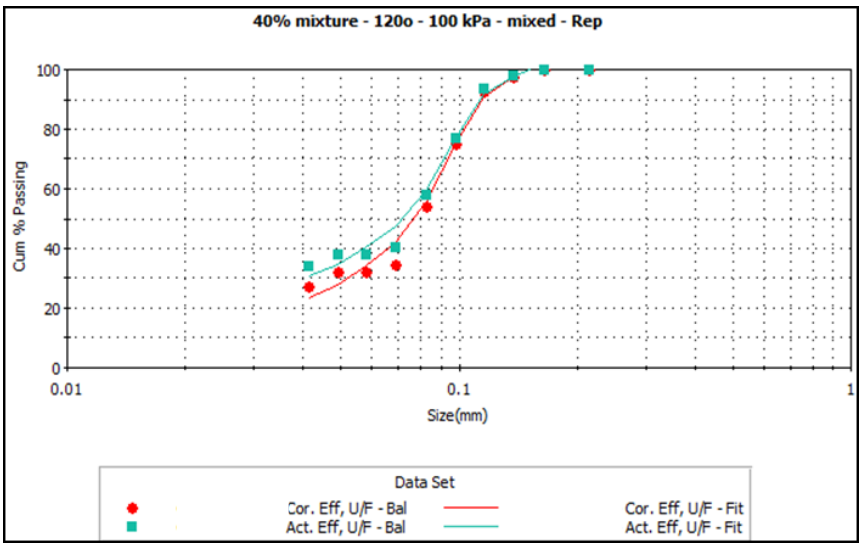

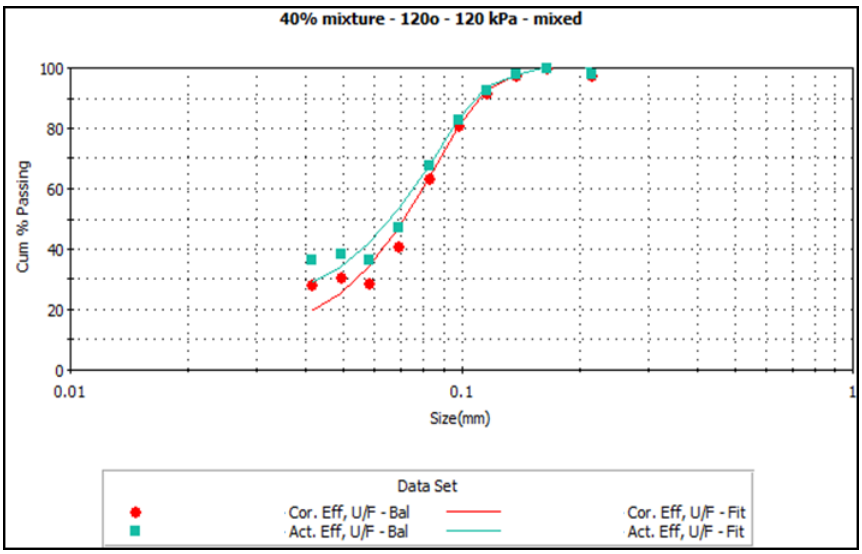
40% mixture - 120o - 120 kPa - mixed
Cum % Passing
100
80
60
40
20
0
0.01
0.1
1
Size(mm)
Data Set
Cor. Eff, U/F - Bal
Act. Eff, U/F - Bal
Cor. Eff, U/F - Fit
Act. Eff, U/F - Fit

Classification curves for experiment using **modified cone** at 135 degree with 40% silica-magnetite mixture feed:

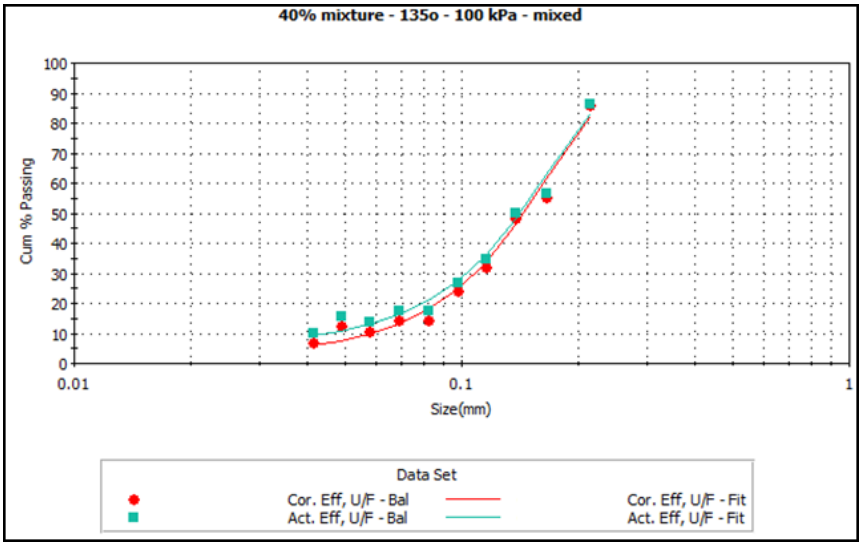

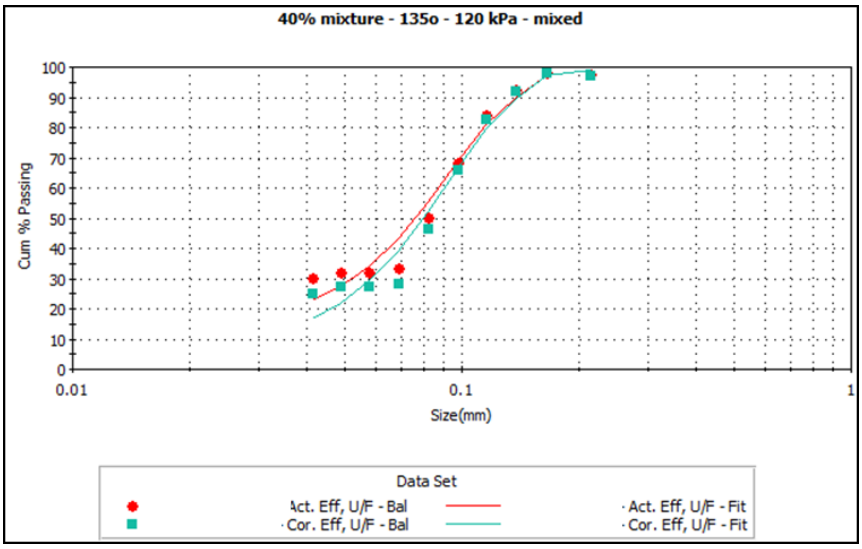

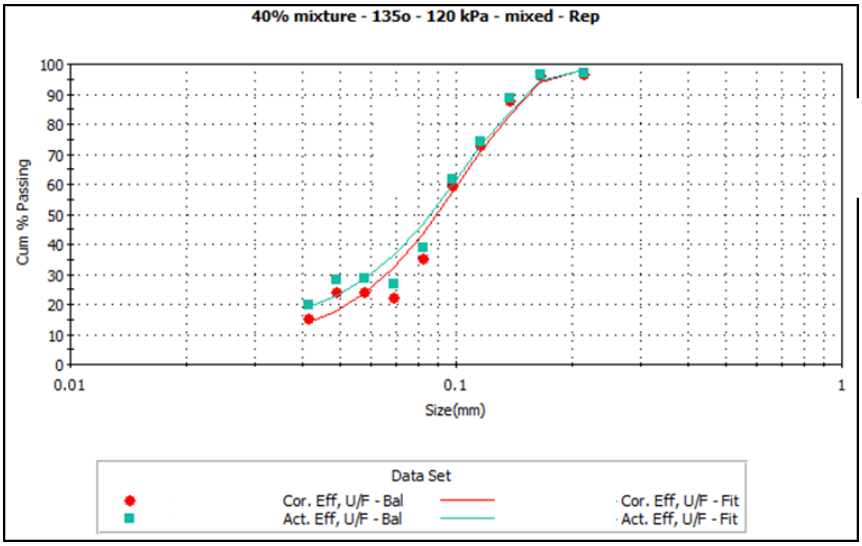

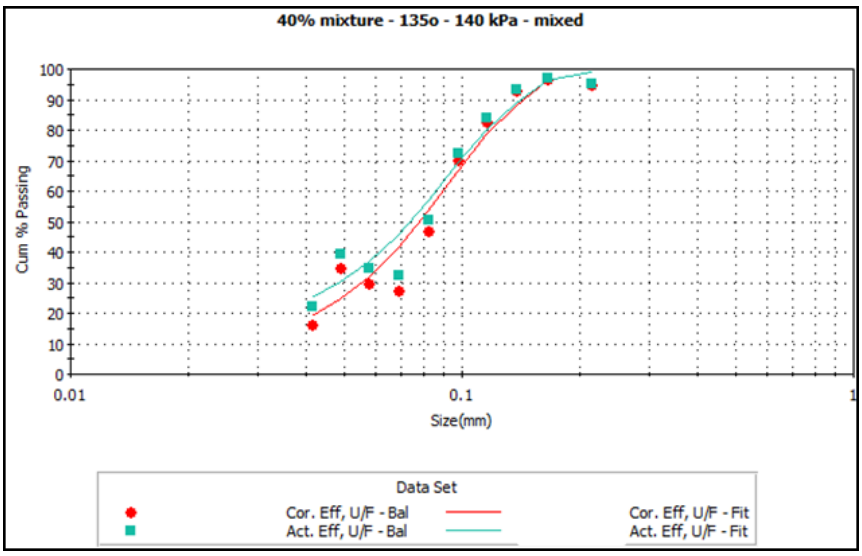
40% mixture - 135o - 140 kPa - mixed
Cum % Passing
100
90
80
70
60
50
40
30
20
10
0
0.01
0.1
1
Size(mm)
Data Set
Cor. Eff, U/F - Bal
Act. Eff, U/F - Bal
Cor. Eff, U/F - Fit
Act. Eff, U/F - Fit

Classification curves for experiment using **modified cone** and **novel vortex finder** at 135 degree with 40% silica-magnetite mixture feed:

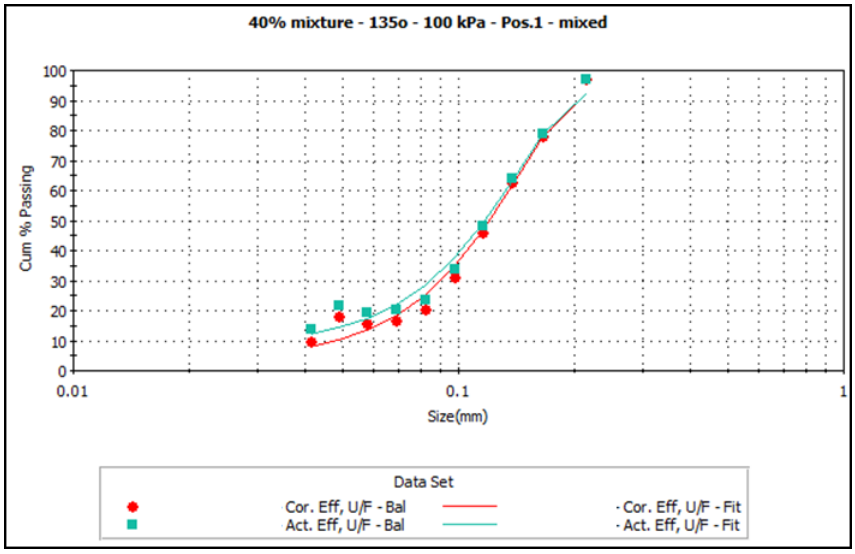

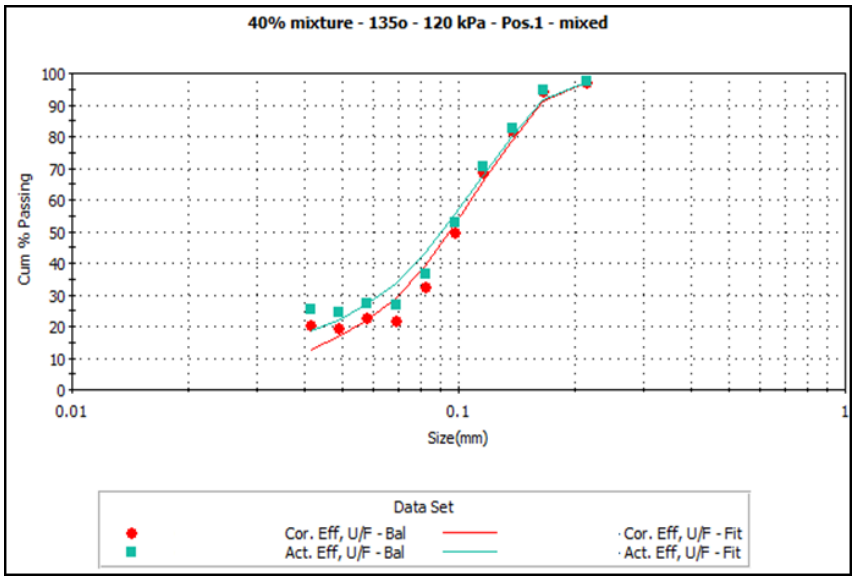

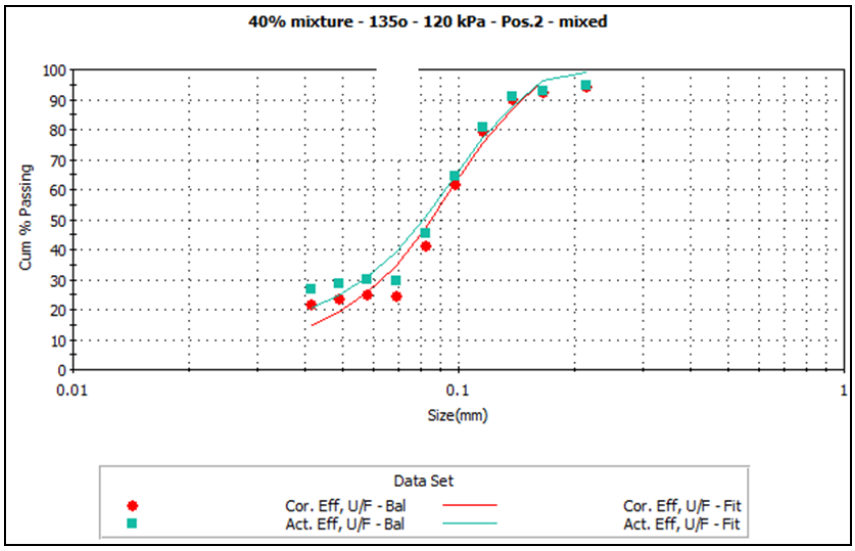

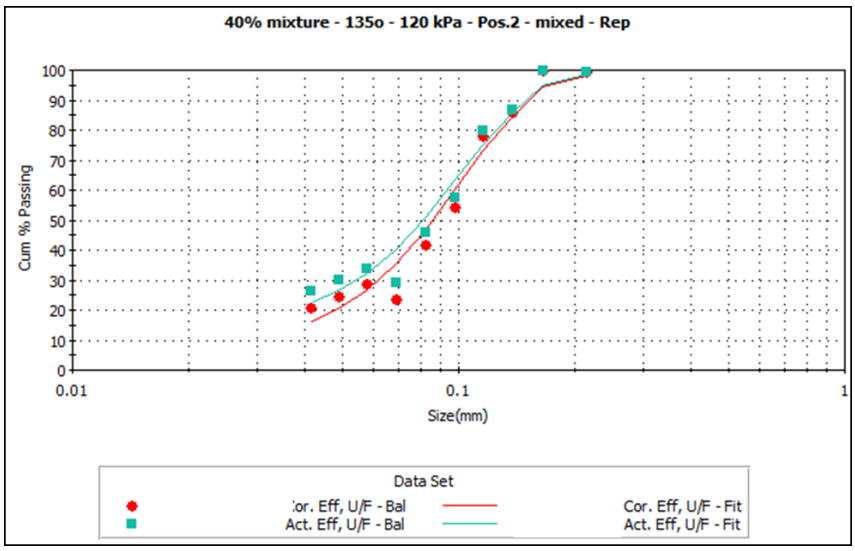
40% mixture - 135o - 120 kPa - Pos.2 - mixed - Rep
Cum % Passing
100
90
80
70
60
50
40
30
20
10
0
0.01
0.1
1
Size(mm)
Data Set
or. Eff, U/F - Bal
Act. Eff, U/F - Bal
Cor. Eff, U/F - Fit
Act. Eff, U/F - Fit

Appendix B: **Water Testing Results**

Prior to hydrocyclone experiment, some preliminary test works using water have been performed. The objectives of the testworks are:

1. To confirm that feed water recovery to underflow follows the expected result, which is declining as inclination was set higher.
2. To identify the most suitable spigot size to choose for the experiment.
3. To provide adequate knowledge of working on the hydrocyclone rig environment.

B.1. Experiment Condition

Two different JKMRC hydrocyclones, 150 mm diameter and 250 mm diameter, were utilized in this test works. The smaller diameter hydrocyclone dimension is given in Table B-1. The larger hydrocyclone dimensions and JKMRC hydrocyclone rig schematic picture are given in Chapter 3.

Table B-1: Dimensions of the 150 mm JKMRC hydrocyclone

Dimensions	Size	Unit
Body diameter	150	mm
Cylindrical body length	75	mm
Inlet diameter	76	mm
Vortex finder diameter	50	mm
Spigot diameter	20, 40, and 50	mm
Cone angle	7	degrees

Water testing on 150 mm diameter hydrocyclone was performed at five inclination point: 135^o, 125^o, 90^o, 45^o, and 0^o. Four levels of pressure drop were applied for each inclination point. Feed pressure was set to the targeted level by adjusting feed pump speed. Three spigot sizes were utilised. Spigot replacement was carried out during inclination adjustment. In total, there were 169 data sets of water testing results.

For larger diameter hydrocyclone of 250 mm, five different inclinations of 0^o, 45^o, 90^o, 120^o, and 135^o were applied with three pressure level (80 kPa, 100 kPa, and 120 kPa) varied at each inclination. Two spigot sizes with diameter of 55 mm and 70 mm were used.

Overflow and underflow samples were collected by rotating Vezin sampler. Three sample replications were taken for each operating conditions.

B.2. Experiment Data and Results

Table B-2 gives result of water testing with 150 mm diameter hydrocyclone.

Table B-2: Raw data sets including water recovery to underflow of water testing on 150 mm hydrocyclone

Run	Inclination	Spigot size	Pressure	Pump Speed	Underflow	Overflow	Water recovery to Underflow, Rf
#	(^{o})	(mm)	(kPa)	(rpm)	(kg)	(kg)	(%)
1	120	50	50	40	3.900	4.920	44.2
2	120	50	80	40	6.950	6.400	52.1
3	120	50	110	43.2	8.150	7.450	52.2
4	120	50	140	48	6.780	7.540	47.3
5	120	40	140	47.7	3.001	11.210	21.1
6	120	40	110	43.3	2.200	9.120	19.4
7	120	40	80	43.3	2.976	7.940	27.3
8	120	40	50	43.3	2.257	6.605	25.5
9	135	40	50	43.3	1.864	6.657	21.9
10	135	40	80	43.3	2.764	8.378	24.8
11	135	40	110	43.3	3.622	9.711	27.2
12	135	40	140	47.7	4.332	10.41	29.4
13	135	50	80	39	5.423	6.033	47.3
14	135	50	80	39	5.562	6.268	47.0
15	135	50	50	43.3	3.739	5.263	41.5
16	135	50	50	43.3	3.782	5.217	42.0
17	135	50	110	43.6	6.487	7.141	47.6
18	135	50	110	43.6	6.275	6.893	47.7
19	135	50	140	48	7.767	7.58	50.6
20	135	50	140	48	7.737	7.58	50.5
21	135	20	140	47.8	0.409	13.445	3.0
22	135	20	140	47.8	0.49	13.56	3.5
23	135	20	110	43.3	0.435	11.984	3.5
24	135	20	110	43.3	0.463	12.12	3.7
25	135	20	80	43.3	0.399	10.549	3.6
26	135	20	80	43.3	0.369	10.505	3.4
27	135	20	50	43.3	0.205	8.309	2.4
28	135	20	50	43.3	0.21	8.433	2.4
29	120	20	50	43.3	0.085	8.407	1.0
30	120	20	50	43.3	0.120	8.051	1.5
31	120	20	80	43.3	0.180	10.28	1.7
32	120	20	80	43.3	0.164	10.371	1.6
33	120	20	110	43.3	0.175	12.177	1.4
34	120	20	110	43.3	0.171	11.815	1.4
35	120	20	140	47.4	0.250	13.134	1.9
36	120	20	140	47.4	0.240	13.386	1.8
37	90	20	140	47.4	0.267	13.17	2.0
38	90	20	140	47.4	0.254	13.323	1.9
39	90	20	110	43.3	0.217	11.793	1.8
40	90	20	110	43.3	0.233	11.995	1.9
41	90	20	80	43.3	0.235	10.238	2.2
42	90	20	80	43.3	0.241	10.004	2.4
43	90	20	50	43.3	0.183	8.122	2.2
44	90	20	50	43.3	0.199	8.066	2.4
45	45	20	50	43.3	0.291	7.949	3.5

46	45	20	50	43.3	0.29	7.862	3.6
47	45	20	80	43.3	0.27	9.929	2.6
48	45	20	80	43.3	0.293	9.964	2.9
49	45	20	110	43.3	0.264	11.578	2.2
50	45	20	110	43.3	0.274	11.742	2.3
51	45	20	140	47.4	0.275	13.366	2.0
52	45	20	140	47.4	0.284	13.351	2.1
53	0	20	140	47.4	0.473	14.037	3.3
54	0	20	140	47.4	0.488	13.89	3.4
55	0	20	110	43.3	0.483	12.212	3.8
56	0	20	110	43.3	0.424	12.076	3.4
57	0	20	80	43.3	0.441	10.349	4.1
58	0	20	80	43.3	0.413	10.338	3.8
59	0	20	50	43.3	0.498	8.2898	5.7
60	0	20	50	43.3	0.477	7.89	5.7
61	0	20	50	43.3	0.504	8.2754	5.7
62	0	40	140	47.6	5.722	9.4404	37.7
63	0	40	140	47.6	5.964	9.4786	38.6
64	0	40	110	43.4	5.520	8.0685	40.6
65	0	40	110	43.4	5.471	8.2337	39.9
66	0	40	80	43.4	4.869	6.7555	41.9
67	0	40	80	43.4	4.783	6.8521	41.1
68	0	40	50	43.4	4.427	4.8658	47.6
69	0	40	50	43.4	4.570	4.9413	48.0
70	0	50	140	47.2	9.454	6.2603	60.2
71	0	50	140	47.2	9.694	6.5758	59.6
72	0	50	140	47.2	9.372	6.3685	59.5
73	0	50	110	43.6	8.674	5.6422	60.6
74	0	50	110	43.6	8.636	5.5274	61.0
75	0	50	80	43.6	7.640	4.6298	62.3
76	0	50	80	43.6	8.188	4.4619	64.7
77	0	50	50	43.6	7.842	4.6159	62.9
78	0	50	50	43.6	7.069	3.3945	67.6
79	0	50	50	43.6	6.983	3.3792	67.4

The results amongst three spigot sizes were presented in graphs individually. Those are shown in Fig. B-1, Fig. B-2, and Fig. B-3.

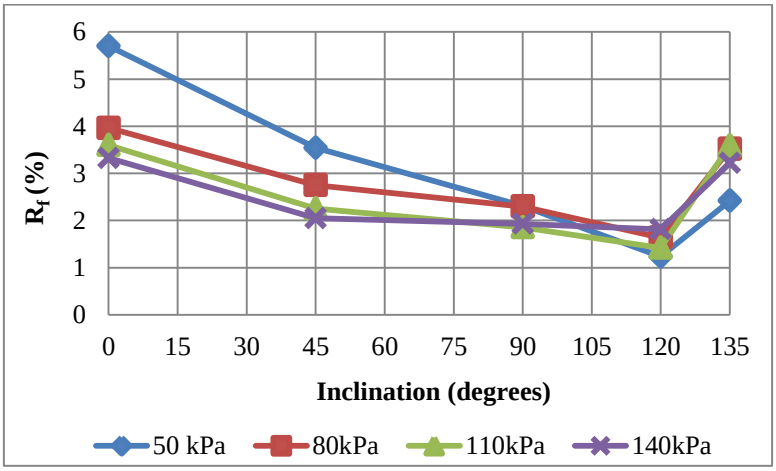

Fig. B-1: Water recovery to underflow response to inclination for 150 mm diameter hydrocyclone with 20 mm spigot

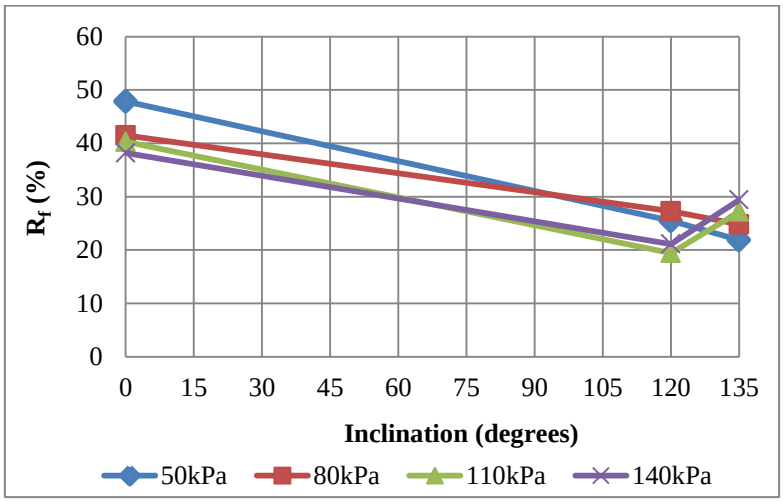

Fig. B-2: Water recovery to underflow response to inclination for 150 mm diameter hydrocyclone with 40 mm spigot

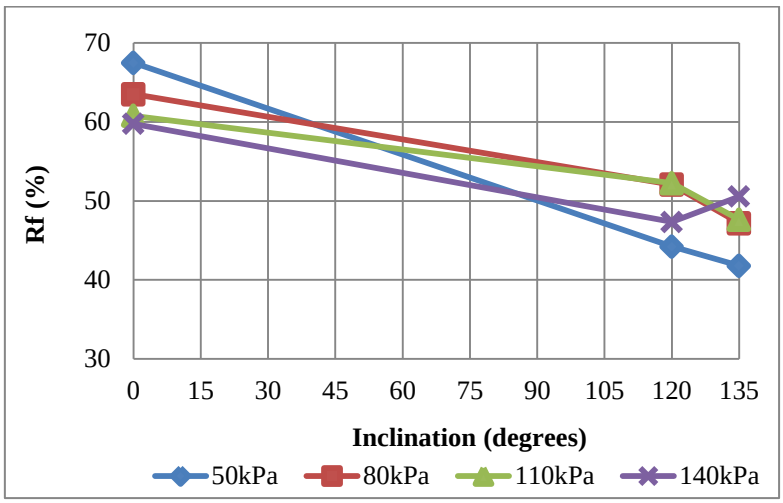

Fig. B-3: Water recovery to underflow response to inclination for 150 mm diameter hydrocyclone with 50 mm spigot

The graph shown by Fig. B-1 illustrates water recovery response with inclination using 20 mm diameter spigot in combination with 50 mm vortex finder. In general, water recovery decreases as inclination goes higher for all different pressure drops with a few exceptions. For instance, vertical operations (or zero inclination) at all pressure levels were giving the most water to underflow. However, at high pressure drop regions of 110 kPa and 140 kPa, water recovery to underflow at 135 degree inclination operation were giving equal values compare to the vertical position. At this particular angle of inclination for all pressure levels, the water recovery rose again after experiencing declining manner.

Fig. B-2 and Fig. B-3 are generated from test using 40 mm spigot size and 50 mm spigot size respectively. Water recoveries are reduced by 13% to 26% at high inclination operations of 120 and 135 degrees compare to conventional vertical operation.

Other interesting features from all three figures are the kick-backs of water reporting to underflow at 135 degree inclination. The reason for this might be that at this specific inclination the hydrocyclone could not more accommodate the rotational flow of water and turbulence was present. It is an indication of operation outside of its optimum range for 150 mm hydrocyclone.

Table B-3: Raw data sets including water recovery to underflow of water testing on 250 mm hydrocyclone

Run	Inclination	Spigot size	Pressure	Pump Speed	Underflow	Overflow	Water recovery to Underflow, Rf
#	(^{o})	(mm)	(kPa)	(rpm)	(kg)	(kg)	(%)
1	0	55	80	47.1	5.74	26.54	17.8
2	0	55	80	47.1	5.84	27.02	17.8
3	0	55	80	47.1	5.82	26.38	18.1
4	0	55	100	51.1	5.38	29.34	15.5
5	0	55	100	51.1	5.04	29.64	14.5
6	0	55	100	51.1	5.22	29.34	15.1
7	0	55	120	55.4	4.94	32.48	13.2
8	0	55	120	55.4	5.1	31.92	13.8
9	0	55	120	55.4	5.16	32.4	13.7
10	0	70	120	55.8	14.78	26.6	35.7
11	0	70	120	55.8	15.02	26.44	36.2
12	0	70	120	55.8	15.06	26.5	36.2
13	0	70	100	51.6	14.54	23.28	38.4
14	0	70	100	51.6	14.3	23.38	38.0
15	0	70	100	51.6	14.36	23.22	38.2
16	0	70	80	47.4	14.24	21.06	40.3
17	0	70	80	47.4	13.94	21.58	39.2
18	0	70	80	47.4	14.04	20.78	40.3
19	45	55	80	47.4	26.20	4.12	13.6
20	45	55	80	47.4	26.10	4.06	13.5
21	45	55	80	47.4	25.70	4.04	13.6
22	45	55	100	52.4	30.50	4.30	12.4
23	45	55	100	52.4	29.72	4.42	12.9
24	45	55	100	52.4	29.86	4.30	12.6
25	45	55	120	57.6	33.56	4.56	12.0
26	45	55	120	57.6	33.90	4.50	11.7
27	45	55	120	57.6	33.66	4.60	12.0
28	45	70	120	58.4	25.70	12.36	32.5
29	45	70	120	58.4	26.06	12.90	33.1
30	45	70	120	58.4	26.66	12.68	32.2
31	45	70	100	54.3	24.78	11.62	31.9
32	45	70	100	54.3	23.96	11.96	33.3
33	45	70	100	54.3	23.78	12.10	33.7
34	45	70	80	50.3	22.44	11.38	33.6
35	45	70	80	50.3	21.76	11.38	34.3
36	45	70	80	50.3	22.04	11.64	34.6
37	90	70	80	46.4	23.58	7.92	25.1
38	90	70	80	46.4	25.14	8.00	24.1
39	90	70	80	46.4	22.20	7.78	26.0

40	90	70	100	50.5	26.62	8.82	24.9
41	90	70	100	50.5	26.32	8.90	25.3
42	90	70	100	50.5	26.86	9.06	25.2
43	90	70	120	55.2	28.87	9.82	25.4
44	90	70	120	55.2	28.54	9.68	25.3
45	90	70	120	55.2	29.06	9.82	25.3
46	90	55	120	54.1	33.24	3.06	8.4
47	90	55	120	54.1	32.76	3.08	8.6
48	90	55	120	54.1	31.97	3.04	8.7
49	90	55	100	49.9	30.28	2.72	8.2
50	90	55	100	49.9	30.98	2.90	8.6
51	90	55	100	49.9	30.60	2.68	8.1
52	90	55	80	46.0	27.30	2.42	8.1
53	90	55	80	46.0	27.54	2.52	8.4
54	90	55	80	46.0	27.22	2.56	8.6
55	120	55	80	45.9	27.22	1.78	6.1
56	120	55	80	45.9	27.80	1.88	6.3
57	120	55	80	45.9	27.40	1.72	5.9
58	120	55	100	50.1	30.88	2.08	6.3
59	120	55	100	50.1	31.66	1.96	5.8
60	120	55	100	50.1	31.80	2.12	6.3
61	120	55	120	54.4	33.96	2.70	7.4
62	120	55	120	54.4	34.44	2.52	6.8
63	120	55	120	54.4	34.32	2.46	6.7
64	120	70	120	54.4	29.36	8.50	22.5
65	120	70	120	54.4	29.40	8.30	22.0
66	120	70	120	54.4	29.62	8.24	21.8
67	120	70	120	50.5	27.14	7.58	21.8
68	120	70	100	50.5	26.06	7.40	22.1
69	120	70	100	50.5	26.90	7.30	21.3
70	120	70	100	46.4	24.24	6.36	20.8
71	120	70	80	46.4	25.34	6.66	20.8
72	120	70	80	46.4	24.50	6.54	21.1
73	135	70	80	46.4	25.28	6.20	19.70
74	135	70	80	46.4	24.80	5.86	19.11
75	135	70	80	46.4	25.16	6.08	19.46
76	135	70	100	51.1	27.28	7.40	21.34
77	135	70	100	51.1	26.96	7.06	20.75
78	135	70	100	51.1	27.38	7.08	20.55
79	135	70	120	55.5	29.74	8.50	22.23
80	135	70	120	55.5	30.02	8.24	21.54
81	135	70	120	55.5	30.24	8.14	21.21
82	135	55	120	53.9	34.90	2.28	6.13
83	135	55	120	53.9	34.42	2.26	6.16
84	135	55	120	53.9	35.26	2.16	5.77
85	135	55	100	49.9	31.66	1.88	5.61
86	135	55	100	49.9	30.66	1.76	5.43
87	135	55	100	49.9	31.76	1.84	5.48
88	135	55	80	46.4	28.10	1.42	4.81
89	135	55	80	46.4	28.66	1.44	4.78
90	135	55	80	46.4	27.86	1.60	5.43

Data from Table B-3 are illustrated into graphs in Fig. B-4 and Fig. B-5.

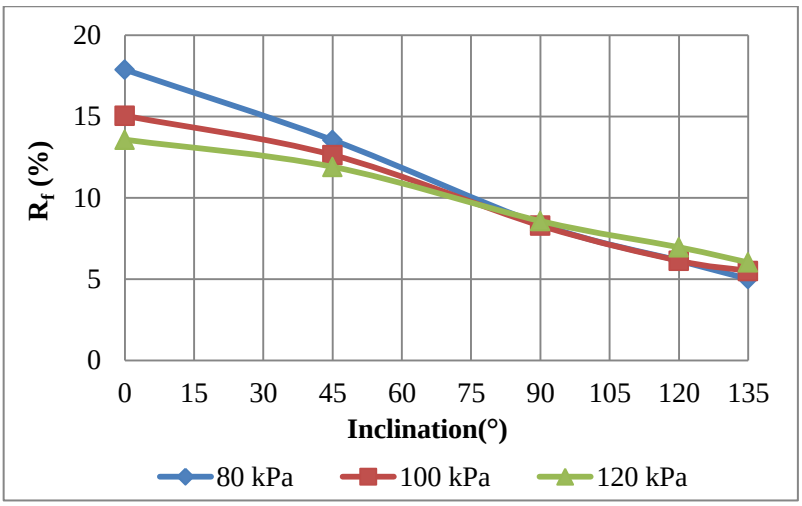

Fig. B-4: Water recovery to underflow response to inclinations on 250 mm diameter hydrocyclone using 55 mm spigot

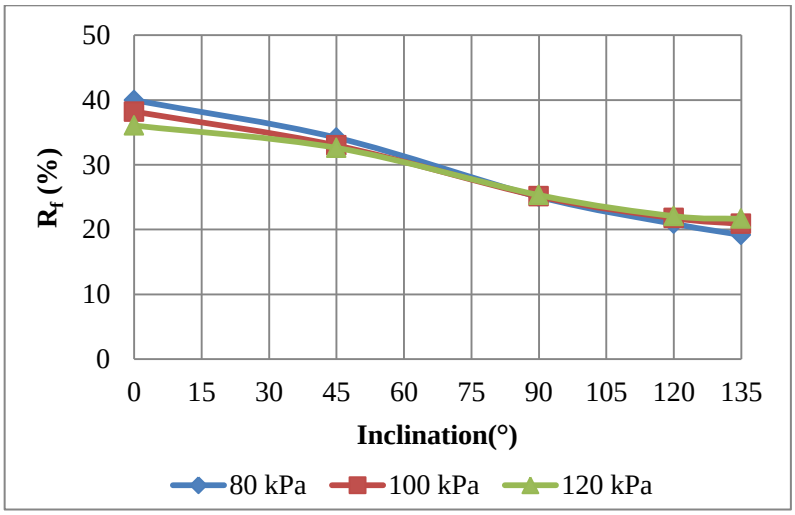

Fig. B-5: Water recovery to underflow response to inclinations on 250 mm diameter hydrocyclone using 70 mm spigot

From Fig. B-4 and Fig. B-5, it can be argued that water recovery responds inversely to inclinations. Compare to 150 mm diameter hydrocyclone results, 250 mm diameter hydrocyclone has wider operating pressure, which is signified by the continuous decreasing trend of water recovery to underflow at 135 degrees.

Operation with 55 mm spigot diameter can suppress water recovery to underflow down to five percent on semi-inverted operations from around fifteen per cent at vertical operations.